Sapienza University of Rome
XIII PhD Course in Environmental Engineering

Alkaline activation of incinerator bottom ash for use in structural applications

Roberta Onori

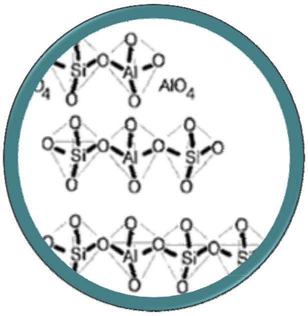

SAPIENZA
UNIVERSITÀ DI ROMA

Sapienza University of Rome

XIII PhD Course in Environmental Engineering

“Alkaline activation of incinerator bottom ash for use in structural applications”

Ing. Roberta Onori

Supervisor:

Prof. Ing. A. Polettini

Contents

Contents I

List of Figures III

List of Tables VII

Abstract IX

Sintesi XI

Introduction 1

Alkali-activated waste materials 1

References 4

1. State of the art 5

1.1 State of the art of waste management in the EU and role of incineration 5

1.2 Bottom Ash from waste incineration 10

1.3 Physical characteristics 11

1.4 Chemical characteristics 13

1.5 Mineralogical Characteristics 15

1.6 Recycling of incinerator BA for the formulation of blended cements. 17

1.7 Geopolymers 19

1.7.1 History 20

1.7.2 Chemistry aspects 21

1.7.3 Geopolymerization process 23

1.7.4 Applications 28

References 30

2. Materials and methods 41

2.1 Bottom Ash 41

2.1 Activation of bottom ash for use in Portland cement blends 43

2.2 Production of geopolymeric materials from bottom ash 53

References 57

3. Results and Discussion: Bottom ash characterization 61

3.1 Size classification 61

3.2 LOI determination 62

3.3 Elemental Composition 62
3.4 EN 12457-2 test 64
3.5 ANC TEST....................66
3.6 Mineralogical and morphological characterization of BA Sample 2....................68
References....................73
4. Results and Discussion: BA activation for blended cement formulation....................75
4.1 Mechanical properties....................75
4.2 Analysis of variance (ANOVA) of results 81
4.3 TGA analysis of selected samples....................87
4.4 ANC leaching test on selected mixtures 88
4.5 Visual Minteq results....................90
4.6 Results of leaching tests for trace metals 95
References....................101
5. Results and Discussion: BA based geopolymer materials....................107
5.1 Mechanical properties of geopolymer products 107
5.2 SEM (Secondary Electron Images) interpretation....................110
5.3 TGA interpretation....................115
5.4 FT-IR (Fourier transform infrared spectroscopy) analysis 116
5.5 XRD interpretation....................119
RAMAN interpretation 121
5.6 ANC test on selected samples....................124
References....................127
6. Conclusions 133
Papers 137
WASCON 2009: Sustainable Management of waste and recycled materials in construction....................137
3rd BOKU Waste Conference April 15 - 17, 2009 Vienna, Austria....................150
2010 International Solidification/Stabilization Technology Forum 15th-17th June 2010 Cape Breton University (Canada)....................160
35th International Conference on Advanced Ceramics & Composites (ICACC) 2011...172
Waste Management....................184
Acknowledgements....................197

List of Figures

Figure 1: Classification of different subset of AAMs with comparisons to OPC. The gray level in the circles represents the alkali content, the higher content corresponding to darker grey level 3
Figure 2: Example of general schematics of policy and legislative system (Costa et al., 2010) 7
Figure 3: Municipal Waste generated in the Member States in 2008 (Eurostat, 2009) 7
Figure 4: Municipal Waste Treated Methods in UE Member States (Eurostat, 2009) 8
Figure 5: Amount of Municipal Waste Landfilled (Eurostat 2009) 8
Figure 6: Distribution and classification of solid residues from an incineration plant 10
Figure 7: quenching unit and storage site 11
Figure 8: Main oxides (a) and trace elements (b) of BA as a function of particle size 12
Figure 9 Types of polysialate units 22
Figure 10: Main components used to produce geopolymeric materials 23
Figure 11: Main steps and reaction associated in a geopolymerization process 24
Figure 12:Cubic moulds for cement mixtures 45
Figure 13: Cylindrical steel moulds and geopolymer samples obtained 55
Figure 14: quartering (a), wet sample (b), dry sample (c) 61
Figure 15: particle size distribution for Sample 2, comparison of class weights between Sample 1 and Sample 2 62
Figure 16: ANC curves for Sample 1 (a), for Sample 2 (b) and comparison between both Samples 67
Figure 17: Sample 1 - Metals leaching 67
Figure 18: Sample 2 - Metals leaching 68
Figure 19: SEM micrograph (a and b) and results of EDAX spot analysis (c) for powdered BA (Sample 2) 69
Figure 20: FT-IR spectra for CF+FF fraction of sample 2 and position of the main peaks 69
Figure 21: Raman spectra collected for the CF+FF of Sample 2 in three main areas: grey (G), white (W), black (B) 70
Figure 22: XRD spectra for BA sample 2 72

Figure 23: Unconfined Compressive Strength (UCS) UCS of mixtures containing the CF of BA ____ 75
Figure 24: UCS vs. curing time for mixtures containing 20% BA (CF) and 2% and 4% activator ____ 77
Figure 25 : Specific Unconfined Compressive Strength (SUCS) of mixtures containing the CF of BA ____ 78
Figure 26: UCS and SUCS of mixtures containing the CF, FF and CF+FF of BA activated with Ca-based compound ____ 80
Figure 27: UCS and SUCS of mixtures containing the CF, FF of BA activated with Ca-based compound; method 1 ("_1) and method 2 ("_2") ____ 81
Figure 28: Response surfaces for UCS as derived from model as per equation (1) – values in MPa ____ 84
Figure 29: Response surfaces for UCS as derived from model as per equation (2) – values in MPa ____ 86
Figure 30. TGA/DSC measurements of selected mixtures ____ 88
Figure 31 ANC curves for Ca-based activator-containing mixtures at all the curing days together with reference samples (control and mixture containing untreated BA) ____ 89
Figure 32: ANC curves for Ca based activator-containing mixtures at 7 and 56 curing days for "Method 1" and "Method 2", the first marked with "_1", the latter marked with the "_2" ____ 90
Figure 33. Results of geochemical modeling for Ca, Si and SO_4^{2-} for the control, U20c and C20-2c mixtures at 7-day curing (A: anhydrite; Ca_ox: Ca oxychloride; CSH-l: C–S–H (Ca/Si = 0.5); CSH-m: C–S–H (Ca/Si = 0.8); E: ettringite; G: gypsum; M: monosulphate, $C_4FS^*H_{12}$ ____ 93
Figure 34: Results of geochemical modeling for Ca, Si and SO42- for the control, U20c and C20-2c mixtures at 56-day curing (A: anhydrite; CSH-l: C–S–H (Ca/Si = 0.5); CSH-m: C–S–H (Ca/Si = 0.8); E: ettringite; G: gypsum; Gh: gehlenite hydrate; M: monosulphate; MCr: Cr-Monosulphate; Q: quartz ____ 94
Figure 35: Metal leaching as a function of pH in the ANC test for reference and $CaCl_2$-containing mixtures (activation method 1) ____ 98
Figure 36: Metal leaching as a function of pH in the ANC test for $CaCl_2$- and $CaSO_4$-containing mixtures at 7 and 56 curing days (activation methods 1 and 2) ____ 99

Figure 37: Results of geochemical modelling of Pb leaching on account of surface complexation by HFO and AAM (SCM = surface complexation model) for sample C20-2c ____ 100
Figure 38: Results of UCS testing on geopolymerized materials (error bars are drawn at one standard deviation of values) ____ 107
Figure 39: Relationship between UCS and the Si/Al ratio at given NaOH concentrations in the alkaline medium ____ 108
Figure 40: SEM micrographs of fracture surfaces for samples (a) S-2.29-7.5 at 7 curing days (b) S-2.29-5 at 7 curing days and (c) S-2.29-5 at 28 curing day ____ 111
Figure 41: SEM micrographs and zone selected for EDAX spot analysis: ____ 112
Figure 42: Main elements indentified in geopolymer samples through EDAX analysis ____ 113
Figure 43: SEM micrograph and results of EDAX spots analysis for powder samples (a) S-2.29-7.5 at 7 day-curing (b) sample S-2.29-5 at 7 day-curing (c) sample S-1.69-7.5 at 7 day-curing (d) sample S-1.28-7.5 at 7 day-curing ____ 114
Figure 44: (a) TGA and (b) DTA curves for samples O, J, P and Q at 7 day curing ____ 116
Figure 45: FT-IR spectra at 7- and 28-day curing (a) and comparison of relative peak intensities (b) for BA-based geopolymers ____ 117
Figure 46: XRD patterns for geopolymer samples at 7-day curing and BA ____ 119
Figure 47: XRD patterns for geopolymer samples and BA with details about the position of amorphous broad hump ____ 121
Figure 48: Examples of the areas where the spectra have been collected (sample S-2.29-5 28 d) ____ 122
Figure 49: Raman spectra of geopolymer samples at 7 and 28 curing days ____ 123
Figure 50: ANC curves for selected samples ____ 125
Figure 51: Metal leaching as a function of pH in the ANC test for selected samples ____ 126

List of Tables

Table 1: humidity (W%) and LOI (%) values in BA 13

Table 2: Observed concentrations of main and trace elements in BA 15

Table 3: Main mineral phases in BA (Dykstra Eudsen et al., 1999) 15

Table 4: Main chemical activators user to improve pozzolanic reactions of reactivity for different residues 18

Table 5: Composition of the OPC/BA mixtures 44

Table 6: coefficient for orthogonal contrast 46

Table 7: contrast coefficients for interaction effects 46

Table 8: general arrangement for a factorial design (design 3^2; UCS value at 56-day curig) 47

Table 9: the Analysis of Variance Table for 3^2 facorial design 48

Table 10: ANOVA components 48

Table 11: Stability constants of the new mineral phases added to the standard thermodynamic database in Visual MINTEQ, based on the dissolution reactions reported 52

Table 12: Compositional characteristics of mixtures used for geopolymer synthesis 54

Table 13: Samples selected for microstructural and leaching characterization 56

Table 14: Bottom ash elemental composition for CF, FF and CF+FF for Sample 1 and Sample 2 63

Table 15: Comparison between EN 12457-2 test results (natural pH) and regulatory limits for selected heavy metals of both BA samples 65

Table 16: Main RAMAN peaks 71

Table 17: ANOVA results for UCS at the four curing times investigated, expressed in terms of sum of squares (SS) for the individual effect/interaction, the corresponding degrees of freedom (DF) and mean squares (MS) 82

Table 18: ANOVA results for UCS at the four curing times investigated, expressed in terms of sum of squares (SS) for the individual effect/interaction, the corresponding degrees of freedom (DF) and mean squares (MS) 85

Table 19: Comparison between leaching test results (natural pH) and regulatory limits for selected heavy metals 96

Table 20: Values of UCS for geopolymeric samples 108
Table 21: Results of physical characterization for selected samples (mean values ± standard deviation) 110
Table 22: Weight loss for different temperature regions as derived from the TGA curves in Figure 44: (a) TGA and (b) DTA curves for samples O, J, P and Q at 7 day curing 116
Table 23: Position and interpretation of the main FT-IR peaks for geopolymer samples 119
Table 24: Raman shift for main phase characteristics of the bottom ash and geopolymers samples. (http://rruff.geo.arizona.edu/rruff; http://www.geocities.com/ostroum/FTRAMAN) 124
Table 25: Comparison between leaching test results (natural pH) and regulatory limits for selected heavy metals 126

Abstract

The aim of this research was the study and identification of suitable alternatives to develop new materials from industrial residues derived from thermal treatment of waste. In detail, this research was addressed to assess different alkali activation processes of incinerator bottom ash in order to evaluate the recycling potential as a structural material in engineering applications.

Bottom ashes (BAs) from waste incineration are generated in relatively large amounts (>90% of the total solid residues mass) and account for 15-25% by mass of the original waste. The research stems from the observation that BAs are also the residues with technical properties most suited for utilization. The similarities in physical characteristics and major composition of granular construction materials and BA make this residue virtually suited for recycling as a substitute for natural aggregate; construction and building materials are the primary utilization route for BAs in Europe. All the mentioned utilization options rely on the implicit assumption of the predominantly inert characteristics of BA, however, the chemical reactivity of BA under natural conditions has also been widely assessed. Thus, advantage may be taken from the presence of reactive compounds in BA to improve the materials' properties for utilization. Different processing methods have been investigated to improve the mechanical properties of BA in view of engineering applications, which are mostly based on preliminary activation of the material by means of mechanical, chemical or thermal methods (or a combination of the three).

The experimental study conducted includes investigations of two main activation processes of bottom ash:

- Alkaline activation using different alkaline compounds in order to improve the natural reactivity of bottom ash for blended cement formulation;
- Geopoymerization process aimed at producing a mechanically resistant material without binder addition.

Considering mechanical activation (i.e., increase of specific surface area) as a preliminary step required for both processes, the two experimental studies differ mainly for the alkali activation method used (type and concentration of activator, contact time, process temperature).

In the first process, a slurry-phase activation method of bottom ash with the selected activator at 90° C for 3h was applied. Different sodium-, potassium- and calcium-based activators were tested at different dosages (0, 0.4 and 0.8 wt %). The activated bottom ash was then mixed in different proportions (0, 20 and 40 wt %) with Portland cement to produce blended cements. The materials obtained were characterized in terms of mechanical characteristics, leaching properties; a detailed study of the hydration process evolution was also conducted in order to gain information about the main differences with respect to the hydration process of pure cement. The results indicated that Ca-based activators exhibited by far the best effects on the evolution of the hydration process of the mixtures and metal leaching from the hardened material.

In the latter activation process a preliminary study concerning the identification of the main parameters controlling the geopolymerization process of bottom ash was conducted. The activation process involves lower temperatures (~ 75°C) than the previous one. Different mixtures were investigated for geopolymer production, which differed for the Si/Al ratio (obtained upon addition of sodium silicate and metakaolin) and the NaOH concentration in the alkaline medium. The obtained geopolymeric materials were characterized in terms of physical and mechanical properties, mineralogical and microstructural characteristics as well as chemical durability. While the physical and mechanical properties correlated well with the Si/Al ratio, no clear trend was found with the NaOH concentration; however, although the strength development upon geopolymerization was clear, the experimental data suggested that the optimal Si/Al ratio was probably beyond the investigated range. Microstructural and leaching tests showed that, although the onset of the geopolymer-formation reactions was clear, the degree of matrix restructuring was relatively poor, indicating the need for further investigation to promote the development of the geopolymerization reactions.

Sintesi

Lo scopo di questa ricerca è stato quello di studiare e identificare possibili alternative per lo sviluppo di nuovi materiali a partire da residui di origine industriale derivanti da processi termici di trattamento dei rifiuti.

In particolare sono stati studiati due processi di attivazione alcalina di scorie di fondo (bottom ash) provenienti da un impianto di incenerimento di rifiuti solidi urbani al fine di valutare le possibilità di riciclo e riuso di questi scarti per la produzione di materiali dotati di buone caratteristiche meccaniche potenzialmente impiegabili per applicazioni ingegneristiche.

Le scorie di fondo (BAs) rappresentano la porzione più abbondante tra tutti i residui solidi prodotti durante il processo di incenerimento (> 90% in massa) e circa il 15-25% in massa dei rifiuti conferiti in impianto. Le scorie di fondo sono residui dotati di caratteristiche tecniche tali da renderle potenzialmente riutilizzabili poiché presentano caratteristiche fisiche e composizione molto simili a quelle possedute dai materiali granulari utilizzati nel settore delle costruzioni. Queste caratteristiche fanno si che questo materiale venga ampiamente studiato allo scopo di riutilizzarlo per applicazioni che lo vedono impiegato come sostituto di aggregati naturali e come materiale da costruzione per sottofondi stradali (in Europa le scorie di fondo sono il materiale maggiormente utilizzato a questo scopo).

Gli impieghi citati, oramai divenuti tradizionali per questo materiale, presuppongono una natura principalmente inerte del residuo. Studi recenti, ma già ampiamente consolidati, hanno però dimostrato l’intrinseca reattività chimica, specie in condizioni naturali e in ambienti alcalini, delle scorie di fondo. La presenza di composti potenzialmente reattivi all’interno della matrice del materiale, dovuta alle modalità di produzione del residuo, fa si che processi di attivazione, meccanica, chimica e termica, o combinazioni di questi tre metodi, vengano testati e sperimentati al fine di migliorare le prestazioni meccaniche e limitare l’impatto sull’ambiente dovuto alla presenza di metalli pesanti.

In questa tesi vengono presentati i risultati di una sperimentazione condotta su due differenti processi di attivazioni delle scorie di fondo:

- attivazione alcalina con utilizzo di differenti composti per promuovere la naturale reattività delle scorie di fondo per la formulazione di cementi di miscela;
- geopolimerizzazione delle scorie per la produzione di materiali dotati di buone resistenze meccaniche anche senza aggiunte di cementi.

Considerando come propedeutica, per entrambi i processi, l'attivazione meccanica, allo scopo di aumentare la superficie specifica, i due filoni di ricerca si sono differenziati principalmente per il metodo di attivazione alcalina utilizzato (tipo e concentrazione di attivatore, tempo di contatto, temperatura di processo).

Nella prima sperimentazione è stato studiato un processo di attivazione in fase slurry miscelando scorie e attivatore a 90°C per 3 h. Gli attivatori alcalini selezionati per questa sperimentazione, testati a differenti dosaggi (0, 0.4 e 0.8 % in peso), sono a base di sodio, potassio e calcio. Le scorie attivate sono successivamente state miscelate con cemento Portland variandone la percentuale nell'impasto (0, 20 e 40 % in peso). I materiali prodotti sono stati caratterizzati da un punto di vista meccanico, sono state studiate le proprietà di rilascio/immobilizzo attraverso test di cessione ed è stato condotto uno studio per valutare le principali modifiche al processo di idratazione rispetto a quello del cemento puro. Dai risultati ottenuti si è evidenziato una buona resa per gli attivatori a base di calcio sia in termini di sviluppo delle resistenze meccaniche sia per quanto concerne l'aspetto legato al rilascio dalla matrice cementizia di contaminanti nell'ambiente.

La seconda sperimentazione ha avuto come oggetto lo studio preliminare di un processo di geopolimerizzazione delle scorie di fondo al fine di individuare i principali parametri controllanti il processo stesso. L'attivazione è stata condotto a temperatura inferiore rispetto a quella utilizzata durante la prima sperimentazione (circa 75°C). Sono state formulate diverse miscele caratterizzate da un diverso rapporto Si/Al (ottenuto con dosaggi differenti di una soluzione di sodio silicato e di metacaolino) e da una diversa concentrazione di NaOH nella soluzione alcalina. I geopolimeri, così ottenuti, sono stati caratterizzati dal punto di vista fisico, meccanico, chimico e micro strutturale; inoltre sono state studiate le caratteristiche di rilascio dei principali metalli pesanti.

I primi risultati hanno evidenziato un'evidente relazione tra le resistenze meccaniche sviluppate ed il rapporto Si/Al delle miscele e un'influenza molto minore della concentrazione di NaOH della soluzione alcalina. Considerando l'evidente relazione tra resistenze sviluppate dai geopolimeri e dosaggio Si/Al è possibile affermare che il rapporto Si/Al nei geopolimeri prodotti è ancora basso rispetto a quello ottimale. I risultati della caratterizzazione microstrutturale e degli studi sul rilascio hanno mostrato che, sebbene il processo di geopolimerizzazione sia stato attivato, il grado di riorganizzazione chimica della struttura ottenuta è ancora basso. Risulta quindi necessario condurre ulteriori studi al fine migliorare le condizioni per uno sviluppo completo delle reazioni di geopolimerizzazione.

Introduction

Alkali-activated waste materials

Over the last years a great deal of scientific research has been conducted to develop new materials from industrial residues including ashes from coal and waste combustion, metallurgical slags, red mud, etc. through the use of alkali activators to allow for beneficial reuse (van Deventer et al., 2010). The research in this area is addressed to produce an alternative to traditional inorganic binder materials such as Portland cement with the double purpose of saving natural resources and reducing the CO_2 emissions associated to cement production (Pacheco-Torgal et al., 2008). It should be considered that in 2008 the global cement production was estimated to be around 2.6 billion tons per annum (Freedonia Group, 2009). Cement production has been identified as a primary contributor to the world greenhouse gas emissions, accounting for ~ 5-8% of all manmade emissions worldwide.

Taking this into account, several alternatives to develop supplementary cementitious materials (SCMs) (Scrivener and Kirkpatrick, 2008) are the subject of research studies all over the world.

In addition, other studies are being conducted in order to assess the most suitable approach to improve the natural reactivity of these materials; different alkaline compounds or combination of reagents have been tested to promote the dissolution of the aluminosilicate matrix thus improving the material's reactivity. Among such compounds, the following have been tested: sodium and potassium silicate, sodium and potassium hydroxide, sodium, potassium and calcium carbonate, sodium aluminate, calcium sulphate and chloride (van Deventer et al., 2010).

The materials produced through the use of alkaline activators are referred to as Alkali Activated Materials (AAMs). In several countries these materials have already found practical applications in a number of construction sectors. For example, incinerator bottom ash is already used as a fine aggregate substitute in hot-mix asphalt wearing surfaces, in emulsified asphalt cold-mix wearing surfaces, occasionally as unbound aggregate or granular material for pavement construction, as a structural fill material for the construction of highway embankments and/or the retaining walls or trenches (U.S. Department of

Transportation, 1997). Despite the presence of track records of successful applications of these materials, this has not been recognized by the market. However, the recent focus on global warming together with the public and consumer preference for “green products” have made AAMs a good alternative to partially replace cementitious materials.

The threshold between materials of different properties in this area is sometimes quite subtle, and various terms are used by the scientific community to refer to such materials, including AAMs, inorganic polymers and geopolymers (Duxson et al., 2007; van Deventer et al., 2010). The definition for each class is provided below and outlined in Figure 1: (van Deventer et al., 2010).

AAMs include any binder system derived by the reaction between an alkali salt or a combination of more alkali salts (either in the solid or dissolved form) and a solid silicate powder (Shi et al., 2006). As mentioned above, the solid can be a calcium silicate or a calcium aluminate-rich precursor such as coal fly ash, bottom ash or another waste material. The alkali salts used include: hydroxides, silicates, carbonates, sulphates, aluminates; essentially any soluble substance which can increase the pH of the reaction medium and accelerate the dissolution of the solid precursor can be used on the process.

Inorganic polymers are, according to the above mentioned classification, a subset of AAMs. Inorganic polymers are characterized by the presence of a disordered silicate network as the primary binding phase. To obtain this, a higher degree of silicate connectivity or, in other words, a higher $(SiO_2+Al_2O_3)/(CaO+Na_2O)$ ratio than that of pure Ordinary Portland Cement (OPC), is required.

Geopolymers are a further subset of inorganic polymers where the binding phase (gel) is almost exclusively made of aluminosilicates. To form this type of gel as a primary binding phase, the calcium availability should be usually low in order to enable the formation a pseudo-zeolitic network characterized by a crystalline structure. This does not mean that the Ca content of the material is low, but simply that Ca availability is low (Yip et al., 2003; 2005; 2008).

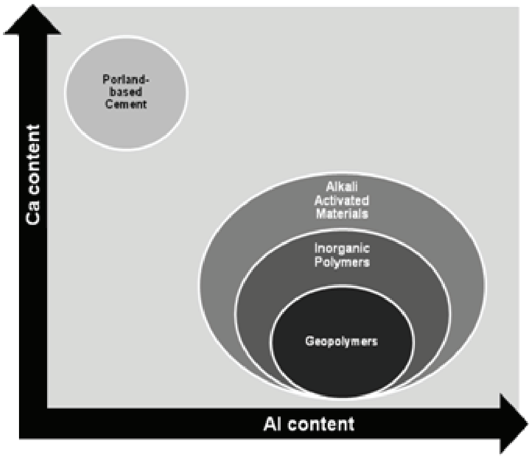

Figure 1: Classification of different subset of AAMs with comparisons to OPC. The gray level in the circles represents the alkali content, the higher content corresponding to darker grey level

References

- ✓ J S.J. van Deventer, J.L. Provis, P. Duxon, D.G. Brice: Chemical Research and Climate Change as Drivers in the Commercial Adoption of Alkali Activated Material; Waste Biomass Valorization (2010) 1: 145-155.
- ✓ U.S. Department of Transportation, Federal Highway Administration: User Guidelines for Waste and Byproduct Materials in Pavement Construction, FHWA-RD-97-148 (1997).
- ✓ P. Duxson, A. Fernandez-Jimenez, J. L. Provis, G.C. Lukey, A. Palomo, J. S. J. van Deventer: Geopolymer technology: the current state of the art; Journal of Material Science (2007) 42: 2917–2933.
- ✓ Freedonia Group (2009) viewed at: http://fredoniagroup.com/WorldCement.html
- ✓ F. Pacheco-Torgal, J. Castro-Gomes, S. Jalali: Alkali-activated binders: A review Part 1. Historical background, terminology, reaction mechanisms and hydration products; Construction and Building Materials (2008) 22: 1305–1314.
- ✓ C.K. Yip and J.S.J. van Deventer: Microanlaysis of calcium silicate hydrate gel formed within a geopolymeric binder; Journal of Material Science (2003) 38: 3851-3860.
- ✓ C.K. Yip, G.C. Lukey, J.S.J. van Deventer: The coesistence of geopolimeric gel and calcium silicate hydrate at the early stage of alkali activation; Cement and Concrete research (2005) 35: 1688-1697.
- ✓ C.K. Yip, G.C. Lukey, J.L. Provis, J.S.J. van Deventer: Effect of calcium silicate sources on geopolymerization; Cement and Concrete research (2008) 38: 554-564
- ✓ K.L. Scrivener and R.J. Kirkpatrick: Innovation in use and research on cementitius material; Cement and Concrete research (2008) 38: 128-136
- ✓ C.Shi, P.V. Krivenko, D. Roy: Alkali-activated cements concretes; Advanced in Cement Research (2006) 18: 179-180

1. State of the art

1.1 State of the art of waste management in the EU and role of incineration

About 30 years ago, the first legislation in the field of environmental policy including waste policy came into force. In the context of increasing awareness of negative environmental and health impacts of anthropogenic activities, the environmental policy established key areas to be covered by legislation. Since then a large number of legal obligations have been set in order to limit or reduce the negative impacts and to protect the environment and human health.

One of the most prominent policy areas in this respect is waste policy, due to the serious environmental and social impacts it may entail. As a consequence, the corresponding European legislation sets standards for the handling, transport, treatment and disposal of waste for the purpose of reducing the negative effects to human health and to the environment. Therefore, Member States shall take appropriate measures for implementation and practical enforcement including the establishment of the necessary administrative and technical infrastructure, permitting, operation procedures, monitoring and effective control.

The Waste Framework Directive 2008/98/EC (former 2006/12/EC) sets the legal framework and basic definitions relevant for waste management. Priority within the European waste hierarchy is given to prevent waste generation. Reuse, recycling and recovery options should be realized whenever suitable in order to reduce the consumption of primary resources and the amount of waste generated. However, a huge amount of waste is currently landfilled.

Concerning the disposal of waste in landfills, the Directive 1999/31/EC on landfilling of waste and the Decision 2003/33/EC on the acceptance criteria set standards for the authorization, design, operation, closure and aftercare of landfills. First, the Landfill Directive (2003/33/EC) had to be applied for new landfills only, and since July 2009 even existing landfills have had to fully comply with the set requirements. Inter alia, landfills have to establish the provisions related to waste characterization and the acceptance of waste in different landfill categories as defined in Annex II to the Landfill Directive. The acceptance criteria and the acceptance process are further specified in Council Decision 2003/33/EC (hereinafter referred to as WAC Decision). This includes a detailed description of waste characterization procedures, limit values for waste composition and leaching behaviour as well as acceptance procedures to be executed at each landfill site. The decision entered into force on 16 July 2004 and the limit values had to be applied in all Member States since 16 July 2005. Member States must ensure that existing landfill sites may not continue to operate unless they comply with the provisions of the Directive as soon as possible (Eurostat, 2009).

The 27 UE Member States according to European directive have developed a national waste strategy according to the each policy and legislation system (Figure 2). For example Italy has not developed a national waste management plan, as the legislation provides the plans are developed at a regional level. However, the National Waste Framework Act gives general criteria for the implementation of regional plans. In particular these criteria are defined in article 199 of the Legislative Decree 152/2006. According to the Directive 1999/31/CE and the European Decision 33/2003 of transposition, Italy has developed a national strategy regarding the reduction of biodegradable municipal waste going to landfills. This strategy identifies some instruments to be implemented in order to achieve the targets. Each region has to establish its own plan for the reduction of biodegradable waste to be landfilled, in order to ensure a suitable management of this kind waste within the regional territory. In accordance to the national framework legislation, regions have developed their own programs in order to achieve an improved waste management within the regional territory. Referring to municipal waste each province has integrated the regional plan defining its own specific plan in order to achieve a proper municipal waste management within the ATO (Eionet, 2009).

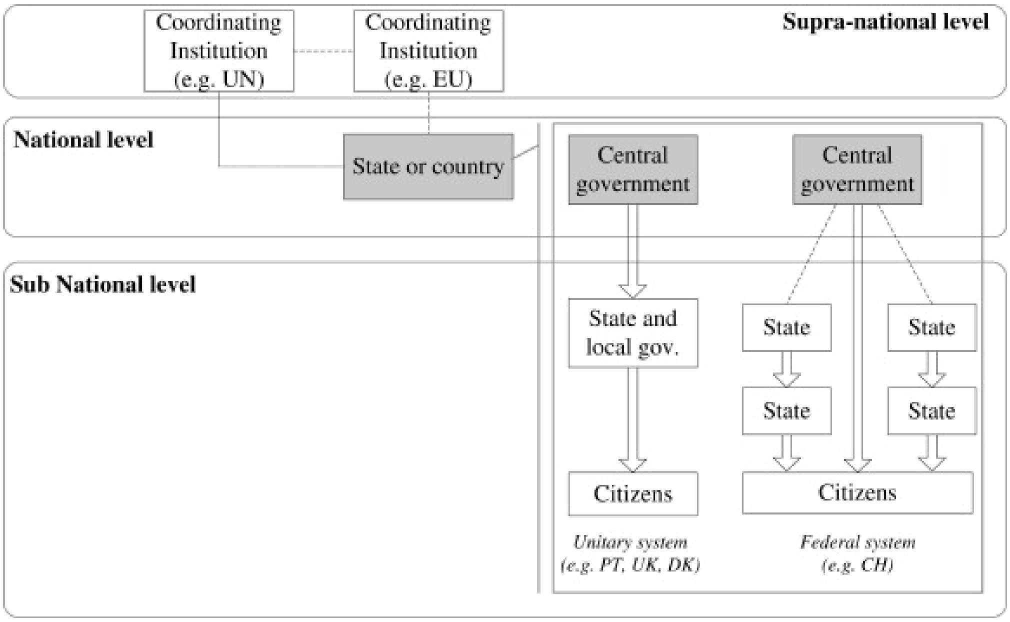

Figure 2: Example of general schematics of policy and legislative system (Costa et al., 2010)

The data about the total amount of wastes produced in the Member States (Figure 3) is very difficult to obtain. Here the data, derived from Eurostat (2009), related to the municipal waste produced without the amount of waste generated from agriculture and industry were presented. The amount of municipal waste generated is about 14% of the total amount of wastes produced. In the 27 Member States 524 kg of municipal waste were generated per person in 2008 (Figure 3) and the amount varies significantly across Member States.

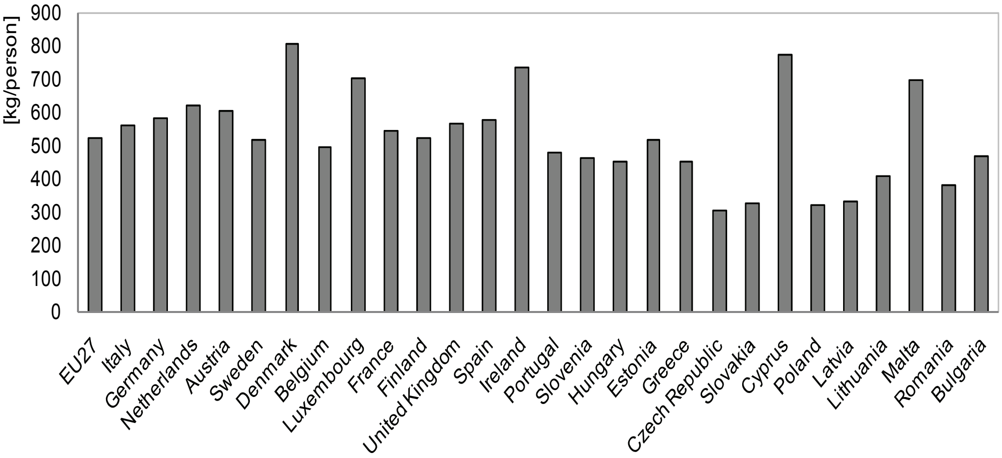

Figure 3: Municipal Waste generated in the Member States in 2008 (Eurostat, 2009)

Between 500 and 600 kg per person of municipal waste were generated in Italy. In terms of treatment methods there are differences between the Members States as shown in Figure 4. A large number of Countries, in particular the new Member States, use landfilling as the main waste management method. Only few countries (Germany, The Netherlands, Austria and some North European States) have significantly reduced the amount of waste landfilled preferring recycling and incineration (Eurostat, 2010). Generally the amount of wastes landfilled in the EU27 countries has decreased from 1997 to 2008 with a more evident trend between 2002 and 2005, as shown in Figure 4 and Figure 5. The same trend has been observed in Italy but only starting from the year 2000 (Figure 5).

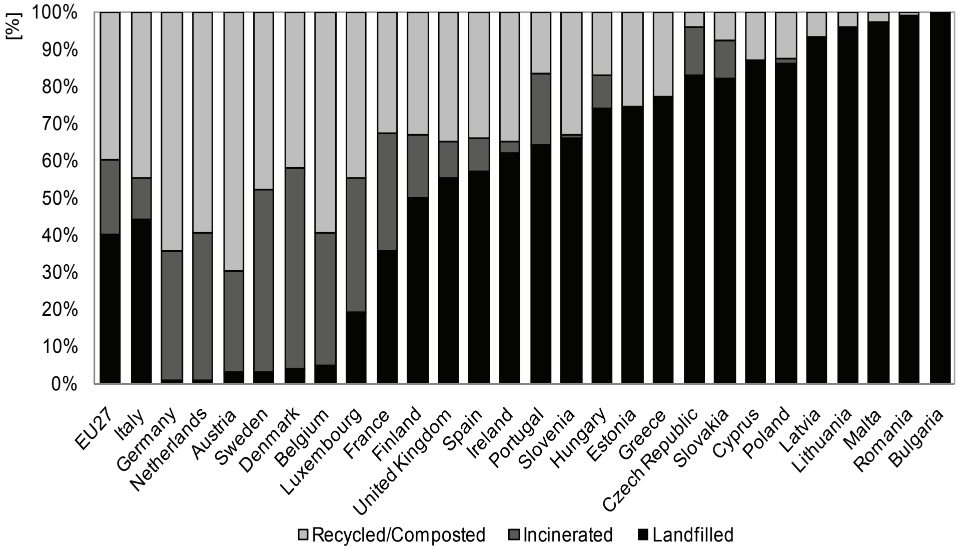

Figure 4: Municipal Waste Treated Methods in UE Member States (Eurostat, 2009)

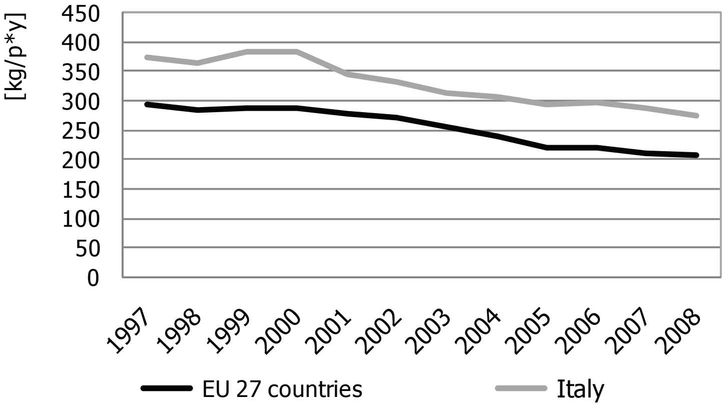

Figure 5: Amount of Municipal Waste Landfilled (Eurostat 2009)

Taking the above figures into account, over the next years an increase in the amount of waste incinerated is expected to occur in order to decrease the volume of waste to final disposal. Therefore, the incineration process, is evolving to reduce its potential environmental impacts, with particular regard to the emissions into the atmosphere. In modern incinerator plants the systems for the reduction of macro- and micro-pollutants in the off-gases are very sophisticated because the regulatory standards for emissions into the atmosphere have been made more and more restrictive. As a result, the contaminants are concentrated in the solid residues of the process which therefore must be managed with particular attention to minimize the environmental impact.

Incinerator residues are of gaseous, liquid and solid nature. In particular, solid residues account for 1/4 of the weight and 1/10 of the volume of the original waste (Sabbas et al., 2003). Typically the solid incinerator residues are classified as listed below and shown in Figure 6 (Lechner et al., 2006; IAWG, 1995; Sabbas et al., 2003):

- bottom ash (BA): generated in the combustion chamber and collected from the quenching unit of this section. The main constituents are inorganic materials and unburned organic fraction. Usually this fraction is collected together with the grate siftings, which comprises the fine fraction of materials with get through the grate in the combustion unit. These fractions together represent about 20-25% by mass of the initial waste;
- heat recovery ash: the material collected at the energy recovery unit. This contains the coarse fraction of solid particulate that is carried over from the combustion section by the off-gases flow and represents about 2-10% by mass of the initial waste;
- fly ash(FA): the fine particulate fraction deriving from the off-gas treatment, before reagent injection, which represents about 1-3% by mass of the initial waste;
- air pollution control residues (APC): the solid particulate deriving from acid gases treatment . These residues can be produced either in a solid, sludge or liquid form depending on whether a dry or a wet treatment system is applied. This residue represents about 2-5% by mass of the initial waste.

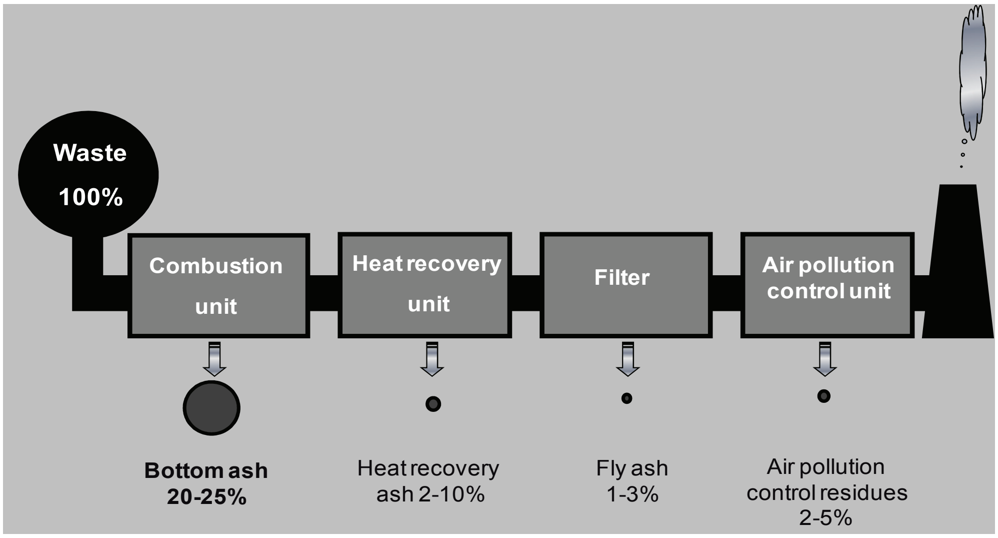

Figure 6: Distribution and classification of solid residues from an incineration plant

Usually a solid residue generated from a municipal solid waste incinerator (MSWI) plant ends up in two ways: disposed in landfill or reused as a secondary raw material (Lam et al., 2010). Taking into account the need to reduce the amount of waste landfilled and to save the consumption of natural resources, the latter way should be pursued as a first priority.

1.2 Bottom Ash from waste incineration

Among waste incineration residues, BAs are those generated in the largest amounts, accounting for more than 90% by mass of the total inventory of solid residues from the process and 15-25% by mass of the original waste, being at the same time the residues with technical properties most suited for utilization.

The minerals present in BA, formed under the high temperatures of the combustion process, are subjected to a fairly rapid cooling down to ambient temperatures during quenching at the exit of the combustion unit (Figure 7). This sudden temperature drop makes most solid phases in BA metastable at ambient temperature and pressure, leading to a series of chemical and mineralogical transformations over time with the production of more stable minerals and mineral assemblages.

Figure 7: quenching unit and storage site

Mineralogical studies on incinerator BA have shown that the fresh material is generally composed of a low-density, impurity-bearing slag or melt phase and a vitreous phase with variable quantities of crystals and glassy material. Silicates (quartz), alumino-silicates of Ca and Na (feldspars, gehlenite, pyroxene, olivine, alite, belite), metal oxides, hydroxides (portlandite), sulphates (anhydrite, gypsum), carbonates (calcite, siderite), as well as metals and alloys are recognized as the most common phases in municipal solid waste incineration (MSWI) BA (Eighmy et al., 1994; IAWG 1995; Clozel-Leloup et al., 1999; Eusden et al., 1999).

1.3 Physical characteristics

BA can include more than 20% wt of materials with sizes larger than 10 cm which are primarily composed of ceramics, glass and metal scrap fragments; this fraction is often separated from the BA for reuse process (IAWG, 1997). Except for the mentioned 10-cm oversize fraction, the size distribution of BA is quite homogeneous. Usually the material covers the size ranges typical of gravel and sand. As an example, Chimenos et al., (1999) found that about 30 % wt of their BA sample was characterized by 6-mm oversize particles, while the remaining 70% wt included 3-mm oversize particles. The finer fraction was found to be suitable for reuse in the construction field. There are also finer particles (size < 0.6 mm) mainly on the surface of coarse particles.

The particle size distribution of BA (Chimenos et al., 2003; Speiser et al., 2000) also affects the morphological, microstructural and chemical characteristics of the material (Figure 8). In the fine fraction (particles size < 2 mm) higher concentrations of heavy metals (Pb, Zn, Cu, Ni, Cd) and Mn- Cr- Ti- Cu- Zn- Al- Mg- Si- based iron metal oxides were detected. Particles with sizes < 0.4 mm were found to contain secondary reaction phases such as ettringite ($Ca_6Al_2(SO_4)_3(OH)_{12}*26H_2O$) and portlandite ($Ca(OH)_2$) (Chimenos et al., 1999; Freyssinet et al., 2002; Piantone et al., 2004). In addition the fine fraction was observed to be richer in sulphates (anhydrite and ettringite), and carbonates (calcite and siderite), while the coarse fraction (16-25 mm) was found to be composed mainly by silicate phases such as quartz, gehlenite, plagioclase, pyroxene, by oxides such as magnetite and hematite, as well as by ceramics materials and glass fragments rich in Na.

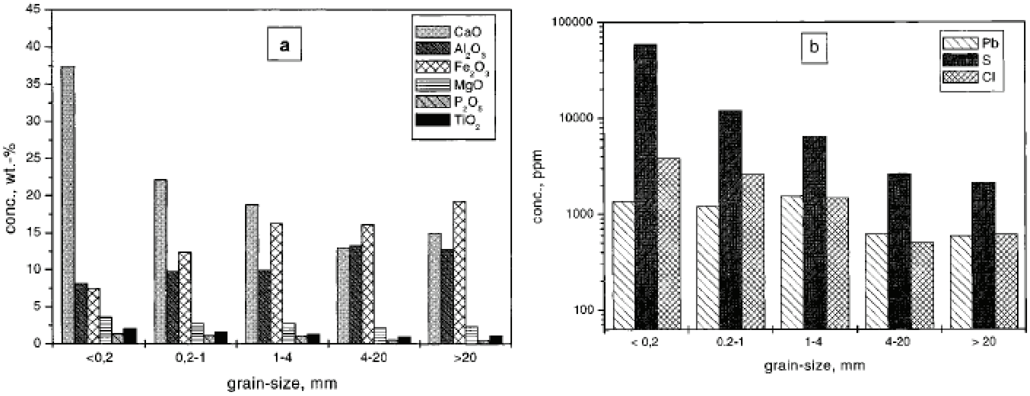

Figure 8: Main oxides (a) and trace elements (b) of BA as a function of particle size

BA is characterised by a high porosity and specific surface of about 50 m^2/g dry weight due to the gas expulsion during the formation process. The humidity is highly variable and values range between 6 and 60% depending on the cooling process in the quenching unit and the transportation method. The more representative range for humidity is around 15-20% wt. The water content could be high enough to reduce the powder emission but not too high to increase the metal leaching during transportation and/or treatment of BA (IAWG, 1997).

The loss on ignition (LOI) of BA gives a rough evaluation of the amount of carbon, hydroxides and hydration phases contained in the material.

In Table 1 the typical ranges observed for LOI and humidity in BA derived from several incineration plants are reported.

Reference	W%	LOI%
Polettini et al., 2004	13.6	3.9
Fernandez Bertos et al., 2004	16.8_21.9*	-
Moller, 2004	12.4_13.5*	-
Polettini et al., 2005	39.3	8
Giampaolo et al., 2002	21.7_39.3*	3.0_8.5*
Izquierdo et al., 2002		2-10**
Qiao et al., 2008 (a & b)		13
Quiao et al., 2009		12.8
Park et al., 2007		6.4
Andrade et al., 2006		2.3
Andrate et al., 2009		4.6
Pan et al., 2008		3.2
Saikia et al., 2007		4.6
Targan et al., 2003		10.2

(*): estimated values for BA derived from different MSWI plants.

(**): range of estimated values for BA derived from different Spanish MSWI plants.

Table 1: humidity (W%) and LOI (%) values in BA

1.4 Chemical characteristics

The composition of incinerator BA is observed to vary over relatively wide ranges, depending on the characteristics of the burned waste, the incineration technology adopted, as well as the operating conditions applied. Both the major and trace constituents may be affected by such factors, in turn influencing different chemical and mineralogical characteristics of the material and the associated environmental behavior.

The pH of BA typically ranges between 9.5 and 12.3 (IAWG, 1997; Meima and Comans, 1999; Fernandez Bertos et al., 2004; Moller, 2004; Rendek et al., 2007) due mainly to the high content of alkaline elements and metal oxides that generate hydroxides (for example, portlandite $Ca(OH)_2$; Johnson et al., 1995) as a result of hydrolysis. The presence of Ca carbonates in the original waste affects the alkalinity of BA: during the combustion process Ca carbonates are decomposed into CO_2 and CaO, the latter being converted to $Ca(OH)_2$ due to hydration during cooling.

The main elements found in BA include Si, Ca, Al, Na, Mg and Fe. The overall content of these elements in the corresponding chemical forms in BA typically accounts for about 80-90% of total weight. The Si content (about 32- 48%) derives mainly from the domestic waste and glass bottles. The Ca content (about 16-23%) derives from paper, alimentary and industrial wastes. The Fe content (6-13%) depends on the presence (and efficiency) of a metal separation process in the incinerator. There are in addition small percentages of sulphate and chlorides. The former is generally present at concentrations of 0.29–0.47% and increases with the increasing of presence of industrial wastes. Chloride accounts for about 0.34-0.84% of the material and is founnd at higher concentrations for higher contents of plastic wastes.

In addition traces of toxic and hazardous elements are found in BA. Table 2 lists the concentrations of the main and trace elements of BA collected from several studies reported as oxides concentration.

Concentration of the oxides (wt.%)									
	Qiao et al., 2008 (a & b)	**Polettini et al., 2009**	**Jurič et al., 2006**	**Kokalj et al., 2005**	**Bertolini et al., 2004**	**Andrade et al., 2007**	**Park et al., 2007**	**Targan et al., 2003**	**Andrade et al., 2009**
SiO_2	36.20	56.99	24.00	24.00	14.71-61.90	50.46	9.78	42.39	56.00
CaO	20.20	13.22	30.00	39.00	13.25-37.32	2.07	11.14	17.57	0.80
Al_2O_3	8.48	9.20	14.80	14.80	6.36-10.72	28.35	20.75	21.35	26.70
Fe_2O_3	6.21	3.97	2.70	2.70	2.6-14.17	10.68	37.10	6.41	5.80
Na_2O	2.93	-	0.90	0.90	1.72-11.34	-	-	-	0.20
SO_3	2.34	-	-	-	1.21-8.49	0.34	-	2.34	0.10
P_2O_5	1.59	0.70	-	-	0.77-1.55	-	2.37	-	-
MgO	1.58	3.46	1.72	1,70	1.99-3.30	-	3.28	1.52	-
K2O	1.04	1.35	0.20	0.20	0.40-6.94	3.81	-	1.11	2.60
TiO_2	0.89	0.49	-	-	0.38-0.85	1.57	-	-	1.30
ZnO	0.37	-	-	-	-	0.03	1.80	-	-
CuO	0.30	-	-	-	-	-	1.85	-	-
PbO	0.24	-		-	-	-	1.65	-	-
MnO	-	0.08	-	-	0.05-0.16	0.07	-	-	-
ZrO	-	-	-	-	-	0.18	-	-	-
V_2O_5	-	-	--	-	-	0.09	-	-	-
Cr_2O_3	-	-		-	-	-	0.78	-	-
NiO	-	-	-	-	-	-	-	-	-
	Jing et al., 2007	**Pan et al., 2008**	**Andreola et al., 2008**	**Gines et al., 2009**	**Kayabali et al., 2000**	**Naganathan et al., 2009**	**Polettini et al., 2005**		
SiO_2	44.00	13.44	46.7	49.38	15.1-57.9	43.85	41.13		
CaO	21.10	50.39	26.3	14.68	2-23.7	4.14	3.85		
Al_2O_3	11.30	1.26	6.86	6.58	7.5-27.8	8.37	11.35		
Fe_2O_3	7.00	8.84	4.69	8.38	3.3-20.3	11.91	6.77		
Na_2O	8.20	12.66	4.62	7.78	0.08-9.9	2.73	2.84		
SO_3	-	1.79	2.18	0.57	traces-13.2	-	-		
P_2O_5	-	3.19	0.85	-	-	1.73	1.84		
MgO	4.20	2.26	2.22	0.32	0.92-4.5	0.79	3.85		
K2O	2.60	1.78	0.89	1.41	0.60-1.14	0.71	1.57		
TiO_2	-	2.36	0.77	-	Traces-1.03	2.71	1.23		
ZnO	-	2.60	-	-	-	-	-		
CuO	-	1.51	-	-	-	-	-		

PbO	-	2.11	-	-	-	-	-
MnO	-	-	-	-	-	0.12	0.11
ZrO	-	-	-	-	-	-	-
V_2O_5	-	-	-	-	-	-	-
Cr_2O_3	-	0.18	-	-	-	-	-
NiO	-	0.16	-	-	-	-	-

Table 2: Observed concentrations of main and trace elements in BA

Even if BA includes only about 1-3% of grate siftings, these residues are the main contributor to the Pb, Al, Cu and Zn concentrations in BA.

The concentrations of PCDDs and PCDFs, polycyclic aromatic hydrocarbons, chlorophenols and cholobenzene are usually lower than 2 ng/g of waste.

1.5 Mineralogical Characteristics

The BA particles can be classified in two major groups: non combusted waste products (15%) from the municipal solid waste feed and melt products (85%) (Dykstra Eudsen et al., 1999). The former include waste minerals (2%), waste glasses (10%), waste metals (2%) and waste organics (1%). The latter include: opaque and metallic glass, schlieren and spinel-group minerals (magnetite, Fe3O4, chromite, FeCr2O4) and melilite-group minerals (gehlenite, Ca2Al2SiO7, akermanite, Ca2(Mg,Fe2+)Si2O7). The melt products are similar to those found in volcanic ashes both for morphology and chemical composition, and present vesicles for about 15-25% of the total volume of the particles providing for a significant measure of particle porosity (Dykstra Eudsen et al., 1999). The main minerals present in BA matrix are listed in Table 3.

	Component
non combusted waste products	Quartz (SiO_2) Feldspars ($(K,Ca,Na)(Al,Si)_4O_8$) Biotite ($K(Mg,Fe)_3AlSi_3O_{10}O_{22}(OH)_2$) Olivine ($(Mg,Fe)_2(SiO_4)$ Pyroxene ($Ca(Mg,Fe)Si_2O_6$)
melt products	Mulilite group (ghelenite ($Ca_2Al_2SiO_7$),akermanite ($Ca_2(Mg,Fe^{2+})Si_2O_7$) Magnetite ($Fe^{2+}(Fe^{3+})_2O_4$), Hematite (Fe_2O_3) Plagioclase feldspar ($(K,Ca,Na)(Al,Si)_4O_8$) Wollastonite ($CaSiO_3$) Chromite ($Fe^{2+}Cr_2O_4$) Ca oxide (CaO)

Table 3: Main mineral phases in BA (Dykstra Eudsen et al., 1999)

Other minerals have also been detected in BA (Kirby and Rimstidt, 1993; IAWG, 1995; Dykstra Eudsen et al. 1999; Speiser et al., 2000), including:

- sulphate-based minerals such as anhydrite ($CaSO_4$), ettringite ($Ca_6Al_2(SO_4)_3(OH)_{12}*26H_2O$) and gypsum ($CaSO_4*2H_2O$) (about 5%);
- carbonate-based minerals such as calcite ($CaCO_3$), accounting for about 20% of BA mass and deriving from reaction between $Ca(OH)_2$ and CO_2. Metal carbonates of Fe, Zn and Cu- have also been detected in BA;
- small percentages of chlorides such as NaCl and $CaCl_2$.

Traditionally incinerator BA has been considered as an inert material. Numerous studies have been conducted in order to use BA as an aggregate substitute in asphalt mixtures and more generally in the field of road construction. A dramatic reduction in heavy metal leaching was observed in such applications (Chen et al., 2008; Pecqueur et al., 2001; Vagas et al., 2008).

However, taking into account the modes of formation of BA and the resulting content of reactive and unstable phases, BA should rather be considered as a reactive material. Among the different treatments applied to promote the reuse and recycling of BA, a novel approach involves taking advantage from the presence of reactive compounds to improve the material's properties for utilization. This approach stems from the consideration that incinerator BA is typically composed of amorphous and vitreous phases, the most abundant constituents being Ca, Si and Al minerals, which are also major components of common pozzolanic materials.

Some researchers have investigated different processing methods to improve the mechanical properties of BA for use in engineering applications, which are based on preliminary activation of the material by means of different, often combined, methods: mechanical activation relies on intensive milling of the material to increase the surface area available for reaction; chemical activation is based on the addition of chemical agents capable of breaking down the structure of alumino-silicate minerals, releasing silicate and aluminate ions which can thereafter be transformed into mechanically resistant phases (e.g., in blends with hydraulic binders such as cement and lime, or in geopolymer products); thermal activation involves a moderate-to-high temperature treatment to allow for mineralogical rearrangement of the solid matrix, producing (depending on treatment temperature) either a zeolitized or a predominantly glassy material, the latter being more reactive in alkaline environments, and at the same time immobilizing trace contaminants within the treated material.

The regulatory framework for BA utilization is quite constraining in Italy; for this reason only about 20% of this residue is used as a raw material in cement kilns or as a daily cover layer in landfills, while about 80 % is landfilled (Baun et al., 2007). As observed by many authors (Freyssinet et al., 2002; Meima and Comans, 1997; 1999; 2002; Sabbas et al., 2003; Polettini et al., 2004), the main critical aspect to be taken into account for reuse is the leaching behavior of the material. Other detrimental effects related to the chemical reactivity of BA involve hydrogen gas production, hydration of Ca and Mg oxides with ettringite formation, with associated expansion and cracking phenomena (Pera et al., 1997; Pecqueur et al., 2001; Sabbas et al., 2003; Ginés et al., 2009) in case of blending with cement materials.

1.6 Recycling of incinerator BA for the formulation of blended cements.

An intensive research is particularly focused on the usability of residues as engineering materials (Kayabali et al., 2000). In particular, a large number of these was aimed at improving the reactivity of coal fly ash (Ma et al., 1994; Sekulić et al., 1998; Kumar et al., 2007; Lam et al., 2000; Arjunan et al., 2001; Lee et al., 2007; Poon et al., 2004; Shi et al., 1995) and industrial slag (Wang et al., 1995; Malolepszy et al., 1994; Donatello et al., 2010; Shi et al., 1999), using mechanical, chemical or thermal activation or a combination of these three methods.

The use of alkaline activators to stimulate the latent pozzolanic properties of different types of residues was studied since 1940's with Purdon's work. He used blast furnace slag as the raw material and sodium hydroxide as the alkali activator. It should however be noted that alkali activation to improve the natural pozzolanic properties of various materials was applied also since times dating back to the Babylonian, Roman and Egyptian period (Roy, 1999; Pacheco-Torgal et al., 2008). The use of appropriate chemical activators - as suggested by a number of investigators for materials of different origin (Poon et al., 2003; 2004; Giergiczny, 2004; Fan et al., 1999; Qiao et al., 2001; Shi et al., 1995; 2000; 2001) - combined with thermal and mechanical activation of different residues, including incinerator BA, was found to promote the development of mechanical strength in Portland cement mixtures (Polettini et al., 2005; 2009; Qiao et al., 2008; 2009).

In Table 4 some of the recent studies conducted to improve the reactivity of different residues using chemical activators are summarized. Among the different alkali activators, the more tested are those based on Ca, Na, and K.

Type of residue	Chemical Activator type	Reference
FA	Na_2SO_4	Lorenzo et al., 2002
BA	Na_2SiO_3, NAOH, KOH, $CaCl_2$, Na_2SO_4,$CaNO_3$	Polettini et al., 2004; 2009
FA	$CaCl_2$, $CaSO_4$, $Ca(OH)_2$	Giergiczny, 2004
FA/BA	NaOH	Arjunan et al., 2001
FA	Na_2SiO_3,$Ca(OH)_2$	Fan et al., 1998
FA	Na_2SO_4, K_2SO_4, triethanolamine	Lee et al., 2002
wastePb	$CaCl_2$	Cheeseman & Asavapisit, 1999
FA	Na_2SO_4, K_2SO_4,$CaCl_2$,$Ca(OH)_2$	Poon et al., 2003
FA,FGD	Na_2SO_4, K_2SO_4,$CaCl_2$,$Ca(OH)_2$, NaOH, KOH	Poon et al., 2004
BA	Ca(OH)2	Qiao et al., 2007 ,2008
BA	Na_2SO_4, K_2SO_4,Na_2CO_3, K_2CO_3, NaOH, KOH,$CaCl_2$, $Ca(OH)_2$	Qiao et al., 2009
FA	Na_2SO_4, NaCl,$CaCl_2$, $Ca(OH)_2$	Shi & Day, 1994
FA	Na_2SO_4, $CaCl_2$, $Ca(OH)_2$	Shi, 1996
Waste mud	Na_2SO_4 $Ca(OH)_2CaCl_2$	Shi et al., 1999
FA,SLAG	Na_2SO_4	Jueshi et al., 2000
BFS	$CaCO_3$, $Ca(OH)_2$, $CaCl_2$, NaCl, $CaBr_2$	Bellan & Stark, 2009
GBS FA	Na_2SiO_3	Zhang et al., 2007

FA: Fly Ash
BA: Bottom Ash
FGD: Flue Gas Desulphurization
wastePb: synthetic 10M NaOH+1M $Pb(NO_3)_2$ exsiccate a 105°C
BFS: Blast furnace slag
GBS: granulated Blast furnace slag

Table 4: Main chemical activators user to improve pozzolanic reactions of reactivity for different residues

Over the last years, the studies on BA activation in blended cements have largely increased (Qiao et al., 2008 (a); 2008 (b); 2007; 2009; Jurić et al., 2006; Rechberger 2001; Andrade et al., 2009; Pan et al., 2008; Jing at al., 2007; Chen et al., 2008). The literature on the utilization of BA is not as plentiful, however, as it is for other types of industrial residues investigated for similar application.

Some evidence was gained of the capability of BA to exhibit pozzolanic properties in cement-based systems (Polettini et al., 2005; 2009; Qiao et al., 2008 (a); 2009) suggesting potential useful applications for blended cement formulation.

Generally, the main positive effect observed when using alkaline activation of industrial ashes in cement-based systems can be summarised as:

- ✓ decrease in volume and amount of pores due to the presence of sulphate and sodium into the microstructure of the material (Lorenzo et al., 2002; Lee et al., 2003);
- ✓ acceleration of the early hydration stage and improvement in mechanical strength (Shi et al., 1995; 1999; Arjunan, 2001; Jueshi et al., 2001; Zhang et al., 2007; Cheeseman and Asavapisit 1999; Lee et al., 2003; Poon et al., 2003; Poon et al., 2004).

All these aspects have been observed as being largely affected by both the starting material and the activator type. The engineering application of blended cement with a partial substitution of treated BA or residues has still some limitations underlined by different studies (Roy, 1999; Rechberger, 2001):

- √ absence of specific standards or guidelines for application;
- √ absence of databases: it is necessary to collect data in order to allow for prediction of the performance of these materials. This aspect is particularly significant taking into account the large variability of the starting materials;
- √ need to learn more about the reaction mechanisms in order to better define the activation effectiveness of different types of alkaline compounds used. It is also important, for prediction of long-term durability and environmental behavior, to more fully characterize the hydration process occurring, specifically in terms of type and strength of hydration products, presence of residual soluble species in the pore solution, and mobility and leaching of inorganic contaminants.

1.7 Geopolymers

In the present work, we intend to gain insights into the feasibility of production of geopolymeric materials from incinerator BA, considering that the material is known to be composed of amorphous and vitreous phases, the most abundant constituents being Ca-, Si- and Al-containing minerals. While other kinds of inorganic industrial wastes as: coal/lignite fly ash (Andini et al., 2007; Chindaprasirt et al., 2006; 2009; Kumar et al., 2011; Panias et al., 2007; Škvára et al., 2009; Temuujin 2009; 2010; van Jaarsveld et al., 2002), biomass ash (Songpiriyakij et al., 2009), coal bottom ash (Chindaprasirt et al., 2009; Xu et al., 2010), blast furnace slag (Cheng et al., 2003; Oh et al., 2010), air pollution control ash from waste incineration (Kourti et al., 2010) and wastewater sludge (Lampris et al., 2009) have been investigated in previous studies for similar applications, to the authors' knowledge no specific study on geopolymer production from incinerator BA has been conducted so far.

1.7.1 History

Geopolymers, also referred to as inorganic polymers, are alumino-silicate materials having the potential of being used in a number of applications, e.g. as structural and non-structural materials, concrete products, reagents for waste and wastewater treatment, structural ceramics, fire resistant composites, etc.

A precursor of geopolymer materials was first developed in the Ukraine in the mid 1950s by Glukhovsky. This researcher in 1930 began investigating the materials used by ancient Romans and Egyptians to build their structures and hypothesized that the superior durability of this ancient concretes resulted from the coexistence of cements containing calcium silicate hydrate (C-S-H) with some form of alkaline aluminosilicate hydrates. Taking these observations into account, he developed a kind of binder named "soil cement" using aluminosilicate wastes such as industrial slag, coal fly ash and other wastes, mixed with alkaline industrial waste solutions (Shi et al., 2006; van Deventer et al., 2010). The research on these materials in Ukraine dramatically increased afterwards and from the 1960s the materials were used for structural applications with a consequent production of a large number of standards and patents. All this research, developed in the last 30 years in the Soviet union, Ukraine, Scandinavia and Eastern Europe remained almost unknown in the Western European and American countries (Pacheco-Torgal et al. 2008 (a); van Deventer et al., 2010).

In Europe and in the rest of the world the research had an exponential increment when the results of Davdovits studies were published. Davidovits in 1972 and onwards began the research on geopolymers starting from observation of inorganic polymers and from a research about new heat resistant materials in the form of non-flammable and non-combustible "plastic materials". He was the first that examined the geopolymer chemistry and coined the term "geopolymers" in 1978 after the development of a patent of a binder obtained from alkali activation of metakaolin (Davidovits, 1994; Kriven et al., 2003; Pacheco-Torgal et al., 2008 (b)). The new theory on the structure of geopolymeric materials was based on the study of inorganic polymer technologies and understanding of zeolite synthesis and chemistry. The name was chosen starting from the observation that the production of the geopolymers is similar to that of synthetic zeolites and a number of tectoaluminosilicate minerals and that inorganic polymeric materials can be considered to be the amorphous equivalent of geological feldspars, but synthesized in a similar manner to that used for thermosetting the organic polymers. Taking this into account, the term "geopolymer" was coined recognizing that this material is an inorganic polymer analogous to conventional organic polymers (Hos et al., 2002). As reported, geopolymers can be seen as analogue amorphous of synthetic zeolites: the chemistry involved is similar, although the resulting products are different in composition and structure (Davidovits, 1991; van Jaarsveld et al., 1997; 1998). Geopolymeric products, however, do not have stoichiometric composition and comprise mixtures of amorphous to semi-crystalline structures and crystalline Al–Si particles as through nano-crystalline zeolites are dispersed in an alumino-silicate gel. During geopolymerisation, when the alumino-silicate powder is mixed with the alkaline solution, a paste forms which quickly transforms into a hard geopolymer, and there is no sufficient time and space for the gel or paste to grow into a well-crystallised structure; this is the main difference between zeolites and geopolymers (Xu et al., 2000; Komnitsas et al., 2007). The geopolymerisation process involves leaching, diffusion, condensation and hardening steps, while zeolite synthesis is due to prenucleation, nucleation and crystal growth but the factors affecting the synthesis of zeolites also affect geopolymerisation and include: temperature, pH, cations concentration, water/solid ratio, curing time and Al_2O_3/SiO_2 ratio in the mix (Komnisas et al., 2007; Khale et al., 2007). As reported by Davidovits in 1991, the temperature required to produce geopolymers is lower than that necessary to zeolite synthesis.

Nowadays, the abundance of names describing these materials, including alkali-bounded ceramics, hydroceramics and alkali-activated cements, maybe misleading however, in all cases alkali activation is essentially involved (Davidovits, 2005). Probably, a more appropriate broad term that describes the produced materials is ‘‘inorganic polymers’’ (Duxon et al., 2007).

1.7.2 Chemistry aspects

Geopolymers are characterized by silicon and aluminium thetraedral structures linked together by oxygen atoms. To describe the three-dimensional geopolymeric structures, a new terminology was proposed by Davidovits during an IUPAC Symposium in 1976. The geopolymer structures includes three classes of inorganic polymers that, depending on the silica/alumina ratio, are based on three different monomeric units followed descibed (Figure 9) (Van Jaaesveld et al., 1997, Davidovits, 1991):

1) Poly(sialate) (PS) with [-Si-O-Al-O-] as the repeating unit, with $SiO_2/Al_2O_3 = 2$;

2) Poly(sialate-siloxo) (PSS) with [-Si-O-Al-O-Si-O-] as the repeating unit, with $SiO_2/ Al_2O_3 = 4$;

3) Poly(sialatedisiloxo) (PSDS) with [-Si-O-Al-O-Si-O-Si-O-] as the repeating unit, with $SiO2/Al_2O_3 = 6$ as repeating unit.

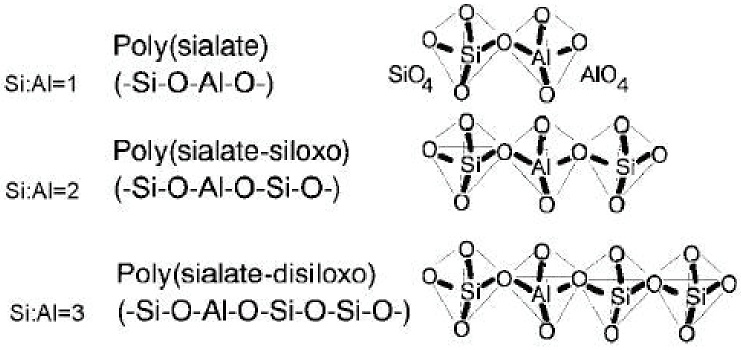

Figure 9 Types of polysialate units

Sialate is an abbreviation for silicon-oxo-aluminate. The sialate network consists of SiO_4 and AlO_4 thetraedra linked alternately by sharing all the oxygens. Positive ions (Na^+, Ca^{++}, K^+…) must be present in the framework cavities to balance the negative charge of Al_3^+ in IV-fold coordination. Poly-sialates have this empirical formula:

$$Mn[–(SiO_2)_z–AlO_2]n•wH_2O$$

Where M is a cation such as potassium, sodium or calcium, n is the degree of polymerization and z is 1, 2 or 3 depending on the type of sialate structure formed . Poly-sialates are chain- and ring-polymers with Si_4^+ and Al_3^+ in IV-fold coordination with oxygen and range from amorphous to semi-crytalline.

For the synthesis of geopolymers three main components are required: raw material, inactive filler and geopolymer liquor (see Figure 10) (Komnitsas et al., 2007):

- raw materials include natural alumino-silicate materials or aluminosilicate wastes such as industrial slag, coal ashes and others. The main role in the geopolymerzation process is to provide the source of Si and Al ions. Although geopolymers are traditionally produced through alkali activation of naturally occurring alumino-silicates, the results of several studies published in the last ten years have shown that industrial residues with high silicon and aluminium contents may be considered as suitable source materials for the production of inorganic polymers;
- the inactive filler is added to increase the amount of Al_3^+ ions. One of the most utilized inactive filler is kaolin or metakaolin (obtained from kaolin calcinations). This filler is required when the Al dissolution rate of the raw material is not sufficient to promote the production of the geopolymer gel. The inactive filler reduces the reactivity of the mixture by increasing the reaction time between the

raw material and the alkali activator, promoting the gel formation and than improving mechanical strength and decreasing the porosity and permeability of the resulting geopolymer;

- the geopolymer liquor is an alkali solution obtained by mixing an alkali metal hydroxide solution with a sodium silicate solution named waterglass. The geopolymer liquor is required to dissolve the raw materials and it plays also the additional role of activator, binder, dispersant and plasticiser.

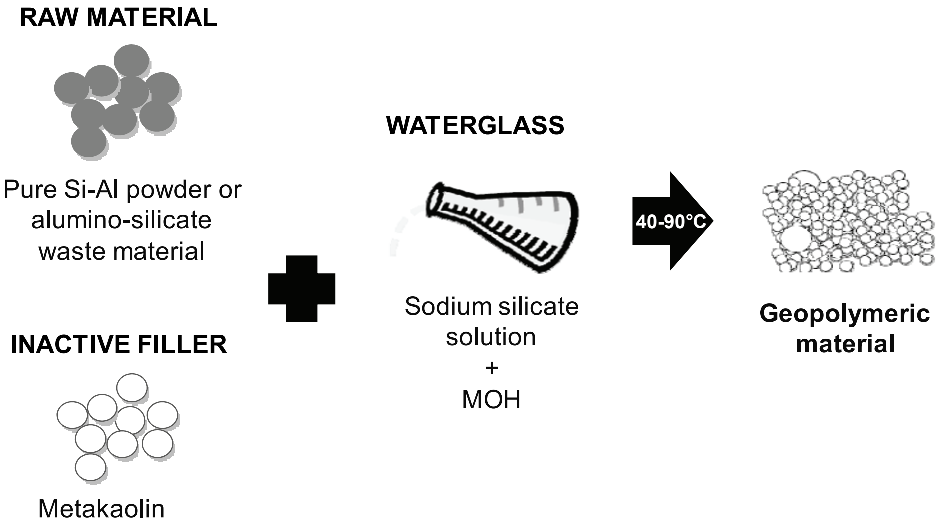

Figure 10: Main components used to produce geopolymeric materials

1.7.3 Geopolymerization process

Geopolymerisation is an exothermic process that include the geosyntetic reaction of alumino-silicate minerals in the presence of an alkali solution at low temperatures (25-80°C); adoption of elevated pressures is not essential and is applied only than lower than the normal porosities of the final product are required (van Jaarsveld et al., 1997; 1998; Davidovits, 1991). The series of geochemical reactions involved is complex and the exact mechanism by which geopolymer setting and hardening occurs is not completely known because the reactions are almost impossible to isolate for individual study (Provis et al., 2009). However, according to a large numbers of the authors, the main steps of the process involve (van Jaarsveld et al., 1997; 1998; Phair et al., 2003; Xu and Van Deventer, 2000; Duxon et al., 2007; Komnitsas et al., 2007):

1) dissolution of solid alumino-silicate structures in the MOH solution with formation of mobile precursor through the complexing action of hydroxide ions;

2) diffusion and transport of the dissolved Al and Si complexes from the particle surface to the among particle space;
3) polycondensation and structural re-organisation with the formation of a gel phase resulting from polymerization between the added silicate solution and Si and Al complexes and reprecipitation where the whole system hardens into an inorganic polymeric structure.

In general alumino-silicate materials react with the MOH solution and the water glass and form a gel layer on the particle surface. The gel grow away from the particle surface and move into the interstitial space between the particles, as a consequence precipitation of the gel followed by the dissolution of new solids from particles occur. When the gel hardens the particles are bound together by the gel (Xu et al., 2000).

A schematic description of the main phases and reactions associated with the geopolymerization process are reported in Figure 11.

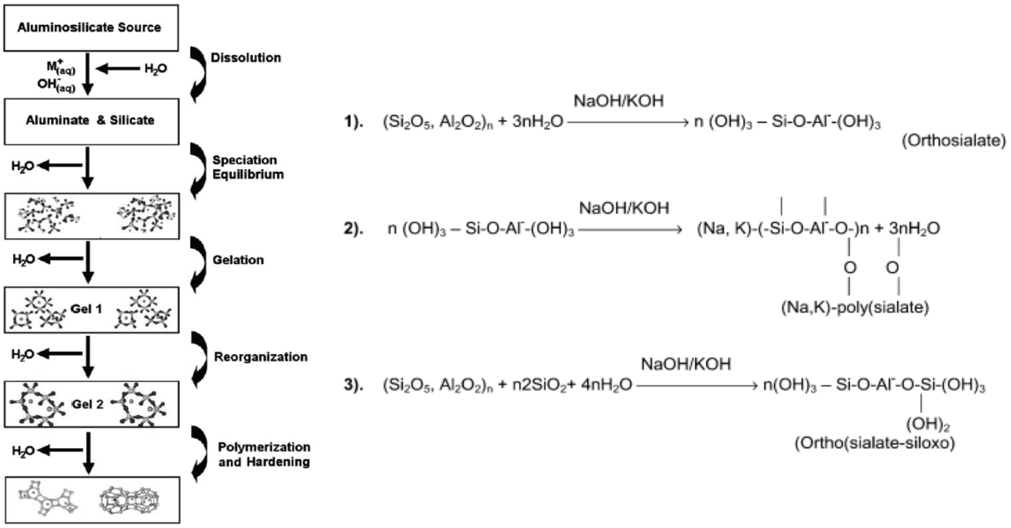

Figure 11: Main steps and reaction associated in a geopolymerization process

During the first step the raw materials dissolution proceeds like in the zeolitization process. The extent of Al and Si dissolution depends from the particle size, the original content of these elements in the materials and the concentration of the alkali solution used. The most important differences between the zeolite formation process and geopolimerization are mainly placed in this step. Zeolites are formed in a more dilute aqueous solution than geopolymers (Khale et al., 2007). Taking this into account, it is possible to observe that the precursors concentration are different for the two process and their mobility too. In particular, lower precursor concentrations and higher mobility make the zeolite structure crystalline because is allowed enough time to undergo proper orientation before bonding into the crystalline structure. Taking this into account, according to several authors (van Jaarsveld et al., 1998; van Jaarsveld et al., 2002) for both processes the H_2O/SiO_2 molar ratio was found to play an important role during both dissolution and polycondensation of zeolite and geopolymer precursor species and therefore deserves attention to evaluate the effect on the final geopolymer properties.

In addition, to perform a good geopolymerization process compositional criteria is also critical. In particular, the following optimal conditions have been determined (Davidovits et al., 1994):

- SiO_2/M_2O molar ratio in the alkaline solution = 4 - 6.6;
- SiO_2/Al_2O_3: molar ratio = 5.5 - 6.5;
- The main part of Aluminium must be in soluble form.

Many authors have demonstrated that such ranges, which were determined for kaolin as the raw material, are only indicative when different raw materials such as industrial waste are used. The surface reaction on waste particles depend on numerous issues like mineralogy, silica and alumina content, fineness, reactive surface area and morphology, all these characteristics being involved in the synthesis reaction. The aluminum contained in most waste materials is in much too stable forms (e.g. mullite) to be dissolved by alkaline solutions, which often requires the Al content to be adjusted to attain suitable values for geopolymerization (van Jaarsveld et al., 1997; 1998; Xu et al., 2000).

Usually, as the secondary source of soluble aluminum either kaolin or its dehydroxylated form metakaolin (which also contains soluble silica) are used.

The main difference between kaolin and metakaolin is that in the latter the octahedral sheer containing aluminium atoms is broken down, forcing aluminum into a tetrahedral coordination (van Jaarsveld et al., 1998; Feng et al., 2004; Khale et al., 2007). An excess in metakaolin dosage negatively affects the mechanical characteristics because of the presence of unreacted metakaolin particles; mixture workability can also be affected due to water absorption and retention (van Jaarsveld et al., 2002).

In the first step the alkali metal salt or hydroxide plays a key role related to a catalytic function promoting raw material dissolution and also governing the condensation reactions. The initial dissolution process is promoted by the presence of OH^- ions and is thought to be independent of the type or concentration of cations (step 3); at the same time if the alkali concentration is too large, the connectivity of silicate anions may be reduced thus resulting in poor polymerisation (Komnitsas et al., 2007; van Jaarsveld et al., 1998; 1999). As alkali elements, theoretically, any alkali and alkali earth cation can be used (Komnitsas et al., 2007). However, the type of metal cation used during geopolymer synthesis affects most of the physical and chemical properties of the final product; the formation of different zeolites is also largely documented by different authors depending on the alkali cation used during geopolymer synthesis. Among the metal cations that can be used in the geopolymerization process the most common are Na^+ and K^+ and to a lower extent Ca^{2+}. In the geopolimerization process metal cations play a charge balancing role of Al^{3+} in IV-fold coordination as already said. In general the optimal polymer properties are obtained when the alkali cation concentration is sufficient to provide the charge balance for the substitution of thetrahedral Si by Al; therefore, the presence of the cation also affect the SiO_2/Al_2O_3 ratio of the products (van Jaarsveld et al., 1999; Komnitsas et al., 2007). The role of the ratio between alkaline hydroxide and waterglass is particularly relevant on mechanical strength of the products, probably because an excess in waterglass (sodium silicate) hinders water evaporation and structure formation (Khale et al., 2007); on the other hand, an excess of the alkaline hydroxide, slowing the hydration rate, reduces mechanical strength and produces an undesirable morphology and an inhomogeneity of hydration products in the paste (Khale et al.2007). For as much as the water content also plays a key role in geopolymer formation as mentioned by various authors (Van Jaarsveld et al., 2002; Khale et al., 2007; Panias et al., 2006; Perera et al., 2007; Zuhua et al., 2009; Panias et al., 2007) and determines the solid to liquid (S/L) ratio of the starting materials in the geopolymeric matrices. Water takes part in different process steps: dissolution and hydrolysis, as well as polycondensation reactions. Providing OH^- ions, the water content acts as a medium for the dissolution of aluminosilicates and facilitates the transfer of various ions, the hydrolysis of Al^{3+} and Si^{4+} and polycondensation of different aluminate- and silicate-hydroxyl species (Zuhua et al., 2009). Generally in a geopolymeric mixture, as the water content decreases, the MOH concentration in the aqueous phase increases substantially and consequently an acceleration in the Si and Al dissolution reactions is observed promoting the start of the geopolymerization process. Additionally, the increase in the Si and Al concentrations in the aqueous phase, due to the dissolution of raw material, enhances the process of Si and/or Si–Al oligomers formation and consequently, polycondensation of oligomers and hardening of the geopolymer (Panias et al., 2007). As a result, the water content has a key effect on geopolymer formation, gel structure and final product properties. As a result, when water/solid ratio increases, mechanical strength decreases drastically as also observed for cementitious materials (Zuhua et al., 2009; Khale et al., 2007).

Another key factor that can affect the properties of geopolymers is the calcium content (Xu et al., 2000; Komnitsas et al., 2007). Nevertheless its role during the geopolymerization process at the moment is unclear (Yip et al. 2007). In general, the presence of calcium gives a positive effect on the mechanical properties of geopolymers due to the formation of a small amount of calcium silicate hydrate C-S-H in addition to the amorphous geopolymeric gel. The major difference between the C-S-H gel and the geopolymeric gel in terms of their elemental composition is the calcium content (Yip et al., 2003; 2005; 2007; Khale et al., 2007).

The nature of the end products obtained upon alkali activation of an alumino silicate source containing calcium depends on various factors such as: elemental composition, mineralogy, particle size distribution, surface properties, curing conditions and type of alkali metal cation used.

In particular some studies (Yip et al., 2005; 2007) demonstrated that only in some cases does the coexistence of the geopolymer gel and C-S-H occurs and this depends on the level of alkalinity (concentration of MOH in the solution) and also on the ratio between the amount of aluminum, silicon and calcium of the matrix. The chemical mechanisms responsible for the formation of these products were proposed by Yip (Yip et al., 2003; 2005; 2008). The dissolution of silicon, calcium and aluminum from the raw material depends on the alkali concentration (the different elements have a different dissolution rate which depends on the alkalinity); the concentration of each elements in the solution determines the subsequent reactions including polymerization and other precipitation processes. It can be observed two main cases:

- at high concentration of MOH in the aqueous solution, the raw materials will be saturated with hydroxyl ions. Only a small amount of calcium will be dissolved from the particles surface of raw material and diffuse into the solution. Here the calcium dissolved will react with the OH^- groups to precipitate as $Ca(OH)_2$. When the quantity of this precipitate will be too match, the dissolution and diffusion of calcium from raw material will be more difficult due also to the presence of OH^- thick layer. In this situation the small amount of dissolved calcium from particles remains within the particles and forms a new nucleation seed in which amorphous C-S-H can be produced only as a secondary product. The lack of dissolved calcium inhibits the formation of C-S-H;

- at low MOH concentrations, the OH^- layer is slim and a certain quantity of calcium will be able to be dissolved and diffused out. When the amount of calcium is sufficient and the respective amount of silicon and aluminium dissolved is not enough to promote the geopolymer gel formation, the formation of C-S-H will be favoured since the $Ca(OH)_2$ concentration won't be as high to reduce the available space for C-S-H nucleation. The results, in this case, will be the simultaneous formation of C-S-H and calcium silicate aluminate hydrate (CSAH) (Yip et al., 2003; 2008; Temuujin et al., 2009).

1.7.4 Applications

It may be interesting to compare the engineering characteristics of geopolymers whit those of ordinary cement (Khale et al., 2007). First of all geopolymer production is associated with lower CO_2 emissions and production cost: the production of geopolymer concrete, without considering the activator, may be from 10 to 30% cheaper than that of Portland cement concrete (Komnitsas et al., 2007). Further positive characteristics of gepolymers include high early strength and fast setting (generally geopolymers attain 70% of the final compressive strength within the first 4 hours of setting), long-term durability, low shrinkage and permeability, freeze-thaw resistance, sulphate resistance, corrosion resistance, acid resistance (unlike the Portland cement, geopolymer cements do not rely on lime and are not dissolved by acidic solutions), fire resistance (the compressive strength of Portland cement decreases dramatically above 300°C, whereas geopolymer cements are stable up to 600°C) and no dangerous alkali-aggregate reactions (Khale et al., 2007; Whalla et al., 2006; Davidovits, 1994; van Jaarsveld et al., 1997; 1999 (a & b)). Geopolymer material are suitable to several practical industrial applications such as automobile and aerospace, non-ferrous foundries and metallurgy, civil engineering and plastics industries. In particular one of the main potential fields of application of geopolymeric materials is in toxic waste management because geopolymers have similar behaviour to zeolitic materials that have a known ability to absorb toxic chemicals from wastes (Whalla et al., 2006). In particular, based on the application field, a number of suitable applications may be indentified (van Jaarsveld et al., 1998):

Hydrogeology:

- ✓ dam construction;
- ✓ vertical barriers and water control structures where water deflection is needed, both above and below the surface.

Construction:

- ✓ structural surfaces like floor and storage areas as well as runways;
- ✓ pre-casting of simple structures used in non-specialist applications such as fences, paving materials and low cost pipes. Generally the mould-ability of geopolymeric pastes is very good and together with their relatively low shrinkage compared to Portland cement, any such non-specialist application should be suitable.

Waste management:

- ✓ surface capping of waste dumps and landfill sites where a stiff high strength structure is needed to prevent contact by rainwater and provide a solid and safe cover which can also assist in utilizing the area for building purposes;
- ✓ low permeability base liners where minimum leakage of contaminants into the groundwater is desired or where fresh water reservoirs need a lining to prevent water from seeping away as in regions where not enough clay is present in the soil;
- ✓ intermittent horizontal barriers in waste masses, used to keep waste masses stable and prevent contact between various layers stacked on top of one another;
- ✓ immobilization of metal-containing toxic waste. This is possibly one of the major areas where geopolymerisation can impact heavily on the status quo;
- ✓ inexpensive but durable encapsulation of hazardous waste such as radioactive wastes.

As already reported, one of the main perspectives of geopolymers application in waste management is related to their capacity to immobilize toxic waste like heavy, toxic and radioactive elements, This capacity derives from the similar behaviour of geopolymers, zeolites and feldsphatoids. Unlike the traditional binders used for stabilization/solidification of inorganic wastes, geopolymers can also be used in the presence of: sodium salt, arsenate, borate, phosphate, iodate and sulphide as well as magnesium, tin, zinc, copper, lead salts.

References

- ✓ L.B. Andrade, J.C. Rocha, M. Cheriaf: Evaluation of concrete incorporating bottom ash as a natural aggregates replacement; Waste Management (2007) 27: 1190-1199.
- ✓ L.B. Andrade, J.C. Rocha, M. Cheriaf: Influence of coal bottom ash as fine aggregate on fresh properties of concrete; Construction and Building Materials (2009) 23: 609-614.
- ✓ S. Andini, R. Cioffi, F. Colangelo, T. Grieco, F. Montagnaro, L. Santoro: Coal fly ash as raw material for the manufacture of geopolymer-based products; Waste Manage (2008) 28(2):416-423.
- ✓ P- Arjunan, M. R. Silsbee, M. Roy: Chemical Activation of Low Calcium Fly Ash Part II; (2001) Effect of Mineralogical Composition on Alkali Activation Fly Ash library home www.flyash.info.
- ✓ ASTM C150/C150M – 09 Standard Specfication for Portland Cement.
- ✓ D.L. Baun, B. Kamuk, P. Avanzi: Treatment of bottom ash from waste to energy plants: overview and experiences; Proceedings Sardinia 2007, Eleventh International Waste Management and Landfill Symposium S.Margherita di Pla, Cagliari, Italy; 1-5 October 2007.
- ✓ F. Belleman and J. Stark: Activation of blast furnace slag by a new method; Cement and Concrte Research (2009) 39: 644-650.
- ✓ L. Bertolini, M. Carsana, D. Cassago, M. Collepardi, A. Quadrio Curzio: MSWI ashes as mineral additions in concrete; Cement and Concrete Research (2004) 34: 1899-1906.
- ✓ C.R. Cheeseman and S. Asavapisit: Effect of calcium chloride on the Hydration and leaching of lead-retarded cement; Cement and Cocrete Research (1999) 29: 885-892.
- ✓ Q.Y. Chen, M. Tyrer, C.D. Hills, X.M. Yang, P. Carey: Immobilitazion of heavy metal in cement-based solidification/ stabilitazion: A review; Waste Management (2009) 29: 390-403.
- ✓ J.S. Chen, P.Y. Chu, J.E. Chang, H.C. Lu, Z.H. Wu, K.Y. Lin: Engineering and Environmental Characterization of Municipal Solid Waste Bottom Ash as an Aggregate Substitute Utilized for Asphalt Concrete; Journal of Materials in Civil Engineering (2008) 20 (6):432-438.

- ✓ T.W. Cheng and J. P. Chiu: Fire-resistant geopolymer produced by granulated blast furnace slag; Minerals Engineering (2003) 16: 205-210.
- ✓ J. M. Chimenos, M. Sagarra, M.A. Fernandez, F. Espiell: Characterization of the bottom ash in municipal solid waste incinerator; Journal of Hazardous Materials A (1999) 64: 211-222.
- ✓ J. M. Chimenos., A.I. Fernandez, L. Miralles, M. Sagarra, F. Espiell: Short-term natural weathering of bottom ash as a function of particle size; Waste Management (2003) 23: 887-895.
- ✓ P. Chindaprasirt, T. Chareerat, V. Sirivivatnanon: Workability and strength of coarse high calcium fly ash geopolymer; Cement Concrete Composite (2006) 29: 224-229.
- ✓ P. Chindaprasirt, C. Jaturapitakkul, W. Chalee, U. Rattanasak: Comparative study on the characteristics of fly ash and bottom ash geopolymers; Waste Management (2009) 29: 539-543.
- ✓ I. Costa, G. Massard, A. Agarwal: Waste management policies for industrial symbiosis development: case studies in European countries; Journal of Cleaner Production (2010) 18: 815-822.
- ✓ G. Cornelis, C.A. Johnson, T. Van Gerven, C. Vandecasteele: Leaching mechanisms of oxyanionic metalloid and metal species in alkaline solid wastes: A review; Applied Geochemistry (2008) 23: 955-976.
- ✓ B. Clozel-Leloup, F. Bodénan, P. Piantone: Bottom ash from municipal solid waste incineration: mineralogy and distribution of metals; In: Mehu J., Keck G., Navarro A. (eds.). Proc. STAB & ENV 99., International Conference on Waste Stabilization and Environment. Lyone Villeurbanne, France, (1999):46-51.
- ✓ G. Cornelis, C.A. Johnson, T. Van Gerven, C.Vandecasteele: Leaching mechanisms of oxyanionic metalloid and metal species in alkaline solid wastes: A review; Applied Geochemistry (2008) 23: 955-976.
- ✓ Council Directive 99/31/EC, 1999. Landfill of waste. Official Journal L 182, 16/07/1999, 0001-0019.
- ✓ B.S. Crannel, T.T. Eighmy, J.E. Krzanowski, J.D. Eusden Jr, E.L. Shaw, C.A. Francis: Heavy metal stabilization in municipal solid waste combustion bottom ash using soluble phosphate; Waste Management (2000) 20: 135-148.
- ✓ J. Davidovits: Geopolymers: inorganic polymeric new materials; Journal of thermal analysis (1991) 37: 1633-1656.

- ✓ J. Davidovits: Properties of geopolymer cement; Proceeding first international conference on Alkaline Cements and Concretes, Institute of Binders and Materials, Kiev State Technical university,Kiev, Ukraine (1994): 131-149.
- ✓ J. Davidovits, M. Davidovics, N. Davidovits: Process for obtaining a geopolymeric alumino silicate and products thus obtained; (1994) U.S. Patent no.5,342,595.
- ✓ J S.J. van Deventer, J.L. Provis, P. Duxson, D.G. Brice: Chemical Research and Climate Change as Drivers in the Commercial Adoption of Alkali Activated Material; Waste Biomass Valorization (2010) 1: 145-155.
- ✓ Decreto Legislativo 3 aprile 2006, n. 152 "Norme in materia ambientale" G.U. n. 88 del 14 aprile 2006 - Supplemento Ordinario n. 96.
- ✓ Directive 2006/12/EC of the European Parliament and of the Council of 5 April 2006 on waste (Text with EEA relevance).
- ✓ Directive 2008/98/EC of the European Parliament and of the Council of 19 November 2008 on waste (Text with EEA relevance).
- ✓ Directive 2003/33/EC of the European parliament and of the council of 26 May 2003 on the approximation of the laws, regulations and administrative provisions of the Member States relating to the advertising and sponsorship of tobacco products (Text with EEA relevance).
- ✓ S. Donatello, A. Freeman-Pask, M. Tyrer, C.R. Cheeseman: Effect of milling and acid washing on the pozzolanic activity of incinerator sewage ash; Cement and Concrete Composite (2010) 32: 54-61.
- ✓ P. Duxon, A. Fernandez-Jimenez, J. L. Provis, G.C. Lukey, A. Palomo, J. S. J. van Deventer: Geopolymer technology: the current state of the art; Journal of Materials Science (2007) 42: 2917-2933.
- ✓ J. Dykstra Eudsen, T. Eighmy, K. Hockert, E. Holland, K. Marsella: Petrogenesis of municipal solid waste combustion bottom ash; Applied Geochemistry (1999) 14: 1073-1091.
- ✓ T. Eighmy, J. Eudsen, K. Marsella, J. Hogan, D. Domingo, J. Kranowski, D. Stampfli: Particle petrogenesis and speculation of elements in MSW incineration bottom ashes; Environmental aspects of Construction with Waste Materialials (1994): 111-136.
- ✓ Eionet: European Topic Centre on Sustainable Consumption and Production EEA European Environment Agency: Country fact sheets on waste policies - 2009 edition viewed at http://scp.eionet.europa.eu/facts/factsheets_waste/2009_edition.

- ✓ European Commission, Brussels assessing legal compliance with and implementation of the waste acceptance criteria and proceduresby the EU-15 07.0307/2008/510910/SER/G4 (December 2009) Final Report 23.
- ✓ Eurostat data relate to waste production on 2008 viewed at: http://epp.eurostat.ec.europa.eu/portal/page/portal/environment/data (2009).
- ✓ Eurostat Newsrelease: Environment in the EU27 40% of municipal waste recycled or composted in 2008 Half a tonne of waste generated per person, (19th March 2010) 43/2010.
- ✓ M. Fernandez Bertos, X. Li, S.J.R. Simons, C.D. Hills, P.J.Carey: Investigation of accelerated carbonation for the stabilization of MSW incinerator ashes and the sequestration of CO_2; Green Chemistry (2004) 6: 428-436.
- ✓ Y. Fan, S. Yin, Z. Wen, J. Zhong: Activation of fly ash and its effects on cement properties; Cement and Concrete Research (1999): 467-472.
- ✓ D. Feng, H. Tan, J.S.J. van Deventer: Ultrasound enhanced geopolymerisation; Journal of materials science (2004) 39: 571-580.
- ✓ P. Freyssinet, P. Piantone, M. Azaroual, Y. Itard, B. Clozel-Leloup, D. Guyonnet, J.C. Baubron: Chemical changes and leachate mass balance of municipal solid waste bottom ash submitted to weathering; Waste Management (2002) 22: 159-172.
- ✓ C. Giampaolo, S. Lo Mastro, A. Polettini, R. Pomi, P. Sirini: Acid neutralisation capacity and hydration behaviour of incineration bottom ash–Portland cement mixtures; Cement and Concrete Research (2002) 32: 769-775.
- ✓ O. Ginés, J.M. Chimenos, A. Vizcarro, J. Formosa, J.R. Rosell: Combined use of MSWI bottom ash and fly ash as aggregate in concrete formulation: environmental and mechanical considerations; Journal of Hazardous Material (2009) 169: 643-650.
- ✓ Z. Giergiczny: Effect of some additives on the reactions in fly ash/$Ca(OH)_2$ system; Journal of Thermal Analysis and Calorimetry (2004) 76: 747-754.
- ✓ V.D. Glukhovsky, G.S. Rostovskaja, G.V. Rumyna: High strength slag-alkaline cements; International Congress on the Chemistry of Cement, Paris (1980) 3 Theme 5: 164-168.
- ✓ J.P. Hos, P.G. McCormick, L.T. Byrne: Investigation of a synthetic aluminosilicate inorganic polymer; Journal of materials science (2002) 37: 2311-2316.

- ✓ Z. Jing, N. Matsuoka, F. Jin, T. Hashida, N. Yamasaki: Municipal incineration bottom ash treatment using hydrothermal solidification; Waste Management (2007) 27: 287-293
- ✓ IAWG (International Ash Working Group: A.J. Chandler, T.T. Eighmy, J. Hartlén, O. Hjelmar, D. Kosson, S.E. Sawell, H.A. van der Sloot, J. Vehlow) In: Municipal Solid Waste Incinerator Residues, Studies in Environmental Sciences (1997) 67, Elsevier Science, Amsterdam.
- ✓ C. A. Johnson, S. Brandenberger, P. Baccini: Acid neutralizing capacity of municipal waste Incinerator bottom ash; Environmental Science and Technology (1995) 29: 142-147.
- ✓ C.A. Johnson, M. Kersten, F. Ziegler, H.C. Moor: Leaching behaviour and solubility controlling solid phases of heavy metals in municipal solid waste incineration ash; Waste Management (1996) 16: 129-134.
- ✓ Q. Jueshi. S. Caijun, W. Zhi: Activation of blended cement containing fly ash; Cement and Concrete Research (2001) 31: 1121-1127.
- ✓ B. Jurić, L. Hanžič, R. Ilić, N. Samec: Utilization of municipal solid waste bottom ash and recycled aggregate in concrete; Waste Management (2006) 26: 1436-1442.
- ✓ P. Lechner, A. Polettini, T. Van Gerven: Characterization and treatment of waste combustion residues; Proceeding Venice 2006, Biomass and Waste to Energy Symposium Venice, Italy; 29 November – 1 December 2006.
- ✓ L. Lam, Y.L. Wong, C.S. Poon: Degree of hydration and gel/space ratio of high-volume fly ash/cement system; Cement and Concrete Research (2000) 30: 747-756.
- ✓ C.H.K. Lam, A.W.M. Ip, J.P. Barford, G. McKay: Use of incinerator MSW Ash: A Review; Sustainability (2010) open acces ISSN 2071-1050 www.mdpi.com/journal/sustainability.
- ✓ C. Lampris, R. Lupo, C.R. Cheeseman: Geopolymerisation of silt generated from construction and demolition waste washing plants; Waste Management (2009) 29: 368–373.
- ✓ C.Y. Lee, H.K. Lee, K.M. Lee: Strength and microstructural characteristics of chemically activated fly ash-cement system; Cement and Concrete Research (2003) 33: 425-431.
- ✓ M.P. Lorenzo, S. Goňi, A. Guerrero: Activation of Pozzolanic Reaction of Hydrated Portland Cement Fly Ash Pastes in Sulfate Solution; Journal of American Ceramic Society (2002) 85: 3071-3075.

- ✓ K. Kayabali and G. Bulus: The usability of bottom ash as an engineering material when amended with different matrices; Engineering Geology (2000) 56: 293-303.
- ✓ D. Khale and R. Chaudhary: Mechanism of geopolymerization and factors influencing its development: a review; Journal of Materials Science (2007) 42: 729-746.
- ✓ C.S. Kirby and J.D. Rimstidt: Mineralogy and surface properties of municipal solid waste ash; Environmental Science and Technology (1993) 27: 652-660.
- ✓ F. Kokalj, N. Samec, B. Jurl: Utilization of bottom ash from the incinerator of separated wastes as a cement substitute; Waste Management & Resarch (2005) 23: 468-472.
- ✓ K. Komnitsas and D. Zaharaki: Geopolymerisation: A review and prospects for the minerals industry; Minerals Engineering (2007) 20: 1261-1277.
- ✓ W.M. Kriven, J.L. Bell, M.Gordon: Microsructure nd microchemistry of fully reacted geopolymers and geopolymer matrix composites; Ceramic Transactions (2003) 153: 227-250.
- ✓ I. Kourti, D. A. Rani, D. Deegan, A.R. Boccaccini, C.R. Cheeseman: Production of geopolymers using glass produced from DC plasma treatment of air pollution control (APC) residues; Journal of Hazardous Materials (2010) 176: 704-709.
- ✓ R. Kumar, S. Kumar, S.P. Mehrotra: Towards sustainable solution for fly ash through mechanical activation; Resources, Conservation and Recycling (2007) 52: 157-179.
- ✓ W. Ma and P.W. Brown: Hydrothermal reactions of fly ash with $Ca(OH)_2$ and $CaSO_4*2H_2O$; Cement and Concrete Research (1997) 27: 1237-1248.
- ✓ J. Malolepszy and J. Deja: Immobilization of heavy metal ions by the alkali activated slag cementitious materials; Environmental Aspects od Construction with Waste Materials (1994): 519-524.
- ✓ J.A. Meima and R.N.J. Comans: Geochemical modeling of weathering reactions in municipal solid waste incinerator bottom ash; Environmental Science Technologies (1997) 31: 1269-1276.
- ✓ J.A. Meima and R.N.J. Comans: The leaching of trace elements from municipal solid waste incinerartor bottom ash at different stages of weathering; Applied Geochemistry (1999) 14: 159-171.
- ✓ J. A., Meima, R.D. van der Weijden, T.T. Eighmy, R.N.J. Comans: Carbonation processes in municipal solid waste incinerator bottom ash and their effect on leaching of copper and molybdenum; Applied Geochemistry (2002) 17: 1503-1513.

- ✓ H. Moller: Sampling of heterogeneous bottom ash from municipal waste incineration plants; Chemometrics and Intelligent Laboratory Systems (2004) 74: 171-176.
- ✓ S. Naganathan and H. A Razak: Effect of kaolin addition on the performance of controlled low-strength material using industrial waste incinerator bottom ash; Waste Management & Research (2009) 00: 1-13.
- ✓ .E. Oh, P.J.M. Monteiro, S.S. Jun, S. Choi, S.M. Clark: The evolution of strength and crystalline phases for alkali-activated ground blast furnace slag and fly ash-based geopolymers; Cement and Concrete Research (2010) 40: 189-196.
- ✓ J.R. Pan, C. Huang, J.J. Kuo,. S.H. Lin: Recycling MSWI bottom and fly ash as raw materials for Portland cement; Waste Management (2008) 28: 1113-1118.
- ✓ J.S. Park, Y.J. Park, J. Heo: Solidification and recycling of incinerator bottom ash through the addition of colloidal silica (SiO_2) solution; Waste Management (2007) 27: 1207-1212.
- ✓ D. Panias, I.P. Giannopoulou, T. Perraki: Effect of synthesis parameters on the mechanical properties of fly ash-based geopolymers; Colloids and Surfaces A: Physicochemical and Engineering Aspects (2007) 301: 246-254.
- ✓ G. Pecqueur, C. Crignon, B. Quénée: Behaviour of cement-treated MSWI bottom ash; Waste Management (2001) 21: 229-233.
- ✓ D. S. Perera, O. Uchid, E. R. Vance, K. S. Finnie: Influence of curing schedule on the integrity of geopolymers; Materilas Science (2007) 42: 3099-3106.
- ✓ J.W. Phair, J.S.J. van Deventer, J.D. Smith: Effect of Al source and alkali activation on Pb and Cu immobilization in fly ash based “geopolymers”; Applied Geochemistry (2004) 19: 423-434.
- ✓ P. Piantone, F. Bodenan, L. Chatelet-Snidaro: Mineralogical study of secondary mineral phases from weathered MSWI bottom ash: implications for the modeling and trapping of heavy metals; Applied Geochemistry (2004) 19: 1891-1904.
- ✓ A. Polettini and R. Pomi: The leaching behavior of incinerator bottom ash as affected by accelerated ageing; Journal of Hazardous Materials B (2004) 113: 209-215.
- ✓ A. Polettini, R. Pomi, G. Carcani: The effect of Na and Ca salts on MSWI bottom ash activation for reuse as a pozzolanic admixture; Resources, Conservation and Recycling (2005) 43: 403-418.
- ✓ A. Polettini, R. Pomi, E. Fortuna: Chemical activation in view of MSWI bottom ash recycling; Journal of Hazardous Materials (2009) 162: 1292-1299.
- ✓ C.S. Poon, X.C. Qiao, Z.S. Lin: Pozzolanic properties of reject fly ash in blended cement pastes; Cement and Concrete Research (2003): 1857-1865.

- ✓ C.S. Poon, X.C. Qiao, Z.S. Lin: Effects of flue gas desulphurization sludge on the pozzolanic reaction of reject-fly-ash-blended cement pastes; Cement and Concrete Research (2004): 1907-1918.
- ✓ J.L. Provis, C. Zheng Yong, P. Duxson, J.S.J. van Deventer: Correlating mechanical and thermal properties of sodium silicate-fly ash geopolymers; Colloids and Surfaces A: Physicochemical and Engineering Aspects (2009) 336: 57-63.
- ✓ A.O. Purdon: The action of alkalies on blast furnace slags; Indian Journal of Chemistry (1940) 59:191-202.
- ✓ X.C. Qiao, C.S. Poon, C.R. Cheeseman: Investigation into the stabilization/solidification performance of Portland cement through cement clinker phases; Journal of Hazardous Waste (2007) 139 (B): 238-243.
- ✓ X.C. Qiao, M. Tyrer, C.S. Poon, C.R. Cheeseman: Novel cementitious materials produced from incinerator bottom ash; Resources, Conservation and Recycling (2008 (a)) 52: 496-510.
- ✓ X.C. Qiao, M. Tyrer, C.S. Poon, C.R. Cheeseman: Characterization of alkali-activated termally treated incinerator bottom ash; Waste Management (2008 (b)) 28: 1955-1962.
- ✓ X.C. Qiao, C.S. Poon, C.R. Cheeseman: Influences of chemical activators on incinerator bottom ash; Waste Management (2009) 29: 544-549.
- ✓ H. Rechberger: The use of statistical entropy to evaluate the utilization of incinerator ashes for the production of cement; Waste Management & Research (2001) 19: 262-268.
- ✓ E. Rendek, G. Ducom, P. Germain: Influence of waste input and combustion technology on MSWI bottom ash quality; Waste Management (2007).
- ✓ D.M. Roy: Alkali-activated cements. Opportunities and challenges; Cement and Concrete Research (1999) 29: 249-254.
- ✓ Ž. Seculić, S. Popov, M. Duričić, A. Rosić: Mechanical activation of cement with addition of fly ash; Materials Letters (1999) 39: 115-121.
- ✓ T. Sabbas, A. Polettini, R. Pomi, T. Astrup, O. Hjelmar, P. Mostbauer, G. Cappai, G. Magel, S. Salhofera, C. Speiserg , S. Heuss-Assbichler, R. Klein, P. Lechner (members of the pHOENIX working group on Management of MSWI Residues): Management of municipal solid waste incineration residues; Waste Management (2003) 23: 61–88.
- ✓ C. Shi and R.L. Day: Acceleration of the reactivity of fly ash by chemical activation; Cement and Concrete Research (1995) 25: 15-21.

- ✓ C. Shi: Early microstructure development of activated lime/fly ash pastes; Cement and Concrete Research (1996) 26: 1351-1359.
- ✓ C. Shi, P.E. Grattan/Bellew, J. A. Stegemann: Conversion of waste mud into pozzolanic material; Construction and Building Materials (1999) 13: 279-284.
- ✓ C.Shi and J. Qian: High performance cementing materials from industrial slags - a review; Resources, Conservation and Recycling (2000) 29: 195-207.
- ✓ C.Shi, P.V. Krivenko, D. Roy: Alkali-activated cements concretes; Taylor and Francis, London,2006 Advanced in Cement Research (2006) 18: 179-180.
- ✓ S. Songpiriyakij, T. Kubprasit, C. Jaturapitakkul, P. Chindaprasirt: Compressive strength and degree of reaction of biomass- and fly ash-based geopolymer; Construction and Building Materials (2009) 24: 236-240.
- ✓ C. Speiser, T. Baumann, R.Niessner: Morphological and chimica characterization of calcium-hydrate phases formed in alteration processes of deposited municipal solid waste incinerator bottom ash; Environmental Science and Technology (2000) 34: 5030-5037.
- ✓ F. Skvára, L. Kopecky, V. Smilauer, Z. Bittnar: Material and structural characterization of alkali activated low-calcium brown coal fly ash; Journal of Hazardous Materials (2009) 168: 711-720.
- ✓ S. Targan, A. Olgun, Y. Erdogan, V. Sevinc: Influence of natural pozzolan, colemanite ore waste, bottom ash, and fly ash on the properties of Portland cement; Cement and Concrete Research (2003) 33: 1175-1182.
- ✓ J. Temuujin, A. van Riessen, R. Williams: Influence of calcium compounds on the mechanical properties of fly ash geopolymer pastes; Journal of hazardous materials (2009)167: 82-88.
- ✓ J. Temuujin, A. van Riessen, K.J.D. MacKenzie: Preparation and characterisation of fly ash based geopolymer mortars; Construction Building Matererials (2010) 24: 1906-1910.
- ✓ F.P.Torgal, J.C.Gomes, S. Jalali: Alkali-activated binders: A review. Part 2. About materials and binders manufacture; Construction and Building Materials (2008 (a)) 22: 1315-1322.
- ✓ F.P.Torgal, J.C.Gomes, S. Jalali: Alkali-activated binders: A review Part 1. Historical background, terminology, reaction mechanisms and hydration products; Construction and Building Materials (2008 (b)) 22: 1305-1314.

- ✓ J.G.S. van Jaarsveld, J.S.J van Deventer, L. Lorenzen: The potential use of geopolymeric materials to immobilize toxic metals: part I theory and applications; Minerals Engineering (1997) 10 (7): 659-669
- ✓ J.G.S. van Jaarsveld, J.S.J van Deventer, L. Lorenzen: Factor affecting the immobilitazion of metals in geopolymerized fly ash; Metallurgical and materials transactions(1998) 29 (B): 283-291.
- ✓ J.G.S. van Jaarsveld, J.S.J van Deventer, A. Schwartzman: The potential use of geopolymeric materials to immobilize toxic metals: part II materials and leaching characteristics; Minerals Engineering (1999 (a)) 12 (1): 75-91.
- ✓ J. G. S. van Jaarsveld and J. S. J. van Deventer: Effect of the Alkali Metal Activator on the Properties of Fly Ash-Based Geopolymers; Industrial & Engineering Chemistry Research (1999 (b)) 38: 3932-3941.
- ✓ J.G.S. van Jaarsveld, J.S.J. van Deventer, G.C. Lukey: The effect of composition and temperature on the properties of fly ash- and kaolinite-based geopolymers; Chemical Engineering Journal (2002) 89: 63-73.
- ✓ H.A. Van der Sloot, D.S. Kosson, O. Hjelmar: Characteristics, treatment and utilization of residues from municipal waste incineration; Waste Management (2001) 21: 753-765.
- ✓ I. Vagas, J.A. Ibaňez, J.T. San José, A. Urzelai: Construction demolition wastes, Waelz slag and MSWI bottom ash: A comparative technical analysis as material for road construction; Waste Management (2008) 28: 565-574.
- ✓ H. Zhang, P.J. He, L.M. Shao, X.L. Li: Leching behaviour of heavy metals from municipal solid waste incineration bottom ash and its geochemical modelling; Waste Management (2008) 10: 7-13.
- ✓ D. Zhang, W. Liu, H. Hou, X. He:Strength, leachability and microstructure characterization of Na_2SiO_3/activated ground granulated clast/furnace slag solidifiated MSWI fy ash; Waste Management and Research (2007) 25: 402-407.
- ✓ C. Zevenbergen and R.N.J. Comans: Geochemical factors controlling the mobilization of major elements during weathering of MSWI bottom ash. In: Goumans, J.J.J.M., van der Sloot, H.A., Aalbers, Th.G. (Eds.), Environmental Aspects of Construction with Waste Materials, Studies in Environmental Sciences 60. Elsevier Sci., Amsterdam, pp. 179-194.
- ✓ Z. Zuhua, Y. Xiao, Z. Huajun, C. Yue : Role of water in the synthesis of calcined kaolin-based geopolymer; Applied Clay Science (2009) 43: 218-223.

- ✓ H. Xu and J.S.J. van Deventer: The geopolymerization of alumino-silicate minerals; The International Journal of Mineral Processing (2000) 59: 247-266.
- ✓ H. Xu, L. Quin, I. Shen, W. Wang, J. Zhai: Synthesis of thermostble geopolyem from circulating fluidized bed combustion (CFBC) bottom ashes; Journal of Hazardous Materials (2010) 7: 198-204.
- ✓ C.K. Yip and J.S.J. van Deventer: Microanlysis of calcium silicate hydrate gel formed within a geopolymeric binder; Journal of Matererials Science (2003) 38: 3851-3860.
- ✓ C.K. Yip, G.C. Lukey, J.S.J. van Deventer: The coesistence of geopolimeric gel and calcium silicate hydrate at the early stage of alkali activation; Cement and Concrete Research (2005) 35: 1688-1697.
- ✓ C.K. Yip, G.C. Lukey, J.L. Provis, J.S.J. van Deventer: Effect of calcium silicate sources on geopolymerization; Cement and Concrete Research (2008) 38: 554-564.
- ✓ S.E. Wallah and B. V. Rangan: Low-Calcium fly ash based geopolymer concrete: long term properties; Research Report GC 2 Faculty of Engineering Curtin University of Technology Perth, Australia 2006.
- ✓ S.D. Wang and K.L. Scrivener: Hydration products of alkali activated slag cement; World Business Council for Sustainable Development: Cement Sustainability Initiative http://www.wbcsdcement.org; Cement and Concrete Research (1995) 25: 561-571.

2. Materials and methods

2.1 Bottom Ash

The BA used in the present study comes from an Italian grate-type refuse derived fuel (RDF) incinerator located in central Italy, having a nominal size of 90,000 t/y and a BA production of ~12,000 t/y. Two sampling campaigns were performed for each experimental study conducted. The BA used for the alkali activation experiments on blended cement formulation will be named Sample 1 while the BA used to study the geopolymerization process will be named Sample 2. The fresh bottom ash was sampled at the exit of the quenching unit, homogenized by quartering, and oven-dried at 60°C to constant weight.

Both samples were sieved using a shaker equipped with a standard mesh series to produce two different size classes: a coarse fraction (CF), having $12.5 > \Phi > 0.425$ mm and a fine fraction (FF), having $\Phi < 0.425$ mm. In addition, the CF was also sieved to separate some other fraction: class A $12.5 > \Phi > 5.6$ mm; class B $5.6 > \Phi > 2$ mm and class C $2 > \Phi > 0.425$ mm; while only for Sample 1 the FF was also separated considering in two additional classes: class D, having $0.425 > \Phi > 0.150$ mm and class E, having $\Phi < 0.150$ mm. The 12.5 mm oversize fraction (~ 6% wt of total bottom ash mass in both cases) was primarily composed of ceramics, glass and metal scrap fragments, therefore they were judged unsuitable for subsequent processing and discarded. The individual size classes were separately characterized for physical and chemical properties.

The physical and chemical characterization involved determination of: water content, loss on ignition, elemental composition, anion content, leaching behaviour; and for Sample 2 microstructure and mineralogy was also investigated.

The elemental composition was determined by atomic absorption spectrometry (AAS-Perkin-Elmer 3030B) after alkaline digestion at 1050 °C in platinum melting pots using lithium tetraborate as the melting agent. Anions were analyzed by Metrohm 761 Compact IC ion chromatographer after dissolution according to the Italian UNI 8520 methods.

Chloride and acid-soluble sulphates were measured using the Italian standard test procedure UNI 8520, which involves dissolution with hot deionised water and titration with $AgNO_3$ for chloride analysis, whereas dissolution with 3% HCl followed by spectrometric analysis for sulphates. The carbonate content of untreated and carbonated BA was measured with a Dietrich–Frühling calcimeter (only for Sample 2). The loss on ignition (LOI) at 1000°C and the water content of the BA were determined according to the ASTM C25 and ASTM D2216 procedures.

The leaching behaviour was investigated on bottom ash samples, on activated bottom ash mixed with cement and also on geopolymeric materials produced, using the EN 12457-2 batch compliance test and the CEN/TS 14429 pH-dependence leaching test for evaluation of the acid neutralization capacity (ANC).

The EN 12457-2 was applied to asses the material's compliance with both the European regulatory limits for disposal into inert waste landfills (EU Council Directive 99/31/EC, 1999) and the Italian limits regulatory for waste utilization (annex 3 D.M. 05/02/1998, Ministero dell'Ambiente della Repubblica Italiana, 1998). The EN 14429 (ANC) leaching test was applied to evaluate the material's capacity to neutralize pH variations and to acquire information about the material's durability upon acid addition; furthermore the analysis of contaminants concentrations in the ANC eluates was performed to derive information on the solubility curves as a function of pH, which in turn were used to infer about possible leaching-controlling mechanisms. Understanding the mechanisms governing the release of toxic species from the treated waste is indeed considered of key importance in order to estimate potential environmental impacts. The ANC test was carried out over a 48 h period by contacting a number of material sub-samples with nitric acid solutions (L/S = 10 ml/g) having increasing acid concentrations. The acid addition schedule was arranged so as to cover pHs in the final eluate ranging from the material-controlled value to approximately four or three units. The equivalents of acid added were, therefore, dependent on the ANC of the individual sample tested. Agitation was accomplished through tumbling. After 48 h, the pH was measured in the suspension, and the liquid phase was extracted through centrifugation followed by 0.45 μm filtration and acidified with 1:1 v/v HNO_3 for the subsequent chemical analyses. Metals and major elements were analyzed by means of atomic absorption spectrometry.

Scanning Electron Microscope (SEM) analysis were conducted using a Phillips XL- 30 microscope with an operating voltage of 25 kV a spot size of 200 nm; a tilt angle of 35º; a take-off angle of 61.34º, equipped with an energy dispersive EDAX DX-4 spectrometer set with a count rate of about 1200 cps and a live time of 50 s. The samples were first impregnated with an ultra-low viscosity resin and then polished. A carbon film (about 3 nm) was deposited onto the polished surfaces of samples under vacuum to prevent charging.

FT-IR absorbance spectra were collected with an Impact 420 Nicolet instrument in the wavenumber range 400–4000 cm^{-1} with a resolution of 4 cm^{-1} on pellets with KBr; the

pellets were prepared by pressing a mixture of 1 mg of sample with 300 mg of KBr.
Raman spectroscopy analysis were carried out using an Horiba Jobin Yvon LABRAM Infinity spectrometer coupled with an Olympus BX 40 microscope and equipped with an optical notch filter, a charge coupled device detector, and a 20mW He–Ne laser standard HR 800 (k = 632.817 nm). The X-Ray Diffraction (XRD) analysis were performed using a Siemens D 501 diffractometer with Cu Kα radiation scanning the unoriented powder solids from 20° to 80° 2θ with a 0.04° 2θ step interval and a 1s per step counting.

2.1 Activation of bottom ash for use in Portland cement blends

The aims of this experimental study, concerning the alkali activation of BA for blended cement formulation, are:

- the investigation of the main effects of the activators in the BA reactivity promotion;
- the study of the main changes on the hydration process of the cement mixtures;
- the understanding of the influence of activated BA on the mechanical strength development.

Both mechanical and chemical activation were adopted during the experiments. Mechanical activation involved ball-milling of the material to a final maximum particle size of 150 μm, in order to increase the surface area thus improving the potential reactivity. Chemical activation has been made using different inorganic compounds to promote the conversion of original Ca-Si-Al matrix of the waste into hydration phases with adequate mechanical strength. In detail different Ca-, Na- and K-based compounds, including $CaCl_2 \cdot 2H_2O$, $CaSO_4 \cdot 2H_2O$, NaOH, KOH (reagent-grade compounds), were selected as BA activators on the basis of a literature survey and the results from previous studies (Shi and Day, 1995; 2000 (a),(b); 2001; Fan et al., 1999; Qian et al., 2001; Giampaolo et al., 2002; Filipponi et al., 2003; Polettini et al., 2005; 2009; Pacewska et al., 2008; Qiao et al., 2008; 2009). The chemical activation procedure was applied using two different methods. According to Method 1, slurries (L/S = 2 ml/g) containing the ball-milled bottom ash and the chemical activator were heated at 90°C for 3 h and subsequently oven-dried at 60°C. Cementitious mixtures were prepared by blending different proportions of activated BA and Ordinary Portland Cement (OPC) type I 42.5 R at a water/total solids weight ratio of 0.4. The investigated BA/(BA + OPC) ratios were 20 and 40 wt%, while the activator additions adopted (expressed as activator/BA ratio) were 2 and 4 wt%. Control samples containing 0, 20 and 40 wt% of un-activated BA were also prepared for reference purposes. According to the second activation method, Method 2, the milled BA and the mixing water containing the required dissolved amount of the chemical activator were simply added to cement without any pre-processing stage. The second activation method was only applied with Ca-based activators ($CaCl_2$ and $CaSO_4 \cdot 2H_2O$). For selected mixtures Table 5shows the different mixtures tsted during the experimental campaign.

	Mixture composition									
	(g/100 g)			**(%)**					**Activation method**	
Mix no.	**OPC**	**BA**	**Act.**	**BA /(BA+OPC)**	**Activator /BA**	**Activator type**	**symbol**	**BA size fraction**	**Method 1**	**Method 2**
control	100			0						
U20c	80	20		20				CF		
U40c	60	40		40				CF		
U20f	80	20						FF		
ref. C20-2	100		0.04	0		$CaCl_2$	C			
ref. C20-4	100		0.08	0		$CaCl_2$	C			
ref. C40-2	100		0.08	0		$CaCl_2$	C			
ref. C40-4	100		1.06	0		$CaCl_2$	C			
ref. S20-2	100		0.04			$CaSO_4$	C			
ref. S20-4	100		0.08			$CaSO_4$	C			
K20-2c	80	20	0.04	20	2	KOH	K	CF	X	
K20-4c	80	20	0.08	20	4	KOH	K	CF	X	
K40-2c	60	40	0.08	40	2	KOH	K	CF	X	
K40-4c	60	40	1.06	40	4	KOH	K	CF	X	
N20-2c	80	20	0.04	20	2	NaOH	N	CF	X	
N20-4c	80	20	0.08	20	4	NaOH	N	CF	X	
N40-2c	60	40	0.08	40	2	NaOH	N	CF	X	
N40-4c	60	40	1.06	40	4	NaOH	N	CF	X	
C20-2c	80	20	0.04	20	2	$CaCl_2$	C	CF	X	X
C20-4c	80	20	0.08	20	4	$CaCl_2$	C	CF	X	X
C40-2c	60	40	0.08	40	2	$CaCl_2$	C	CF	X	X
C40-4c	60	40	1.06	40	4	$CaCl_2$	C	CF	X	X
S20-2c	80	20	0.04	20	2	$CaSO_4$	S	CF	X	X
S20-4c	80	20	0.08	20	4	$CaSO_4$	S	CF	X	X
C20-2f	80	20	0.04	20	2	$CaCl_2$	C	FF	X	X
C20-4f	80	20	0.08	20	4	$CaCl_2$	C	FF	X	X
S20-2f	80	20	0.04	20	2	$CaSO_4$	S	FF	X	X
C20-2cf	80	20	0.04	20	2	$CaCl_2$	C	CF+FF	X	
S20-2cf	80	20	0.04	20	2	$CaSO_4$	S	CF+FF	X	

Table 5: Composition of the OPC/BA mixtures

The blends were cast in 30-mm cubic moulds (Figure 12), stored at 40 °C and relative humidity (RH) > 90% for 24 h, then demoulded and allowed to cure at 40 °C and RH >90% for 7, 28, 56 and 90 days.

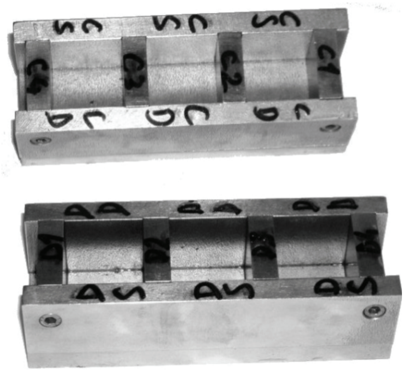

Figure 12:Cubic moulds for cement mixtures

Measurements of unconfined compressive strength (UCS) were made on triplicate specimens according to the ASTM C109 method. and expressed as specific unconfined compressive strength, SUCS (Pu, 1999). The SUCS is defined as the mechanical strength of a given mixture divided by its cement content and was used to identify any additional contribution of cement admixtures to mechanical strength other than that produced by the cement hydrates.

The experiments were arranged according to two main factorial designs and the analysis of variance (ANOVA; Box et al., 2005; Montgomery, 2005) was applied to the experimental data. The ANOVA is a statistical method to derive information on the statistical significance of the main interaction effects between the factors as well as the error of the experiments.

The first design (design 1) included the “activator type”, “bottom ash content” and “activator dosage” as the three factors. A mixed design was obtained with different levels of variation for the selected factors:

- three variation levels for the “activator type”, $CaCl_2$, NaOH and KOH (qualitative factor);
- two variation levels for “activator dosage”, 0.04 and 0.08 wt % (quantitative factor);
- two variation levels for “bottom ash content”, 20 and 40 wt % (quantitative factor).

Due to the number of levels used in design 1 for the two quantitative factors “BA dosage” and “activator addition”, only linear main effects and interactions between factors could be estimated.

The latter design (design 2) was arranged only for $CaCl_2$ activator. The selected factors were the “bottom ash content” and “activator dosage” according to a 3^2 full factorial design. The variation levels of the factors were:

- three variation levels for the “activator dosage”, 0, 0.04 and 0.08 wt %;
- three variation levels for the “bottom ash content”, 0, 20 and 40 wt %.

Since in this case three variation levels of each factor were used, statistical processing of the experimental data allowed for estimation of both linear and quadratic main effects and interactions. To evaluate the linear and quadratic effects of each factor the coefficients for orthogonal contrast (c_j) were used (Table 6).

Coefficient for orthogonal contrast	
Linear	Quadratic
-1	1
0	-2
1	1

Table 6: coefficient for orthogonal contrast

Taking into account the factors selected in the design 2 it was possible to subset the interaction between the two factors (activator dosage (A) and bottom ash content (S)) in four main components, each of these with 1 degree of freedom: AxS_{LXL}; AxS_{LXQ}; AxS_{QXL} and AxS_{QXQ}. The interaction effects were determined through the contrast coefficients shown in Table 7.

AxS_{LxL}			
		S_L	
A_L	-1	0	1
-1	1	0	-1
0	0	0	0
1	-1	0	1

AxS_{QxL}			
		S_L	
A_Q	-1	0	1
1	-1	0	1
-2	2	0	-2
1	-1	0	1

AxS_{LxQ}			
		S_Q	
A_L	1	-2	1
-1	-1	2	-1
0	0	0	0
1	1	-2	1

AxS_{QxQ}			
		A_Q	
A_Q	1	-2	1
1	1	-2	1
-2	-2	4	-2
1	1	-2	1

Table 7: contrast coefficients for interaction effects

The designs were generally arranged as reported in Table 8 (e.g. results for design 2 at 56-day curing).

			S (%)			
			1	**2**	**b**	
			0	*20*	*40*	**yi..**
A(%)	**1**	*0*	46.3	22.61	24.7	
			41.5	29.78	24.6	
			49.6	26.19	25.7	
			137.5	**78.58**	**75.1**	**291.1**
	2	*2*	58.6	43.4	45.1	
			66.9	40.5	49.9	
			45.2	46.2	37.1	
			170.7	**130.0**	**132.2**	**433.0**
	a	*4*	78.14	62.65	39.41	
			41.26	31.52	41.19	
			47.38	39.51	39.59	
			166.7	**133.6**	**120.1**	**420.6**
		y.j.	**475.0**	**342.2**	**327.5**	**1144.9**	**y…**

Table 8: general arrangement for a factorial design (design 3^2; UCS value at 56-day curig)

Where, $y_{i..}$ denote the total of all observations under the i_{th} level of factor “acvtivator dosage“ (A); $y_{.j.}$ denote the total of all observations under the j_{th} level of factor “bottom ash content” (S); $y_{ij.}$ denote the total of all observations under in the ij_{th} cell and $y_{...}$ denote the grand total of all the observations. Mathematically these components are computed as:

$$y_{i..} = \sum_{j=1}^{b} \sum_{k=1}^{n} y_{ijk} \qquad y_{i..} = \sum_{j=1}^{b} \sum_{k=1}^{n} y_{ijk}$$

$$y_{ij.} = \sum_{k=1}^{n} y_{ijk} \qquad y_{ij.} = \sum_{k=1}^{n} y_{ijk}$$

Where: i = 1,2…a; j = 1.2...b and k = 1,2…n (in the case of design 2 a=b=n= 3).

The ANOVA results were expressed in terms of sum of squares (SS) degrees of freedom (DF), mean squares (MS) and Fischer distribution (F_0), as reported in Table 9.

Sum of squares (SS)		DF	Mean sq. (MS)	F_0
SS_A	1372.0	2	686.00	7.2
SS_S	1467.1	2	733.58	7.7
SS_{INT}	85.9	4	21.50	0.2
SS_E	1707.8	18	94.88	
SS_T	4632.9	26	178.1	
$SSAxS_{LxL}$	20.8	1	20.8	0.2
$SSAxS_{LxQ}$	35.6	1	35.6	0.3
$SSAxS_{QxL}$	28.3	1	28.3	0.3
$SSAxS_{QxQ}$	1.1	1	1.1	0.01
SSA_L	930.9	1	930.9	9.8
SSA_Q	441.0	1	441.0	4.6
SSS_L	1209.1	1	1209.1	12.7
SSS_Q	258.0	1	258.0	2.7

Table 9: the Analysis of Variance Table for 3^2 facorial design

Mathematically these components are computed using the equations shown in Table 10.

$SS_A = \frac{\left(\sum_{i=1}^{a} y_{i..}^2\right)}{bn} - \frac{(y_{...})^2}{abn}$	$MS = \frac{SS}{DF}$	$DF_{SS_S} = b - 1$
$SS_S = \frac{\left(\sum_{j=1}^{b} y_{.j.}^2\right)}{an} - \frac{(y_{...})^2}{abn}$	$F_0 = \frac{MS}{MS_{(SS_E)}}$	$DF_{SS_A} = a - 1$
$SS_{INT} = \frac{\left(\sum_{i=1}^{a}\sum_{j=1}^{b} y_{ij.}^2\right)}{n} - \frac{(y_{...})^2}{abn} - SS_A - SS_S$	$DF_{SS_E} = ab(n-1)$	$DF_T = abn - 1$
$SSAxS_{(L)(Q)x(L)(Q)} = \frac{\left(\sum_{i=1}^{a}\sum_{J=1}^{b} c_{ij} y_{ij}\right)^2}{n\sum_{i=1}^{a}\sum_{j=1}^{b} c_{ij}^2}$	$DF_{SS_{INT}} = (a-1) * (b-1)$	

Table 10: ANOVA components

For both factors, different predictive models were derived for each investigated curing time. The calculated main effects and interactions, in both cases, were processed through least-squares linear regression to derive a predictive model for each design, describing the so-called response surface, for the variables of interest. The analytical formulation of the predictive models were as follows for design 1 and design 2, respectively:

$$y = a_0 + a_1 x_1 + a_2 x_2 + a_3 x_3 + a_{12} x_1 x_2 + a_{13} x_1 x_3 + a_{23} x_2 x_3 + a_{123} x_1 x_2 x_3 \quad (1)$$

$$y = a_0 + a_1 x_1 + a_{11} x_1^2 + a_2 x_2 + a_{22} x_2^2 + a_{12} x_1 x_2 + a_{112} x_1^2 x_2 + a_{122} x_1 x_2^2 + a_{1122} x_1^2 x_2^2 \quad (2)$$

In the two equations above, only significant effects were used to derive the model, implying that, case by case, non-significant terms were removed from the general formulations.

The meaning of terms in equation (1) is as follows:

- y is the response variable (e.g., UCS);
- x_1, x_2 and x_3 are the levels of the three factors “activator type”, “bottom ash content” and “activator dosage”;
- $a_{i(j)(k)}$ are the coefficients of the polynomial function.

while the meaning of terms in equation (2) is:

- y is the response variable (e.g., UCS);
- x_1, x_2 are the levels of the two factors “activator type” and “bottom ash content”;
- $a_{(i)(j)(j)}$ are the coefficients of the polynomial function.

In both cases the ANOVA results for UCS were computed for the four curing times investigated (7, 28, 56, 90 days).

Simultaneous thermogravimetric (TGA) and differential scanning calorimetry (DSC) analyses were performed, for a number of selected samples, a thermal analyzer operating at a heating rate of 10°C/min in static air over a temperature range of 20-1000°C was used.

The EN 14429 (ANC) leaching test was applied after mechanical strength testing on ball-milled (Φ<150 μm) and oven-dried (60°C) specimens to assess the pH-dependent leaching of both major elements and trace metals from the hardened matrices.

To derive information on both the evolution of the hydration process and the mechanisms governing the leaching of contaminants from the hardened materials for a number of selected samples (those that shown the best results), geochemical modeling of the ANC eluates was conducted using Visual Minteq as the mathematical code. To allow for a better description of the speciation of eluates from the cement-based materials, the standard thermodynamic database, which presently does not include solid phases typical of hydrated cementitious systems, was thoroughly updated and extended including the stability constants of several cement hydrates from different literature sources (U.S. Department of Energy, 2004; Astrup et al., 2006; Lothenbach and Winnefeld, 2006; Blanc et al., 2007; Hills, 2009; Hyks et al., 2009), which are listed in Table 11 with reference to the corresponding dissolution reaction. In some cases it was required to rearrange the dissolution reaction to fit with the type of components used by Visual MINTEQ, and recalculate the stability constant accordingly. The application of the geochemical speciation code followed a three-step procedure:

(1) the program was run using the measured eluate concentrations and pHs as the input data and suppressing precipitation for all solid phases;

(2) potential solubility-controlling minerals where chosen among those displaying saturation indices (SI) in the range $-1.5 \le SI \le +1.5$ and on the basis of the likelihood of formation in cementitious systems;

(3) the predicted concentrations of each element in equilibrium with the selected mineral phases were derived according to the following empirical equation (3) (Astrup et al., 2006):

$$C_{eq} = C_{meas}\left(10^{-SI}\right)^{1/n} \qquad (3)$$

where C_{eq} and C_{meas} are the theoretical and measured element concentrations, respectively, while n is the stoichiometric coefficient of the element in the mineral of concern. In the modeling calculations, the hypothesis of oxidizing conditions was always assumed.

Mineral	**Dissolution reaction**	**log K**
Sulphate minerals		
K_2SO_4	$K_2SO_4 \rightarrow 2\ K^+ + SO_4$	-1.87 [6]
Pentasalt	$(CaSO_4)_5 \cdot K_2SO_4 \cdot H_2O \rightarrow 5\ Ca^{2+} + 2\ K^+ + 6\ SO_4 + 6\ H_2O$	-29.3 [6]
$PbSO_4 \cdot PbO$	$PbSO_4 \cdot PbO + 2\ H^+ \rightarrow 2\ Pb^{2+} + SO_4 + H_2O$	-0.19 [1]
Syngenite	$K_2Ca(SO_4)_2 \rightarrow Ca^{2+} + 2\ K^+ + 2\ SO_4$	-7.45 [6]
C-S-H phases		
Afwillite	$3CaO \cdot 2SiO_2 \cdot 3H_2O + 6\ H^+ \rightarrow 3\ Ca^{2+} + 2\ H_4SiO_4 + 2\ H_2O$	46.90 [6]
C-S-H(0.8)	$0.8CaO \cdot SiO_2 \cdot 2.2H_2O + 1.6\ H^+ \rightarrow 0.8\ Ca^{2+} + H_4SiO_4 + H_2O$	11.08 [6]
C-S-H(1.1)	$1.1CaO \cdot SiO_2 \cdot 3.9H_2O + 2.2\ H^+ \rightarrow 1.1\ Ca^{2+} + H_4SiO_4 + 3\ H_2O$	16.72 [6]
C-S-H(1.7)	$1.7CaO \cdot SiO_2 \cdot 2.617H_2O + 3.4\ H^+ \rightarrow 1.7\ Ca^{2+} + H_4SiO_4 + 2.317\ H_2O$	29.52 [2]
C-S-H(1.8)	$1.8CaO \cdot SiO_2 \cdot 5.2H_2O + 3.6\ H^+ \rightarrow 1.8\ Ca^{2+} + H_4SiO_4 + 5\ H_2O$	32.60 [6]
Jennite	$1.5CaO \cdot 0.9SiO_2 \cdot (OH)_{4.8} \cdot 0.9H_2O + 3\ H^+ \rightarrow 1.5\ Ca^{2+} + 0.9\ H_4SiO_4 + 2.1\ H_2O$	26.40 [4]
Tobermorite	$2CaO \cdot 2.4SiO_2 \cdot 4H_2O + 4\ H^+ \rightarrow 2\ Ca^{2+} + 2.4\ H_4SiO_4 + 1.2\ H_2O$	27.81 [4]
AFm phases		
C_4AH_{13}	$2CaO \cdot Al_2O_3 \cdot 13H_2O + 14\ H^+ \rightarrow 4\ Ca^{2+} + 2\ Al^{3+} + 20\ H_2O$	104.42[4]
C_4AH_{19}	$4CaO \cdot Al_2O_3 \cdot 19H_2O + 14\ H^+ \rightarrow 4\ Ca^{2+} + 2\ Al^{3+} + 26\ H_2O$	100.60[2]
C_4FH_{13}	$2CaO \cdot Fe_2O_3 \cdot 13H_2O + 14\ H^+ \rightarrow 4\ Ca^{2+} + 2\ Fe^{3+} + 20\ H_2O$	99.50 [4]
C_2AH_8	$2CaO \cdot Al_2O_3 \cdot 8H_2O + 10\ H^+ \rightarrow 2\ Ca^{2+} + 2\ Al^{3+} + 13\ H_2O$	60.43 [4]
C_2FH_8	$2CaO \cdot Fe_2O_3 \cdot 8H_2O + 10\ H^+ \rightarrow 2\ Ca^{2+} + 2\ Fe^{3+} + 13\ H_2O$	55.51 [4]
C_2ASH_8	$2CaO \cdot Al_2O_3 \cdot SiO_2 \cdot 8H_2O + 10\ H^+ \rightarrow 2\ Ca^{2+} + 2\ Al^{3+} + H_4SiO_4 + 11\ H_2O$	49.35 [4]
C_2FSH_8	$2CaO \cdot Fe_2O_3 \cdot SiO_2 \cdot 8H_2O + 10\ H^+ \rightarrow 2\ Ca^{2+} + 2\ Fe^{3+} + H_4SiO_4 + 11\ H_2O$	44.44 [4]

$C_4AS'H_{12}$	$3CaO\cdot Al_2O_3\cdot CaSO_4\cdot 12H_2O + 12 H^+ \rightarrow 4 Ca^{2+} + SO_4^{2-} + 2 Al^{3+} + 18 H_2O$	74.29 [4]
Cr-monosulphate	$3CaO\cdot Al_2O_3\cdot CaSO_4\cdot 15H_2O + 12 H^+ \rightarrow 4 Ca^{2+} + CrO_4^{2-} + 2 Al^{3+} + 21 H_2O$	71.62 [7]
$C_4FS'H_{12}$	$3CaO\cdot Fe_2O_3\cdot CaSO_4\cdot 12H_2O + 12 H^+ \rightarrow 4 Ca^{2+} + SO_4^{2-} + 2 Fe^{3+} + 18 H_2O$	69.37 [4]
$C_4AC'H_{11}$	$3CaO\cdot Al_2O_3\cdot CaCO_3\cdot 11H_2O + 12 H^+ \rightarrow 4 Ca^{2+} + CO_3^{2-} + 2 Al^{3+} + 17 H_2O$	70.52 [4]
$C_4FC'H_{11}$	$3CaO\cdot Fe_2O_3\cdot CaCO_3\cdot 11H_2O + 12 H^+ \rightarrow 4 Ca^{2+} + CO_3^{2-} + 2 Fe^{3+} + 17 H_2O$	65.60 [4]
$C_4AC'_{0.5}H_{12}$	$3CaO\cdot Al_2O_3\cdot 0.5Ca(OH)_2\cdot 0.5CaCO_3\cdot 11.5H_2O + 13 H^+ \rightarrow 4 Ca^{2+} + 0.5 CO_3^{2-} + 2 Al^{3+} + 18.5 H_2O$	86.23 [4]
$C_4FC'_{0.5}H_{12}$	$3CaO\cdot Fe_2O_3\cdot 0.5Ca(OH)_2\cdot 0.5CaCO_{30.5}\cdot 11.5H_2O + 13 H^+ \rightarrow 4 Ca^{2+} + 0.5 CO_3^{2-} + 2 Fe^{3+} + 18.5 H_2O$	85.63 [4]
Fiedel's salt	$3CaO\cdot Al_2O_3\cdot CaCl_2\cdot 10H_2O + 12H^+ \rightarrow 4 Ca^{2+} + 2 Al^{3+} + 2Cl^- + 16 H_2O$	72.04 [6]
Kuzel's salt	$3CaO\cdot Al_2O_3\cdot 0.5CaCl_2\cdot 0.5CaSO_4\cdot 12H_2O + 12H^+ \rightarrow 4 Ca^{2+} + 2 Al^{3+} + Cl^- + 0.5 SO_4^{2-} + 18 H_2O$	71.94 [6]
AFt phases		
Cl-ettringite	$3CaO\cdot Al_2O_3\cdot 3CaCl_2\cdot 30H_2O + 12H^+ \rightarrow 6 Ca^{2+} + 2 Al^{3+} + 6 Cl^- + 36H_2O$	56.84 [6]
Cr-ettringite	$3CaO\cdot Al_2O_3\cdot 3CaCrO_4\cdot 32H_2O + 12 H^+ \rightarrow 6 Ca^{2+} + 2 Al^{3+} + 3 CrO_4^{2-} + 38 H_2O$	60.54 [7]
Fe-ettringite	$3CaO\cdot Fe_2O_3\cdot 3CaSO_4\cdot 32H_2O + 12 H^+ \rightarrow 6 Ca^{2+} + 2 Fe^{3+} + 3 SO_4^{2-} + 38 H_2O$	51.98 [4]
Tricarboaluminate	$3CaO\cdot Al_2O_3\cdot 3CaCO_3\cdot 32H_2O + 12 H^+ \rightarrow 6 Ca^{2+} + 2 Al^{3+} + 3 CO_3^{2-} + 38 H_2O$	60.69 [4]
(Hydro)garnets		
C_3AS_3	$3CaO\cdot Al_2O_3\cdot 3SiO_2 + 12 H^+ \rightarrow 3 Ca^{2+} + 2 Al^{3+} + 3 H_4SiO_4$	52.55 [6]
C_3AH_6	$3CaO\cdot Al_2O_3\cdot 6H_2O + 12 H^+ \rightarrow 3 Ca^{2+} + 2 Al^{3+} + 12 H_2O$	79.53 [4]
$C_3AS_{0.5}$	$3CaO\cdot Al_2O_3\cdot 0.5SiO_2\cdot 5H_2O + 12 H^+ \rightarrow 3 Ca^{2+} + 2 Al^{3+} + 0.5 H_4SiO_4 + 10 H_2O$	74.12 [6]
C_3ASH_4	$3CaO\cdot Al_2O_3\cdot SiO_2\cdot 4H_2O + 12 H^+ \rightarrow 3 Ca^{2+} + 2 Al^{3+} + H_4SiO_4 + 8 H_2O$	69.37 [6]
C_3FH_6	$3CaO\cdot Fe_2O_3\cdot 6H_2O + 12 H^+ \rightarrow 3 Ca^{2+} + 2 Fe^{3+} + 12 H_2O$	74.61 [4]
CAH_{10}		
CAH_{10}	$CaO\cdot Al_2O_3\cdot 10H_2O + 8 H^+ \rightarrow Ca^{2+} + Al^{3+} + 14 H_2O$	38.51 [4]
Mg phases		
Hydrotalcite	$Mg_4Al_2(OH)_{14}\cdot 3H_2O + 14 H^+ \rightarrow 2 Al^{3+} + 4 Mg^{2+} + 17 H_2O$	73.96 [4]
CO_3-hydrotalcite	$Mg_4Al_2(OH)_{12}\cdot CO_3\cdot 2H_2O + 12 H^+ \rightarrow 4 Mg^{2+} + CO_3^{2-} + 2 Al^{3+}$	50.85 [4]
Other phases		
Akermanite	$Ca_2MgSi_2O_7 + 6 H^+ + H_2O \rightarrow 2 Ca^{2+} + Mg^{2+} + 2 H_4SiO_4$	46.08 [5]
Anorthite	$CaAl_2Si_2O_8 + 8 H^+ \rightarrow Ca^{2+} + 2 Al^{3+} + 2 H_4SiO_4$	25.31 [5]
CA	$CaO\cdot Al_2O_3 + 8 H^+ \rightarrow Ca^{2+} + 2 Al^{3+} + 4 H_2O$	45.73 [2]
CA_2	$CaO\cdot 2Al_2O_3 + 14 H^+ \rightarrow Ca^{2+} + 4 Al^{3+} + 7 H_2O$	61.77 [2]
C_2S	$2CaO\cdot SiO_2 + 4 H^+ \rightarrow 2 Ca^{2+} + H_4SiO_4$	38.82 [2]
C_3S	$3CaO\cdot SiO_2 + 6 H^+ \rightarrow 3 Ca^{2+} + H_4SiO_4 + H_2O$	73.66 [2]
C_3A	$3CaO\cdot Al_2O_3 + 12 H^+ \rightarrow 2 Al^{3+} + 3 Ca^{2+} + 6 H_2O$	113.05[6]
C_4AF	$4CaO\cdot Al_2O_3\cdot Fe_2O_3 + 20 H^+ \rightarrow 2 Al^{3+} + 2 Fe^{3+} + 4 Ca^{2+} + 10 H_2O$	140.51[6]
$C_{12}A_7$	$12CaO\cdot 7Al_2O_3 + 66 H^+ \rightarrow 12 Ca^{2+} + 14 Al^{3+} + 33 H_2O$	487.20[2]
Ca oxychloride	$3CaO\cdot CaCl_2\cdot 16H_2O + 6 H^+ \rightarrow 4 Ca^{2+} + 2Cl^- + 19 H_2O$	68.75 [6]
Ca zincate	$CaZn_2(OH)_6\cdot 2H_2O + 6 H^+ \rightarrow Ca^{2+} + 2 Zn^{2+} + 8 H_2O$	43.90 [3]
Ca-zeolite P	$CaO\cdot Al_2O_3\cdot 2.6SiO_2\cdot 3.2H_2O + 8 H^+ \rightarrow Ca^{2+} + 2 Al^{3+} + 2.6 H_4SiO_4 + 2 H_2O$	20.20 [6]

Chabazite	$CaAl_2Si_4O_{12} \cdot 6H_2O + 8\ H^+ \rightarrow Ca^{2+} + 2\ Al^{3+} + 4\ H_4SiO_4 + 2\ H_2O$	13.63[6]
Forsterite	$Mg_2SiO_4 + 4\ H^+ \rightarrow 2\ Mg^{2+} + H_4SiO_4$	28.60[5]
Gehlenite	$Ca_2Al(AlSi)O_7 + 10\ H^+ \rightarrow 2\ Ca^{2+} + 2\ Al^{3+} + H_4SiO_4 + 3\ H_2O$	55.23[5]
Leucite	$KAl(SiO_3)_2 + 2\ H_2O + 4\ H^+ \rightarrow K^+ + Al^{3+} + 2\ H_4SiO_4$	6.42[3]
Merwinite	$Ca_3Mg(SiO_4)_2 + 8\ H^+ \rightarrow 3\ Ca^{2+} + Mg^{2+} + 2\ H_4SiO_4$	69.28[5]
Na-zeolite P	$Na_2O \cdot Al_2O_3 \cdot 2.6SiO_2 \cdot 3.2H_2O + 8\ H^+ \rightarrow Ca^{2+} + 2\ Al^{3+} + 2.6\ H_4SiO_4 + 2\ H_2O$	26.40[6]
$ZnFe_2O_4$	$ZnFe_2O_4 + 8\ H^+ \rightarrow Zn^{2+} + 2\ Fe^{3+} + 4\ H_2O$	9.85[1]
$ZnSiO_3$	$ZnSiO_3 + H_2O + H^+ \rightarrow Zn^{2+} + H_4SiO_4$	2.93[3]
Wairakite	$Ca \cdot Al_2Si_4O_{12} \cdot 2H_2O + 2\ H_2O + 8\ H^+ \rightarrow Ca^{2+} + 2\ Al^{3+} + 4\ H_4SiO_4$	18.87[3]
Wollastonite	$CaSiO_3 + H_2O + H^+ \rightarrow Ca^{2+} + H_4SiO_4$	12.99[3]

[1] Dijkstra et al., 2002 ; [2] U.S. Department of Energy, 2004; [3] Astrup et al., 2006; [4] Lothenbach and Winnefeld, 2006; [5] Blanc et al., 2007; [6] Hills, 2009; [7] Hyks et al., 2009

Table 11: Stability constants of the new mineral phases added to the standard thermodynamic database in Visual MINTEQ, based on the dissolution reactions reported

To improve the modelling predictions for trace metals, additional runs of the geochemical speciation program for selected cases were performed, accounting for the binding of trace metals onto the surface of hydrous ferric oxide (HFO). This was described using the diffuse layer model (DLM) proposed by Dzombak and Morel (1990) which is incorporated in the Visual Minteq code. The thermodynamic database for surface complexation was modified by increasing the log K of the complexation reaction of Pb onto high-capacity/low-affinity sites from 0.3 to 1.7, as suggested by Meima and Comans (1998) and also used by other investigators (see e.g. Martens et al., 2010). Surface sorption onto amorphous aluminum minerals (AAM), which have been demonstrated to have a binding capacity towards metal ions (Stumm and Morgan, 1995; Meima and Comans, 1998), was also taken into account by means of the same surface complexation model as before. Due to the lack of a consistent thermodynamic data set for complexation by AAM, HFO was used as a surrogate sorbent mineral for AAM, considering the similarities in the degree of coordination, charge and reactivity of Fe(III) and Al(III) in such (hydr)oxide forms (Meima and Comans, 1998); the same specific surface area and concentration of binding sites as HFO were used in the calculations, assuming a 1:1 molar equivalence between HFO and AAM. The measured leachate concentrations of Fe and Al at pH < 2 were taken as a measure of the total amount of HFO and AAM in the samples, as suggested by Engelsen et al. (2009). The amount available for sorption was estimated from low-pH eluates for trace metal cations and from alkaline pH leachates for Cr.

2.2 Production of geopolymeric materials from bottom ash

The aim of this experimental study is to investigate the feasibility to produce geopolymers starting from incinerator BA materials. Taking into account the relatively few experience of the research fiel the present study is addressed to identify the process, and corresponding process parameters, that could be applied to this material in order to obtain a good level of matrix geopolymerization. In addition, the investigation has been also addressed to better understand the geopolymer chemistry. The interest on geopolymers production starts from the assumption that this material could represent a new “raw material” for cement production or to replace use of binders because it possesses its own structural strength with no need of adding cement or any other blending material.

Bottom ash was selected as a potential candidate for the geopolymer production process on account of its composition, being assumed to provide Ca, Si and Al elements to the reacting medium. As reported in the introduction section, the last two elements are considered to be the most important in view of formation of the geopolymer network. BA pre-treatment involved ball-milling the dried as-received material to a final mean particle size below 425 μm taking into account that the finesses plays an important role in the development of mechanical strength in alkali-activated mixtures (Khale et al., 2007; Fernandez Jimenes and Palomo, 2003).

The alkaline activator used for geopolymerization included a sodium silicate solution (SiO_2 = 26.91%; Na_2O = 8.68%; SiO_2/Na_2O = 3.1 w/w) and an NaOH solution (10-15.5 M), which were mixed in different proportions to provide the desired reacting medium. Metakaolin (MK) was used to adjust the Si/Al ratio in the desired range of values; metakaolin was obtained from commercial-grade kaolin by calcination at 800°C for 2 hours in air. Milled BA was mixed with the alkaline activator at a solid-to-liquid (S/L) ratio of 4 kg/l except for pastes with the highest metakaolin content, where additional water was required to ensure a suitable workability, resulting in a S/L ratio of 3.3.

Different pastes were tested for the geopolymerization process by varying the Si/Al molar ratio (1.28-2.29) and the NaOH concentration (5-9 M) in the alkaline medium as a source of metallic cations to the dissolving medium, which are known to be required to attain a neutrally charged matrix during geopolymer synthesis (Table 12).

The first two steps (dissolution of solid alumino-silicate oxides, diffusion and transportation of dissolved Al and Si complex) of the geopolymerization process occur in the mixing stage (Feng et al., 2004).

The paste preparation procedure was performed as described below:

- preparation of the activator solution. This involved dissolving NaOH pellets in deionised water to reach the desired concentration. The strongly exothermic reaction required cooling the solution to ambient temperature before use. The NaOH solution was mixed with the Na silicate solution for 5 minutes using a magnetic stirrer at 600 rpm);
- hand-mixing of the dry BA and metakaolin for 2 minutes;
- hand-mixing for additional 7 minutes of the resulting dry mixture with previously blended Na silicate and NaOH solutions to obtain a homogeneous paste.

		Mixture components						Final values	
Name	Sample code	BA (g)	MK (g)	Na silicate sol. (ml)	NaOH sol. (M)	NaOH sol. (ml)	S/L ratio (g/ml)	Si/Al (mol/mol)	NaOH (M)
A	S-2.29-6	15.8	4.2	3	15	2	4	2.29	6
B	S-1.69-6	11.7	8.3	3	15	2	4	1.69	6
C	S-1.28-6	4.6	15.4	3.5	14.5	2.5	3.3	1.28	6
D	S-2.29-9	16.2	3.8	2	15	3	4	2.29	9
E	S-1.69-9	12.3	7.7	2	15	3	4	1.69	9
F	S-1.28-9	5.7	14.3	2.5	15.5	3.5	3.3	1.28	9
G	S-2.29-12	16.7	3.3	1	15	4	4	2.29	12
H	S-1.69-12	13	7	1	15	4	4	1.69	12
I	S-1.28-12	7.2	12.8	1	14.5	5	3.3	1.28	12
J	S-2.29-5	16	4	2.5	10	2.5	4	2.29	5
L	S-1.69-5	12	8	2.5	10	2.5	4	1.69	5
M	S-1.28-5	5.2	14.8	3	10	3	3.3	1.28	5
O	S-2.29-7.5	16	4	2.5	15	2.5	4	2.29	7.5
P	S-1.69-7.5	12	8	2.5	15	2.5	4	1.69	7.5
Q	S-1.28-7.5	5.2	14.8	3	15	3	3.3	1.28	7.5

Table 12: Compositional characteristics of mixtures used for geopolymer synthesis

The resulting pastes were cast in 20-mm diameter, 45-mm height cylindrical steel moulds (Fugure 13) manually compacted with a steel piston to reduce the presence of voids in the specimen, and de-moulded afterwards.

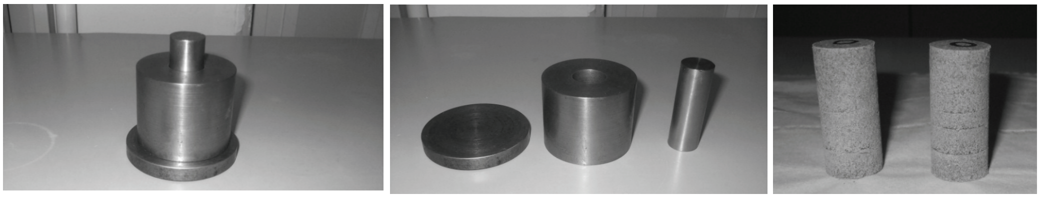

Figure 13: Cylindrical steel moulds and geopolymer samples obtained

The cylindrical specimens were transferred to an oven where they were heated at 75°C for 24 hours; such operating values were selected on the basis of the results from preliminary tests. After the heat treatment the specimens were wrapped in parafilm foils to prevent oxidation, carbonation and evaporation, and cured at room temperature for 7, 28 and 56 days. After the selected curing times, the products were tested for physical, mechanical, mineralogical, microstructural and leaching properties.

Physical and mechanical characterization involved triplicate measurements of unconfined compressive strength (UCS). On the basis of the results obtained for mechanical strength, a number of representative samples were also characterized in terms of wet apparent unit weight (measured on the humid sample using the volume displacement principle), total porosity and solids unit weight (pycnometric measurement), mineralogical and microstructural characteristics, in order to better understand the unfold of the geopolymerization process (see Table 13). These selected samples are:

- samples S-2.29-7.5 and S-2.29-5 (which gave the best results in terms of UCS), characterized by the same Si/Al molar ratio (2.29) and different NaOH molar concentrations in the alkaline solution (7.5 and 5 M respectively);
- samples S-1.69-7.5 and S-1.28-7.5 (which yielded the lowest UCS values), with the same NaOH concentration as that of sample S-2.29-7.5, but with a different Si/Al molar ratios (1.69 for sample S-1.69-7.5 P and 1.27 for sample S-1.28-7.5).

Mineralogy and microstructure were investigated through SEM/EDAX, FT-IR, XRD, RAMAN spectroscopy and TGA/DTA analyses; while SEM observations were carried out on specimen fragments obtained from mechanical testing, the other analytical techniques were applied on powdered samples.

SEM analyses was conducted using a Phillips XL- 30 microscope with an operating voltage of 25 kV a spot size of 200 nm; a tilt angle of 35°; a take-off angle of 61.34°, equipped with an energy dispersive EDAX DX-4 spectrometer set with a count rate of about 1200 cps and a live time of 50 s). The samples were first impregnated with an ultra-low viscosity resin and then polished. A carbon film (about 3 nm) was deposited onto the polished surfaces of samples under vacuum to prevent charging.

FT-IR absorbance spectra were collected with an Impact 420 Nicolet instrument in the wavenumber range 400–4000 cm^{-1} with a resolution of 4 cm^{-1} on pellets with KBr.

The X-Ray Diffraction (XRD) analysis was performed using a Siemens D 501 diffractometer with Cu Kα radiation scanning the unoriented powder solids from 20 to 80° 2θ with a 0.04 2θ step interval and a 1 s per step counting. Raman spectra were collected between 100 and 1800 cm^{-1} using using an Horiba Jobin Yvon LABRAM Infinity spectrometer coupled with an Olympus BX 40 microscope and equipped with an optical notch filter, a charge coupled device detector, and a 20mW He–Ne laser standard HR 800 (k = 632.817 nm).

Simultaneous TGA/DTA analyses were performed at a heating rate of 10 °C/min in static air over a temperature range of 20–1000°C.

Name		O		J		P		Q		BA
Sample code		S-2.29-7.5		S-2.29-5		S-1.69-7.5		S-1.28-7.5		
Curing time		7	28	7	28	7	28	7	28	
Physical Charact.		x		x		x		x		
SEM/EDX	(piece)	x		x	x					
	(powder)	x		x		x		x		x
TGA/DTA	(powder)	x		x		x		x		
XRD	(powder)	x		x		x		x		x
ANC	(powder)	x		x		x		x		x
Raman	(powder)	x	x	x	x	x	x	x	x	x
FT-IR	(powder)	x	x	x	x	x	x	x	x	x

Table 13: Samples selected for microstructural and leaching characterization

The EN 14429 (acid neutralization capacity, ANC) leaching test was applied after mechanical strength testing on ball-milled (<425 μm) specimens to evaluate the pH-dependent leaching of the main trace metals (Zn, Cr, Cu, Ni and Pb) from the geopolymeric matrices to infer on metal immobilization yield. This test was conducted on the same samples characterized in terms of microstructure at 7-day curing; the leaching for samples cured for longer periods was not investigated assuming that for geopolymeric materials a period of 7 days was long enough to allow for the most relevant mineralogical transformations to occur.

References

- ✓ ASTM C109/C109 M: Test Method for Compressive Strength of Hydraulic Cement Mortars, DOI: 10.1520/C0109_C0109M-08.
- ✓ T. Astrup, J. Dijkstra, R.N.J. Comans, H.A. van der Sloot, T.H. Christensen: Geochemical modelling of leaching from MSWI air-pollution-control residues; Environmental Science & Technology (2006) 40: 3551-3557.
- ✓ P. Blanc, A. Lassin, C. Nowak, A. Burnol, P. Piantone, L. Chateau: THERMODDEM: a thermodynamic database for waste materials; Available on-line at http://thermoddem.brgm.fr/ fichiers/Phreeqc_thermoddem_lvl1_no-org.txt (2007).
- ✓ G.E. Box, S.J. Hunter, W.G. Hunter: Statistics for Experimenters. Design, Innovation and Discovery. Second edition, John Wiley & Sons, Hoboken, New Jersey (2005)CEN/TS 14429: Characterization of waste - Leaching Behaviour Tests – Influence of pH on leaching with initial acid/base addition; European Committee for standardization; Management Centre Brussels (October 2005).
- ✓ Council Directive 99/31/EC, 1999. Landfill of waste. Official Journal L 182, 16/07/1999, 0001-0019.
- ✓ U.S. Department of Energy: Qualification of thermodynamic data for geochemical modeling of mineral-water interactions in dilute systems, document no. ANL-WIS-GS-000003 (2004).
- ✓ J.J. Dijkstra, H.A. van der Sloot, R.N.J. Comans: Process identification and model development of contaminant transport in MSWI bottom ash; Waste Management (2002) 22: 531-541.
- ✓ D.A. Dzombak and F.M.M. Morel: Surface complexation modeling: hydrous ferric oxide; John Wiley & Sons, Inc., New York (1990).
- ✓ C.J. Engelsen, H.A. van der Sloot, G. Wibetoe, G. Petkovic: Release of major elements from recycled concrete aggregates and geochemical modeling; Cement and Concrete Research (2009) 39: 446-459.
- ✓ Y. Fan, S. Yin, Z. Wen, J. Zhong: Activation of fly ash and its effects on cement properties; Cement and Concrete Research.(1999) 29: 467-472.
- ✓ D. Feng, H. Tan, J.S.J. van Deventer: Ultrasound enhanced geopolymerisation; Journal of Materials Science (2004) 39: 571-580.
- ✓ A. Fernandez-Jiménez and A. Palomo: Characterisation of fly ashes Potential reactivity as alkaline cements; Fuel (2003) 82: 2259-2265.

- ✓ P. Filipponi, A. Polettini, R. Pomi, P. Sirini: Physical and mechanical properties of incineration bottom ash-based cements; Waste Managegement (2003) 23: 145-156.
- ✓ C. Giampaolo, S. Lo Mastro, A. Polettini, R. Pomi, P. Sirini,: Acid neutralization capacity and hydration behavior of incineration bottom ash–Portland cement mixtures; Cement and Concrete Research (2002) 32: 769-775.
- ✓ G.K. Glass and N.R. Buenfeld: Differential acid neutralization analysis; Cement and Concrete Research. (1999) 29: 1681.
- ✓ C.D. Hills,: Personal communication. University of Greenwich (2009).
- ✓ J. Hyks, T. Astrup, T.H. Christensen: Long-term leaching from MSWI air pollution control residues: leaching characterization and modeling; Journal of Hazardous Materials (2009) 162: 80-91.
- ✓ D. Khale and R. Chaudhary: Mechanism of geopolymerization and factors influencing its development: a review; Journal of Materials Science (2007) 42: 729-746.
- ✓ B. Lothenbach and F. Winnefeld: Thermodynamic modeling of the hydration of Portland cement; Cement and Concrete Research (2006) 36: 209-226.
- ✓ E. Martens, D. Jacques, T. Van Gerven, L. Wang, D. Mallants: Geochemical modeling of leaching of Ca, Mg, Al, and Pb from cementitious waste forms; Cement and Concrete Research (2010) 40: 1298-1305.
- ✓ Ministero dell'Ambiente della Repubblica Italiana, 1998. D.M. 05/02/1998. Individuazione dei rifiuti non pericolosi sottoposti alle procedure semplificate di recupero ai sensi degli articoli 31 e 33 del decreto legislativo 5 febbraio 1997, n. 22. Suppl. Ord. G.U. 16/04/1998 n. 88 (as amended by D.M. 05/04/2006, n. 186).
- ✓ J.A. Meima and R.N.J. Comans: Application of surface complexation/precipitation modeling to contaminant leaching from weathered municipal solid waste incinerator bottom ash; Environmental Science and Technology (1998) 32: 688-693.
- ✓ D.C. Montgomery: Design and Analysis of the Experiments. Sixth edition; John Wiley & Sons, Hoboken, New Jersey (2005).
- ✓ B. Pacewska, I. Wilinska, G. Blonkowski: Investigations of cement early hydration in the presence of chemically activated fly ash; Journal of Thermal Analysis and Calorimetry (2008) 93: 769-776.
- ✓ A. Polettini, R. Pomi, P. Sirini, F. Testa: Properties of Portland cement-stabilized MSWI fly ashes; Journal of Hazardous Materials B (2001) 88: 123-138.

✓ A. Polettini, R. Pomi, G. Carcani: The effect of Na and Ca salts on MSWI bottom ash activation for reuse as a pozzolanic admixture; Resources, Conservation and Recycling (2005) 43: 404-418.

✓ A. Polettini, R. Pomi, E. Fortuna: Chemical activation in view of MSWI bottom ash recycling in cement-based systems; Journal of Hazardous Materials (2009) 162: 1292-1299.

✓ X. Pu: Investigation on pozzolanic effect of mineral additives in cement and concrete by specific strength index; Cement and Concrete Research (1999) 29: 951-955.

✓ J. Qian, C. Shi, Z. Wang: Activation of blended cements containing fly ash; Cement and Concrete Research (2001) 31: 1121-1127.

✓ X.C. Qiao, M. Tyrer, C.S. Poon, C.R. Cheeseman: Novel cementitious materials produced from incinerator bottom ash; Resources, Conservation and Recycling (2008) 52: 496-510.

✓ X.C. Qiao, C.R. Cheeseman, C.S. Poon: Influences of chemical activators on incinerator bottom ash; Waste Management (2009) 29: 544-549.

✓ C. Shi and R.L. Day: Acceleration of the reactivity of fly ash by chemical activation; Cement and Concrete Research (1995) 25: 15-21.

✓ C. Shi and R.L. Day . Pozzolanic reaction in the presence of chemical activators Part I Reaction kinetics; Cement and Concrete Research (2000 (a)) 30: 51-58.

✓ C. Shi and R.L. Day: Pozzolanic reaction in the presence of chemical activators. Part II. Reaction products and mechanism; Cement and Concrete Research (2000 (b)) 30: 607-613.

✓ C. Shi and R.L. Day: Comparison of different methods for enhancing reactivity of pozzolans; Cement and Concrete Research. (2001) 31: 813-818.

✓ W. Stumm and J.J. Morgan: Aquatic Chemistry: Chemical Equilibria and Rates in Natural Waters; third ed., John Wiley & Sons, Inc., New York (1995).

✓ UNI EN 12457-2:2004: Characterisation of waste - Leaching - Compliance test for leaching of granular waste materials and sludges - Part 2: One stage batch test at a liquid to solid ratio of 10 l/kg for materials with particle size below 4 mm (without or with size reduction), 2004-10-01.

3. Results and Discussion: Bottom ash characterization

Fresh bottom ash was sampled at the exit of the quenching unit, homogenized by quartering (Figure 14 (a)), and dried at 60°C (until constant weight, about 48 hours) (Figure 14 (b) and (c)).

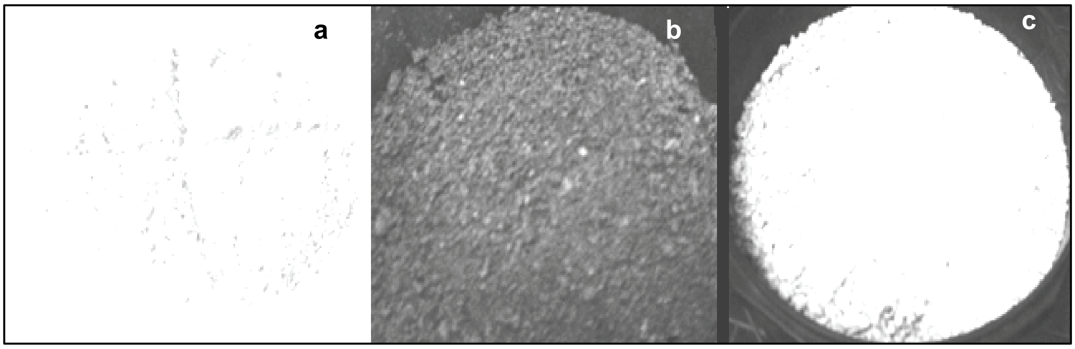

Figure 14: quartering (a), wet sample (b), dry sample (c)

During quartering the coarse fractions with a size between 15 and 40 cm were separated by hand. The total amount of these fractions, mainly composed by coarse glass, plastics and metal objects, accounted for about 6% wt of the materials for each BA sample and was discarded for the subsequent treatment. The humidity was also determinate for both samples; Sample 1 resulted more humid than Sample 2: 25.54% versus 14.67% respectly.

3.1 Size classification

The bottom ash were sieved into several size classes to identify the particle size distribution shown in Figure 15 a for sample 2. After sieving, 4 classes were separated from both samples: class A [12.5>Φ>5.6 mm], class B [5.6>Φ>2mm], class C [2>Φ>0.425mm] and class DE [Φ<0.425 mm]. Class C was more aboundant in Sample 1 than in Sample 2 (47 wt% and 36 wt% respectively). All the other classes, instead, were more abundant in sample 2: class A 15 wt% in Sample 2 versus 10 %wt in Sample 1, class B 36 wt% in Sample 2 versus 35 wt% in Sample 1 and class DE 13 wt% versus 9 wt%. Only for Sample 1 the finer fraction (DE) was also separated in two parts: class D [0.425>Φ>0.150 mm], accounted for about 6 wt%, and class E [Φ<0.150 mm], accounted for about 3 wt%. Considering the three coarse fractions (A, B, C) together (CF), they represent 91 wt% of Sample 1 and 87 wt% of Sample 2. Class DE, that rapresents the fine fraction (FF) of the material was equal to 9 wt% of Sample 1 and 13 wt% of Sample 2.

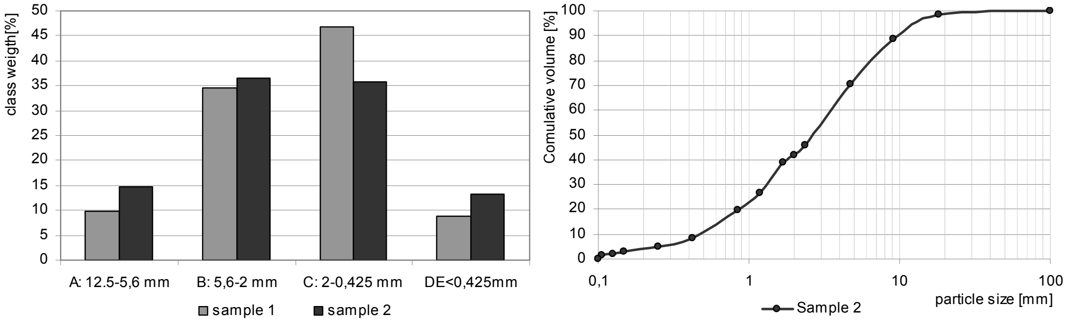

Figure 15: particle size distribution for Sample 2, comparison of class weights between Sample 1 and Sample 2

3.2 LOI determination

The LOI for CF was equal to 19.70% for Sample 1 and 5.08% for Sample 2. Conversely for FF the LOI value of Sample 1 was lower than for Sample 2, (11.24% and 14.11% respectively). In addition while for Sample 1 the LOI value of CF was higher than the LOI of FF in the case of sample 2 the trend is opposite.

In particular, the LOI values measured for the CF of Sample 2 were in good agreement with the results of other studies (Izquierdo et al., 2002; Giampaolo et al., 2002), and the relatively high values measured for the FF could be associated with chemically bound water in hydroxide species, carbonates and with organic matter. In order to confirm this last results the carbonates were also measured. The carbonate values measured were around 10% for CF and about 14% for FF.

3.3 Elemental Composition

The elemental composition and anion content of the size classes for both samples are reported in Table 14. The corresponding values for the combined classes are also reported to highlight the contribution of each size class to the chemical composition of the original sample.

	Concentration (mg/kg) ± std. error (%)					
	Sample 1			Sample 2		
Element /Anion	**CF**	**FF**	**CF+FF**	**CF**	**FF**	**CF+FF**
Al	59691 ± 8%	44051 ± 6%	58322 ± 8%	41836 ± 2%	37142 ± 2%	41213 ± 2%
As	2.1 ± 25%	1.2 ± 26%	2.0± 25%	3.6 ± 6%	2.3 ± 6%	3.4 ± 6%
Ca	248567 ± 9.0%	272715 ± 11%	250680 ± 10%	271073 ± 6%	299977 ± 13%	274910 ± 7%
Cd	25.2 ± 25%	14.0 ± 25%	23.2 ± 25%	4.6 ± 25%	32.0 ± 25%	8.3 ± 15%
Cr	478 ± 4%	517 ± 4%	481 ± 4%	368 ± 4%	510 ± 1%	387 ± 4%
Cu	6278 ± 21%	6790 ± 18%	6322 ± 19%	6021 ± 17%	4920 ± 9%	5875 ± 16%
Fe	18467 ± 16%	17725 ± 19%	18401 ± 17%	29398 ± 3%	2925 ± 4%	29377 ± 3%
K	5110 ± 11%	4470 ± 5%	5054 ± 11%	3935 ± 2%	3440 ± 1%	3869 ± 2%
Mg	18029 ± 9%	17829 ± 6%	18011 ± 8%	18820 ± 5%	19627 ± 2%	18927 ± 4%
Mn	488 ± 6%	490 ± 4%	488 ± 6%	706 ± 5%	778 ± 5%	715 ± 5%
Mo	12.8 ± 11%	14.4 ± 14%	24.0 ± 15%	30.2 ± 3%	31.4 ± 10%	30.4 ± 4%
Na	17851 ± 20%	14695 ± 17%	17575 ± 20%	17630 ± 1%	16619 ± 3%	17496 ± 1%
Ni	110 ± 21%	152 ± 13%	114 ± 19%	171 ± 22%	186 ± 19%	173 ± 22%
Pb	3064 ± 18%	4235 ± 25%	3166 ± 19%	1318 ± 11%	1931 ± 17%	1399 ± 12%
Sb	39.5 ± 25%	34.8 ± 22%	39.0 ± 25%	130 ± 16%	187 ± 9%	137 ± 15%
Si	104422 ± 21%	66640 ± 25%	101115 ± 25%	154076 ± 3%	120359 ± 6%	149600 ± 3%
Zn	2194 ± 17%	1964 ± 13%	2173 ± 17%	6363 ± 7%	4949 ± 2%	6175 ± 6%
Cl^-	22522 ± 5%	17865 ± 7%	22114 ± 6%	48718 ± 5%	91688 ± 4%	54423 ± 5%
SO_4^{2-}	11912 ± 8%	10331 ± 1%	11773 ± 7%	2416 ± 5%	15058 ± 2%	4095 ± 5%

Table 14: Bottom ash elemental composition for CF, FF and CF+FF for Sample 1 and Sample 2

The elemental composition was similar for both samples analyzed. Considering the total sample, the main differences were related to the concentrations of heavy metals. Sample1 was richer by about 48% in Cd, about 11% in Cr and about 39% in Pb. The Cu concentration was very similar for both classes, with a difference by 4% more in Sample 1. Conversely sample 2 was richer in Ni (about 21%) and in Zn (about 48%). Considering the main constituents, in particular Al, Ca and Si: Sample 1 presented 17% more of Al than Sample 2, that was 5% and 19% richer in Ca and Si respectively.

Other differences among the two samples were the concentrations of sulphate and chloride: the former was more abundant in Sample 1 (by about 48%) while the latter in Sample 2 (by about 42%).

A comparison between the CF and the FF, for each sample, confirms the results of a previous study (Chimenos et al., 2003) which indicated a larger amount of heavy metals in the FF in comparison to the CF. This result was valid for all trace metals in Sample 1 except for Zn, while for all metals in Sample 2 except for Zn and Cu.

Sample 1 was used to test different types of alkaline activators to promote the pozzolanic reactions and the performance of BA when used to produce blended cement. For this experimental study, it was decided to test separately the CF and the FF, starting from the assumption that the FF was more reactive than the CF. The different results obtained especially in terms of mechanical strength were studied in order to better understand if the differences in the original particle size and composition can play a key role in the performance of the final products obtained. At the end of the experimental study some tests were also conducted using the combined material (CF+FF) testing only on the best conditions identified.

Sample 2 was used for a preliminary study on geopolymer materials production. The main elements relevant for the geopolymerization process are Si, Al and Ca. These three main elements were present at similar concentrations in both classes, even if the CF was richer in Si and Al (154.08 and 41.84 g/kg respectively) than the FF (120.36 and 37.14 g /kg) and less abundant in Ca (271.07 g/kg for CF versus 299.98 for FF). Also the Fe, Na, K, Mg and Mn concentrations appeared to be equally distributed among the two classes. Taking these observations into account, with a view to a possible future industrial application it may be judged more appropriate to use BA without any preliminary size separation. The combination of CF and FF presented, in terms of the main oxides of concern, the following concentrations: 15.57% of Al_2O_3, 32.06% of SiO_2 and 38.47% of CaO. These values were judged to be satisfactory in view of the application for geopolymers production. In addition, the FF in the original sample was present in quite a low amount and, even if this fraction was richer in heavy metals, its larger fineness could have a good effect on improving the mechanical strength of the geopolymer materials.

3.4 EN 12457-2 test

The results of the EN 12457-2 compliance test indicated that both size fractions of each sample were alkaline in nature, with a pH ranging between 12.4 and 12.9 (see Table 15). These clearly alkaline characteristics were due to the large presence of alkaline metal oxides that, during an hydrolysis process, are transformed into hydroxides like portlandite ($Ca(OH)_2$) (Johnson et al., 1995), as confirmed also through the high LOI values measured that, as already explained, are related to the hydroxide and carbonates content in the materials.

Element	Concentration (mg/l)							
	pH		**Cd**		**Cr**		**Cu**	
	Sample 1	Sample 2	Sample 1	Sample 2	Sample 1	Sample 2	Sample 1	Sample 2
CF	12.56	12.40	<0.0005	<0.0005	0.01	0.01	0.02	*0.26*
FF	12.67	12.88	<0.0005	<0.0005	*0.06*	0.02	0.09	0.09
CF+FF	12.71	11.84	<0.0005	n.a.	0.04	0.02	0.08	0.06
EU LD (hazardous waste)			**0.2**		**7**		**10**	
EU LD (non hazar. waste)			**0.0129**		**1**		**5**	
EU LD (inert waste)			*0.004*		*0.05*		*0.20*	
DM 05/02/1998 (reuse)	5.5÷12.0		0.005		0.05		0.05	
Detection limit			0.0005		0.002		0.002	

Element	**Ni**		**Pb**		**Zn**	
	Sample 1	Sample 2	Sample 1	Sample 2	Sample 1	Sample 2
CF	0.004	0.01	***2.11***	*0.32*	0.09	*0.45*
FF	0.01	<0,002	***5.89***	***2.1***	0.11	*0.47*
CF+FF	0.03	<0,002	***2.52***	0.04	0.06	0.06
EU LD (hazardous waste)			**5.0000**		**20**	
EU LD (non hazar. waste)			**1.0000**		**5**	
EU LD (inert waste)	---		*0.05*		*0.40*	
DM 05/02/1998 (reuse)	0.01		0.05		3.00	
Detection limit	0.002		0.002		0.02	

Table 15: Comparison between EN 12457-2 test results (natural pH) and regulatory limits for selected heavy metals of both BA samples

For both samples and all fractions analyzed Pb was highly mobile. The leachate concentrations were found to be above the limit established by the EU regulation for non-hazardous waste landfills for CF and CF+FF of Sample 1 and FF of Sample 2, while the concentration for FF of Sample 1 was even above the limit for hazardous waste landfills. For Sample 2 CF and the combination of CF and FF were above the limits for inert waste landfills.

Zn showed for all classes of Sample 2 leachate concentrations above the limit established by the EU regulation for inert waste landfills, while for all the fractions of Sample 1 the values measured were all below the regulatory limits. The Cu leachate concentration for both Samples 1 and 2 was higher than the Italian limit for reuse, while the CF of Sample 2 showed a value above the limit established by the EU regulatory for inert waste landfills.

The Ni concentrations in the leachate from FF of Sample 1 and CF of Sample 2 showed values equal to the Italian regulatory limit for waste reuse. The Cr concentration in the eluate from the FF of Sample 1 was above the Italian regulatory limit for reuse while all the other fractions analysed for both samples were all below all the regulatory limits. Finally the Cd concentrations were always below the detection limit.

3.5 ANC TEST

For Sample 1 the ANC test was conducted separately for each size class analysed: class A [12.5>Φ>5.6 mm], class B [5.6>Φ>2mm], class C [2>Φ>0.425mm], class D [0.425>Φ>0.150 mm] and class E [Φ<0.150 mm].

For Sample 1 (see Figure 16) notably different acid neutralization behaviours were observed for the five size classes investigated. Differences in the titration curves were evident in both the pH values at which the plateaus occurred and in the amount of acid required to reach specific pH values. In terms of total acid neutralization capacity, fraction E followed by fraction D displayed the strongest total buffering behavior, while the weakest value was presented by fraction A. Fractions B and C, although starting from different natural pHs, showed similar trends of the titration curves. Fraction E also displayed a pH plateau of appreciable width at a pH of ~7, indicating the presence of a specific buffering phase in this pH region.

For Sample 2 the ANC test was conducted on theCF, FF and CF+FF fractions. As it is shown in Figure 16, the ANC curves obtained for the CF and the CF + FF had a very similar buffering behavior. This result confirms the low influence of FF on the mixture due mainly to its small amount. As obtained also in the ANC analysis of Sample 1 the strongest buffering capacity was shown by the finer fraction. In particular, the titration curve for the FF of Sample 2 resembled the curve for fraction D of Sample 1 (Figure 16).

Concerning metal leaching, the concentrations in the leachates from Sample 1 (Figure 17) were appreciably different for the various size fractions only in the case of Cr, for which the finer classes were found to displayed a higher release particularly at pHs above 6. For the other metals the variations between the leaching curves were less evident, with generally more similar release trends as a function of pH.

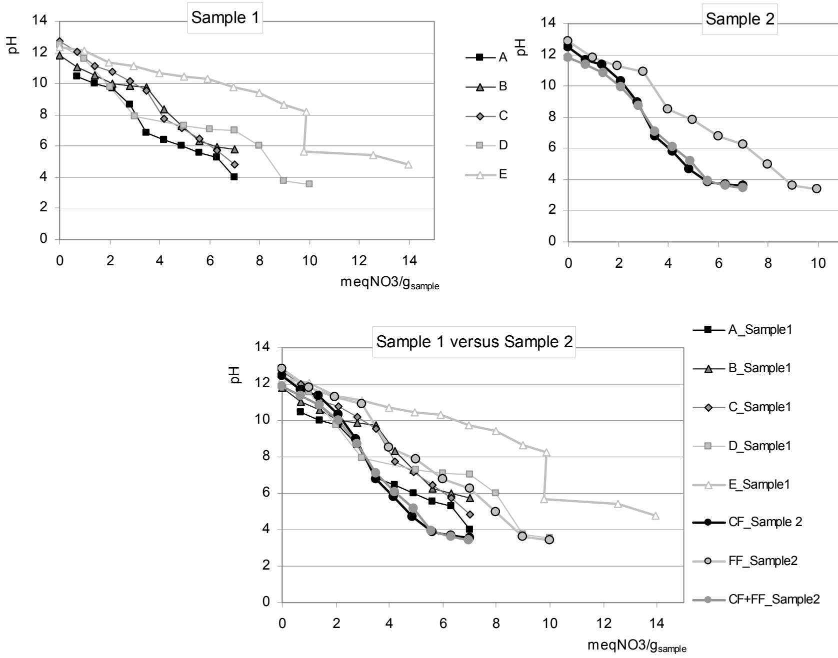

Figure 16: ANC curves for Sample 1 (a), for Sample 2 (b) and comparison between both Samples

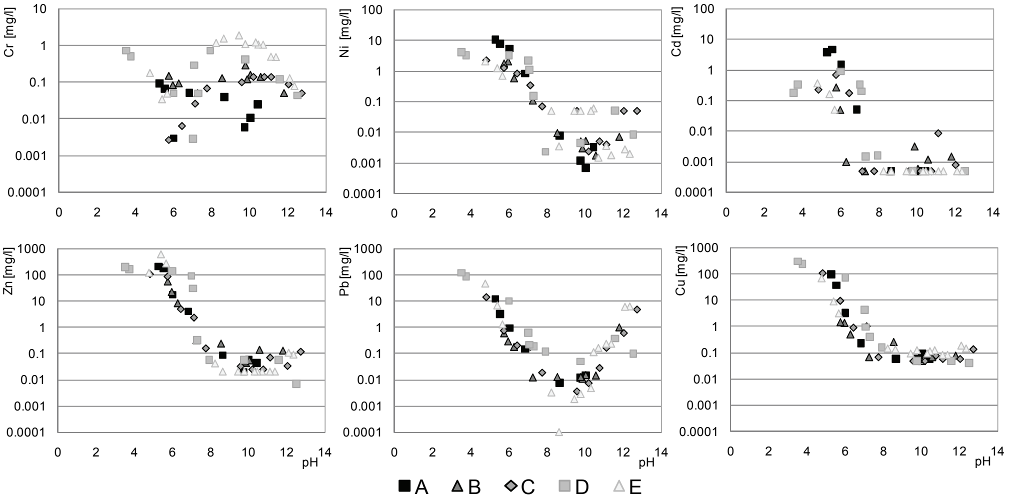

Figure 17: Sample 1 - Metals leaching

For Sample 2 (Figure 18) the raw material (CF+FF) and CF showed very similar metals leaching curves, likely for the same reason indicated above to explain the trend of the titration curves (slight influence of the FF). In addition, similarly to what observed for

Sample 1, Cr was found to be released in higher amounts by the FF as compared to the other materials.

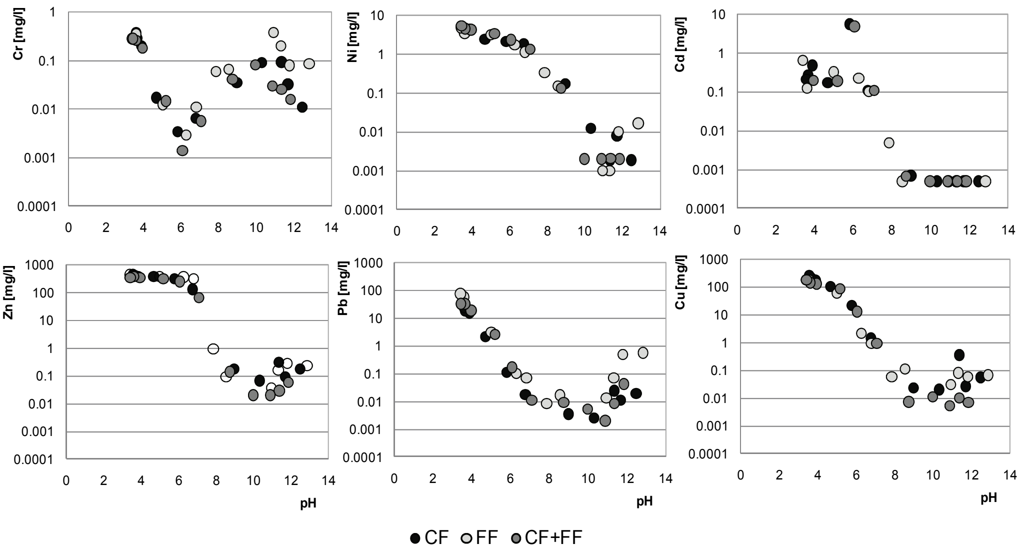

Figure 18: Sample 2 - Metals leaching

3.6 Mineralogical and morphological characterization of BA Sample 2

The mineralogical and morphological characterization was conducted only on the whole Sample 2 to better understand the influence of BA on the geopolymer formation process and to evaluate the differences between the BA structure and that of the geopolymeric products.

SEM micrographs (100× magnification) were collected to study the morphology of the materials (Figure 19(a)). The picture showed loose particles with large areas characterized by a dark grey level (P2 area) intermixed with light gray zones (P3 area) of more limited extension more visible in the zoomed image (Figure 19 (b)). In addition some small white inclusions (P1 area) were visible.The three different areas were analyzed for elemental composition through EDAX analysis (Figure 19 (c)). The EDAX measurements showed a similar composition for both grey zones (dark and light), while the white area was characterized by larger amounts of heavy metals (in particular Pb). In detail:

- the light grey area (P3) mainly contained Ca (16 mol%), Si (13.5 mol%) and Al (5.4 mol%), which could roughly be described by the presence of CaO, SiO_2 and Al_2O_3 at molar ratios of 6:5:1; lower contents of C (4.6 mol%), Na (3.7 mol%), Cl (1.9 mol%) and Mg (1.3 mol%) were also detected;

- dark grey zones (P2) mainly contained Si (24.4 mol%), Na (9.8 mol%) and Ca (7.3 mol%), with smaller concentrations of C (3.9 mol%), Al (2.8 mol%) and Mg (1.4 mol%).

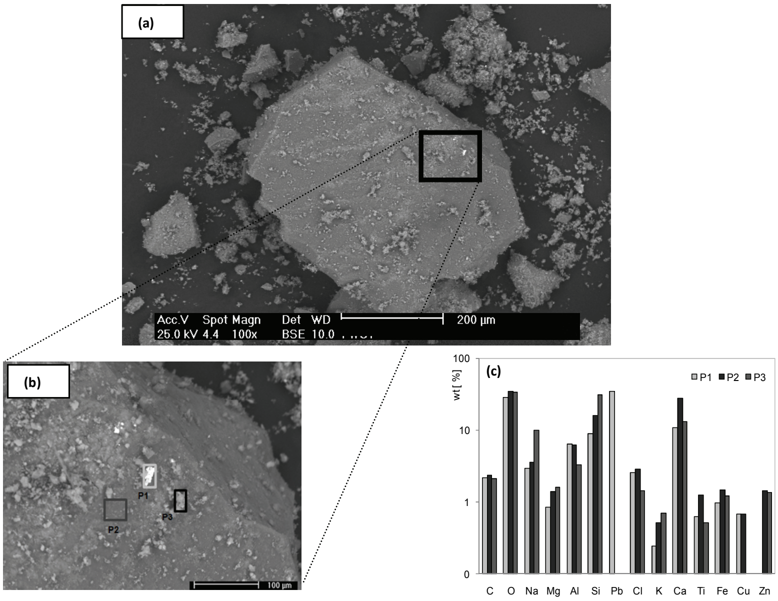

Figure 19: SEM micrograph (a and b) and results of EDAX spot analysis (c) for powdered BA (Sample 2)

Infrared spectra (Figure 20) of the same sample were also acquired to have a comparison between the raw material and new geopolymer materials produced.

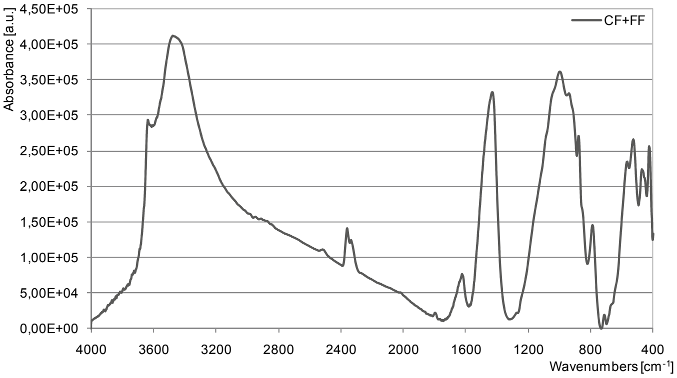

Figure 20: FT-IR spectra for CF+FF fraction of sample 2 and position of the main peaks

The main peaks identified are placed around:

- ✓ 3690 cm^{-1} associated to O–H stretching in the Ca(OH)$_2$ structure (Yousuf et al., 1995);
- ✓ 1640–1660 cm^{-1} and 3440–3460 cm^{-1} associated to stretching and deformation vibrations of OH and H–O–H groups (Chindaprasirt et al., 2009; Barbosa et al., 2003; Lee et al., 2002; Palomo et al., 1999);
- ✓ 1450 cm^{-1} associated to the presence of O–C–O stretching vibration in carbonate (Barbosa et al., 2003, Andini et al., 2008, Mozgawa et al., 2009, Lee et al., 2003);
- ✓ 980-1040 cm^{-1} associated to asymmetric stretching vibrations of Si–O/Al–O bonds (Barbosa et al., 2000, Phair et al., 2002);
- ✓ 450–470 cm^{-1} assigned to the in-plane bending vibration of Si–O–Si (Barbosa et al., 2000, Phair et al., 2002).

According to previous studies (Barbosa et al., 2000, Phair et al., 2002), the peaks centred at 980–1040 cm^{-1} and 450–470 cm^{-1} were assumed as the main molecular vibration fingerprints of geopolymeric materials. While the latter was not present in the BA, the former appeared but with a different shape and intensity if compared to the peak of the geopolymeric materials (Figure 45).

The BA was also characterized through RAMAN spectroscopy. Several Raman spectra (one for each area characterized by a different colour) were collected. Figure 21shows the results of the anlaysis.

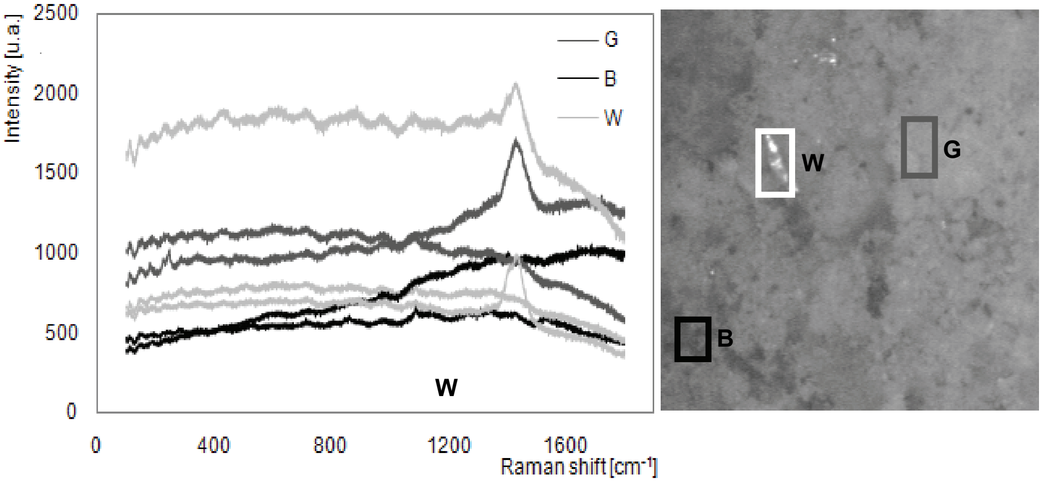

Figure 21: Raman spectra collected for the CF+FF of Sample 2 in three main areas: grey (G), white (W), black (B)

In the white zone a double peak around 1400 cm^{-1} was observed, probably associated to alumina. The same peak, although less pronounced, was also detected in the Raman spectrum of the grey zone. In a spectrum associated to the black zone some small peaks around 1050 cm^{-1}, 700 cm^{-1} and between 150 and 300 cm^{-1} were detected which were likely associated to calcite. In the grey zone a large numbers of peaks ranging from 150 and 300 cm^{-1}, around 500 cm^{-1} and between 600 and 1000 cm^{-1} were identified, which could be attributed to several phases listed in Table 16 including gehlenite, hematite, quartz, amorphous and crystalline silica or C-S-H. Unfortunately the noise of the spectra probably due to the amorphous nature of the material, makes a more accurate spectra interpretation difficult. This is the main restriction of RAMAN spectroscopy application to amorphous materials, even if RAMAN spectroscopy could provide a good support for the mineralogy characterisation when coupled with other techniques (e.g. XRD).

cm^{-1}	Raman shift							
Alumina	1381	1410						double peak
Silicon	520							
Amorphous silica	540							broad peak
Calcite	155	281	711	1087				not all visible
Quartz	130	208	466					not all visible
Gehlenite	620	656	690	910				not all visible
Hematite	225	245	291	410	490	610	660	not all visible
CSH	650							broad peak

Table 16: Main RAMAN peaks

The analysis of XRD spectra confirmed the results of elemental analysis and RAMAN measurements. In detail the results of XRD for the CF+FF (Figure 22) confirm the findings of other literature studies (Chimenos et al., 1999; Eusden et al., 1999; Freyssinet et al., 2002; Piantone et al., 2004).

Gehlenite ($Ca_2Al_2SiO_7$), a mineral of the melilite group, showed the most intense diffraction peaks together with quartz and hydrocalumite ($Ca_2Al(OH)_6[Cl_{1\_x}O_x]\cdot 3H_2O$). Calcite ($CaCO_3$), which is typically formed as a result of hydration and carbonation reactions during quenching and storage, was also identified.

Other important phases detected by XRD analysis included dicalcium silicate (Ca_2SiO_4) and hematite (Fe_2O_3).

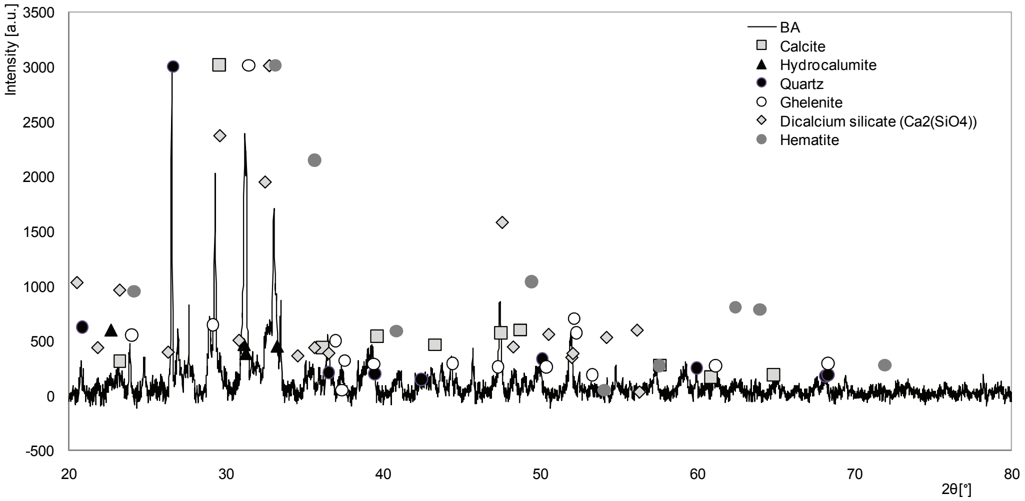

Figure 22: XRD spectra for BA sample 2

References

- ✓ S. Andini, R. Cioffi, F. Colangelo, T. Grieco, F. Montagnaro, L. Santoro: Coal fly ash as raw material for the manufacture of geopolymer-based products; Waste Manage (2008) 28(2): 416-423.
- ✓ V.F.F. Barbosa, K.J.D MacKenzie, C. Thaumaturgo: Synthesis and characterisation of materials based on inorganic polymers of alumina and silica: sodium polysialate polymers; Journal of Inorganic Matererials, (2000) 2: 309-317.
- ✓ V.F.F. Barbosa and K.J.D. MacKenzie: Thermal behavior of inorganic geopolymers and composites derived from sodium polysialate; Material Research Bulletin (2003) 38: 319-331.
- ✓ J. M. Chimenos, M. Sagarra, M.A. Fernandez, F.Espiell: Characterization of the bottom ash in municipal solid waste incinerator; Journal of Hazardous Materials A (1999) 64: 211-222.
- ✓ P. Chindaprasirt, C. Jaturapitakkul, W. Chalee, U. Rattanasak: Comparative study on the characteristics of fly ash and bottom ash geopolymers; Waste Management (2009) 29: 539-543.
- ✓ J.D. Eusden, T.T. Eighmy, K. Hockert, E. Holland, E. Marsella: Petrogenesis of municipal solid waste combustion bottom ash; Applied Geochemistry (1999) 14: 1073-1091.
- ✓ P. Freyssinet, P. Piantone, M. Azaroual, Y. Itard, B. Clozel-Leloup, D. Guyonnet, J.C. Baubron: Chemical changes and leachate mass balance of municipal solid waste bottom ash submitted to weathering; Waste Management (2002) 22: 159-172.
- ✓ C. Giampaolo, S. Lo Mastro, A. Polettini, R. Pomi, P. Sirini: Acid neutralization capacity and hydration behavior of incineration bottom ash–Portland cement mixtures; Cement Concrete Ressearch (2002) 32: 769-775.
- ✓ M. Izquierdo, A. Lopez-Soler, E. Vazquez Ramonich, M. Barra, X. Querol: Characterisation of bottom ash from municipal solid waste incineration in Catalonia; Journal of Chemical Technology and Biotechnology (2002) 77: 576-583.
- ✓ C.A. Johnson, S. Brandenberger, P. Baccini: Acid neutralizing capacity of municipal waste incinerator bottom ash; Environmental Science and Technology (1995) 29: 142-147.

- ✓ C.Y. Lee, H.K. Lee, K.M. Lee: Strength and microstructural characteristics of chemically activated fly ash-cement system; Cement and Concrete Research (2003) 33: 425-431.
- ✓ W. Mozgawa and J. Deja: Spectroscopic studies of alkaline activated slag geopolymers; Journal of Molecular Structure (2009) 434-441.
- ✓ A. Palomo, M.W. Grutzeck, M.T. Blanco: Alkali-activated fly ashes A cement for the future; Cement and Concrete Research (1999) 29: 1323-1329.
- ✓ J.W. Phair and J.S.J. Van Deventer: Effect of the silicate activator pH on the microstructural characteristics of waste-based geopolymers; The International Journal of Mineral Processing (2002) 66: 121-143.
- ✓ P. Piantone, F. Bodenan, L. Chatelet-Snidaro L: Mineralogical study of secondary mineral phases from weathered MSWI bottom ash: implications for the modeling and trapping of heavy metals; Applied Geochemistry (2004) 19: 1891-1904.
- ✓ M. Yousuf, A. Mollah, P. Palta, T.R. Hess, R.K. Vempati, D.L. Cocke: Chemical and physical effects of sodium lignosulfonate superplasticizer on the hydration of portland cement and solidification/stabilization consequences;. Cement Concrete Research (1995) 25: 671-682.

4. Results and Discussion: BA activation for blended cement formulation

4.1 Mechanical properties

The results from mechanical characterization of the cementitious materials are reported in Figure 23 (activation Method 1) in terms of UCS values for the coarse BA fraction (CF).

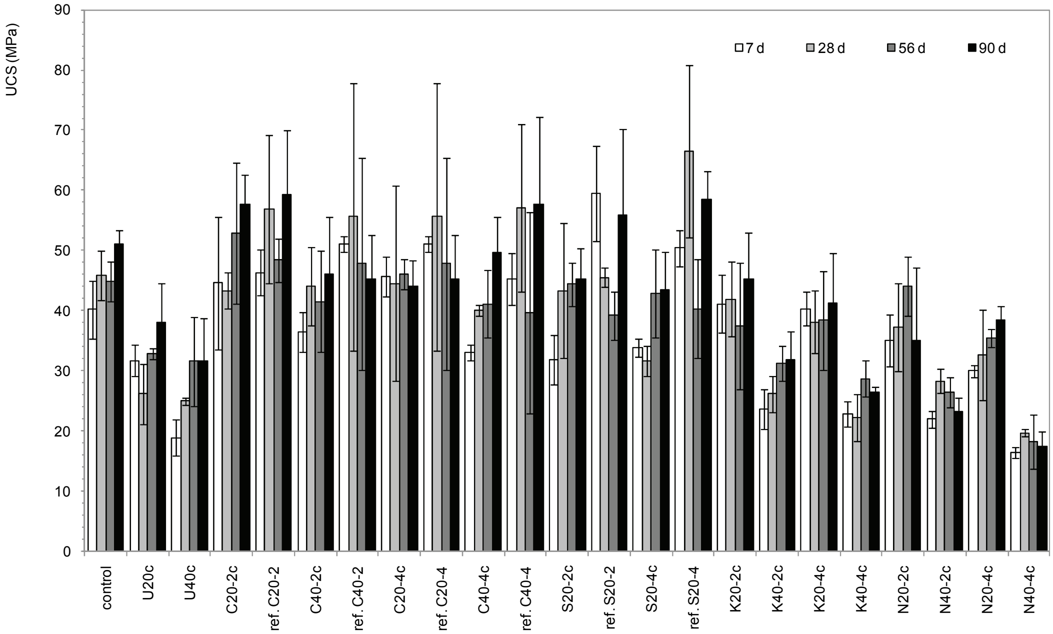

Figure 23: Unconfined Compressive Strength (UCS) UCS of mixtures containing the CF of BA

The addition of un-activated BA (samples U20c and U40c) was observed to result in decreased mechanical strength values in comparison to the control mixture (100%OPC). When activated BA was used as a cement admixture, the effects produced on mechanical strength were dependent on the type of chemical activator added. As a general feature, the four activators tested always produced a gain in mechanical strength in respect to the specimens without activator addition (samples U20c and U40c), however the UCS values were largely variable depending on the individual activator used. In particular, as already observed in a previous study on a BA sample from a different source (Polettini et al., 2005;

2009), $CaCl_2$ was capable of improving the mechanical characteristics of cementitious blends in respect to the control mixture, as also observed by other authors in the activation of natural pozzolans (Shi and Day, 2001). The addition of small amounts of $CaCl_2$ is known to decrease the solubility of $Ca(OH)_2$, at the same time increasing its dissolution rate, thus improving the rate of pozzolanic reactions (Shi and Day, 2000 (a)). Furthermore, $CaCl_2$ is known to decrease the setting time, as well as to promote the formation of monochloroaluminate, $C_3A{\cdot}CaCl_2{\cdot}10H_2O$ (Shi, 1998). In the present study the best results were obtained for a 20% BA content at 2% $CaCl_2$ addition, with UCS values of 44.6, 43.3, 52.9 and 57.7 MPa after 7, 28, 56 and 90 days, as opposed to 42.0, 45.8, 44.9 and 51.1 MPa measured for the control sample (100% OPC); increasing the $CaCl_2$ addition from 2% to 4% appeared to exert a minor effect on strength improvement. When the BA addition was increased to 40%, mechanical strength was reduced only slightly below that of the control specimen.

As for the other activators, there was still a positive effect on mechanical strength compared to the un-activated material, although this was less pronounced. The two activators $CaSO_4$ and KOH affected similarly the mechanical properties of the material. The positive effect of sulphate-based activators is known to be associated to the enhanced formation of AFt phases (Shi and Day, 2000 (b); Poon et al., 2003 (b)). Gypsum also appeared to play a role in the dissolution of the glassy phase of fly ashes (Poon et al., 2003 (b)). In addition, to the specific mechanisms described above for $CaCl_2$ and $CaSO_4$, the favourable contribution of Ca-based activators to the hydration process of systems containing alkaline waste materials has been indicated by other authors (Bellmann and Stark, 2009) and associated to modified precipitation equilibria resulting from the increased Ca concentration in the pore solution. Concerning the KOH at both the dosages (2 and 4%) and for lower BA (20%) addition it was possible to observe that this activator was capable of promoting the hydration process at early curing (7 days) yielding UCS values above that of the control (41.1 and 40.3 MPa, respectively for 2% and 4% activator addition, as opposed to 40.2 MPa for the control mixtures), no similar gain was observed at longer curing times. In addition, unlike noted for $CaCl_2$, the decreasing in UCS with the BA content when KOH was used as the activator was still considerable at all curing times. This suggested that KOH was only capable to affect hydration to some extent during the early stages of the process and for low BA dosages. Although NaOH is reported in the literature to be a valid activator for a variety of materials, particularly ashes rich in C_2AS (Shi and Qian, 2000), the effect on strength development has been found to differ depending on the composition of the material to be activated (Shi and Qian, 2000). In this research the mechanical properties were worsened when NaOH was added to the mixtures, showing that this species was not suited to significantly contribute to strength development, irrespective of the amount of both BA and activator added to the mixtures. When comparing the effects of the two alkaline hydroxides used in the present study the negative effect of NaOH on strength development is believed to be associated to either the higher alkalinity induced in comparison to KOH at the same weight addition, or by an excess of sodium in the pore solution which modified the precipitation equilibria of the main hydration phases. Some investigators have also indicated detrimental effects of NaOH in terms of altered morphology and reduced microstructural uniformity of the hydration products at both early and late ages (Wang et al., 2004). The same authors also highlighted that this negative effect on microstructure is enhanced at elevated curing temperatures, which may explain the results obtained in these experiments.

Considering the influence of the BA content of the mixtures, irrespective of the specific activator tested an increase from 20 to 40% was observed to considerably decrease mechanical strength.

From the statistical analysis of UCS values, an increase in the activator dosage at any of the investigated curing times was also generally found to produce only a minor effect on mechanical strength, indicating the BA content as the main factor affecting the mechanical properties of the hardened materials.

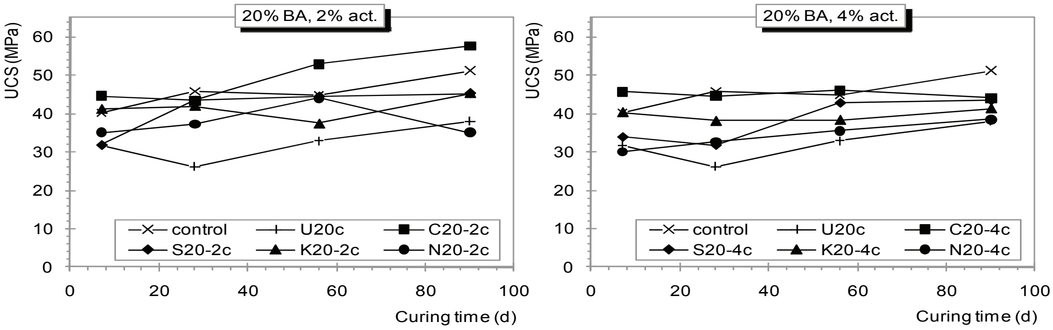

Figure 24: UCS vs. curing time for mixtures containing 20% BA (CF) and 2% and 4% activator

The UCS evolution as a function of curing time for mixtures containing 20% of the coarse BA fraction and 2% and 4% activator are reported in Figure 24.

It is evident that, in addition to producing higher mechanical strengths, $CaCl_2$ was also shown to exhibit a higher strength gain with time in comparison to all the other mixtures tested, including the control one in the case of 2% activator dosage. For an activator addition of 4% the results were very similar, although UCS was observed to decrease at longer curing times (≥ 28 days) in comparison to the control mixture. Furthermore, $CaSO_4$ and KOH yielded UCS values comparable to that of the control mixture up to 28-day curing, while the residual gain in mechanical strength upon prolonged curing was lower than that of the pure OPC specimen in both cases of 2% and 4% activator dosages. Mixtures containing $CaSO_4$-activated BA at 4% activator addition also showed a trend in UCS similar to that displayed by mixtures containing $CaCl_2$-activated BA.

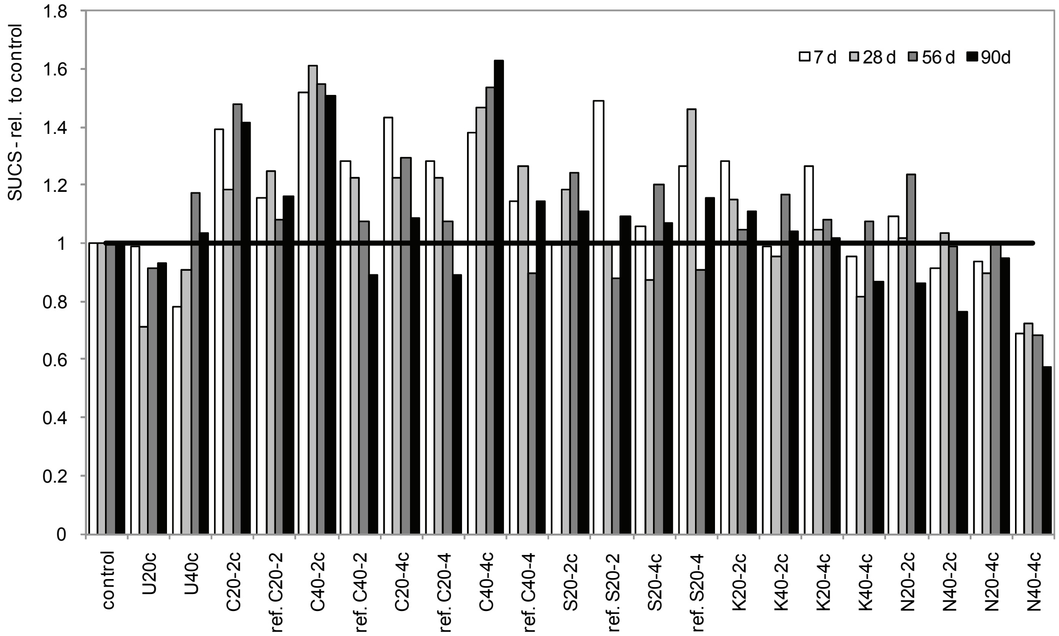

Figure 25 : Specific Unconfined Compressive Strength (SUCS) of mixtures containing the CF of BA

The findings commented above become more clear when interpreted in terms of specific strength values. SUCS (Pu, 1999) is defined as the mechanical strength of a given mixture divided by its OPC content and, is used to identify any additional contribution of cement admixtures to mechanical strength other than that produced by the OPC hydrates. As shown in Figure 25, while the SUCS of $CaCl_2$-contaning mixtures were all well above the corresponding values for the control specimen, the strength gain was less pronounced for $CaSO_4$ and KOH and much less visible (or absent at all) for NaOH.

Comparing the results obtained using the different activators, it was decided for the follow-up of the study to investigate in more detail the effects of the Ca-based activators. In particular, for these activators, additional mixtures were formulated to assess the real activation potential of BA displayed by these compounds and to separate any possible effect on the improvement of the hydration process of cement only.

Additional reference mixtures (ref.) were formulated using $CaCl_2$ and $CaSO_4$ added to cement at the same dosages (2 and 4 %wt) used for activated BA-containing mixtures. The SUCS results showed that the positive influence of $CaCl_2$ and $CaSO_4$ on cement strength, although visible at all curing times , was less pronounced than that observed for the mixtures containing activated BA. For example, while mixture C20-2c at 7-day curing had an SUCS (relative to that of the control mixture) of 1.39, the corresponding value for the reference mixture (ref.C20-2) was 1.16. Thus, it may be concluded that the strength gain recorder for mixture C20-2c was related to two main contributions: one due to the contribution of the activator on the hydration process of cement (probably the same observed for mixture ref.C20-2) and the other related to the activation effect of BA.

In terms of absolute UCS values the effects commented above were less evident, since they were probably masked by the reduced cement content in the BA-containing mixtures. For the same mixtures mentioned above as an example, the UCS values at 7-day curing were 44.6 MPa for the C20-2c mixture and 46.3 MPa for the ref.C20-2 mixture, as opposed to 40.20 MPa of the control specimen.

A comparison was also made between the effects of $CaCl_2$ and $CaSO_4$ on mechanical strength in the case of mixtures containing the FF of BA. The results in terms of UCS, compared with the corresponding mixtures formulated with CF and CF+FF and the reference and control mixtures are shown in Figure 26. It is evident that the FF of the material generally exhibited lower UCS values than the coarse fraction, due to its lower content of alumino-silicate minerals as evidenced by the elemental composition. The mixtures containing the fine fraction also displayed mechanical strength values well below that of the control mixture, even upon chemical activation. When the two size fractions were blended together in the cementitious mixtures, the mechanical behaviour was quite similar to that displayed by the coarse material, obviously due to the prevalence of this in the raw BA. It was also found that, while for the fine material $CaCl_2$ and $CaSO_4$ produced comparable results in terms of UCS, for the coarse fraction $CaCl_2$ was capable of appreciably improving the mechanical properties, with an increase in UCS by 12-26% (depending on curing time) as compared to the corresponding mixture containing the fine fraction.

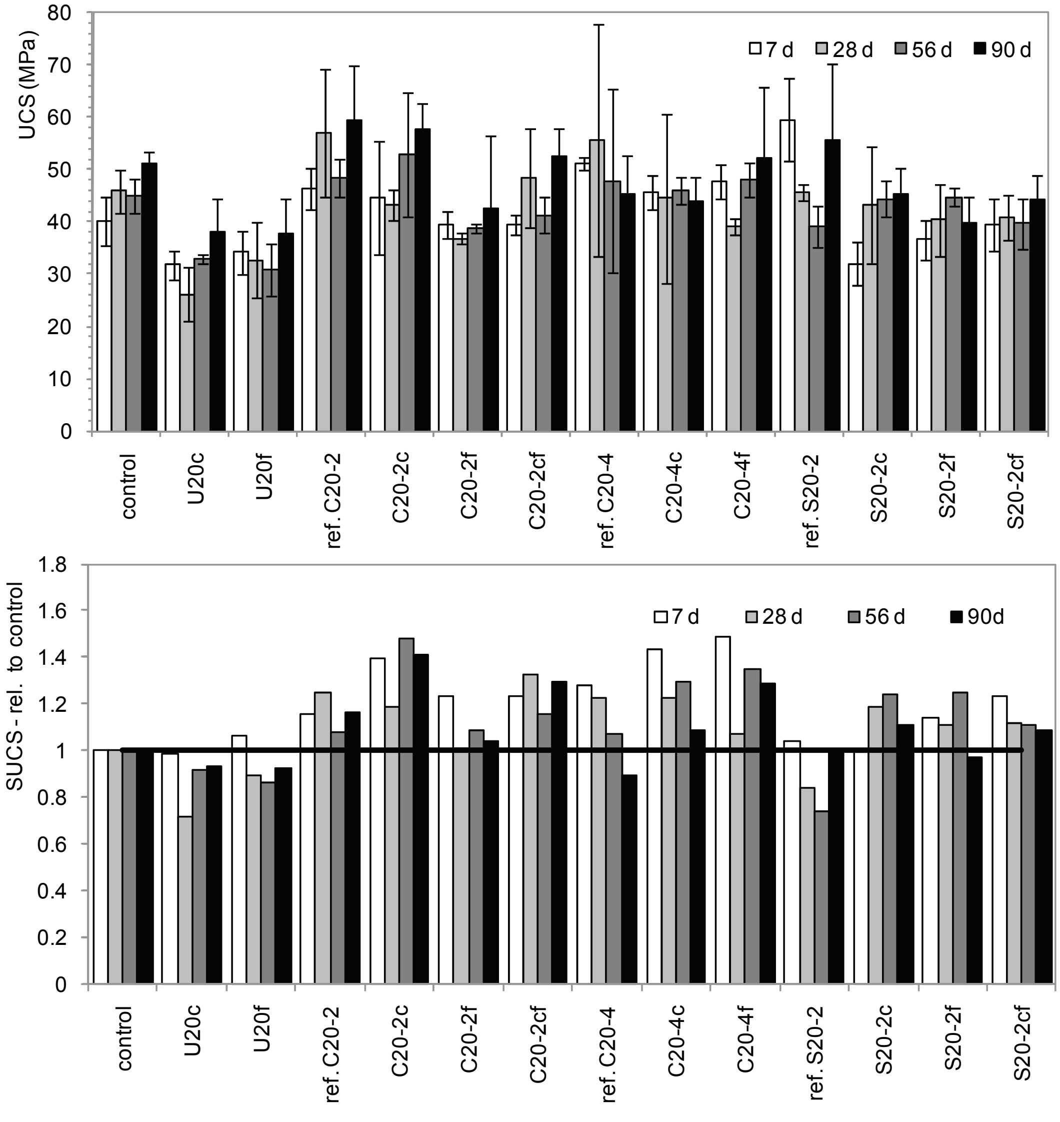

Figure 26: UCS and SUCS of mixtures containing the CF, FF and CF+FF of BA activated with Ca-based compound

The influence of the type of alkaline activation method applied is depicted in Figure 27 in the case of Ca-based activators; the mixtures obtained with activation method 2 were marked with “_2” while the mixtures obtained with activation method 1 were marked with “_1”. The results obtained show that the activation process with a pretreatment at 90°C was capable of promoting an increase in mechanical strength of the mixtures more than the other method (method 2).

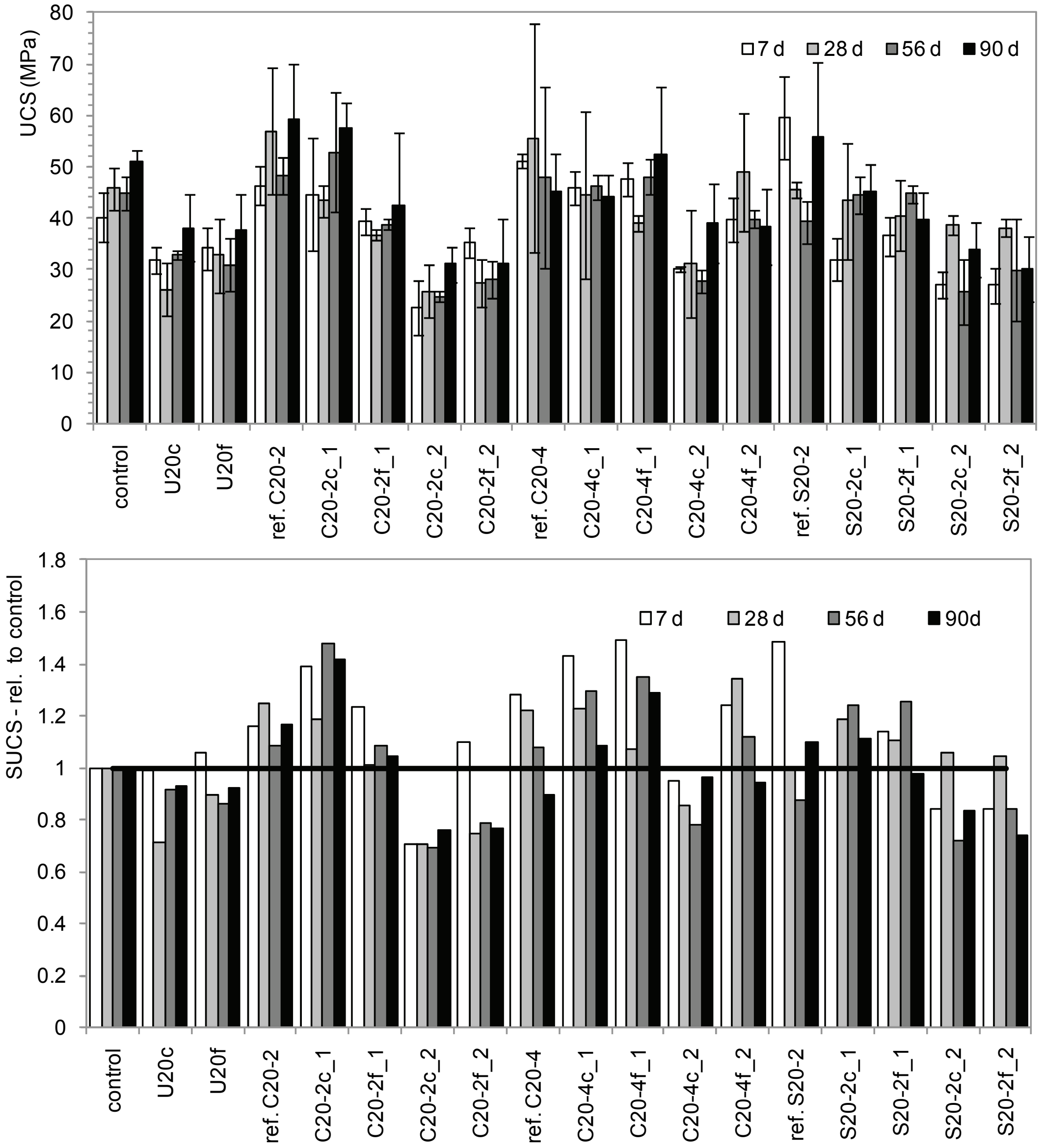

Figure 27: UCS and SUCS of mixtures containing the CF, FF of BA activated with Ca-based compound; method 1 ("_1) and method 2 ("_2")

4.2 Analysis of variance (ANOVA) of results

The results of mechanical strength measurements were processed through the ANOVA, which was used to judge the statistical significance of factor effects and interactions, required to build the predictive model described by equation (1) and (2).

For the first factorial design which included three factors: “bottom ash content”, “activator type” and “activator dosage”, set at 2, 3 and 2 levels, respectively, the ANOVA results for UCS at the four curing times investigated (7, 28, 56 and 90 days) are shown in Table 17. The results are expressed in terms of sum of squares (SS) for the individual effect/interaction, the corresponding degrees of freedom (DF) and mean squares (MS). The bold values in Table 17 indicate the significant effects at a 10% significance level. Due to the number of levels used for the two quantitative factors “BA dosage” and “activator addition”, only linear main effects and interactions between factors could be estimated, resulting in a linear predictive model for the response variables (equation 1).

	t = 7 d			t = 28 d		
	SS	DF	MS	SS	DF	MS
SS_t	1194.7	2	**597.3**	1231.2	2	**615.6**
SS_S	1693.3	1	**1693.3**	814.8	1	**814.8**
SS_A	53.1	1	**53.1**	139.9	1	**139.9**
SS_{tS}	75.0	2	**37.5**	298.4	2	**149.2**
SS_{tA}	36.3	2	**18.1**	40.3	2	**20.2**
SS_{SA}	6.3	1	**6.3**	22.1	1	**22.1**
SS_{tSA}	9.5	2	**4.8**	10.9	2	**5.4**
SS_E	301.8	24	**12.6**	1034.0	24	**43.1**
SS_T	3369.9	35	**96.3**	3591.7	35	**102.6**
	t = 56 d			t = 90 d		
	SS	DF	MS	SS	DF	MS
SS_t	1374.6	2	**687.3**	2646.5	2	**1323.3**
SS_S	1123.4	1	**1123.4**	1126.3	1	**1126.3**
SS_A	164.4	1	**164.4**	118.8	1	**118.8**
SS_{tS}	177.2	2	**88.6**	305.7	2	**152.9**
SS_{tA}	87.7	2	**43.9**	25.8	2	**12.9**
SS_{SA}	2.6	1	**2.6**	10.1	1	**10.1**
SS_{tSA}	37.6	2	**18.8**	279.3	2	**139.7**
SS_E	990.1	24	**41.3**	972.9	24	**40.5**
SS_T	3957.6	35	**113.1**	5485.4	35	**156.7**

t = “activator type”; S = “BA dosage”; A = “activator addition”
E = error; T = total

Table 17: ANOVA results for UCS at the four curing times investigated, expressed in terms of sum of squares (SS) for the individual effect/interaction, the corresponding degrees of freedom (DF) and mean squares (MS)

The response surfaces obtained using this approach are plotted in Figure 28 at constant values for factor “activator type” (level 1 = $CaCl_2$, level 2 = KOH and level 3 = NaOH) separately for each curing time.

On the whole, the analysis of the contour plots shows, in agreement with UCS results, the minor effect of an increase in activator dosage for all the investigated curing times; conversely, UCS was more negatively affected by a corresponding increase in BA dosage.

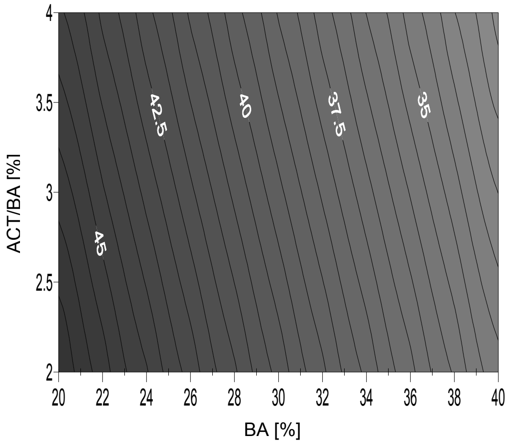
$CaCl_2$ 7 days

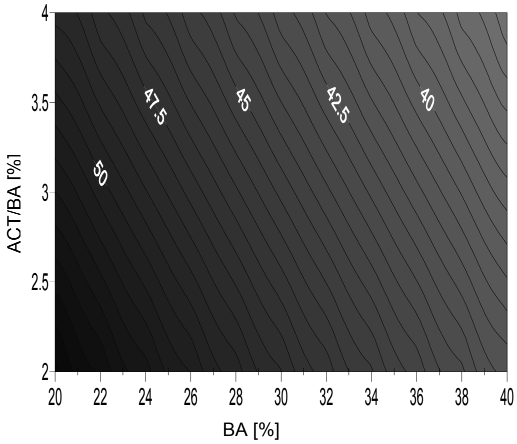
$CaCl_2$ 28 days

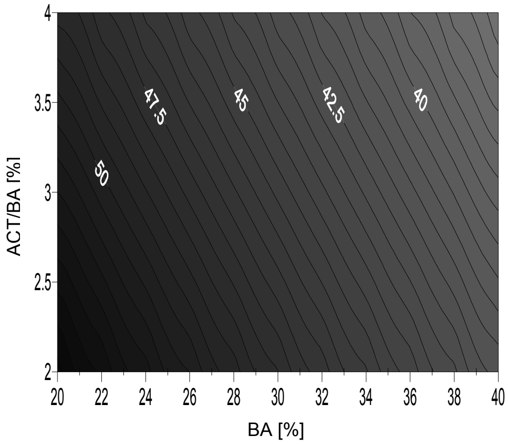
$CaCl_2$ 56 days

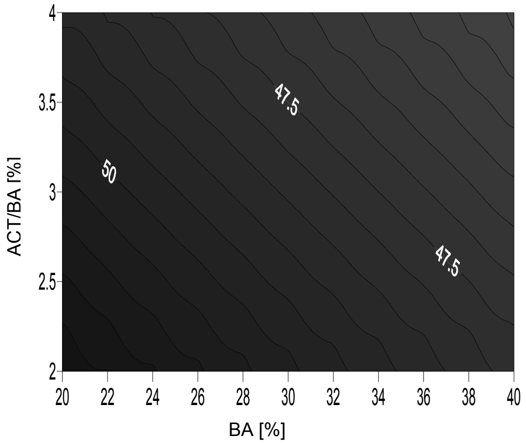
$CaCl_2$ 90 days

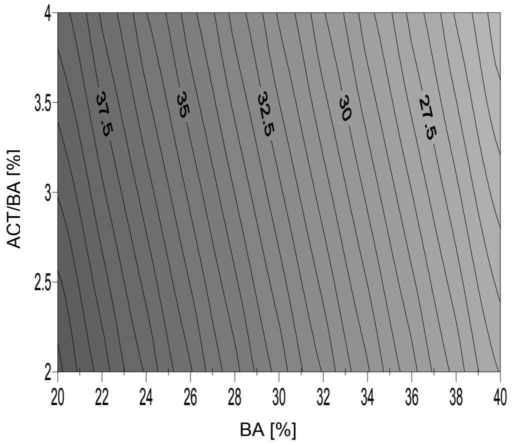
KOH 7 days

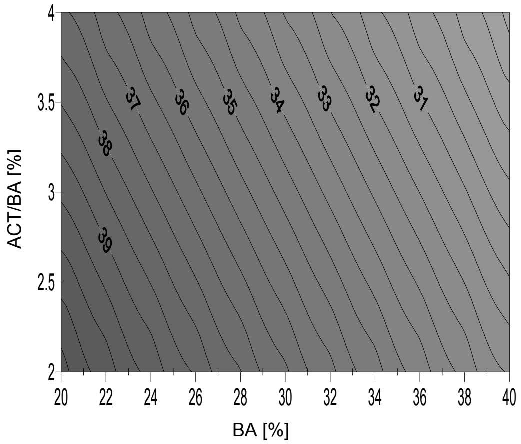
KOH 28 days

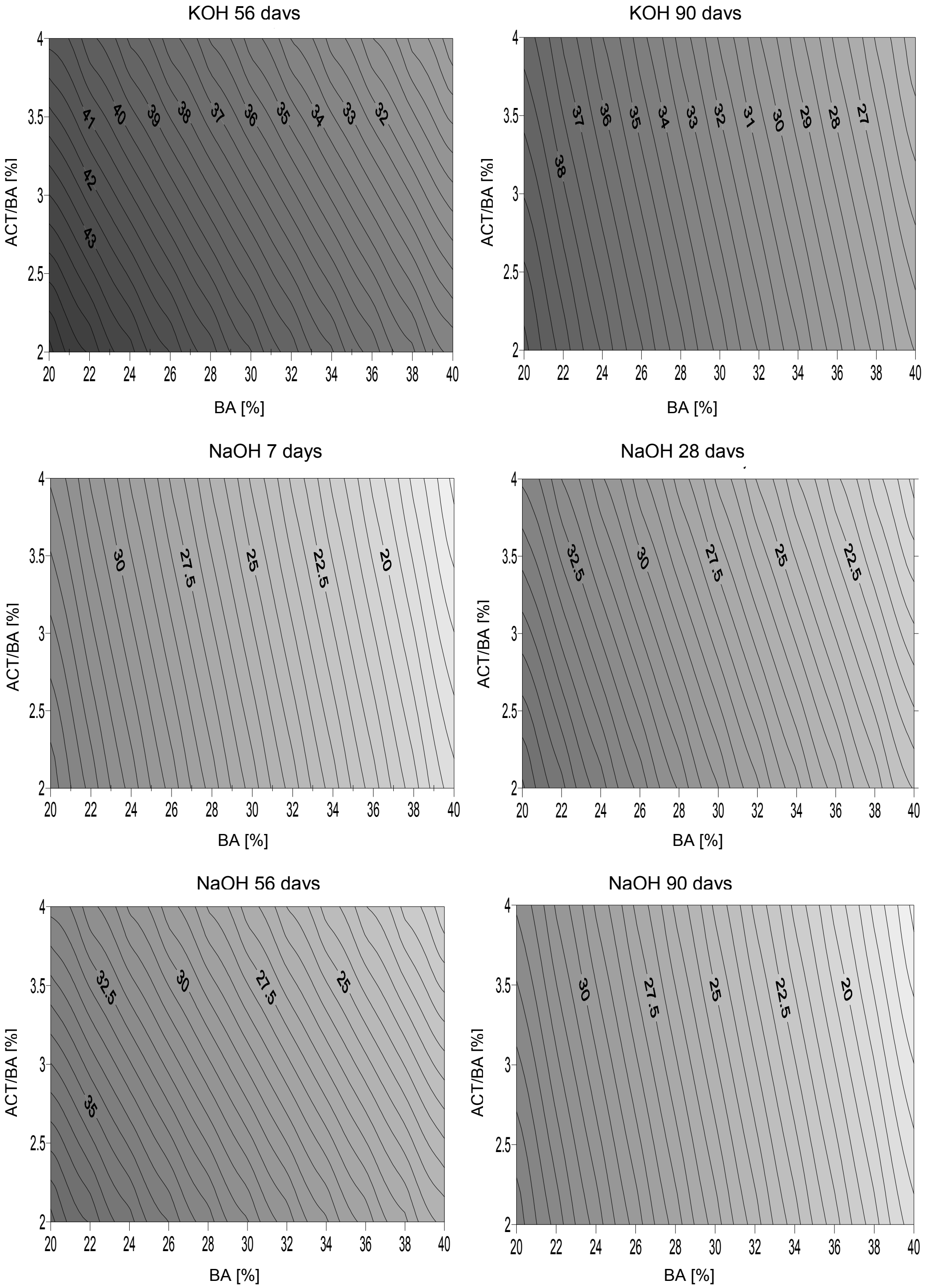

Figure 28: Response surfaces for UCS as derived from model as per equation (1) – values in MPa

The minor influence of the activator dosage is more visible in the case of KOH and NaOH especially at low (7 days) and longe (90 days) curing times.

In the case of $CaCl_2$ the influence of BA content is again quite relevant, although some influence, even if rather weak, of the activator dosage can also be recognized.

For this reason and taking into account the good results obtained using $CaCl_2$ on mechanical strength development, a full 3^2 factorial design was arranged in this case in order to better evaluate higher-order effects/interactions of factors. In Table 18 the ANOVA results for UCS at the three curing times investigated are reported. The bold values indicate significant effects at a 5% significance level considering the Fischer distribution. Considering the significant effects identified by the ANOVA, a predictive model for UCS as described by equation (2) was built. The response surfaces obtained using this approach are plotted separately for each curing time in Figure 29.

	t = 7 d			**t = 28 d**			**t = 56 d**			**t = 90 d**		
	SS	**DF**	**MS**	**SS**	**DF**	**MS**	**SS**	**DF**	**MS**	**SS**	**DF**	**MS**
SS_A	956.2	2	**478.1**	1372.0	2	**686.0**	614.3	2	**307.2**	1505.7	2	**752.9**
SS_S	1270.8	2	**635.4**	1467.2	2	**733.6**	373.0	2	**186.5**	545.2	2	**272.6**
$SS_{Interaction}$	106.7	4	**26.7**	86.0	4	**21.5**	218.5	4	**54.6**	902.3	4	**225.6**
SS_E	248.7	18	**13.8**	1707.8	18	**94.9**	989.6	18	**55.0**	1684.5	18	**93.6**
SS_T	2582.3	26	**99.3**	4633.0	26	**178.2**	2195.4	26	**84.4**	4637.7	26	**178.4**
SS_{AxSLxL}	7.9	1	**7.9**	20.9	1	**20.9**	31.8	1	**31.8**	420.2	1	**420.2**
SS_{AxSLxQ}	2.1	1	**2.1**	35.7	1	**35.7**	48.2	1	**48.2**	160.2	1	**160.2**
SS_{AxSQxL}	96.6	1	**96.6**	28.3	1	**28.3**	10.0	1	**10.0**	32.8	1	**32.8**
SS_{AxSQxQ}	0.1	1	**0.1**	1.1	1	**1.1**	128.5	1	**128.5**	289.2	1	**289.2**
SS_{AL}	761.4	1	**761.4**	931.0	1	**931.0**	330.3	1	**330.3**	472.3	1	**472.3**
SS_{AQ}	194.8	1	**194.8**	441.0	1	**441.0**	284.0	1	**284.0**	1033.4	1	**1033.4**
SS_{SL}	1215.5	1	**1215.5**	1209.1	1	**1209.1**	361.5	1	**361.5**	405.1	1	**405.1**
SS_{SQ}	55.3	1	**55.3**	258.0	1	**258.0**	11.5	1	**11.5**	140.1	1	**140.1**

t = “activator type”; S = “BA dosage”; A = “activator addition”; E = error; T = total; L: linear; Q: quadratic

Table 18: ANOVA results for UCS at the four curing times investigated, expressed in terms of sum of squares (SS) for the individual effect/interaction, the corresponding degrees of freedom (DF) and mean squares (MS)

.

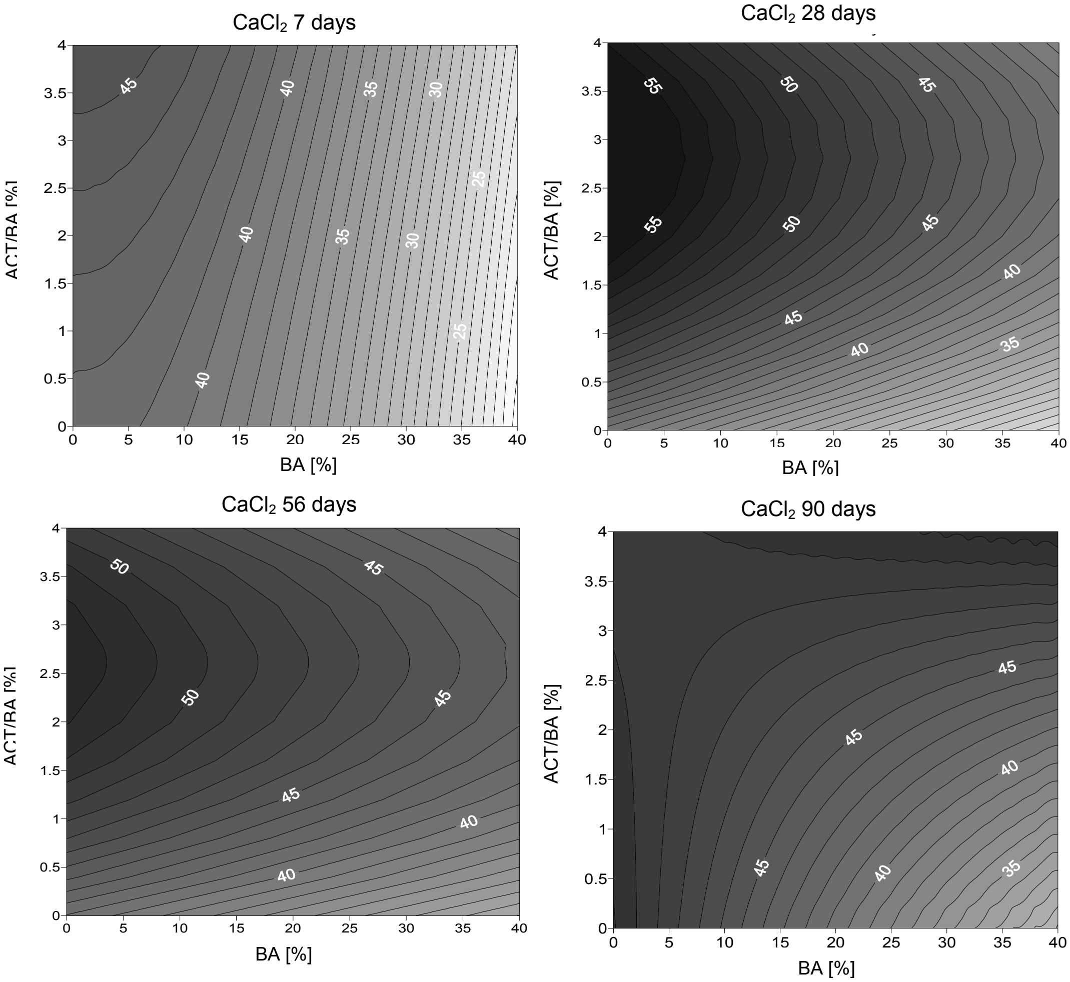
$CaCl_2$ 7 days

$CaCl_2$ 28 days

$CaCl_2$ 56 days

$CaCl_2$ 90 days

Figure 29: Response surfaces for UCS as derived from model as per equation (2) – values in MPa

The analysis of the contour plots confirms again the minor effect of an increase in activator dosage at all investigated curing times; conversely, UCS was more negatively affected by a corresponding increase in the BA dosage. From the analysis of the response surfaces it can be observed that the best results in terms of mechanical strength were obtained for BA dosages below 20% and activator additions between 1.5 and 3%. In particular it was found that:

- at low curing times (7 days) an increase in BA content above 15% resulting in decreasing UCS irrespective of the activator dosage adopted; this played a role, although quite limited, only for BA contents below 15%. This is mirrored by the pseudo-vertical trend of the reponse curves for BA contents >15% and by the larger curvature of the lines below this threshold;

- the trend of the response curves at 28 and 56 curing was comparable. The main influence on mechanical strength was, even in this case, exerted by the BA content. However, the influence of activator dosage was more evident and appeared to exert a higher influence on strength development at dosages up to 2%. For additions above 3%, the activator effect involved reducing mechanical strength, while in the intermediate range the influence of the activator was much less evident;
- at 90-day curing an increase in BA content was again found to decrease UCS , while an increase in the activator dosage was observed to improve mechanical strength at all BA dosages. It was also evident that for activator additions above 3% mechanical strength was approximately independent from the BA content.

4.3 TGA analysis of selected samples

The TGA/DSC patterns for the control, U20c and C20-2c mixtures at 28-day curing are reported in Figure 30. Five main regions can be identified on the basis of the characteristic temperature range (Alarcon-Ruiz et al., 2005):
1) 20-105°C, corresponding to the loss of the evaporable and part of the bound water;
2) 110-170°C, due to the dehydration of gypsum (displaying a double endothermic peak associated to the subsequent loss of the two water molecules), ettringite and part of the carboaluminate hydrates;
3) 180-300°C, related to the dehydration of C–S–H and carboaluminate phases;
4) 450-550°C, associated to the decomposition of portlandite ($Ca(OH)_2$);
5) 700-900 C, corresponding to the loss of CO_2 from carbonates.
On the basis of the experimental results depicted in Figure 30, the weight loss associated to the portlandite peak corresponded to a $Ca(OH)_2$ content of 11.5, 10.9 and 6.2 wt% for the control, U20c and C20-2c mixtures, respectively, which were then corrected to account for the carbonate content in the materials, yielding values of 22.3, 18.5 and 16.0 wt%. The difference in the portlandite content between the control and the un-activated BA mixture suggests that BA addition to cement produced merely a dilution effect of the hydrate system. When $CaCl_2$ was used as the activator, the portlandite content was found to decrease further, however, given the observed accompanied improvement in mechanical strength (see above), this may be interpreted as a positive influence of chemical activation on the hydration reactions. In other terms, the lower amount of portlandite measured in the mixture where $CaCl_2$ was added, along with its improved mechanical properties, may

suggest an effect of activation by $CaCl_2$ upon the development of pozzolanic reactions within the cementitious system.

The total weight loss (excluding the loss of free water) recorded in the TGA measurements for the control, U20c and C20-2c samples (19.1, 19.4 and 20.4 wt%, respectively) seems to confirm the increase in the total amount of hydration phases in the presence of $CaCl_2$.

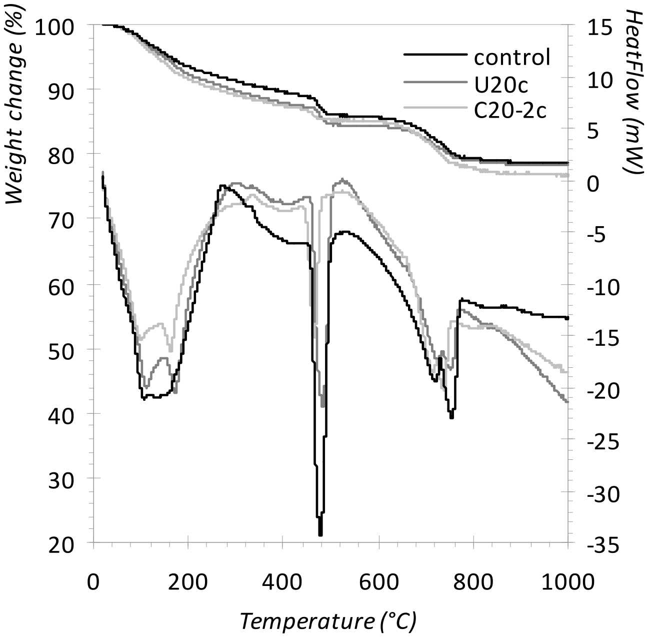

Figure 30. TGA/DSC measurements of selected mixtures

4.4 ANC leaching test on selected mixtures

As for the acid neutralization behaviour of the hydrated mixtures, Figure 31 compares the titration curves obtained for the Ca based activator-containing samples at all the curing days analysed. The acid neutralization capacity was observed to decrease with the BA content, as indicated by the increasing slope of the titration curves. Comparing the titration curves, especially considering those at 7 and 56 days, it is possible to observe that below pH 10 the addition of $CaCl_2$ was also found to reduce the buffering capacity of the material, and this effect became more appreciable at a 40% BA dosage.

In detail it is observed that the ANC to pH 10, which gives a rough estimation of the main hydration phases formed, decreased by about 1-2 meq/g (depending on curing time) as the BA content increased from 20 to 40%. The trend of the investigated titration curves for $CaSO_4$-activated mixtures was similar to the shape of the corresponding curves for mixtures containing $CaCl_2$.

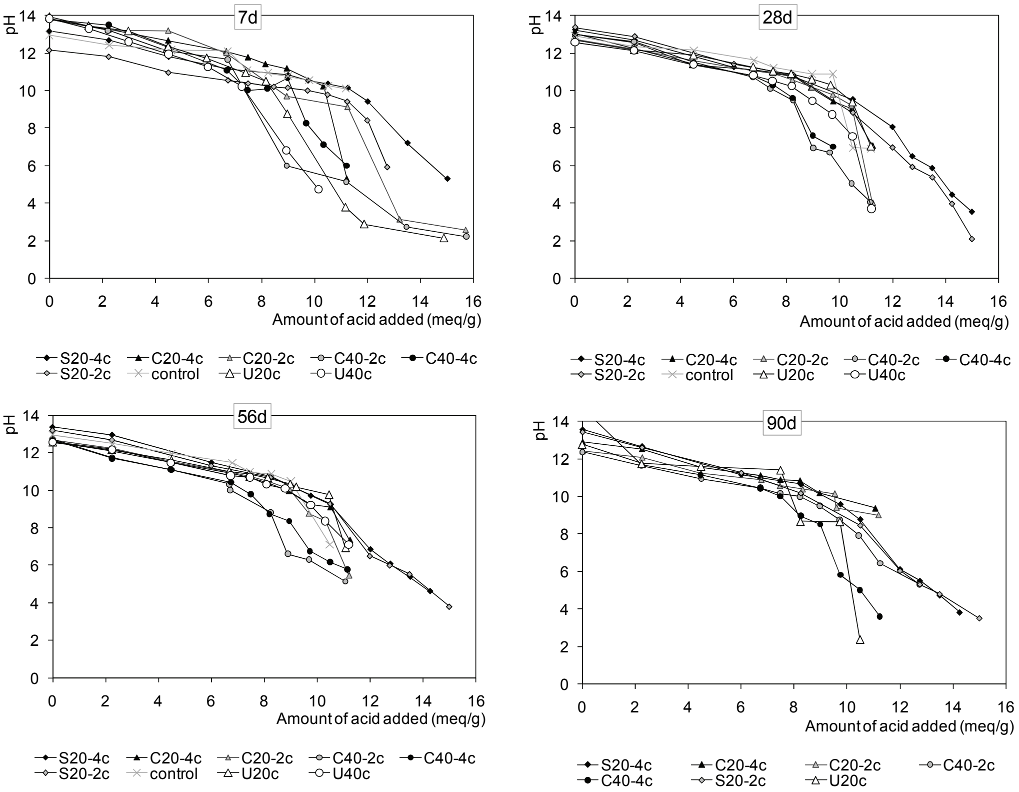

Figure 31 ANC curves for Ca-based activator-containing mixtures at all the curing days together with reference samples (control and mixture containing untreated BA)

In Figure 32 the ANC titration curves for mixtures containing Ca-based activators and separately for $CaCl_2$ ad $CaSO_4$, at 7 and 56 curing days are shown, which also include a comparison with the corresponding mixtures where the activation method used was method 2. It is possible to observe that the influence of increasing the BA content was similar for both activation methods (1 and 2). Furthermore, activation according to method 2 was found to produce a decrease in acid neutralization capacity if compared to method 1.

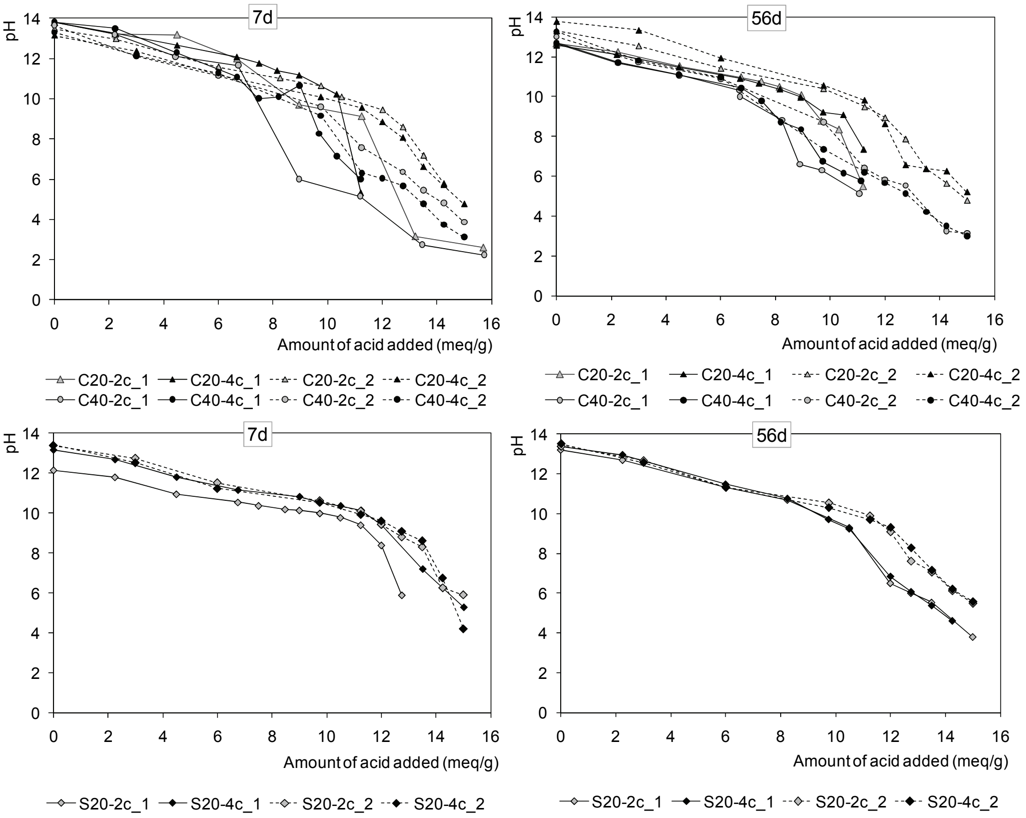

Figure 32: ANC curves for Ca based activator-containing mixtures at 7 and 56 curing days for “Method 1” and “Method 2”, the first marked with “_1”, the latter marked with the “_2”

4.5 Visual Minteq results

Figure 33 and Figure 34 report the experimental leaching data for Ca, Si and SO_4^{2-} as obtained from the ANC leaching test on the reference mixtures and the C20-2c sample at curing times of 7 and 56 days; the theoretical curves of the solubility-controlling minerals identified on the basis of geochemical modeling results are also reported. Modelling calculations were conducted to gain a better insight into the evolution of the hydration process of OPC in the presence of BA and the activator and derive information on the mechanisms governing the leaching of major elements and trace metals from the solid matrices. The behavior of the major solid matrix constituents is deemed particularly important to understand the mechanisms of trace contaminant release from the material, since major phases are able to control the leachate pH (which is a key parameter for metal leaching) and to interact with trace elements through several mechanisms including co-precipitation, incorporation, sorption, ion exchange and others. In general, depending on the nature of the mixture tested, different hydration phases were found to control the solubility of major elements/species.

For the control sample, at early curing (7 days) at pH < 11 two AFm phases including gehlenite hydrate (also known as strätlingite, having the composition $2CaO{\cdot}Al_2O_3{\cdot}SiO_2{\cdot}8H_2O$, or C_2ASH_8 in the cement chemistry notation) and $3CaO{\cdot}Fe_2O_3{\cdot}(CaSO_4){\cdot}12H_2O$ ($C_4F\overline{S}H_{12}$) were found to describe the leaching of Ca; such two phases also appeared to govern the leaching of, respectively, Si and sulphate in the same pH range. At more alkaline pH values (12-13), the only phase which could explain the release of Ca as well as Si was C-S-H with a Ca/Si ratio of 0.5. The occurrence of C–S–H phases with low Ca/Si ratios as potential solubility-controlling minerals may be explained on account that, due to the large solubility of portlandite in water, even from Ca-rich solutions the equilibrium precipitate has been reported to be always low in Ca/Si ratio (Kersten, 1996). It is thus still possible that, although not apparent from the analysis of the ANC eluates, other calcium silicate hydrate phases with higher Ca/Si ratios were actually present in the solid material. In the control sample at early curing the leaching solutions were calculated to be oversaturated by ~1 order of magnitude with respect to ettringite ($Ca_6Al_2(SO_4)_3(OH)_{12}{\cdot}26H_2O$), although the shape of the theoretical solubility curve for this phase was very similar to the experimental leaching curve.

At longer curing times (56 days) Ca leaching from the control mixture was comparably well described by both ettringite and C_2ASH_8 at pHs in the range 10-12. Ettringite was also a good candidate for solubility control of sulphate within the same pH range. Ca leaching at pH>12 appeared to be better controlled by two AFm phases including monosulphate ($Ca_4Al_2(SO_4)(OH)_{12}{\cdot}6H_2O$ or $C_4A\overline{S}H_{12}$, which also showed a good fit with sulphate concentration data within the same pH range) and chromium monosulphate ($Ca_4Al_2(CrO_4)(OH)_{12}{\cdot}9H_2O$). The appearance of Cr-monosulphate as a potential solubility-controlling mineral for both Ca and Cr may well explain the incorporation of Cr within the hydration products of Portland cement as the hydration proceeded, with an associated decrease in the release levels as indicated by the corresponding leaching curves (see Figure 35 below). The fit between Si leaching data from the control mixture and the theoretical solubility curves of the above mentioned phases was relatively poor. Only C_2ASH_8 in a limited pH interval (10.5-11.5) appeared to somehow describe the experimental data, while Ca/Si=0.5 C-S-H, which gave a good fit with the measured Ca concentrations (see above), was not found to adequately explain the leaching behavior of

Si. As far as the reference mixture containing un-activated BA (U20c) was concerned, at 7-day curing either anhydrite or gypsum were identified as potential solubility-controlling minerals for both Ca and sulphate in the pH range 8.5-11.5. In the alkaline range (pH>12), while the leaching of Ca was described by Ca oxychloride ($3CaO \cdot CaCl_2 \cdot 15H_2O$), no solubility-controlling minerals could be identified for sulphate, with eluates being oversaturated by 1-2 orders of magnitude with respect to both ettringite and monosulphate. It is tempting to hypothesize that the absence of such sulphate-bearing phases in the U20c sample indicates a delay in the hydration process of cement when un-activated BA was added to the mixture.

In the case of Si, again Ca/Si=0.5 C–S–H was identified as the potential leaching-controlling mineral below pH 12.5, while no suitable phases were found to describe Si leaching at higher pH levels. At 56-day curing ettringite appeared to be a good candidate for solubility control for both Ca and sulphate at pH values in the range 9.5-12, although approximately in the same pH interval (10-13) C_2ASH_8 was also found to display a good match with Ca and Si leaching data. At pH values below ~9.5, when ettringite becomes unstable as widely reported in the literature (Damidot and Glasser, 1992; 1993; Perkins and Palmer, 1999), gypsum appeared to control Ca and sulphate leaching from the material.

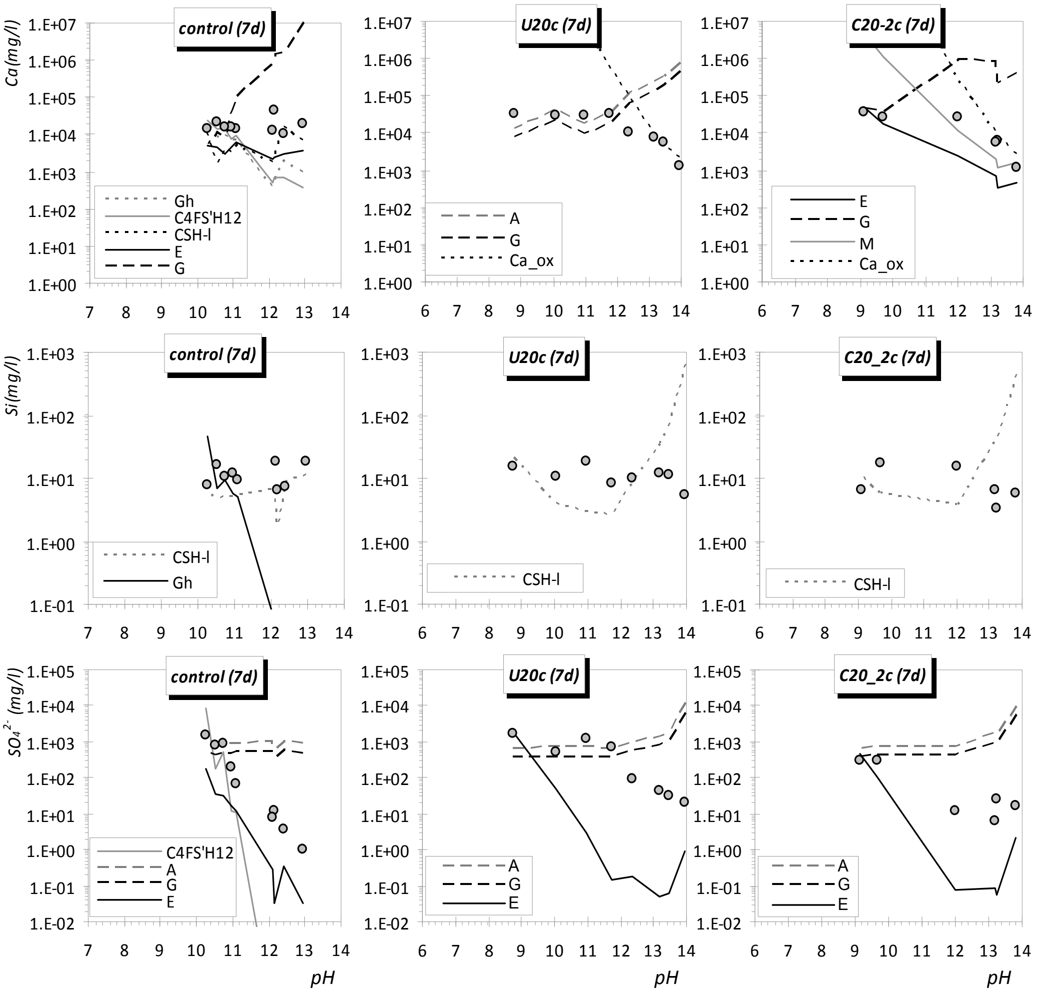

Figure 33. Results of geochemical modeling for Ca, Si and SO_4^{2-} for the control, U20c and C20-2c mixtures at 7-day curing (A: anhydrite; Ca_ox: Ca oxychloride; CSH-l: C–S–H (Ca/Si = 0.5); CSH-m: C–S–H (Ca/Si = 0.8); E: ettringite; G: gypsum; M: monosulphate, $C_4FS^*H_{12}$

When $CaCl_2$-activated BA was added to cement (specimen C20-2c), at 7-day curing gypsum at pH < 9 was found to be the most probable candidate for solubility control of both Ca and sulphate. In the case of Ca, monosulphate and Ca oxychloride were also identified as solubility controlling solids in the pH ranges 12-13.8 and 13-13.8, respectively. On the other hand, in the alkaline range (pH > 9) sulphate concentrations in the leaching solutions always showed oversaturation with respect to ettringite by about 2 orders of magnitude, and no mineral was found suitable to explain the release of sulphate from the hardened material.

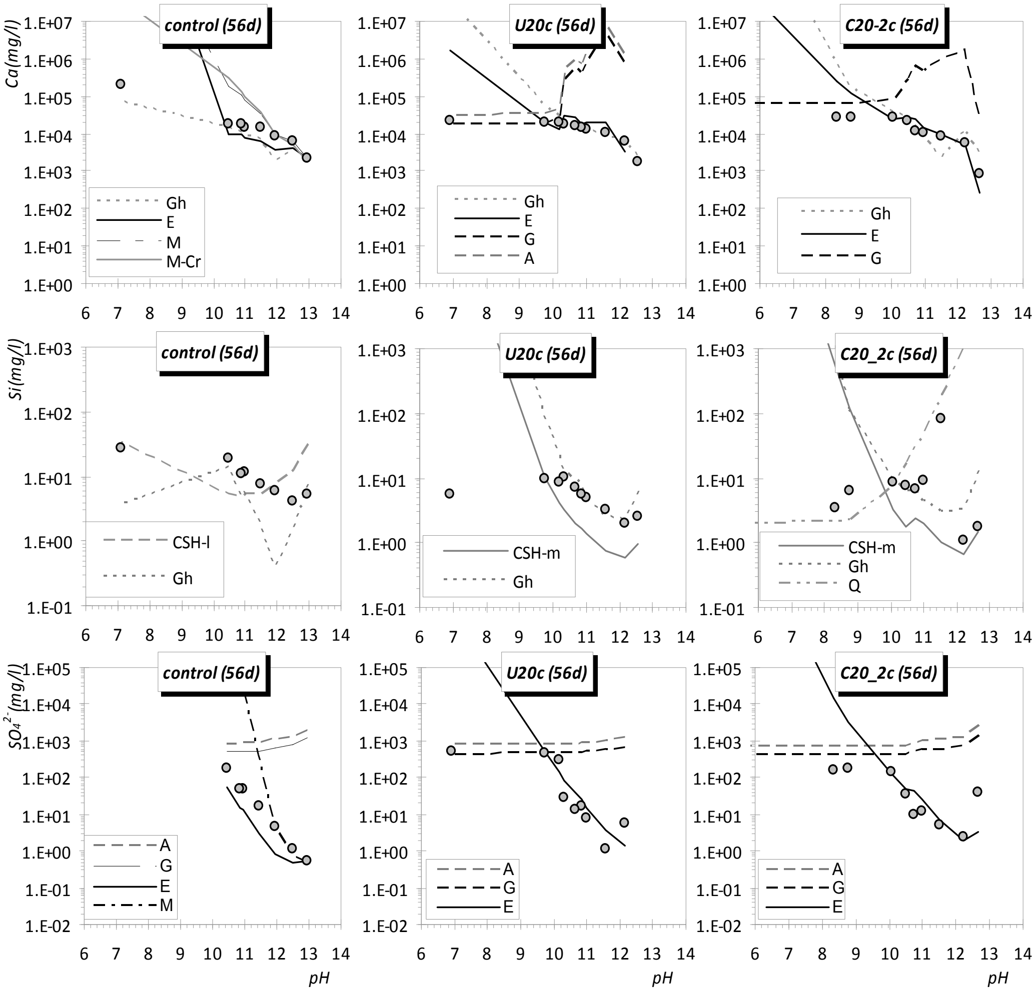

Figure 34: Results of geochemical modeling for Ca, Si and SO42- for the control, U20c and C20-2c mixtures at 56-day curing (A: anhydrite; CSH-l: C–S–H (Ca/Si = 0.5); CSH-m: C–S–H (Ca/Si = 0.8); E: ettringite; G: gypsum; Gh: gehlenite hydrate; M: monosulphate; MCr: Cr-Monosulphate; Q: quartz

As mentioned above for the sample containing un-activated BA, the only mineral describing Si leaching (although again with relatively poor fitting of the measured data) was Ca/Si = 0.5 C-S-H at pH < 10, while at higher pH values none of the phases included in the expanded thermodynamic database was capable of matching the experimental leaching curves. Upon prolonged curing (56 days), the minerals responsible for solubility control of the major elements/species were found to change. Again, at pH < 9 gypsum was selected as the leaching-controlling mineral for both Ca and sulphate; on the other hand, ettringite appeared to be the best candidate for solubility control at pH > 10 for both species, with a very good fit with the measured concentrations.

It should also be mentioned that at the same pH values C_2ASH_8 appeared to adequately describe the release of Ca as well, along with that of Si. In other pH ranges, the dissolution of this element was found to be dictated by quartz (pH < 9) and Ca/Si = 0.8 C-S-H (pH = 12-13).

4.6 Results of leaching tests for trace metals

The results of the ANC leaching test at natural pH for the trace metals Cd, Cr, Cu, Ni, Pb and Zn are compared in

Table *19* with the European regulatory limits for hazardous, non hazardous and inert waste landfills (EU Council Directive 99/31/EC, 1999) and with the limits established by the Italian law for waste utilization (annex 3 D.M. 05/02/1998, Ministero dell'Ambiente della Repubblica Italiana, 1998).

		Concentration (mg/l)					
Element	pH	Cd	Cr	Cu	Ni	Pb	Zn
raw bottom ash	12.71	<0.0005	0.04	0.08	0.0034	***2.52***	0.06
control (7d)	12.95	<0.0005	***3.52***	0.018	<0.002	<0.002	0.022
control (28d)	12.92	0.0009	*0.151*	0.009	<0.002	0.007	<0.01
control (56d)	12.95	0.0008	*0.065*	0.061	0.002	***1.9***	*0.179*
C20-2c (7d)	13.8	<0.0005	*0.09*	*0.39*	0.06	*0.54*	*0.15*
C20-2c (28d)	12.74	<0.0005	0.05	0.04	0.06	*0.14*	0.032
C20-2c (56d)	12.66	0.0005	*0.09*	0.054	0.013	*0.1*	0.016
C20-2c (90d)	12.42	<0.0005	*0.06*	0.041	0.033	*0.005*	0.021
C20-4c (7d)	13.8	<0.0005	0.04	0.05	0.06	*0.09*	0.031
C20-4c (28d)	13.01	<0.0005	*0.08*	0.05	0.004	0.023	0.05
C20-4c (56d)	12.58	***0.0111***	*0.08*	0.027	0.05	*0.061*	0.045
C40-2c (7d)	13.82	<0.0005	*0.05*	*0.43*	0.004	*0.5*	*0.225*
C40-2c (28d)	13.01	*0.005*	*0.08*	0.11	0.004	*0.15*	0.051
C40-2c (56d)	12.71	<0.0005	*0.07*	0.09	<0.002	*0.12*	0.031
C40-2c (90d)	12.37	<0.0005	*0.12*	0.14	2.3	*0.27*	0.025
C40-4c (7d)	13.79	<0.0005	*0.06*	0.13	<0.002	*0.27*	0.052
C40-4c (28d)	13.03	<0.0005	*0.05*	0.07	0.003	<0.002	0.038
C40-4c (56d)	12.65	<0.0005	*0.07*	0.09	0.05	*0.16*	0.041
S20-2c (7d)	12.16	n.a	*0.07*	0.06	n.a	*0.11*	0.029
S20-2c (56d)	13.2	n.a	*0.1*	*0.23*	n.a	*0.18*	0.023
S20-4c (7d)	13.16	n.a	0.06	0.06	n.a	*0.125*	<0.01
S20-4c (56d)	13.36	n.a	0.04	0.02	n.a	*0.13*	0.059

C20-2cF (7d)	13.48	n.a	0.01	0.03	n.a	0.013	0.015
C20-2cF (56d)	13.3	n.a	0.03	0.03	n.a	0.014	0.013
C20-4cF (7d)	13.14	n.a	*0.05*	0.04	n.a	*0.21*	0.037
C20-4cF (56d)	13.78	n.a	0.02	0.06	n.a	*0.09*	0.017
C40-2cF (7d)	13.65	n.a	*0.05*	0.09	n.a	*0.27*	<0.01
C40-2cF (56d)	13.1	n.a	0.03	0.05	n.a	*0.29*	0.029
C40-4cF (7d)	13.3	n.a	0.03	0.06	n.a	*0.32*	0.035
C40-4cF (56d)	13.27	n.a	0.02	0.07	n.a	*0.17*	0.042
S20-2cF (7d)	13.39	n.a	0.04	0.06	n.a	0.03	0.048
S20-2cF (56d)	13.4	n.a	0.02	0.03	n.a	*0.08*	0.04
S20-4cF (7d)	13.4	n.a	0.01	0.02	n.a	*0.13*	0.041
S20-4cF (56d)	13.5	n.a.	0.03	0.02	n.a.	*0.05*	0.022
EU LD (hazardous waste)		**0.2**	**7**	**10**		**5**	**20**
EU LD (not hazar. waste)		**0.0129**	**1**	**5**		**1**	**5**
EU LD (inert waste)		*0.004*	*0.05*	*0.2*	---	*0.05*	*0.4*
DM 05/02/1998 (reuse)	5.5 -12.0	0.005	0.05	0.05	0.01	0.05	3
Detection limit		0.0005	0.002	0.002	0.002	0.002	0.02

Table 19: Comparison between leaching test results (natural pH) and regulatory limits for selected heavy metals

Other trace elements of environmental concern, including the oxyanion-forming elements As, Mo, Sb and V, were not analyzed since for the raw BA either their total content or the leaching levels were below the detection limits. In general the leachate concentrations for the investigated heavy metals were found to decrease, in some cases appreciably, with curing, indicating a progressive immobilization with time. According to the values presented in Table 19, it is also clear that the critical elements for the materials include Cr and Pb. As evident from the leaching curves as a function of pH presented Figure 35, the high leaching levels measured for Cr are by no means caused by the contribution of the cement used, with the control specimen releasing more than 35 mg Cr/kg at 7-day curing; the presence of BA and $CaCl_2$ decreased the leaching level for this metal, however for the majority of the samples tested the Cr concentration in the leaching solutions exceeded the regulatory threshold limits. This result claims for a very careful control of the chemical composition of the raw materials used for cement production, as this can negatively affect the environmental behaviour of the hardened products obtained, even when they do not include waste materials as admixtures. As for Pb, notwithstanding the significant decrease in leaching observed in comparison to the raw BA, the release was often above the regulatory limits due to the typical strongly amphoteric behaviour of this metal. The leaching levels were also found to benefit from prolonged curing, although with some fluctuations likely due to changes in the pH of the leaching solutions; the best results in terms of Pb release were obtained for the C20-2c specimen after 90 days of curing, with a leachate concentration well below the limits established for both disposal in inert waste landfills and utilization.

The results of the ANC leaching test in terms of trace metal leaching as a function of pH are depicted in Figure 35 for the control mixture and those containing $CaCl_2$-activated BA (coarse fraction) and compared to the corresponding leaching data obtained for the raw BA sample. Blending BA with cement produced largely different effects on the leaching behaviour depending on the trace metal under concern. It is clear from the leaching curves obtained that curing time significantly affected the extent of trace metal leaching, producing a progressive immobilization of metals within the hydrated matrix. Metal leaching as a function of pH showed no large differences between the different mixtures investigated. However, as also observed for mechanical strength, $CaCl_2$ addition at a 20% BA content gave the best results, especially upon prolonged curing.

Among the trace metals of interest, Cr was observed to be released to an appreciably higher degree by the control mixture than by the samples containing BA, due to the contribution of OPC itself. Cr in the control mixture was however found to get progressively more immobilized with curing time, likely due to the incorporation in the hydration phases as indicated by the results from geochemical modelling discussed above. At all ages, an addition of 4% $CaCl_2$ was also observed to exert a more positive effect on Cr leaching in comparison to the 2% dosage. For both Cu and Pb, the control sample displayed appreciably lower release levels at all pHs since early hydration, however the differences in leaching with the BA-containing mixtures became fairly less evident as curing progressed, with a similar behaviour being observed for Zn as well.

The results of the ANC leaching test in terms of trace metal leaching as a function of pH are depicted also in Figure 36 for the mixtures containing CaCl2-activated BA (CF) and CaSO4-activated BA (CF) at 7- and 56-day curing, in order to make a comparison between the two activation methods tested. Irrespective of curing time, the effect of activation method 1 was not evident, in particular for Cu and Cr the leaching levels were higher than the corresponding values obtained for samples activated according to activation method 2. In the case of Pb and Zn leaching, the results of the two methods were very similar. For all the elements under concern, also in this case, the immobilization degree was found to be positively related to curing time.

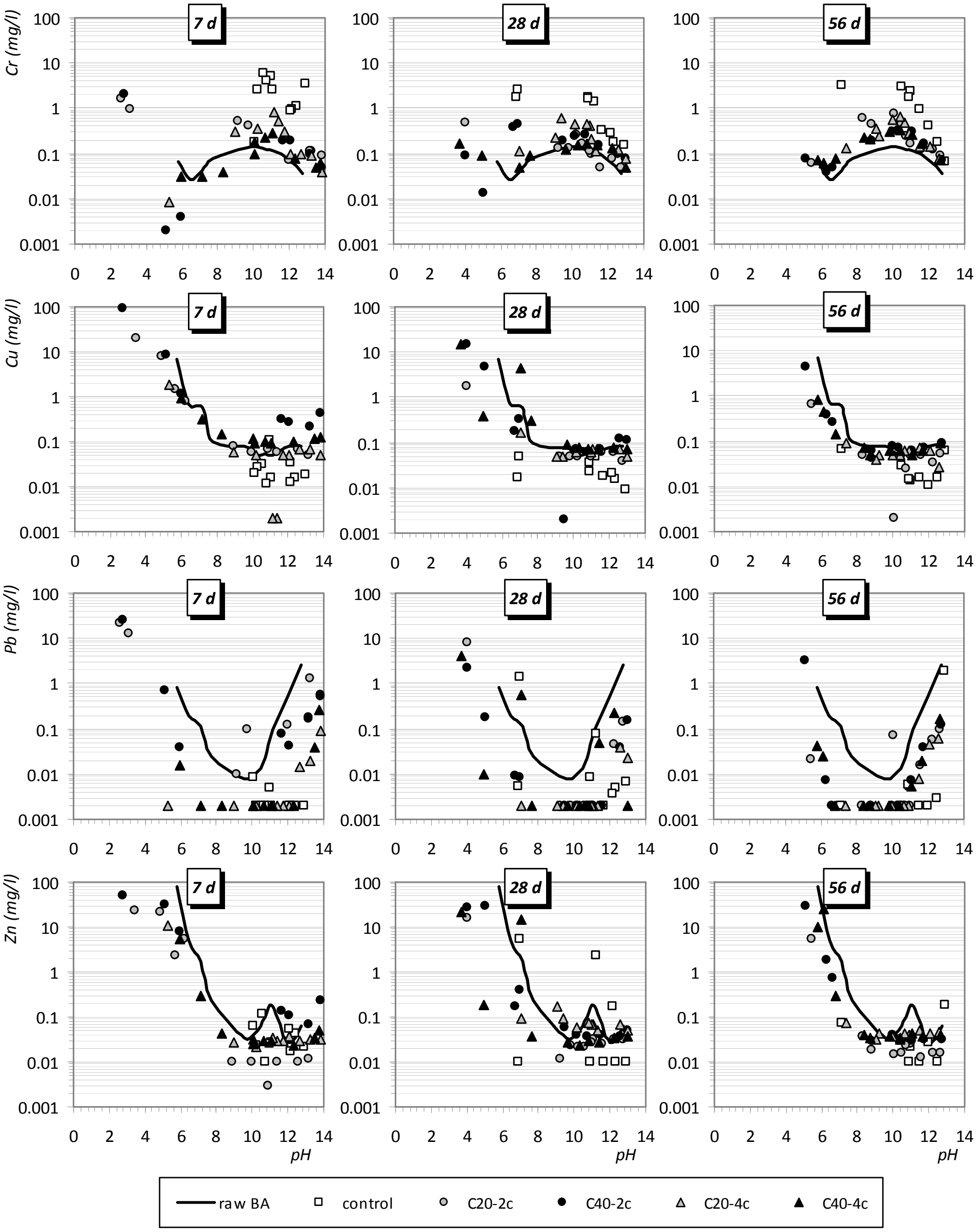

Figure 35: Metal leaching as a function of pH in the ANC test for reference and $CaCl_2$-containing mixtures (activation method 1)

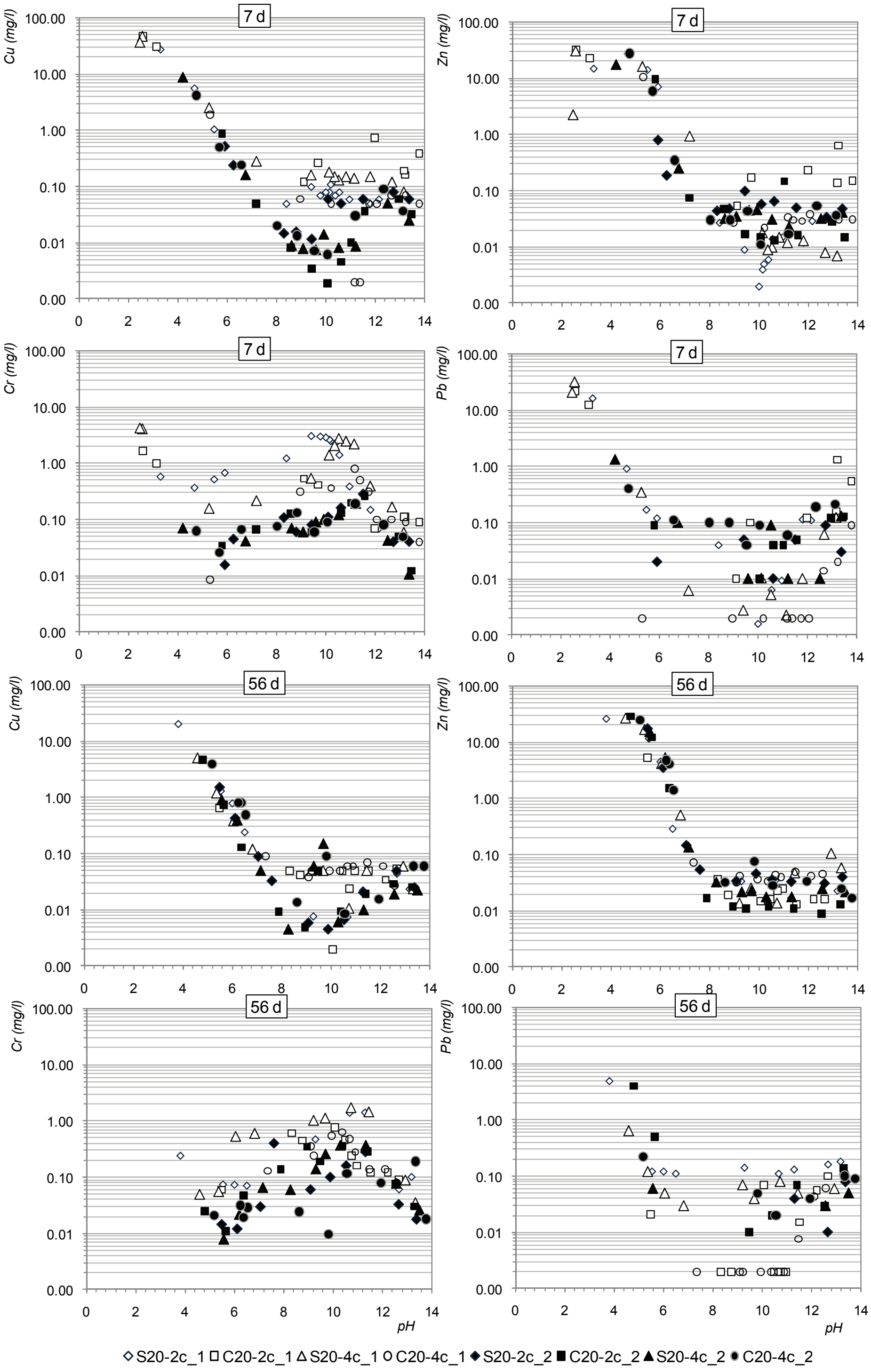

Figure 36: Metal leaching as a function of pH in the ANC test for $CaCl_2$- and $CaSO_4$-containing mixtures at 7 and 56 curing days (activation methods 1 and 2)

The results of geochemical modelling for the investigated trace metals showed that it was not possible to identify common secondary minerals including metal (hydr)oxides, carbonates and sulphates as potential solubility-controlling solids, with leaching solutions being always undersaturated in respect to such phases. This is the reason why the modelling predictions were not shown in Figure 35 and Figure 36 When surface complexation was accounted for in the modelling calculations, the results showed reliable predictions only in the case of Pb (see Figure 37 as an example of the results obtained for specimen C20-2c), which was found to be largely bound to HFO and AAM species in all samples tested (>95% of total leachable Pb, except at pH > 13.5 where the predominantly anionic speciation of Pb in solution likely reduced the amount sorbed). Surface complexation by Fe and Al minerals was thus likely the reason for the strong reduction in Pb leaching within the whole pH range investigated as compared to the raw BA sample. For the other trace metals of concern, the surface complexation model was not able to adequately predict the observed leaching levels, so that the solution concentrations were always strongly overestimated. Clearly, the difference between the observed and model-predicted leachate concentrations is caused by the role played by additional mechanisms (not accounted for in the model) in the immobilization of trace metals within the investigated materials. This is believed to be related to the presence of trace metals as complex minerals or phase assemblages which can hardly be described in a univocal manner from the viewpoint of both chemical composition and thermodynamic data.

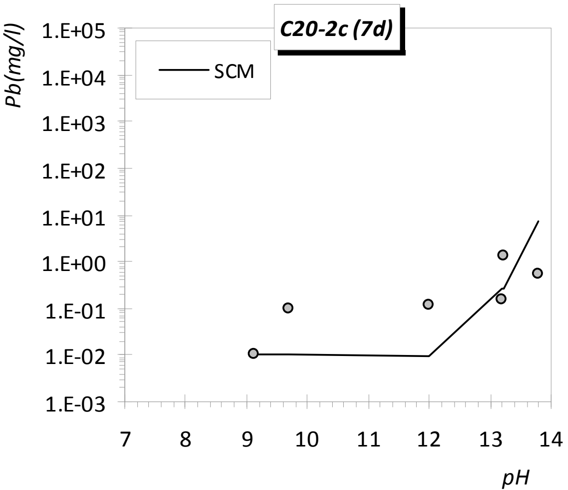

Figure 37: Results of geochemical modelling of Pb leaching on account of surface complexation by HFO and AAM (SCM = surface complexation model) for sample C20-2c

References

- ✓ L. Alarcon-Ruiz, G. Platret, E. Massieu, A. Ehrlacher: The use of thermal analysis in affecting the effect of temperature on a cement paste; Cement and Concrete Research (2005) 35: 609-613.
- ✓ T. Astrup, J. Dijkstra, R.N.J. Comans, H.A. van der Sloot, T.H. Christensen: Geochemical modelling of leaching from MSWI air-pollution-control residues; Environmental Science & Technology (2006) 40: 3551-3557.
- ✓ T. Astrup, P. Lechner, A. Polettini, R. Pomi, T. Van Gerven, A. van Zomeren: State-of-the-art and outlook on management of waste-to-energy bottom ashes, Part 2; Utilization. Proc. Sardinia 2007, Eleventh International Waste Management and Landfill Symposium, S. Margherita di Pula (CA), 1-5 October 2007, session A13 (on CD ROM).
- ✓ P. Blanc, A. Lassin, C. Nowak, A. Burnol, P. Piantone, L. Chateau: THERMODDEM: a thermodynamic database for waste materials; Available on-line at http://thermoddem.brgm.fr/ fichiers/Phreeqc_thermoddem_lvl1_no-org.txt (2007).
- ✓ B. Clozel-Leloup, F. Bodénan, P. Piantone: Bottom ash from municipal solid waste incineration: mineralogy and distribution of metals; In: Mehu J., Keck G., Navarro A. (eds.). Proc. STAB & ENV 99., International Conference on Waste Stabilization and Environment. Lyone Villeurbanne, France, (1999): 46-51.
- ✓ Council Directive 99/31/EC, 1999. Landfill of waste. Official Journal L 182, 16/07/1999, 0001-0019.
- ✓ D. Damidot and F.P. Glasser: Thermodynamic investigation of the $CaO–Al_2O_3–CaSO_4–H_2O$ system at 50 °C and 85 °C; Cement and Concrete Research (1992). 22: 1179-1191.
- ✓ D. Damidot and F.P. Glasser: Thermodynamic investigation of the $CaO–Al_2O_3–CaSO_4–H_2O$ system at 25 °C and the influence of Na_2O; Cement and Concrete Research (1993) 23: 221-238.
- ✓ D.A. Dzombak and F.M.M. Morel: Surface complexation modeling: hydrous ferric oxide; John Wiley & Sons, Inc., New York (1990).
- ✓ T.T: Eighmy, J.D. Eusden, K. Marsella, J. Hogan, D. Domingo, J.E. Krzanowski, D.Stämpfli: Particle petrogenesis and speciation of elements in MSW incineration bottom ashes; In: Goumans J.J.J.M., van der Sloot H.A., Aalbers Th.G. (eds). Waste Materials in Construction, Elsevier Science Publication B.V., Amsterdam, (1991): 111-136.

✓ C.J. Engelsen, H.A. van der Sloot, G. Wibetoe, G. Petkovic: Release of major elements from recycled concrete aggregates and geochemical modeling; Cementent and Concrete Research (2009) 39: 446-459.

✓ J.D. Eusden, T.T. Eighmy, K. Hockert, E. Holland, E. Marsella: Petrogenesis of municipal solid waste combustion bottom ash, Applied Geochemistry (1999) 14: 1073-1091.

✓ Y. Fan, S. Yin, Z. Wen, J. Zhong: Activation of fly ash and its effects on cement properties; Cement and Concrete Research (1999): 467-472.

✓ P. Filipponi, A. Polettini, R. Pomi, P. Sirini: Physical and mechanical properties of incineration bottom ash-based cements; Waste Managegement (2003) 23: 145-156.

✓ C. Giampaolo, S. Lo Mastro, A. Polettini, R. Pomi, P. Sirini: Acid neutralization capacity and hydration behavior of incineration bottom ash–Portland cement mixtures; Cement and Concrete Research (2002) 32: 769-775.

✓ Z. Giergiczny: Effect of some additives on the reactions in fly ash/$Ca(OH)_2$ system; Journal of Thermal Analysis and Calorimetry (2004) 76: 747-754.

✓ O. Ginés, J.M. Chimenos, A. Vizcarro, J. Formosa, J.R. Rosell: Combined use of MSWI bottom ash and fly ash as aggregate in concrete formulation: environmental and mechanical considerations; Journal of Hazardous Material (2009) 169: 643-650

✓ C.D. Hills: Personal communication. University of Greenwich (2009).

✓ IAWG (International Ash Working Group: A.J. Chandler, T.T. Eighmy, J. Hartlén, O. Hjelmar, D. Kosson, S.E. Sawell, H.A. van der Sloot, J. Vehlow); In: Municipal Solid Waste Incinerator Residues, Studies in Environmental Sciences 67, Elsevier Sci., Amsterdam, 1997.

✓ J. Hyks, T. Astrup, T.H. Christensen: Long-term leaching from MSWI air pollution control residues: leaching characterization and modeling; Journal of Hazardous Materials (2009) 162: 80-91.

✓ M. Kersten: Aqueous Solubility Diagrams for Cementitious Waste Stabilization Systems. 1. The C–S–H Solid-Solution System; Environmental Science & Technology (1996) 30: 2286-2293.

✓ D. Li, Y. Chen, Y., J. Shen, J. Su, X. Wu: The influence of alkalinity on activation and microstructure of fly ash; Cement and Concrete Research. (2000) 30: 881-886.

✓ B. Lothenbach and F. Winnefeld: Thermodynamic modeling of the hydration of Portland cement; Cement and Concrete Research (2006) 36: 209-226.

- ✓ E. Martens, D. Jacques, T. Van Gerven, L. Wang, D. Mallants: Geochemical modeling of leaching of Ca, Mg, Al, and Pb from cementitious waste forms; Cement and Concrete Research (2010) 40: 1298-1305.
- ✓ J.A. Meima and R.N.J. Comans: Geochemical modeling of weathering reactions in municipal solid waste incinerator bottom ash; Environmental Science & Technology (1997) 31: 1269-1276.
- ✓ J.A. Meima and R.N.J. Comans : Application of surface complexation/precipitation modeling to contaminant leaching from weathered municipal solid waste incinerator bottom ash; Environmental Science & Technology(1998) 32: 688-693.
- ✓ J.A. Meima and R.N.J. Comans: The leaching of trace elements from municipal solid waste incinerartor bottom ash at different stages of weathering; Applied Geochemistry (1999) 14:159-171.
- ✓ Ministero dell'Ambiente della Repubblica Italiana, 1998. D.M. 05/02/1998. Individuazione dei rifiuti non pericolosi sottoposti alle procedure semplificate di recupero ai sensi degli articoli 31 e 33 del decreto legislativo 5 febbraio 1997, n. 22. Suppl. Ord. G.U. 16/04/1998 n. 88 (as amended by D.M. 05/04/2006, n. 186).
- ✓ R. Onori, A. Polettini, R. Pomi, R: An investigation of RDF bottom ash activation for blended cement formulation. Méhu, J., Goumans, J.J.J.M., Heynen, J.J.M. (eds.). Proc. WASCON 2009, International Conference on Sustainable Management of Waste and Recycled Materials in Construction, Lyon (FR), 3-5 October 2009.
- ✓ G. Pecqueur, C. Crignon, B. Quénée: Behaviour of cement-treated MSWI bottom ash; Waste Management (2001) 21: 229-233.
- ✓ J. Pera, L. Coutaz, J. Ambroise, M. Chababbet: Use of incinerator bottom ash in concrete; Cement and Concrete Research (1997) 27: 1-5.
- ✓ R.B. Perkins and C.D. Palmer: Solubility of ettringite $Ca_6[Al(OH)_6]2(SO_4)_3 \cdot 26H_2O$ at 5–75 °C; Geochimica et Cosmochimica Acta (1999) 63: 1969-1980.
- ✓ A. Polettini, R. Pomi, G. Carcani: The effect of Na and Ca salts on MSWI bottom ash activation for reuse as a pozzolanic admixture; Resources, Conservation and Recycling (2005) 43: 403-418.
- ✓ A. Polettini, R. Pomi, E. Fortuna: Chemical activation in view of MSWI bottom ash recycling; Journal of Hazardous Materials (2009) 162: 1292-1299.
- ✓ B. Pacewska, I. Wilinska, G. Blonkowski: Investigations of cement early hydration in the presence of chemically activated fly ash; Journal of Thermal Analysis and Calorimetry (2008) 93: 769-776.

✓ C.S. Poon, X.C. Qiao, Z.S. Lin: Pozzolanic properties of reject fly ash in blended cement pastes; Cement and Concrete Research (2003) 9: 1857-1865.

✓ J. Qian, C. Shi, Z. Wang: Activation of blended cements containing fly ash; Cement and Concrete Research (2001) 31: 1121-1127.

✓ X.C. Qiao, M. Tyrer, C.S. Poon, C.R. Cheeseman: Novel cementitious materials produced from incinerator bottom ash; Resources, Conservation and Recycling (2008) 52: 496-510.

✓ X.C. Qiao, C.S. Poon, C.R. Cheeseman: Influences of chemical activators on incinerator bottom ash; Waste Management (2009) 29: 544-549.

✓ T. Sabbas, A. Polettini, R. Pomi, T. Astrup, O. Hjelmar, P. Mostbauer, G. Cappai, G. Magel, S. Salhofera, C. Speiserg , S. Heuss-Assbichler, R. Klein, P. Lechner (members of the pHOENIX working group on Management of MSWI Residues): Management of municipal solid waste incineration residues; Waste Management (2003) 23: 61-88.

✓ C. Shi and R.L. Day: Acceleration of the reactivity of fly ash by chemical activation; Cement and Concrete Research (1995) 25: 15-21.

✓ C. Shi and R.L. Day: Pozzolanic reaction in the presence of chemical activators Part I Reaction kinetics; Cement and Concrete Research. (2000 (a)) 30: 51-58.

✓ C. Shi and R.L. Day: Pozzolanic reaction in the presence of chemical activators. Part II. Reaction products and mechanism; Cement and Concrete Research (2000 (b)) 30: 607-613.

✓ C. Shi and R.L. Day: Comparison of different methods for enhancing reactivity of pozzolans; Cement and Concrete Research. (2001) 31: 813-818.

✓ W. Stumm and J.J. Morgan: Aquatic Chemistry: Chemical Equilibria and Rates in Natural Waters. third ed., John Wiley & Sons, Inc., New York (1995).

✓ U.S. Department of Energy: Qualification of thermodynamic data for geochemical modeling of mineral-water interactions in dilute systems; Document no. ANL-WIS-GS-000003 (2004).

✓ C. Zevenbergen and R.N.J. Comans: Geochemical factors controlling the mobilization of major elements during weathering of MSWI bottom ash; In: Goumans, J.J.J.M., van der Sloot, H.A., Aalbers, Th.G. (Eds.); Environmental Aspects of Construction with Waste Materials, Studies in Environmental Sciences Elsevier Sci., Amsterdam, (1994) 60: 179-194.

✓ C. Zevenbergen, L.P. Van Reeuwijk, J.P. Bradley, R.N.J. Comans: Mechanism and conditions of clay formation during natural weathering of MSWI bottom ash; Clays and Clay Minerals (1996) 44: 546-552.

5. Results and Discussion: BA based geopolymer materials

5.1 Mechanical properties of geopolymer products

The results from mechanical characterization of the geopolymeric matrices are shown in Figure 38 and in Table 20 in terms of average UCS values and corresponding standard deviations of measurements. Depending on paste composition, large variations in the mechanical properties were observed, with values ranging:

- at 7 curing days from a minimum of < 0.1 MPa for sample S-1.28-7.5 to a maximum of 7.38 MPa for sample S-2.29-7.5;
- at 28 curing days from a minimum of < 0.1 MPa for sample S-1.69-12 to a maximum of 9.99 MPa for sample S-2.29-7.5;
- at 56 curing days from a minimum of < 0.1 MPa for sample S-1.69-5 to a maximum of 8.28 MPa for sample S-2.29-7.5.

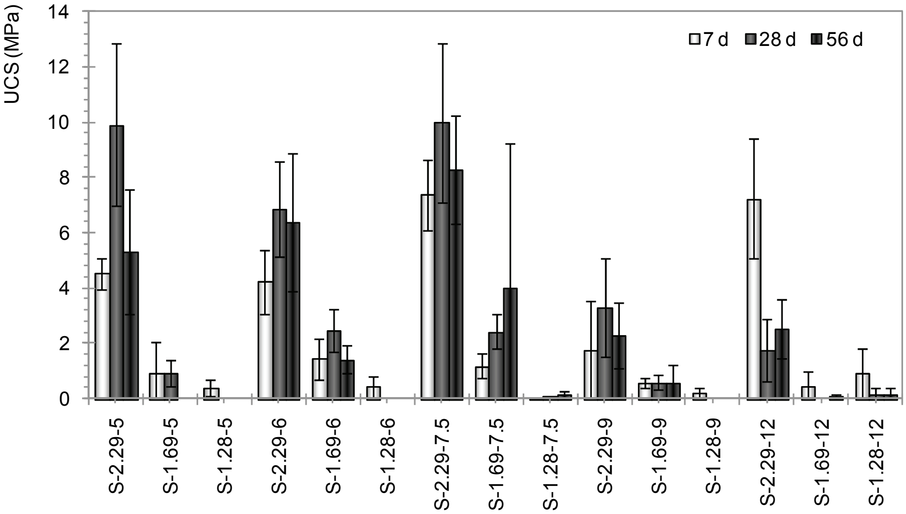

Figure 38: Results of UCS testing on geopolymerized materials (error bars are drawn at one standard deviation of values)

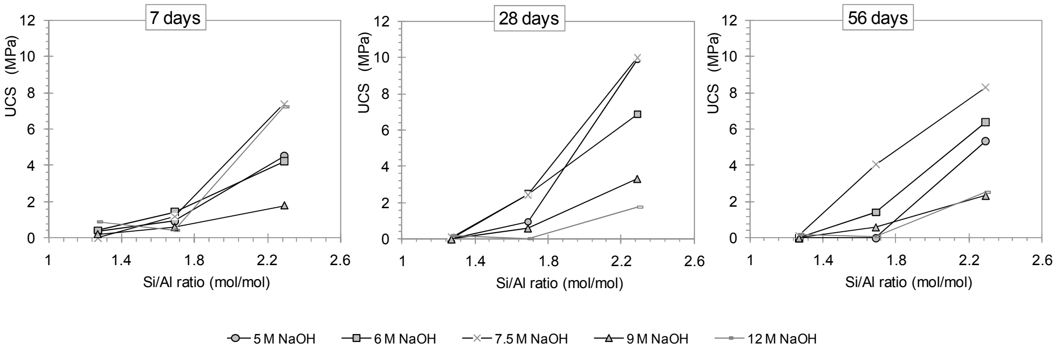

Figure 39: Relationship between UCS and the Si/Al ratio at given NaOH concentrations in the alkaline medium

		Media UCS (MPa)			Dev. st. (MPa)			Si/Al	NaOH
Name	Sample code	7 d	28 d	56 d	7 d	28 d	56 d	(mol/mol)	(M)
A	S-2.29-6	4.23	6.86	6.37	1.17	1.73	2.49	2.29	6
B	S-1.69-6	1.44	2.48	1.42	0.73	0.79	0.51	1.69	6
C	S-1.28-6	0.43	n.a	n.a	0.40	n.a	n.a	1.27	6
D	S-2.29-9	1.78	3.32	2.32	1.74	1.79	1.19	2.29	9
E	S-1.69-9	0.58	0.60	0.60	0.17	0.28	0.60	1.69	9
F	S-1.28-9	0.19	n.a	n.a	0.19	n.a	n.a	1.27	9
G	S-2.29-12	7.23	1.75	2.53	2.16	1.14	1.04	2.29	12
H	S-1.69-12	0.44	0.00	0.07	0.56	0.00	0.06	1.69	12
I	S-1.28-12	0.90	0.17	0.17	0.90	0.21	0.21	1.27	12
J	S-2.29-5	4.52	9.90	5.32	0.59	2.93	2.23	2.29	5
L	S-1.69-5	0.93	0.94	0.00	1.11	0.48	0.00	1.69	5
M	S-1.28-5	0.40	n.a	n.a	0.28	n.a	n.a	1.27	5
O	S-2.29-7.5	7.38	9.99	8.28	1.29	2.86	1.97	2.29	7.5
P	S-1.69-7.5	1.18	2.43	4.04	0.45	0.62	5.17	1.69	7.5
Q	S-1.28-7.5	0.00	0.10	0.13	0.00	0.01	0.15	1.27	7.5

Table 20: Values of UCS for geopolymeric samples

While an increase in the Si/Al ratio appeared to improve compressive strength (see Figure 39), the influence of NaOH concentration in the reacting medium was less clear, so that at this stage of the investigation it is not possible to derive any conclusive information about the optimal NaOH dosage. However, at longer curing times (28 and 56 days) it can be observed that the mechanical characteristics were worsened atNaOH concentrations of 9 and 12 mol/l. For the Si/Al ratio, the results shown in Figure 39 appear to indicate that the optimum value for mechanical strength development probably lies beyond the investigated range. Decreasing the Si/Al molar ratio a considerable decrease in mechanical characteristics was observed for all samples and for all the NaOH concentrations investigated. While the measured UCS values were relatively weak at the operating conditions tested, the trend reported in Figure 39 suggests that improved mechanical characteristics may be obtained when increasing the Si/Al molar ratio above 2.29.

The best results in terms of mechanical strength were obtained for the geopolymeric samples with Si/Al=2.29.

Previous studies on geopolymerization of waste materials (Chindaprasirt et al., 2006; 2009; Andini et al., 2008; Kumar et al., 2011; Panias et al., 2007; Škvára et al., 2009; Temuujin et al., 2009; 2010; van Jaarsveld et al., 2002; Songpiriyakij et al., 2009; Xu et al., 2010; Cheng et al., 2003; Oh et al., 2010; Kourti et al., 2010) have shown that a very wide range of mechanical strength values can be obtained depending on the initial material composition and processing conditions. For a more detailed physical and mineralogical/microstructural characterization and to gain knowledge on the microstructure-mechanical strength relationship, four samples were selected among those displaying the best and worst mechanical behaviour and which differed also in the Si/Al ratio and the NaOH concentration; these included:

- sample S-2.29-7.5 (UCS = 7.38 ± 1.29 MPa at 7-day curing; UCS = 9.99 ± 2.86 MPa at 28-day curing and UCS = 8.28 ± 1.97 MPa at 56-day curing);
- sample S-2.29-5 (UCS = 4.52 ± 0.59 MPa at 7-day curing; UCS = 9.90 ± 2.23 MPa at 28-day curing and UCS = 5.32 ± 2.29 MPa at 56-day curing);
- sample S-1.69-7.5 (UCS = 1.18 ± 0.45 MPa at 7-day curing; UCS = 2.43 ± 0.62 MPa at 28-day curing and UCS = 4.04 ± 5.17 MPa at 56-day curing);
- sample S-1.28-7.5 (UCS < 0.1 MPa at 7-day curing; UCS = 0.10 ± 0.01 MPa at 28-day curing and UCS = 0.13 ± 0.15 MPa at 56-day curing).

The unit weight and total porosity values for such samples are reported in Table 21. The wet apparent unit weight was found to vary from 10.5 to 15.6 kN/m^3, the solids unit weight ranged from 25.3 to 28.5 kN/m^3, while total porosity ranged from 40.2 to 66.5%, and all these parameters displayed a good correlation with mechanical strength data.

Name	Sample code	UCS (MPa)	Wet apparent unit weight (kN/m^3)	Porosity (%)	Solids unit weight (kN/m^3)
O	S-2.29-7.5	7.38 ± 1.29	14.96 ± 0.12	42.8 ± 1.2	28.46
J	S-2.29-5	4.52 ± 0.59	15.57 ± 0.15	40.2 ± 0.5	25.33
P	S-1.69-7.5	1.18 ± 0.45	12.02 ± 0.21	58.9 ± 0.9	25.49
Q	S-1.28-7.5	< 0.1	10.54 ± 0.24	66.5 ± 1.2	26.12

Table 21: Results of physical characterization for selected samples (mean values ± standard deviation)

5.2 SEM (Secondary Electron Images) interpretation

After compressive strength tests, crushed geopolymer samples were collected for SEM/EDX analysis.

The morphological studies were focused on the geopolymers surfaces for samples S-2.29-7.5 at 7 day-curing and S-2.29-5 at 7- and 28-day curing. Additional analyses were made for S-2.29-7.5, S-2.29-5, S-1.69-7.5 and S-1.28-7.5 powdered (425-μm undersize particle ≥ 95%) samples at 7-day curing.

The SEM micrographs (200× magnification) of polished fragments for sample S-2.29-7.5 at 7-day curing and samples S-2.29-5 at 7- and 28-day curing are shown in Figure 40.

These samples were those with the best characteristics in terms of mechanical strength. In general, the samples showed an amorphous and quite compact microstructure with some irregularly shaped macropores. The homogeneous microstructure of samples indicates that the geopolymerization process induced microstructural changes which were evenly distributed in the whole sample and the dissolution of the raw material was well started (Temuujin et al., 2009). In detail, morphological observations suggest that individual unreacted particles of different size were still present in the material and were surrounded by a layer of small sheets of reacted solids. This effect has been also observed in geopolymers produced using plasma vitrified incinerator air pollution control residues (Kourti et al., 2010).

In the present case, it is apparent that the external layer of reacting material filled the original pores and acted by forming bridges and interconnections between the original grains. The fact that geopolymerization reactions had occurred within the material appears to be indicated by the relatively low pore volume and small void size visible in the SEM pictures. Visual observation of the amount and size of pores in the investigated samples also appears to confirm the results from total porosity (Table 21) measurements which indicated that sample S-2.29-7.5 was more porous than sample S-2.29-5.

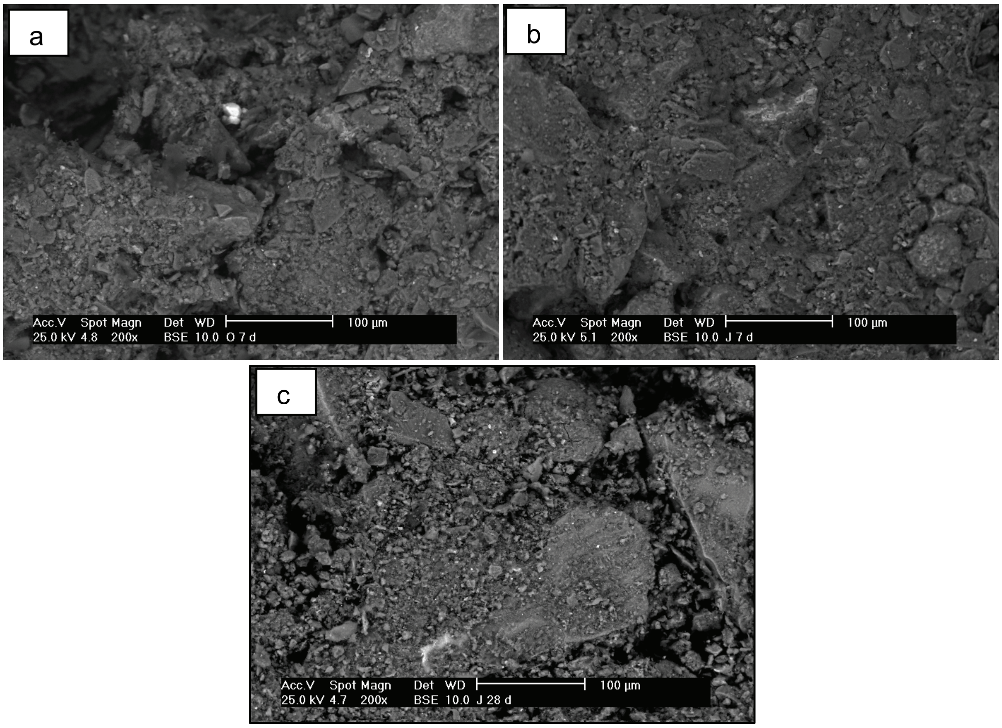

Figure 40: SEM micrographs of fracture surfaces for samples (a) S-2.29-7.5 at 7 curing days (b) S-2.29-5 at 7 curing days and (c) S-2.29-5 at 28 curing day

The EDAX analyses were also done on selected locations on sample surface. In particular, on the basis of differences visually observed in terms of colour and/or morphology, different locations for the analysis were selected. For sample S-2.29-7.5 at 7-day curing two points were selected for the analysis as shown in Figure 41 (a): point P1 was a white particle while point P2 was the matrix portion of the sample.

For sample S-2.29-5 at 7-day and 28-day curing three different points were selected for the analysis as shown in Figure 41 (b) and (c): P1 was a white area (maybe an unreacted metakaolin particle), P2 was the bulk of the matrix and P3 was a grey zone different in color from the matrix.

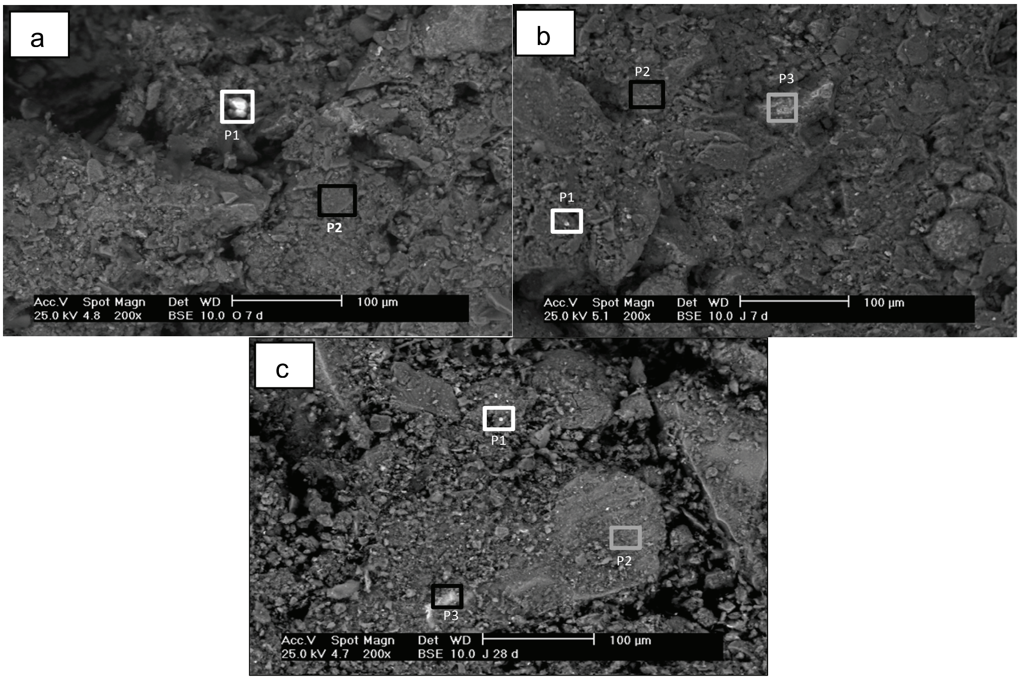

Figure 41: SEM micrographs and zone selected for EDAX spot analysis: samples (a) S-2.29-7.5 at 7-day curing (b) S-2.29-5 at 7-day curing and (c) S-2.29-5 at 28-day curing

EDAX spot analyses (Figure 42) conducted on 10-μm^2 square areas indicated the main presence of Si (20.9 and 18.0 mol% for samples S-2.29-7.5 and S-2.29-5, resp.) and Al (19.8 and 15.7 mol% for samples S-2.29-7.5 and S-2.29-5, resp.), corresponding to Si/Al molar ratios of 1.05 and 1.15. The Si/Al ratio for these samples thus decreased from 2.29 mol/mol to a final value of ~1.0 mol/mol, which may be explained considering that polysialate-type geopolymers [R_n–(–Si–O–Al–O–$)_n$–], having an Si/Al ratio of 1 (Davidovits 2008), were formed under the treatment conditions applied. For sample S-2.29-5 at 28-day curing the main presence of Si (13.6 mol%) and Al (9.03 mol%) corresponded to an Si/Al molar ratio of 1.46. Sample S-2.29-5 at both curing times was also found to have a significant Na content (around 10.8 mol%), which was also appreciably higher than that of sample S-2.29-7.5 (around 2 mol%).

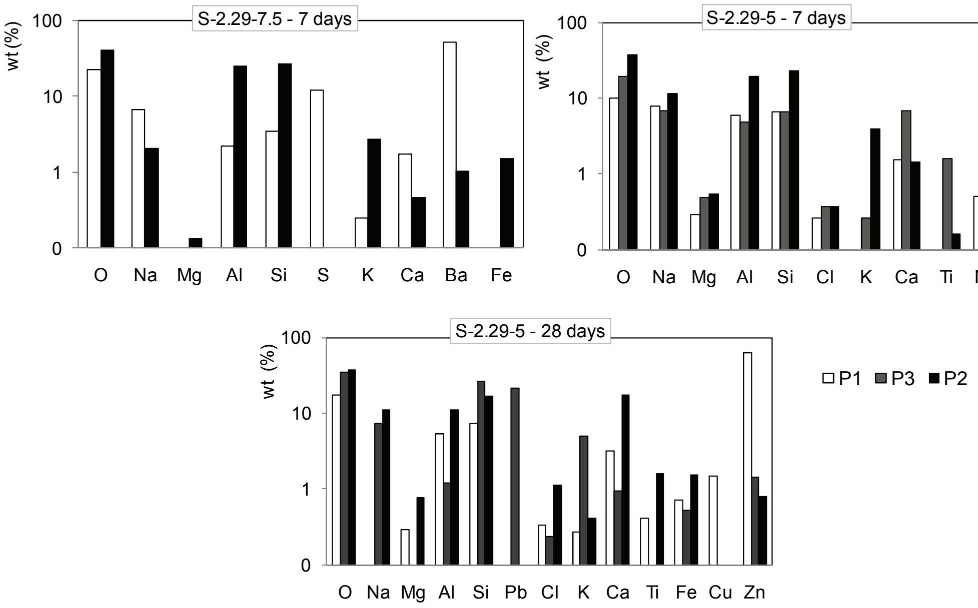

Figure 42: Main elements indentified in geopolymer samples through EDAX analysis

From SEM micrographs and EDAX results for powders (Figure 43) samples, it was possible to observe, a different composition f white zone (P1) in comparison to that of the bulk of matrix (P2). Some of these small areas contain Fe, Ba, Zn, S, Pb, Cl and Ti-rich particles. These elements derive from bottom ash and metakaolin (the kaolin precursor was a commercial) which appear to remain unreacted during geopolymerization and trapped within the geopolymer gel (predominantly hydrated sodium aluminosilicate)(Zhang et al. 2008, Stevenson et al., 2005). Although they appeared to be concentrated into regions of less than 5 µm not uniformly included in the geopolymeric matrix (Zhang et al 2008).

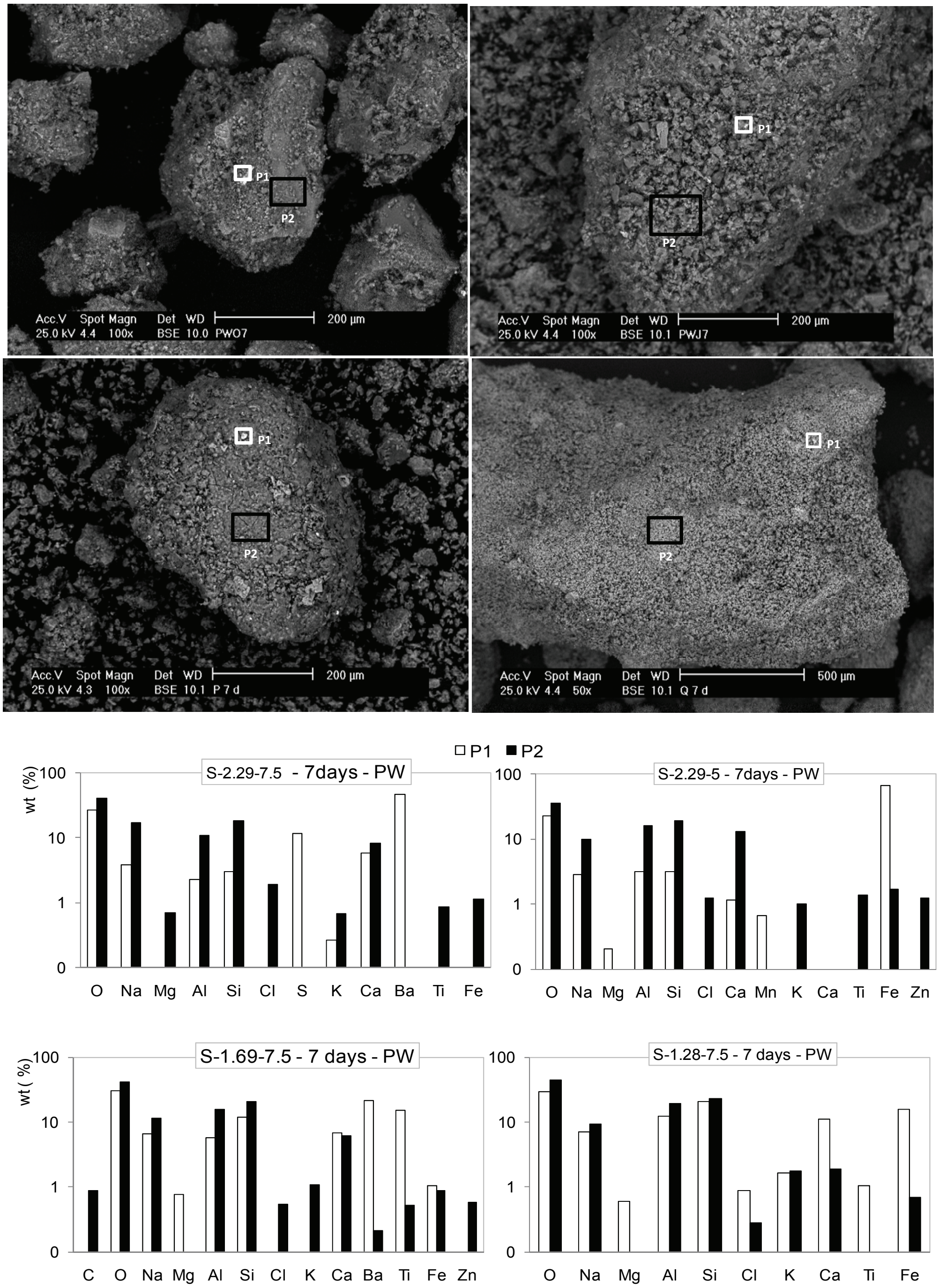

Figure 43: SEM micrograph and results of EDAX spots analysis for powder samples (a) S-2.29-7.5 at 7 day-curing (b) sample S-2.29-5 at 7 day-curing (c) sample S-1.69-7.5 at 7 day-curing (d) sample S-1.28-7.5 at 7 day-curing

5.3 TGA interpretation

The thermal analysis results are reported in Figure 44. for the selected geopolymer samples at 7 curing days. The thermograms displayed basically four regions characterized by different amounts and rates of mass loss in the following ranges: 20-240°C, 240-380°C, 380-700°C and > 700°C. Within the first region, a major weight loss occurred, accounting for 58-75% of the total weight loss recorded over the temperature range investigated. As outlined by numerous studies (Andini e al., 2008; Škvára et al., 2009; Duxson et al., 2006; Kong and Sanjayan, 2010; Pan et al., 2010; Rickard and van Riessen, 2010), a large endothermic peak was observed at temperatures of 120-130 °C, which was related to sample dehydration, with loss of absorbed and loosely bound water. As reported in Table 22, the weight loss associated to the first temperature region ranged from 4.4 to 5.3% and it was larger for samples S-1.69-7.5 and S-1.28-7.5, for which a poorer geopolymerization degree was also indicated by the other characterization analyses.

Further weight decrease was recorded, although at a lower rate (as also noted by other investigators (Kong and Sanjayan, 2010; Rickard and van Riessen, 2010), in the second temperature region and was associated to sample dehydroxylation (Andini et al., 2008; Duxson et al., 2006), the mass loss values ranged from 1.4 to 1.8%. However, in the DTA patterns of samples S-1.69-7.5 and S-1.28-7.5, an exothermic peak was identified at about 330 °C, with an associated weight loss of 1.6 and 1.4%, respectively, which indicates the presence of a different phase for such samples if compared to the other materials investigated. Based on the information available, however, no tentative association with any specific phase, the occurrence of which could reasonably be expected only in samples S-1.69-7.5 and S-1.28-7.5, could be made. If the weight loss associated to the decomposition of this unknown phase is subtracted from the overall weight decrease in the temperature region 240-380 °C, net mass loss values are obtained, as shown in Table 22, which suggested a higher degree of hydration for samples S-2.29-7.5 and S-2.29-5, possibly confirming the larger geopolymerization degree attained for such materials.

An additional, much slower, mass loss was observed between 380 and 700 °C, which mirrors a more stable thermal behaviour of the materials at temperatures above 380 °C and confirms the results obtained from other studies (Kong and Sanjayan, 2010; Prud’homme et al., 2010). Finally, a small weight gain (~1%) was observed in the fourth temperature region (> 700 °C).

Temperature range	Sample code			
	S-2.29-7.5	S-2.29-5	S-1.69-7.5	S-1.28-7.5
0-240 °C	4.42	4.57	4.81	5.27
240-380 °C	1.38	1.45	1.83	1.57
240-380 °C (net)	1.38	1.45	0.21	0.19
380-700 °C	1.36	1.74	1.50	1.24
700-1000 °C	-0.33	0.05	-0.56	-1.03

Table 22: Weight loss for different temperature regions as derived from the TGA curves in Figure 44: (a) TGA and (b) DTA curves for samples O, J, P and Q at 7 day curing

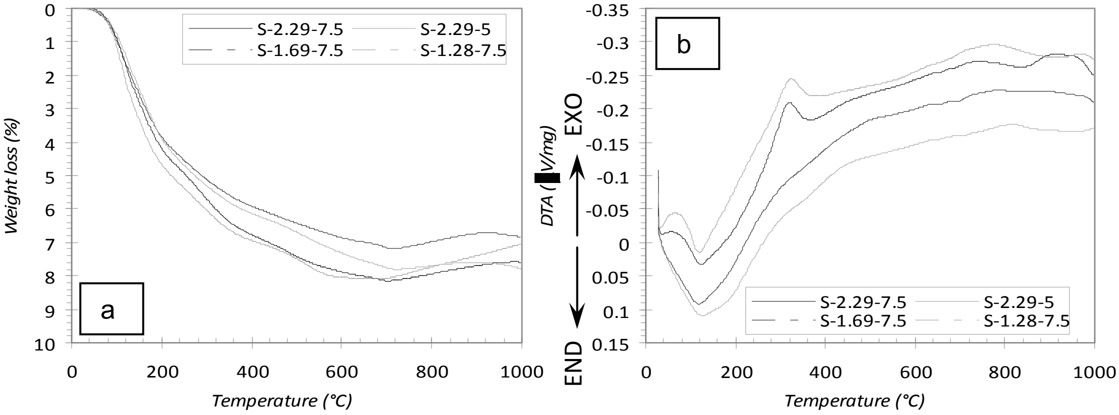

Figure 44: (a) TGA and (b) DTA curves for samples O, J, P and Q at 7 day curing

5.4 FT-IR (Fourier transform infrared spectroscopy) analysis

FTIR absorption spectroscopy is well known for its sensitivity to characterize materials with short-range structural order, and is considered as a useful tool to characterize geopolymer matrices (Guo et al., 2009). Infrared spectra were obtained for selected samples at 7- and 28-day curing (Figure 45 (a)) in order to attain a better description of the structural implications of the degree of silicate polycondensation on the nature of the final product (Phair et al., 2002). Infrared spectra of the unreacted bottom ash sample were also collected for comparison purposes.

Five main adsorption bands can be identified in the FT-IR spectra (Table 23 and Figure 45) of treated materials, namely: a band at 450-470 cm^{-1} associated to in-plain bending vibration of Si–O–Si (Barbosa et al., 2000; Phair et al., 2002) (referred to as peak 1), a second main band at 980-1040 cm^{-1} associated to asymmetric stretching vibrations of

Si–O/Al–O bonds (Barbosa et al., 2000; Mozgawa et al., 2009; Guo et al., 2010; Phair et al., 2002) (referred to as peak 2), a band at ~1450 cm^{-1} due to the presence of O–C–O stretching vibration in carbonate groups (Andini et al., 2008; Barbosa et al., 2000; Mozgawa et al., 2009; Lee et al., 2002) (referred to as peak 3), two broad bands at 1640–1660 cm^{-1} and 3440–3460 cm^{-1} related to stretching and deformation vibrations of OH and H–O–H groups (Chindaprasirt et al., 2009; Barbosa et al., 2000; Lee et al., 2002; Palomo et al., 1999) (referred to as peaks 4 and 5). For the untreated BA, a sharp band (although of low intensity) at ~3690 cm^{-1} was also identified (referred to as peak 6) and associated to O–H stretching in the $Ca(OH)_2$ structure (Yousuf et al., 1995).

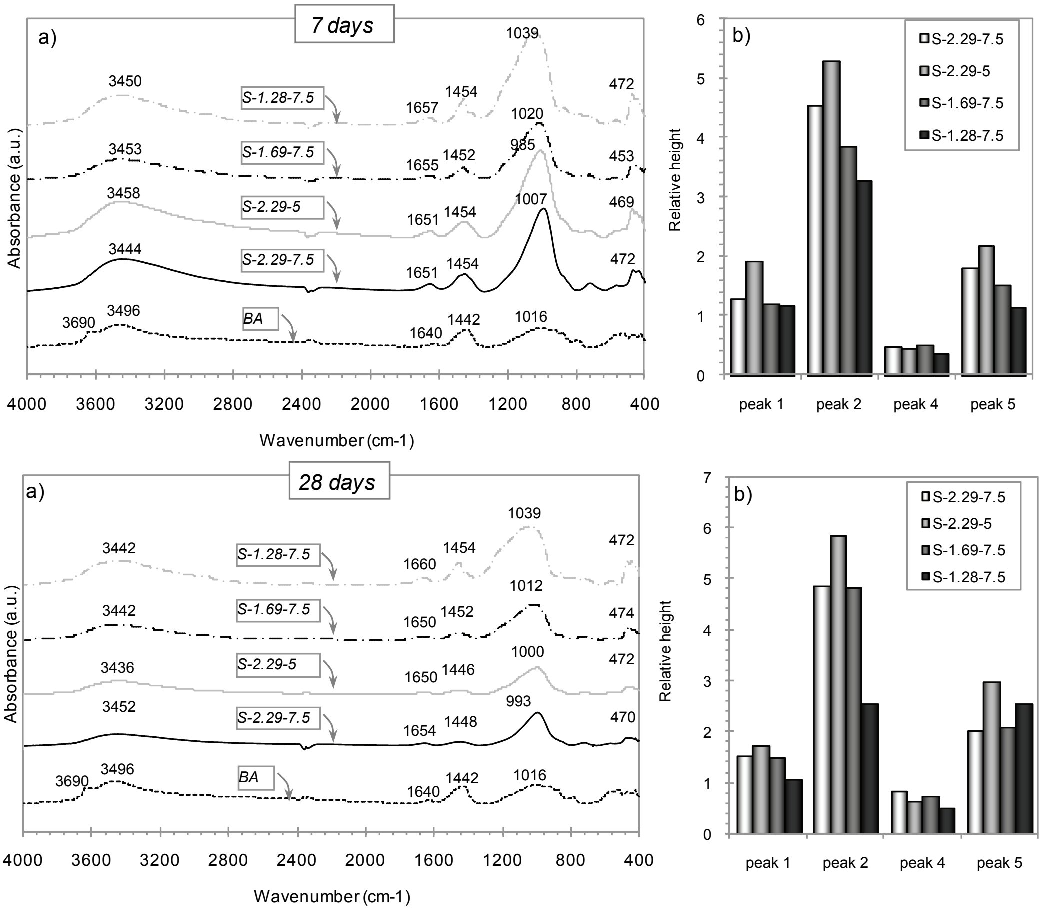

Figure 45: FT-IR spectra at 7- and 28-day curing (a) and comparison of relative peak intensities (b) for BA-based geopolymers

According to previous literature studies (Barbosa et al., 2000; Mozgawa et al., 2009; Guo et al., 2010; Phair et al., 2002), the peaks centred at 980-1040 cm^{-1} and 450-470 cm^{-1}

were assumed as the main molecular vibration fingerprints of geopolymeric materials. While the latter was not present in the original BA and was visible in the treated products, the former appeared in the treated materials with a different shape and intensity if compared to the untreated ash. The absorption characteristics in the range of peak 2 suggest that FT-IR spectra display broad and asymmetric curves, which likely result from the overlapping of several characteristic vibrational bands (Rovnaník 2010); it is thus possible that not only stretching vibrations of Si–O/Al–O bonds were associated to the observed IR peaks, but that additional vibration modes were also hidden in the spectra. However, a quantitative derivation of such additional characteristic bands has not been performed in the present study. Considering the main peak identified as peak 2, its position tended to shift from wavenumbers of 1020-1040 cm^{-1} (samples S-1.69-7.5 and S-1.28-7.5) towards lower values in the range 985-1007 cm^{-1} (samples S-2.29-5 and S-2.29-7.5), which may be taken as an indication of the increase in the degree of geopolymerization associated to the inclusion of tetrahedrally-coordinated Al in the Si–O–Si skeletal structure (Andini et al., 2008; Škvára et al., 2009; Mozgawa et al., 2009; Rovnaník et al., 2010; Rees et al., 2008).

A comparison between the intensities of FT-IR peaks for the four BA-based geopolymers is provided in Figure 45 (b). Data for each sample were calculated as relative intensities of the peaks of interest normalised to the intensity of peak 3, assuming that the degree of carbonation was the same for all samples tested, so that the carbonate peak should have the same height. The most evident difference in peak height could be observed for peak 2, with samples S-2.29-5 and S-2.29-7.5 displaying higher peak intensities than the other two samples, in agreement with the higher strengths measured; however, the fact that sample S-2.29-7.5 showed a higher UCS than the former could not be related to the information provided by FT-IR data. In general, FT-IR data showed that sample S-2.29-5 displayed higher peak intensities than the other samples. The fact that the height of peak 5, associated to absorbed water, followed the same trend already noted for peak 2 may be considered as an indication of the higher degree of hydration attained for samples S-2.29-5 and S-2.29-7.5, as opposed to the other materials investigated.

Another interesting feature noted in the FT-IR spectra was the fact that a small peak appearing at ~800 cm^{-1} for the raw BA, which was attributed to Si–O–Al vibration (Barbosa et al., 2000), disappeared in the treated materials and was replaced by several weaker bands at lower wavenumbers, ranging from 700 to 800 cm^{-1}. This may be interpreted assuming that decomposition of Al-containing chemical structures occurred during geopolymerization and that the resulting Al was afterwards incorporated in alumino-silicate structures indicated by peak 2.

			peak 5	peak 4	peak 3	peak 2	peak 1
	cm $^{-1}$ Name	Sample code	H-O–H DEFORMATION	O–H STRETCING VIBRATION	O-C-O STRETCHING VIBRATION	Al-O Si-O ASYMMETRIC STRETCHING VIBRATION	Si-O-Si BENDING VIBRATION
7 days	**O**	S-2.29-7.5	3444	1651	1454	1007	442
	J	S-2.29-5	3458	1651	1454	985	468
	P	S-1.69-7.5	3453	1655	1452	1020	439
	Q	S-1.28-7.5	3450	1657	1454	1039	467
28 days	**O**	S-2.29-7.5	3452	1654	1448	993	470
	J	S-2.29-5	3436	1650	1446	1000	472
	P	S-1.69-7.5	2442	1650	1452	1012	474
	Q	S-1.28-7.5	3442	1660	1454	1039	472

Table 23: Position and interpretation of the main FT-IR peaks for geopolymer samples

5.5 XRD interpretation

The mineralogy of the ground selected samples was determined by X-ray diffraction (XRD). In Figure 46 are shown the XRD patterns of bottom ash sample as well as those of geopolymers samples at 7-day curing.

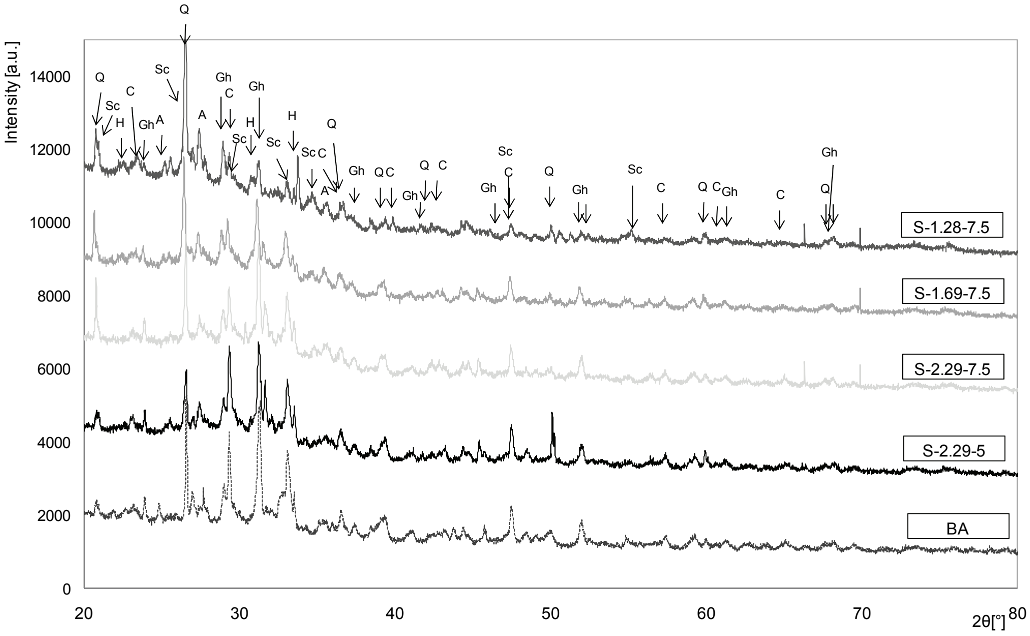

Figure 46: XRD patterns for geopolymer samples at 7-day curing and BA

Q: quartz, Gh: gehelenite, C: calcite, Sc: calcium silicate, A: anorthite, H: hydrocalumite

The XRD patterns of bottom ash, as previously described, displayed peaks associate to some crystalline phases such as: quartz (SiO_2), gehlenite ($Ca_2Al_2SiO_7$), calcite ($CaCO_3$), calcium silicate ($Ca_2(SiO_4)$), anorthite ($Na_{0.05}Ca_{0.95}Al_{1.95}Si_{2.05}O_8$) and hydrocalumite $Ca_2Al(OH)_{6.5}Cl_{0.5}\bullet3(H_2O)$, iron oxides including hematite.

In general, the patterns for geopolymer samples show the same crystalline phases indentified in the bottom ash sample although with reduced peak intensities. The main crystalline phases, including quartz and gehlenite, well detected in all the geopolymers patterns, are relatively inert during the geopolymerization process and the intensity of these peaks generally has not been found to change dramatically (Criado et al., 2007; Rees et al., 2008; Zhang et al., 2008), while the other crystalline phases seem to have more largely decreased as a result of geopolymerization, likely forming amorphous and semi-crystalline phases (Feng et al., 2004).

In BA a broad hump located in the 2θ region around 25-38° with a maximum around 32° 2θ (Figure 47) was detected and associated to the amorphous phases present in BA. Many other studies conducted on similar materials indicated that the same region extended from 20 to 32° 2θ (Alvarez-Ayuso et al. 2008; Bakharev 2005; De Silva et al. 2007; Criado et al., 2007) with a maximum around 24-26° 2θ. The location of the glass diffraction maximum is around 22.7°-27.5° 2θ in ashes containing up to about 20% CaO; while for ashes with CaO contents above 20% the location of the maximum is around 32° 2θ (Diaz et al., 2010). The shift observed in the BA sample investigated could derive from the higher Ca content of the material (38.5 wt %). When BA is mixed with the alkaline solution the original phases in the material are dissolved producing a new amorphous aluminosilicate gel phase in geopolymeric matrices (Alvarez-Ayuso et al., 2008; Panias et al., 2007). For this reason, the major feature of XRD of geopolymers is this large 'hump' (Provis et al., 2005) generally attributed to the amorphous aluminosilicate gel assumed to be the primary binder phase present in geopolymeric systems (Rhaier et al., 1996).

The broad hump, registered between 25-38°2θ in the BA pattern, is shifted towards higher values up to 42° 2θ for the geopolymeric samples S-2.29-7.5 and S-2.29-5. The broad hump from 20-25° 2θ to 38-40° 2θ is typical of a calcium aluminate glass structure that is significantly more reactive with water compared with the siliceous glass structure (Diaz et al., 2010). This leads to the formation of calcium silicate hydrate (C-S-H) compounds in addition to the geopolymeric gel icreasing the mechanical strength of the hardened matrices (Diaz et al., 2010; Guo et al., 2010).

For samples S-1.69-7.5 and S-1.28-7.5 the shift in the hump location is less evident in comparison to the other geopolymeric samples, but the slope is more prominent; however, the maximum remains in the typical range characteristic of materials with high Ca contents. Probably for this reason the mechanical characteristics of both samples were not satisfactory.

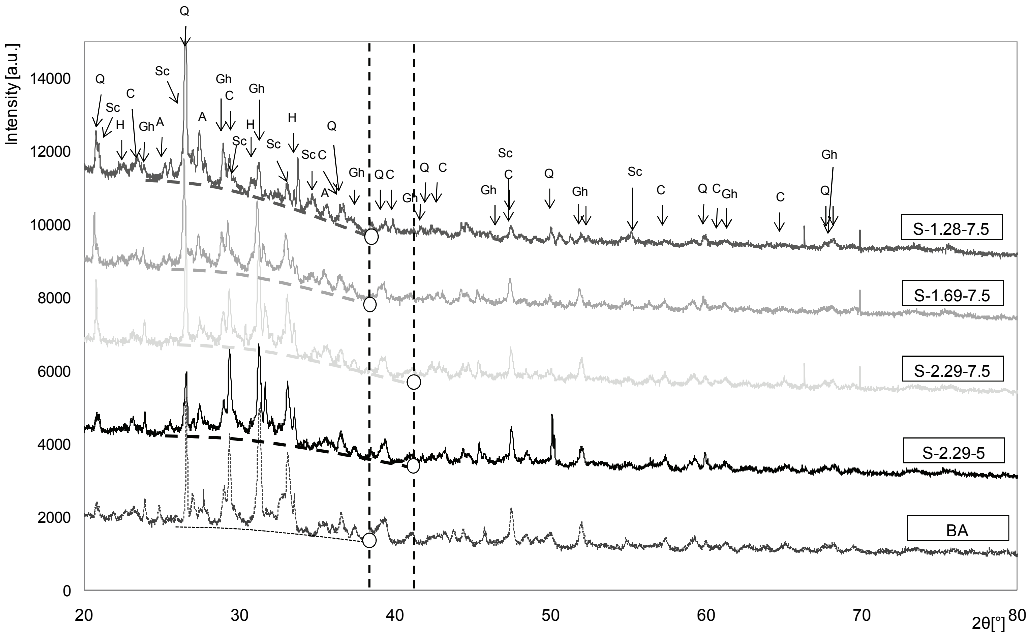

Figure 47: XRD patterns for geopolymer samples and BA with details about the position of amorphous broad hump

RAMAN interpretation

Raman spectra were collected between 100 and 1800 cm-1. In Figure 49 the main Raman spectra for each analyzed samples (S-2.29-7.5, S-2.29-5, S-1.69-7.5 and S-1.28-7.5 at 7- and 28-day curing) are shown. Due to the inhomogeneity of geopolymer samples different spectra were collected for different areas depending on their prevalent colour (grey “G”, white “W” and black “B”, see Figure 48), as already described.

The following features were observed for the investigated samples:

- for sample S-2.29-7.5 at 7-day curing a series of peaks in the region between 100 and 550 cm^{-1}, some peaks around 600 and 800 $cm^{-1}$and a clear double peak between 1380-1400 cm^{-1} could be identified. At longer curing times (28 days) the double peak at around 1400 cm^{-1} was still present;

- for sample S-2.29-5 at 7-day curing there were less clear peaks, likely due to the signal noise, centered at 150, 225, 375, 400, 600 and 1100 cm^{-1}, as well as the double peak at around 1400 cm^{-1}. At longer curing times (28 days) a clear peak around 200 cm^{-1} was identified while the double peak at 1400 cm^{-1} appeared to have considerably broadened and flattened;
- for sample S-1.69-7.5at 7-day curing some small peaks around 400, 430, 720, 1600, 1650 and 1700 cm^{-1} were detected while, at 28-day curing most peaks disappeared with only two peaks at 400 and 720 cm^{-1} remained visible, and a small new peak between 120 and 200 cm^{-1} appeared;
- for sample S-1.28-7.5, at both curing times, it was not possible to identify clear peaks.

Taking these information into account, in Table 24 the main peaks associated to mineral phases also identified by XRD analysis are reported.

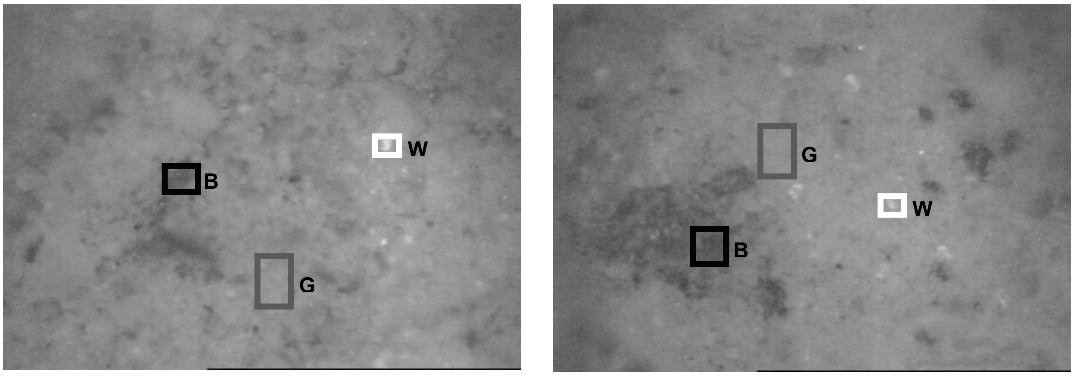

Figure 48: Examples of the areas where the spectra have been collected (sample S-2.29-5 28 d)

According to literature data, the peak at around 1400 cm^{-1} visible in samples S-2.29-7.5 and S-2.29-5, at both curing times analyzed, may be associated to alumina). Similarly, the peaks observed in sample S-2.29-7.5 at 7-day curing and in sample S-2.29-5 at longer curing times at ~520 and ~540 cm^{-1} may be ascribed to silicon (either amorphous or crystalline).

Quartz can be identified, even though not all bands can well be identified, for sample S-2.29-7.5 and S-2.29-5 at 7-day curing (series of peaks in the region between 100 and 550 cm^{-1}). The presence of a peak at 720 cm^{-1} may suggest the presence of calcite in sample S-2.29-7.5 at early curing times.

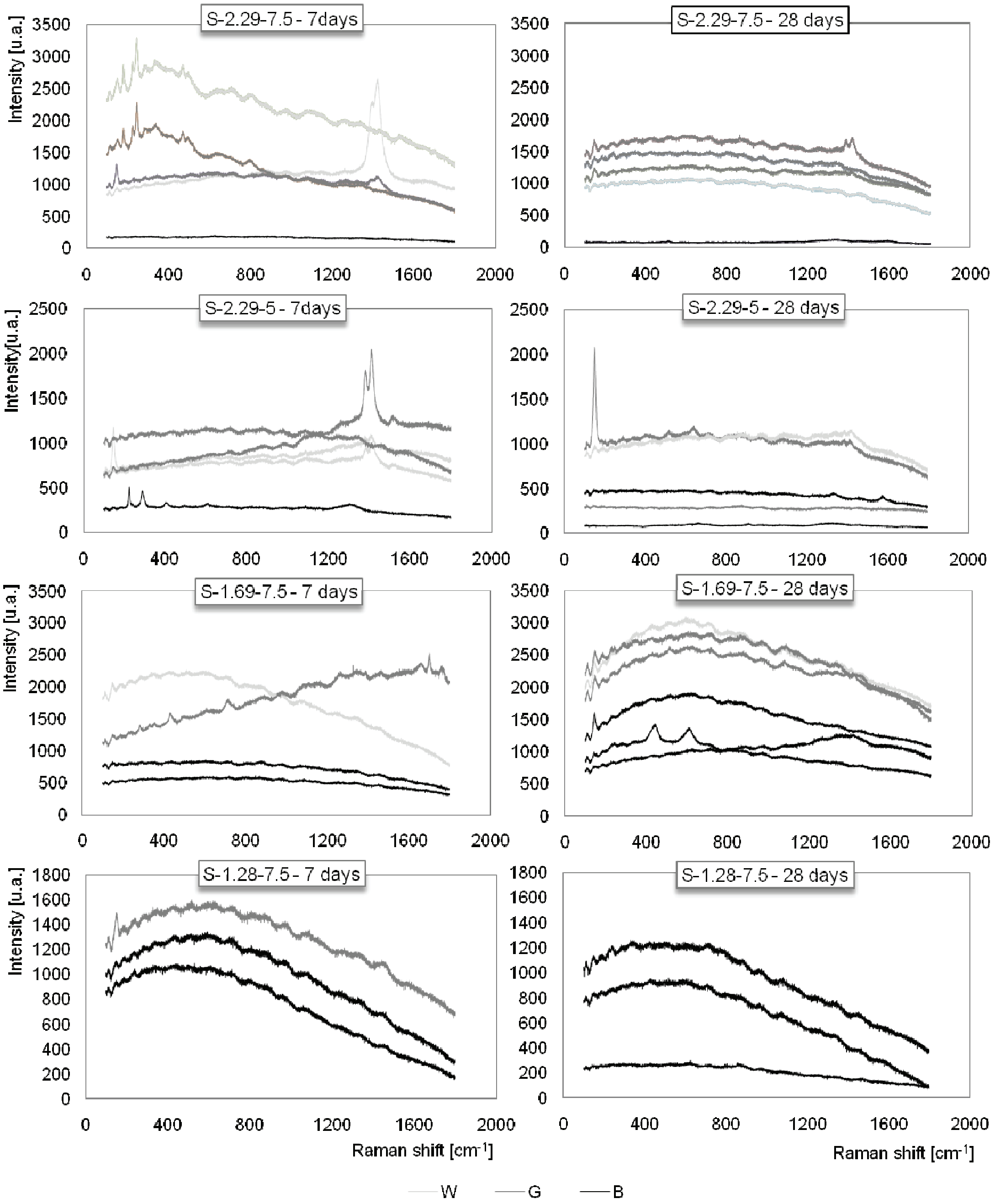

Figure 49: Raman spectra of geopolymer samples at 7 and 28 curing days

cm^{-1}	Raman shift				Notes
Alumina	1381	1410			double peak
Silicon	520				
Amorphous silica	540				broad peak
Calcite	155	281	711	1087	not all visible
Quartz	130	208	466		not all visible
Gehlenite	620	656	690		not all visible
CSH	650				broad peak

Table 24: Raman shift for main phase characteristics of the bottom ash and geopolymers samples. (http://rruff.geo.arizona.edu/rruff; http://www.geocities.com/ostroum/FTRAMAN)

5.6 ANC test on selected samples

The ANC curves of the untreated BA and the BA-based geopolymers (selected samples at 7 curing days) are shown in Figure 50. Significant changes in the buffering capacity were observed in comparison to the raw ash and between the geopolymerized samples. Due to the high alkali amount added to the mixtures, the natural pH of the original BA (11.84) was found to increase by almost two units in the BA-based geopolymers, reaching values in the range 13.02-13.33. The different mineralogical composition of the untreated and treated materials is mirrored by the different shapes of the titration curves: while the raw BA displayed a sort of plateau in the pH range 10-12, the curves of the treated materials were steeper in this pH range, indicating no significant buffering by mineral phases. The acid buffering capacity of the treated material was generally lower than that of the original BA within the whole range investigated: for the purpose of comparison, while the ANC to pH 8 was 3.2 meqH^+/g for the raw BA, it was reduced to 1.6 meqH^+/g (sample S-1.28-7.5) – 2.9 meqH^+/g (sample S-2.29-7.5). Furthermore, samples S-2.29-5 and S-2.29-7.5 displayed similar ANC curves in the entire pH range investigated and showed stronger buffering capacities with respect to the other two samples; these also appreciably differed from each other, with sample S-1.28-7.5 displaying the steepest curve. The lower buffering capacity of samples S-1.28-7.5 and S-1.69-7.5 is assumed to confirm the lower degree of geopolymerization reactions occurred for these materials as indicated by the previous analyses.

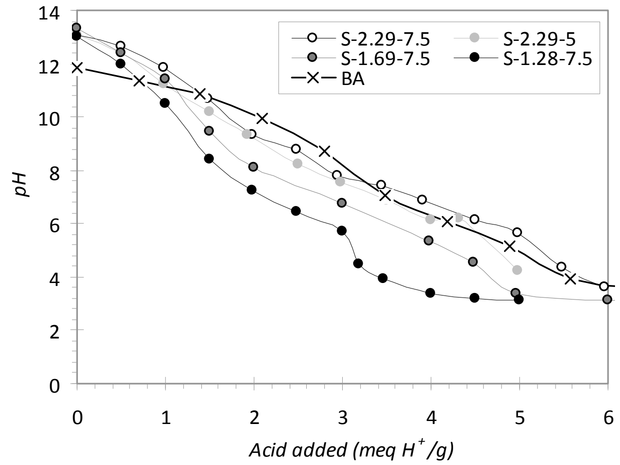

Figure 50: ANC curves for selected samples

The results from the ANC leaching test at the natural pH of the materials for the trace metals Cr, Cu, Ni, Pb and Zn are compared in Table 25 with the European regulatory limits for hazardous, non hazardous and inert waste landfills (EU Council Directive 99/31/EC, 1999) and with the limits established by the Italian law for waste utilization (annex 3 D.M. 05/02/1998, Ministero dell'Ambiente della Repubblica Italiana, 1998).

According to the values shown in Table 25, it is clear that the critical elements for the materials under concern are Cr and Cu, as also evident from the leaching curves as a function of pH shown in Figure 51. As shown, the Cr leaching was higher than the corresponding values measured for BA sample for the pH above 6. In the case of Cu the leaching of contaminants from geopolymer samples shows higher values above pH 10. In general not clearly visible differences in leaching can be detected among the different geopolymer samples under concern.

Element	pH	Cr	Cu	Ni	Pb	Zn
raw bottom ash	11.84	0.02	<u>0.06</u>	<0.002	0.04	0.1
O 7 days	13.08	<u>*0.26*</u>	<u>0.11</u>	0.01	0.04	*0.5*
J 7 days	13.09	<u>*0.29*</u>	<u>0.07</u>	<0.002	0.03	*0.4*
P 7 days	13.33	<u>*0.28*</u>	<u>0.15</u>	<0.002	0.04	0.3
Q7 days	13.02	<u>*0.18*</u>	<u>0.12</u>	<0.002	0.01	0.1
EU LD (hazardous waste)		**7**	**10**		**5**	**20**
EU LD (non hazardous. waste)		**1**	**5**		**1**	**5**
EU LD (inert waste)		*0.05*	*0.2*	*---*	*0.05*	*0.4*
<u>*DM 05/02/1998 (reuse)*</u>	5.5¸12.0	<u>0.05</u>	<u>0.05</u>	<u>0.01</u>	<u>0.05</u>	<u>3</u>
Detection limit (mg/l)		0.002	0.002	0.002	0.002	0.02

Table 25: Comparison between leaching test results (natural pH) and regulatory limits for selected heavy metals

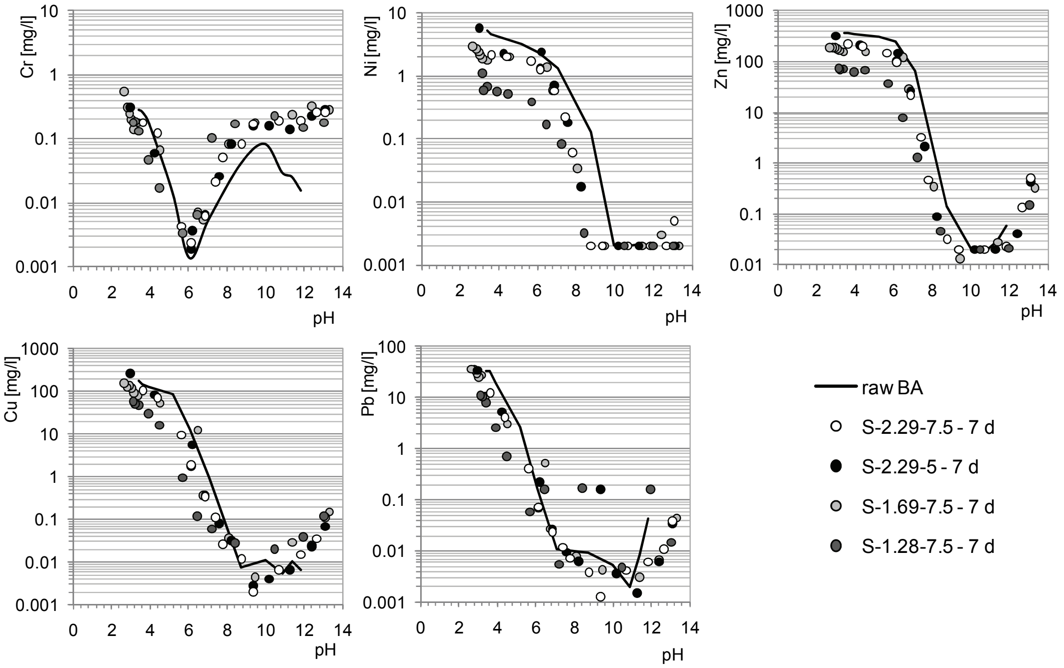

Figure 51: Metal leaching as a function of pH in the ANC test for selected samples

References

- ✓ E. Alvarez-Ayuso, X. Querol, F. Plana, A. Alastuey, N. Moreno, M. Izquierdo, O. Font, T. Moreno, S. Diez, E. V´azquez, M. Barra: Environmental, physical and structural characterisation of geopolymer matrixes synthesised from coal (co-)combustion fly ashes; Journal of Hazardous Materials (2008) 154: 175-183.
- ✓ S. Andini, R. Cioffi, F. Colangelo, T. Grieco, F. Montagnaro, L. Santoro: Coal fly ash as raw material for the manufacture of geopolymer-based products; Waste Manage (2008) 28(2): 416-23.
- ✓ T. Bakharev: Geopolymeric materials prepared using Class F f ly ash and elevated temperature curing; Cement and Concrete Research (2005) 35: 1224- 1232.
- ✓ V.F.F. Barbosa, K.J.D MacKenzie, C. Thaumaturgo: Synthesis and characterisation of materials based on inorganic polymers of alumina and silica: sodium polysialate polymers; Journal of Inorganic Materials.(2000) 2: 309-17.
- ✓ T.W. Cheng, and J. P. Chiu: Fire-resistant geopolymer produced by granulated blast furnace slag; Minerals Engineering (2003) 16: 205-210.
- ✓ P. Chindaprasirt, T. Chareerat, V. Sirivivatnanon: Workability and strength of coarse high calcium fly ash geopolymer; Cement Concrete Composite (2006) 29: 224-229.
- ✓ P. Chindaprasirt, C. Jaturapitakkul, W. Chalee, U. Rattanasak: Comparative study on the characteristics of fly ash and bottom ash geopolymers; Waste Management (2009) 29: 539-543.
- ✓ M. Criado, A. Fernández-Jiménez, A.G. de la Torre, M.A.G. Aranda, A. Palomo: An XRD study of the effect of the SiO_2/Na_2O ratio on the alkali activation of fly ash; Cement and Concrete Research (2007) 37: 671-679.
- ✓ J. Davidovits: Geopolymer chemistry & Applications; cap.15: Physical properties of condense geopolymers; Institut Géopolymère, second edition June 2008.
- ✓ P. De Silva, K. Sagoe-Crenstil, V. Sirivivatnanon: Kinetics of geopolymerization: Role of Al_2O_3 and SiO_2; Cement and Concrete Research (2007) 37: 512–518.
- ✓ E.I. Diaz, E.N. Allouche, S. Eklund: Factors affecting the suitability of fly ash as source material for geopolymers; Fuel (2010) 89: 992-996.
- ✓ P.K. Dutta and M.Puri: Syntesis and structure of zeolite ZSM-5: a Raman spectroscopy study; Journal of Physical Chemistry (1987) 91: 4329-4333.
- ✓ P.K. Dutta, K.M. Rao, J.Y. Park: Correlation of Raman spectra of zeolites with framework architecture; Journal of Physical Chemistry (1991) 95: 6654-6656.

- ✓ P. Duxson, G.C. Lukey, J.S.J. van Deventer: Thermal volution of metakaolin geopolymers: Part1 – Physical evolution; Journal of non crystalline Solids (2006) 352: 4414-5555.
- ✓ Council Directive 99/31/EC, 1999. Landfill of waste. Official Journal L 182, 16/07/1999, 0001-0019.
- ✓ D. Feng, H. Tan, J.S.J. van Deventer: Ultrasound enhanced geopolymerisation; Journal of Material Sciences (2004) 39: 571-580.
- ✓ R.A Fletcher, K.J.D Mackenzie, C.L. Nicholson, S. Shimada: The composition rang of alumino silicate geopolymers; Journal of the European Ceramic Society (2005) 25: 1471-1477.
- ✓ X. Guo, H. Shi, W. A. Dick: Compressive strength and microstructural characteristics of class C fly ash geopolymer; Cement & Concrete Composites (2010) 32: 142-147.
- ✓ J.G.S. van Jaarsveld, J.S.J. van Deventer, G.C. Lukey: The effect of composition and temperature on the properties of fly ash- and kaolinite-based geopolymers; Chemical Engineering Journal (2002) 89: 63-73.
- ✓ I. Kourti, D. A. Rani, D. Deegan, A.R. Boccaccini, C.R. Cheeseman: Production of geopolymers using glass produced from DC plasma treatment of air pollution control (APC) residues; Journal of Hazardous Materials (2010) 176: 704-709.
- ✓ D.L.Y. Kong, and J.G. Sanjayan: Effect of elevated temperatures on geopolymer paste, mortar and concrete; Cement and Concrete Research (2010) 40: 334-339.
- ✓ W.M. Kriven, J.L. Bell, M.Gordon: Microsructure nd microchemistry of fully reacted geopolymers and geopolymer matrix composites; Ceramic Transactions (2003) 153: 22-250.
- ✓ S. Kumar and R. Kumar: Mechanical activation of fly ash: effect on reaction, structure and properties of resulting geopolymer; Ceramics International (2011) 37: 533-541.
- ✓ C. Lampris, R. Lupo, C.R. Cheeseman: Geopolymerisation of silt generated from construction and demolition waste washing plants; Waste Management (2009) 29: 368-373.
- ✓ W.K.W Lee and J.S.J. Van Deventer: The effects of inorganic salt contamination on the strength and durability of geopolymers; Colloids and Surfaces A (2002) 211: 115-126
- ✓ Ministero dell'Ambiente della Repubblica Italiana, 1998. D.M. 05/02/1998. Individuazione dei rifiuti non pericolosi sottoposti alle procedure semplificate di

recupero ai sensi degli articoli 31 e 33 del decreto legislativo 5 febbraio 1997, n. 22. Suppl. Ord. G.U. 16/04/1998 n. 88 (as amended by D.M. 05/04/2006, n. 186).

- ✓ W. Mozgawa and J. Deja: Spectroscopic studies of alkaline activated slag geopolymers; Journal of Molecular Structure (2009) 434-441.
- ✓ N. Murayama, H. Yamamoto; J. Shibata: Mechanism of zeolite synthesis from coal fly ash by alkali hydrothermal reaction; International Journal of Mineral Processing (2002) 64: 1-17.
- ✓ J.E. Oh, P.J.M. Monteiro, S.S. Jun, S. Choi, S.M. Clark: The evolution of strength and crystalline phases for alkali-activated ground blast furnace slag and fly ash-based geopolymers; Cement and Concrete Research (2010) 40: 189-196.
- ✓ A.Palomo, M.W. Grutzeck, M.T. Blanco: Alkali-activated fly ashes A cement for the future; Cement and Concrete Research (1999) 29: 1323-1329.
- ✓ Z. Pan and J.G. Sanjayan: Stress–strain behaviour and abrupt loss of stiffness of geopolymer at elevated temperatures; Cement and Concrete Composite (2010) 32: 657-664.
- ✓ D. Panias, I. P. Giannopoulou, T. Perraki: Effect of synthesis parameters on the mechanical properties of fly ash-based geopolymers; Colloids and Surfaces A: Physicochemical and Engineering Aspects (2007) 301: 246-254.
- ✓ J.W. Phair and J.S.J. Van Deventer: Effect of the silicate activator pH on the microstructural characteristics of waste-based geopolymers; International Journal of Mineral Processing (2002) 66: 121-143.
- ✓ J.L. Provis, G.C. Lukely, J.S.J. van Deventer: Do geopolymers actually contain nanocrystalline zeolites? A reexamination of existing results; Chemistry of Materials (2005) 17: 3075-3085.
- ✓ E. Prud’homme, P. Michaud, E. Joussein, C. Peyratout, A. Smith, S. Arrii-Clacens, J.M. Clacens, S. Rossignol: Silica fume as porogent agent in geo-materials at low temperature; Journal of the European Ceramic Society (2010) 7: 1641-1648.
- ✓ H. Rahier, B. Van Mele, M. Biesemans, J. Wastiels, X. Wu: Low-temperature synthesized aluminosilicate Glasses Part I Low-temperature reaction stoichiometry and structure of a model compound; Journal of Material Sciences (1996) 31: 71-79.
- ✓ C.A. Rees, J.L. Provis, G.C. Lukey, J.S.J. van Deventer: The mechanism of geopolymer gel formation investigated through seeded nucleation; Colloids and Surfaces A: Physicochemical and Engineering Aspects (2008) 318: 97-105.

- ✓ W.D.A. Rickard and A. van Riessen: Thermal character of geopolymers synthesized from class f fly ash containing high concentrations of iron and α-quartz; International Journal of Applied Ceramic Technology (2010) 7: 81-88.
- ✓ P. Rovnaník: Effect of curing temperature on the development of hard structure of metakaolin-based geopolymer; Construction and Building Matererials (2010) 24: 1176-1183.
- ✓ M. Rowles and B. O'Connor: Chemical optimisation of the compressive strength of aluminosilicate geopolymers synthesised by sodium silicate activation of metakaolinite; Jounal of Matererial Chemistry (2003) 13: 1161-1165.
- ✓ M. Stevenson and K. Sagoe-Crentsil: Relationships between composition, structure and strength of inorganic polymers Part I Metakaolin-derived inorganic polymers; Journal of Materials Science (2005) 40: 2023- 2036.
- ✓ F. Skvára, L. Kopecky, V. Smilauer, Z. Bittnar: Material and structural characterization of alkali activated low-calcium brown coal fly ash; Journal of Hazardous Materials (2009) 168: 711-720
- ✓ S. Songpiriyakij, T. Kubprasit, C. Jaturapitakkul, P. Chindaprasirt: Compressive strength and degree of reaction of biomass- and fly ash-based geopolymer; Construction and Building Materials (2009) 24: 236-240.
- ✓ J. Temuujin, R.P.Williams, A. van Riessen: Effect of mechanical activation of fly ash on the properties of geopolymer cured at ambient temperature; Journal of Materials Processing Technology (2009) 209: 5276-5280.
- ✓ J. Temuujin and A. van Riessen: Effect of fly ash preliminary calcination on the properties of geopolymer; Journal of Hazardous Materials (2009) 164: 634-639
- ✓ H. Xu, L. Quin, I. Shen, W. Wang, J. Zhai: Synthesis of thermostble geopolyem from circulating fluidized bed combustion (CFBC) bottom ashes; Journal of Hazardous Materials (2010) 17: 198-204.
- ✓ Z. Yunsheng, S. Weia, C. Qianlia, C. Lina: Synthesis and heavy metal immobilization behaviors of slag based geopolymer; Journal of Hazardous Materials (2007) 143: 206-213.
- ✓ M. Yousuf, A. Mollah, P. Palta, T.R. Hess, R.K. Vempati, D.L. Cocke: Chemical and physical effects of sodium lignosulfonate superplasticizer on the hydration of portland cement and solidification/stabilization consequences; Cement and Concrete Research (1995) 25: 671-682.
- ✓ J. Zhang, J.L. Provis, D. Feng, J.S.J. van Deventer: Geopolymers for immobilization of Cr^{6+}, Cd^{2+}, and Pb^{2+}; Journal of Hazardous Materials (2008) 157: 587-598.

On line database:

- http://rruff.geo.arizona.edu/rruff/
- http://www.geocities.com/ostroum/FTRAMAN.htm

6. Conclusions

In this research different alkali activation processes of incinerator bottom ash were investigated with the purpose of evaluating the recycling potential as a structural material in engineering applications.

The results obtained from the first process, involving the use of alkaline activators to enhance the reactivity of bottom ash in cementitious blends, showed the positive effect of some of the chemical activators tested on the development of mechanical properties of the materials. In all the analysed cases, activation contributed to increasing mechanical strength if compared to untreated bottom ash. CaCl2 was found to be the most effective activator, being able to increase UCS above that of Portland cement. The effect of CaCl2 appeared to promote the onset of pozzolanic reactions in the cementitious mixtures, with an increase in the total amount of hydration phases present. CaSO4 was also found to increase mechanical strength, while KOH gave positive results in terms of mechanical strength development only in a few cases, and NaOH was found to not be particularly effective.

The environmental performance of the material, investigated for mixtures containing Ca-based activator, was also evaluated through leaching tests, which showed that metal leaching was reduced if compared to the raw bottom ash. The extent of reduction in metal leaching was more relevant as curing time increased, indicating a progressive immobilization of trace metals by the hydrate system. For the mixture giving the best results in terms of mechanical behavior, metal leaching at the natural pH of the material was below the regulatory limits established by the Italian law for utilization; Cr was the only exception, with a release into the leaching solution slightly above the corresponding threshold value, which was attributed to a large extent to the contribution of cement. The theoretical description of the composition of the hydrated materials, gained though geochemical modeling of the leaching solutions, indicated the formation of different hydration phases when bottom ash was added to Portland cement. In the case of un-activated bottom ash, the analysis of the modeling results indicated a possible delay in the hydration process in comparison to the normal evolution of pure cement systems. The modeling results for trace metal leaching indicated a strong contribution of surface complexation by Fe and Al minerals to the immobilization of PbFor the other trace metals investigated, modeling of the leaching solutions resulted in only poor prediction of the observed leaching behaviour. This was likely related to the complex mineral forms in which trace metals were present in the original material, with association to solid phases for which a chemical and thermodynamic description is not currently available.

The second activation process was applied to investigate the feasibility of producing geopolymeric materials starting from incinerator bottom ash and an alkaline medium. A preliminary study concerning the identification of the main parameters controlling the geopolymerization process of bottom ash was conducted Depending on the process conditions adopted (Si/Al ratio, NaOH concentration in the alkaline solution), wide variations in the main characteristics of the materials were observed, indicating a significant influence of the selected process variables on the evolution of the geopolymerization reactions. While the physical and mechanical properties were found to be well correlated with the Si/Al ratio, no clear trend was found with the NaOH concentration in the alkaline medium. For the best combination of the operating variables studied, an appreciable gain in the mechanical characteristics of the material was attained, with unconfined compressive strength values as high as 10 MPa. When examining the trend observed for mechanical strength data as a function of the Si/Al ratio, it is apparent that further investigation on the Si and Al content is required to identify the optimal range of values for inducing the highest possible mechanical properties. It thus appears that further improvement in mechanical strength, in turn resulting from a higher degree of geopolymerization, may be attained if the contents of the relevant elements for the process are appropriately adjusted within the corresponding optimal ranges. This conclusion may also be confirmed by the results from mineralogical characterization (SEM, FT-IR, TG, XRD, RAMAN spectroscopy) of the geopolymeric products, as well as from chemical durability testing, which showed that, although the onset of the geopolymer formation reactions was clearly confirmed, the degree of matrix restructuring was relatively poor, in agreement with the suggestions provided by the analysis of the mechanical properties.

In general terms, the results from the present study show that some benefits may be taken from the reactivity of incinerator bottom ash in alkaline environments, with a view to reuse in engineering applications of various nature. However, the reactivity characteristics of the material are rather weak under normal conditions, and the associated chemical reactions proceed typically with slow rates. As a result, appropriate conditions are required to promote the evolution of the chemical and mineralogical transformations involving the mineral phases in bottom ash at the level imposed by technical requirements. While the present study demonstrated that it is possible to identify suitable conditions for bottom ash activation, the results obtained also indicated that the activation reactions are dramatically dependent on the particular type of activation method applied and the specific composition of the material used. The need is therefore recognized to further improve the knowledge in the reaction mechanisms involved, in order to define a quantitative criterion to identify the optimal activation conditions as a function of material composition.

Papers

WASCON 2009: Sustainable Management of waste and recycled materials in construction

WASCON 2009
3-4-5 June 2009 in Lyon - France
ISCOWA "Sustainable Management of Waste and Recycled Materials in Construction"
eedems évaluation environnementale déchets, matériaux et sols pollués

An investigation of RDF bottom ash activation for blended cement formulation

R. Onori, A. Polettini, R. Pomi
Department of Hydraulics, Transportation and Roads - University of Rome "La Sapienza", Rome, Italy

Abstract

In the present study the feasibility of chemical and mechanical activation to improve the reactivity of incinerator bottom ash in Portland cement mixtures was investigated. Three chemical activators, NaOH, KOH and $CaCl_2$, were selected for the experimental campaign on the basis of the results from previous studies. The experiments were arranged according to a full factorial design of three factors - "bottom ash content", "activator type" and "activator dosage" - set at 2, 3 and 2 levels, respectively. The evolution of mechanical strength and the leaching behavior of activated bottom ash/Portland cement mixtures was a matter of major concern in this study. The results indicated that $CaCl_2$ exhibited by far the best effects on the evolution of the hydration process of the mixtures and metal leaching from the hardened material. As for the other activators used, while an improvement in the mechanical properties was still recognizable when KOH was added to the mixtures, no positive effect could be observed in the presence of NaOH. This study provides some promising indications about the feasibility of incinerator bottom ash utilization for the formulation of blended cements, which however will need to be further assessed through a deeper insight into the mechanisms governing the development of mechanical strength in cementitious systems containing bottom ash.

Background

Bottom ash (BA) represents the major portion of the solid residues generated by waste incineration, accounting for 15-25% by mass of the original waste. The minerals present in BA are formed under high-temperature combustion conditions and are subjected to rapid cooling down to ambient temperatures during quenching at the exit of the combustion unit.

This temperature drop explains the metastability of most of such solid phases and accounts for the chemical reactivity of bottom ash under natural conditions, particularly in alkaline and oxidizing environments (Sabbas et al., 2003; Polettini et al., 1998). Incinerator BA is generally composed of amorphous and vitreous phases, and the most abundant constituents are calcium, silicon and aluminum oxides, which are also major components of typical pozzolanic materials.

Previous studies (Filipponi et al., 2003; Giampaolo et al., 2002) appeared to indicate the capability of bottom ash of exhibiting pozzolanic properties in cement based systems, suggesting potential useful applications for blended cement formulation. Nevertheless, such studies indicated also that the mechanical strength of bottom ash-Portland cement products was always lower than that of pure Portland cement or Portland cement-pozzolanic systems, suggesting the need to enhance the weak pozzolanic properties of bottom ash.

More recently, the use of appropriate chemical activators - as suggested by a number of investigators for different materials (Fan at al.,1999; Quian et al., 2001; Shi et al., 1995, 2000, 2001) - combined with thermal and mechanical activation of BA was found to promote the development of mechanical strength for BA-Portland cement mixtures (Polettini et al., 2005, 2009).

In the present work, further investigation on the role of chemical activators in the development of physical, mechanical and leaching characteristics of RDF incinerator BA/Portland cement mixtures has been conducted.

Materials and methods

The bottom ash used in the present study comes from an Italian grate-type RDF incinerator. Fresh bottom ash was sampled at the exit of the quenching unit, homogenized by quartering and characterized for elemental composition as well as anion content. The material was sieved to produce five size classes, which were separately characterized for physical and chemical properties. The elemental composition was determined by atomic absorption spectrometry after sample digestion according to an alkaline digestion procedure at 1050 °C using lithium tetraborate as the melting agent. Anions were analyzed by ion chromatography after solubilization according to the Italian UNI 8520 method. On the basis of the anticipated different behavior of the finer fractions when blended with cement, in this study only the 0.425–12.0 mm size classes were selected for the experiments.

Different Ca-, Na- and K-based compounds, including $CaCl_2 \cdot 2H_2O$, NaOH, KOH (reagent-grade compounds), were selected as BA activators on the basis of a literature survey and the results from previous studies (Filipponi et al., 2003; Giampaolo et al., 2002; Polettini et al., 2005, 2009; Fan at al.,1999; Quian et al., 2001; Shi et al., 1995, 2000, 2001). The activation procedure applied to BA involved heating at 90 °C for 3 h of slurries (L/S = 2 ml/g) containing the ball-milled (<150 μm) ash and the chemical activator. After the pre-treatment step, BA was oven-dried at 60 °C.

Cementitious mixtures were prepared (see Table 26) by blending different proportions of ball-milled BA and ordinary Portland cement (OPC) at a water/total solids weight ratio of 0.4. The investigated BA/(BA+ OPC) ratios were 20 and 40 wt.%, while the activator additions adopted (expressed as activator/(BA + OPC) ratios) were 2 and 4 wt.%. Control samples containing 0, 20 and 40 wt.% of BA were also prepared for reference purposes. The experiments were arranged according to a full factorial design of the three factors "BA content", "activator type" and "activator dosage", set at 2, 3 and 2 levels, respectively.

Table 26: Composition of the OPC/BA mixtures.

Mixture code	**BA/(BA+OPC) (%)**	**Activator/(BA+OPC) (%)**		
		KOH	NaOH	$CaCl_2$
OPC	0			
C1	20			
C2	40			
A1	20	2		
A2	20	4		
A3	40	2		
A4	40	4		
A5	20		2	
A6	20		4	
A7	40		2	
A8	40		4	
A9	20			2
A10	20			4
A11	40			2
A12	40			4

The blends were cast in 30-mm cubic moulds, stored at 40 °C and relative humidity (RH) > 90% for 24 h, then demoulded and allowed to cure at 40 °C and RH> 90% for 7, 28 and 56 days.

Measurements of unconfined compressive strength (UCS) were made on triplicate specimens according to the ASTM C109 method. The EN14429 ANC test was applied after mechanical strength testing on ball-milled (< 150 μm) and oven-dried (60 °C) specimens.

The analysis of variance (ANOVA) (Box et al., 2005; Montgomery, 2005) was applied to the experimental data to derive an estimation of the statistical significance of the main and linear interaction effects between the factors as well as the error of the experiments. The significant effects were then processed through least-squares linear regression to derive a predictive model, describing the so-called response surface, for the variables of interest. The analytical formulation of the predictive model was as follows:

$$y = a_0 + a_1 x_1 + a_2 x_2 + a_3 x_3 + a_{12} x_1 x_2 + a_{13} x_1 x_3 + a_{23} x_2 x_3 + a_{123} x_1 x_2 x_3 \qquad (1)$$

where y is the response variable (e.g., UCS), x_1, x_2 and x_3 are the levels of the three factors “activator type”, “bottom ash content” and “activator dosage” and $a_{i(j)(k)}$ the coefficients of the polynomial function.

The evolution of the hydration process for the investigated mixtures was also studied by means of geochemical modeling of ANC leaching solutions using Visual Minteq as the mathematical code. To allow for a better description of the eluates from cementitious systems, the standard thermodynamic database was thoroughly updated including the stability constants of several typical cement hydrates from different literature sources (Astrup et al., 2006; Lothenbach and Winnefeld, 2006; Blanc et al., 2007; Hyks et al., 2009). The application of the speciation code followed a three-step procedure: (1) the program was run using the measured concentrations and pHs as input data and suppressing precipitation for all solid phases; (2) potential solubility-controlling minerals where chosen among those displaying saturation indices (SI) in the range $-1.5 \leq SI \leq +1.5$ and on the basis of the likelihood of formation in cementitious systems; and (3) the predicted concentrations of each element in equilibrium with the selected mineral phases were derived according to the following empirical equation (Astrup et al., 2006):

$$C_{eq} = C_{meas}\left(10^{-SI}\right)^{1/n} \tag{2}$$

where C_{eq} and C_{meas} are the theoretical and measured element concentrations, respectively, while n is the stoichiometric coefficient of the element in the mineral of concern.

In all the modeling calculations, the hypothesis of oxidizing conditions was always assumed.

Results and discussion

The chemical composition of the three BA size classes investigated (12.0–5.6 mm; 5.6–2.0 mm and 2.0–0.425 mm) is reported in Table 27.

Table 27: Chemical composition and leaching of the three size fractions investigated

Element	CLASS A (12.0–5.6 mm)		CLASS B (5.6–2.0 mm)		CLASS C (2.0–0.425 mm)	
	TC* (mg/kg)	L** (mg/kg)	TC* (mg/kg)	L** (mg/kg)	TC* (mg/kg)	L** (mg/kg)
Al	64591	57	68087	242	52470	202
As	2	0	3	0	2	0
Ca	228165	663	232945	928	264349	982
Cd	61	0	40	0	7	0
Cr	487	0	467	0	483	0
Cu	6452	0	8499	0	4601	1
Fe	21313	0	18795	0	17632	0
K	4410	221	4852	240	5447	281

Mg	16311	0	16652	1	19403	0
Mn	458	0	475	0	503	0
Mo	128	0	13	0	12	0
Na	14901	242	15175	204	20442	208
Ni	209	0	97	0	100	0
Pb	2441	51	2782	41	3403	83
Sb	102	0	42	0	25	0
Si	118872	5	115175	0	93474	0
Zn	2824	4	2424	1	1892	1
Cl^-	18953		19306		25639	
SO_4^{2-}	13417		10427		8800	

*TC = total content ** L = leachate concentration (EN 12457-2)

The trace metals displaying the highest concentrations in BA were Pb (2400-3400 mg/kg), Zn (1900-2800 mg/kg) and Cu (4600-8500 mg/kg). As far as metal leaching was concerned, the Pb and Cr concentrations exceeded the regulatory limits established by the Landfill Directive for disposal in hazardous waste landfills.

The results from mechanical characterization of cementitious materials are reported in Figure 52 in terms of measured UCS values and calculated specific UCS values (relative to OPC), and in Figure 53 in terms of UCS values as a function of curing time and activator type. SUCS (Pu, 1999) is defined as the mechanical strength of a given mixture divided by its OPC content and is used to identify any additional contribution of cement admixtures to mechanical strength other than that produced by the OPC hydrates.

The addition of BA to the mixtures with no preliminary activation treatment (samples C1 and C2) was observed to result in decreased mechanical strength values if compared to the control mixture (100% OPC). A linear decrease in UCS with the BA content was observed, irrespective of curing time, when KOH or NaOH were used as the activators, indicating a dilution effect of the cement hydrates system by BA; in the case of $CaCl_2$, the UCS decrease was less than proportional to the BA content, suggesting some possible contribution of the material to the development of mechanical properties.

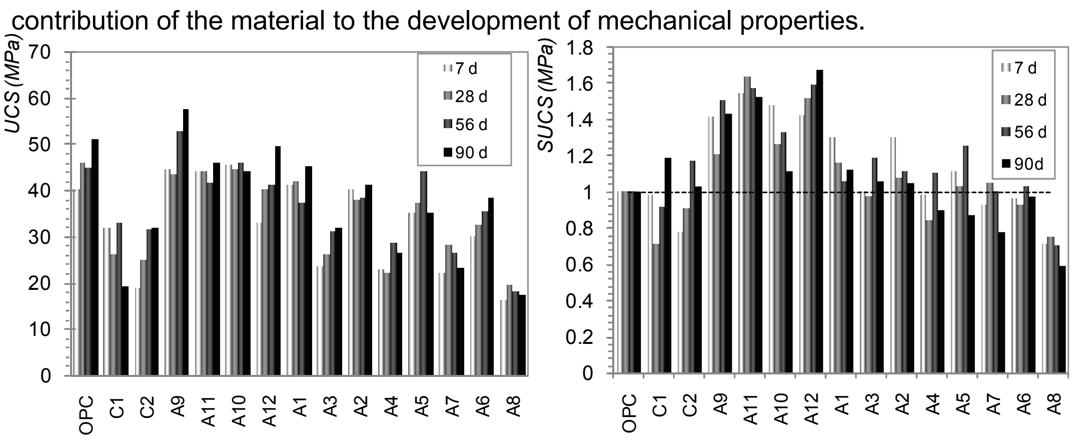

Figure 52: UCS and SUCS values as a function of curing time

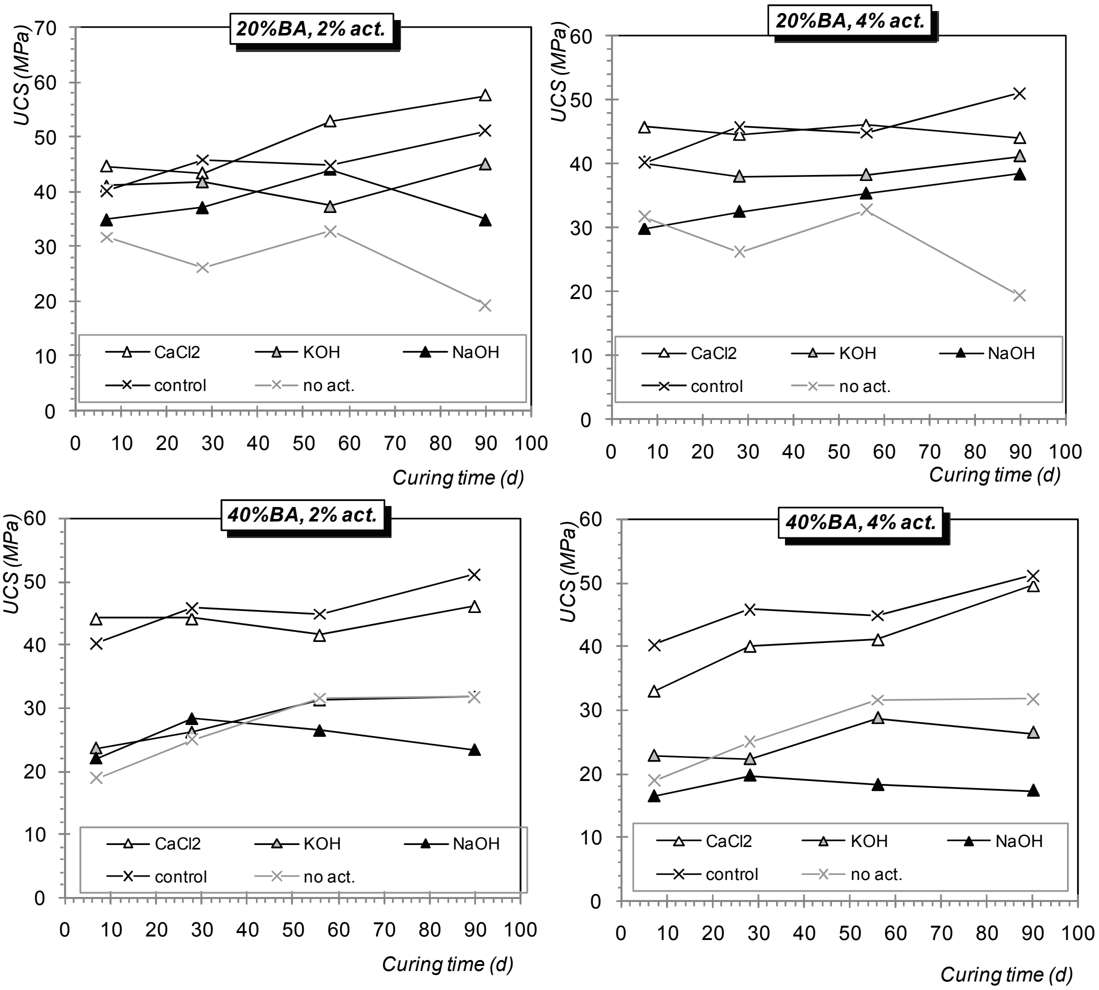

Figure 53: UCS as a function of curing time and activator type

When activated BA was used as a cement admixture, the effects produced on mechanical strength were found to be related to the type of chemical activator used. As a general feature, the three activators tested always resulted in a gain in mechanical strength if compared to the specimens without activator addition. However, the absolute UCS values were found to be largely variable depending on the individual activator used. In particular, as already observed in a previous study on a BA sample from a different source, $CaCl_2$ was found to be capable of improving the mechanical characteristics of cementitious blends in respect to the control mixture. The best results were obtained for a 20% BA content, with UCS values of 44.6, 43.3, 52.9 and 57.7 MPa after 7, 28, 56 and 90 days, as opposed to 42.0, 45.8, 44.9 and 51.1 MPa measured for the control sample; increasing the $CaCl_2$ addition from 2% to 4% appeared to have only a minor effect on strength improvement. When the BA addition was increased to 40%, mechanical strength was reduced only slightly below that of the 100% OPC specimen.

As for the two other activators KOH and NaOH, the positive effect on mechanical strength as compared to the non-activated material was by far less evident. Although at 20% BA addition KOH (at both the 2% and 4% dosages) was capable of promoting the hydration process at early curing (7 days) yielding UCS values above that of the control (41.1 and 40.3 MPa, respectively, as opposed to 40.2 MPa), no similar gain was observed at longer curing times. In addition, unlike noted for $CaCl_2$, the decrease in UCS with the BA content when KOH was used as the activator was still considerable at all curing times. This suggested that KOH was only capable to affect hydration to some extent during the early stages of the process and for low BA dosages.

The results obtained when BA was activated by NaOH showed that this activator was not suited to significantly contribute to strength development. This occurred irrespective of the amount of both BA and activator added to the mixtures. Furthermore, an increase in the NaOH dosage was found to adversely affect UCS, likely due to an excess of sodium in the pore solution. The findings commented above become more clear when interpreted in terms of specific strength values: while the SUCS of $CaCl_2$-contaning mixtures were all well above the corresponding values for the control specimen, the strength gain was less pronounced for KOH and much less visible (or absent at all) for NaOH. For the reasons explained above, in the following discussion more evidence will be devoted to further examine the mechanical and environmental behavior of the BA/OPC mixtures in the presence of $CaCl_2$.

The results of the mechanical strength measurements were processed by means of the ANOVA, which was used to judge the statistical significance of factor effects and interactions, required to build the predictive model described by equation (1). Table 28 reports the ANOVA results for UCS at the three curing times investigated, expressed in terms of sum of squares (SS) for the individual effect/interaction, the corresponding degrees of freedom (DF) and mean squares (MS).

The bold values in Table 28 indicate the significant effects at a 10% significance level. It should be noted that, due to the number of levels used for the two quantitative factors "BA dosage" and "activator addition", only linear main effects and interactions between factors could be estimated, resulting in a linear predictive model for the response variables. The response surfaces obtained using this approach were plotted in Figure 54 at a constant value for factor 1 (activator type = $CaCl_2$) separately for each curing time.

Table 28: ANOVA results for UCS

	t = 7 d			**t = 28 d**		
	SS	**DF**	**MS**	**SS**	**DF**	**MS**
SS_1	1194.7	2	**597.3**	1231.2	2	**615.6**
SS_2	1693.3	1	**1693.3**	814.8	1	**814.8**
SS_3	53.1	1	**53.1**	139.9	1	**139.9**
SS_{12}	75.0	2	**37.5**	298.4	2	**149.2**
SS_{13}	36.3	2	18.1	40.3	2	20.2
SS_{23}	6.3	1	6.3	22.1	1	22.1

SS_{123}	9.5	2	4.8	10.9	2	5.4
SS_E	301.8	24	12.6	1034.0	24	43.1
SS_T	3369.9	35	96.3	3591.7	35	102.6
	t = 56 d			**t = 90 d**		
	SS	**DF**	**MS**	**SS**	**DF**	**MS**
SS_1	1374.6	2	**687.3**	2646.5	2	**1323.3**
SS_2	1123.4	1	**1123.4**	1126.3	1	**1126.3**
SS_3	164.4	1	**164.4**	\118.8	1	**118.8**
SS_{12}	177.2	2	88.6	305.7	2	**152.9**
SS_{13}	87.7	2	43.9	25.8	2	12.9
SS_{23}	2.6	1	2.6	10.1	1	10.1
SS_{123}	37.6	2	18.8	279.3	2	139.7
SS_E	990.1	24	41.3	972.9	24	40.5
SS_T	3957.6	35	113.1	5485.4	35	156.7

1 = “activator type”; 2 = “BA dosage”; 3 = “activator addition”
E = error; T = total

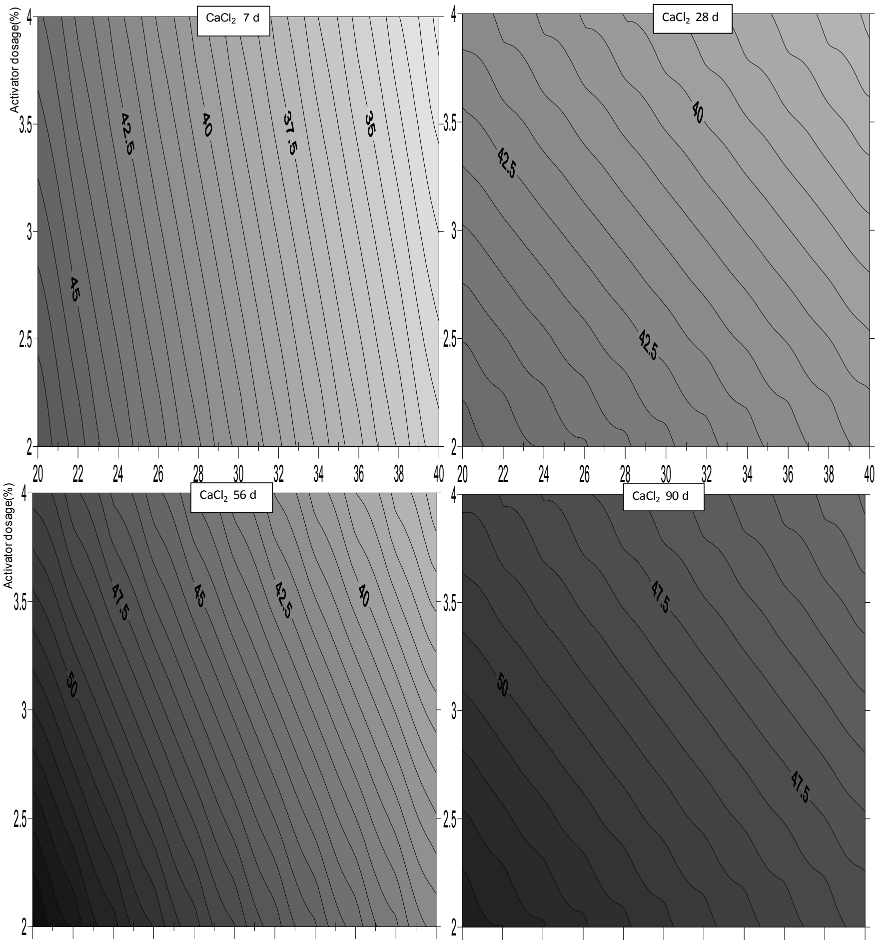

Figure 54: Response surfaces for UCS as derived by equation (1) – values in MPa

The analysis of the contour plots shows the minor effect of an increase in activator dosage at any of the investigated curing times; conversely, UCS was more negatively affected by a corresponding increase in the BA dosage.

The mechanical behaviour of mixtures discussed so far was confirmed by the ANC results. The titration curves for the $CaCl_2$-containing blends, depicted in Figure 55 for curing times of 28 and 56 days, appeared to be affected mainly by the BA content while inappreciably by the activator dosage.

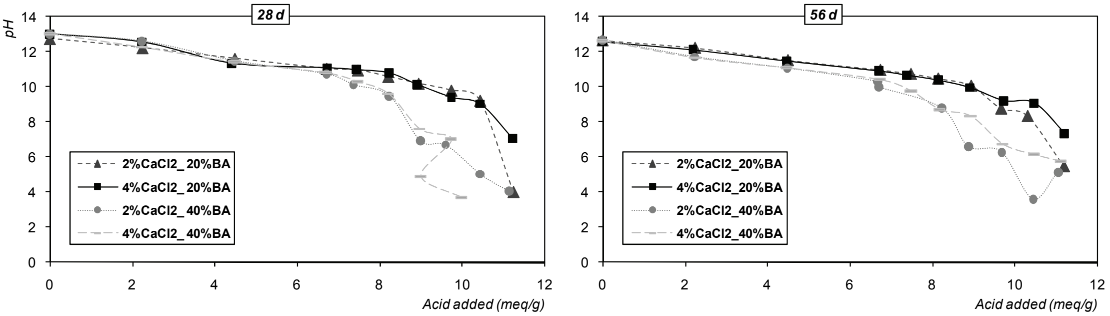

Figure 55: ANC curves for $CaCl_2$-containing blends

It was observed that the ANC to pH 10, which gives a rough estimation of the main hydration phases formed, decreased by about 1-2 meq/g (depending on curing time) as the BA content increased from 20 to 40%.

For all the metals under concern, a very dramatic decrease in leaching was observed if compared to the raw BA sample. Metal leaching as a function of pH showed no large differences between the different mixtures investigated. However, as also observed for mechanical strength, the addition of 4% $CaCl_2$ at 20% BA content gave the best results; in particular, in the pH range above 12 metal immobilization efficiency increased by almost an order of magnitude. This is evident in Figure 5, which shows the leaching results obtained for Pb.

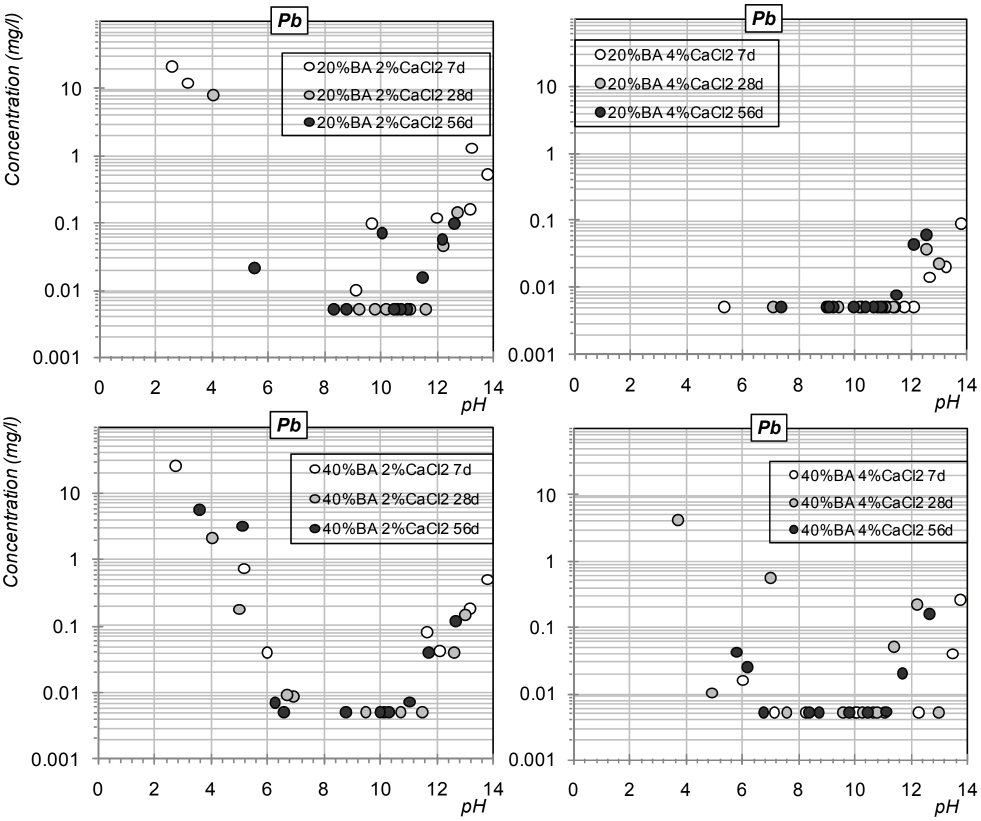

Figure 56: Pb leaching as a function of pH in the ANC test

An attempt was made to infer on the evolution of the hydration process with curing time for the mixtures containing 20% BA and 2% $CaCl_2$. Ca leaching was found to be controlled by different phases as the hydration reactions progressed. In particular, gypsum at low pH values and C_2AH_8 at pH > 12 were the most probable candidates for solubility control at 7-day curing; for longer curing times C_2AH_8 appeared to be replaced by monosulphate; at 56-day curing, additional solubility-controlling phases were identified, consisting of complex Cl-containing hydrates including Friedel's ($3CaO{\cdot}Al_2O_3{\cdot}CaCl_2{\cdot}10H_2O$) and Kuzel's ($3CaO{\cdot}Al_2O_3{\cdot}0.5CaCl_2{\cdot}0.5CaSO_4{\cdot}12H_2O$) salts. This indicates that, as already observed in the literature (Glasser et al., 1999), the AFm phase C_2AH_8 was subjected to changes in its mineral structure, accommodating anion substitutions for Cl^- and SO_4^{2-}.

In the case of Si, no solubility-controlling solids could be identified at low curing times, except for chalcedony at pHs in the range 9-10; as curing progressed, Ca silicate hydrate phases including C-S-H with a Ca/Si ratio = 0.8 and tobermorite (Ca/Si ratio = 0.83) were found to control Si leaching above pH = 9.

As observed for Ca, SO_4^{2-} were observed to be controlled by gypsum at low pHs and, for curing times of 28 and 56 days, by monosulphate at pH > 10. It should be noted that te leaching solutions were always found to be oversaturated with respect to ettringite, although the shape of the theoretical solubility curve for this phase was very similar to the measured concentrations. Further investigation is required to judge about the reliability of the stability constant used in the thermodynamic database for ettringite in the case of impurity-bearing cementitious systems.

Among the major cations, Mg leaching (results not reported graphically here) appeared to be controlled by forsterite at 28- and 56-day curing, while no clear solubility control was observed for lower curing times.

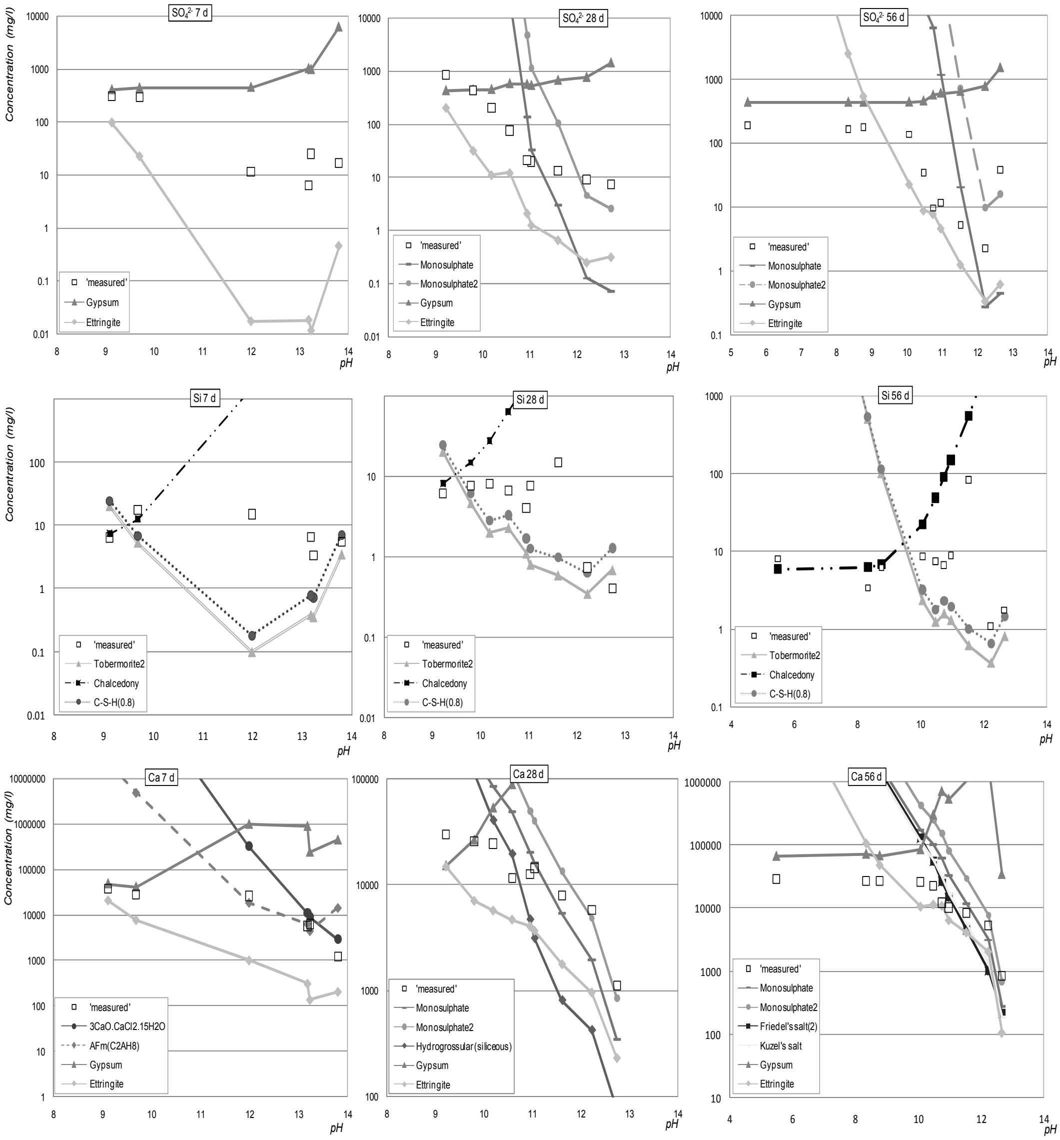

Figure 57: Results of the geochemical speciation modeling for Ca SO_4^{2-}, and Si (20% BA, 2% $CaCl_2$)

Conclusions

The preliminary results of a study on the formulation of blended cements using incinerator bottom ash revealed that in order to attain adequate mechanical strength, an activation pre-treatment was required. In all cases, activation contributed to increasing mechanical strength if compared to untreated bottom ash. However, among the activators tested, $CaCl_2$ only was able to increase UCS above that of Portland cement. The environmental performance of the material was also evaluated through leach testing, which showed that metal leaching was drastically reduced if compared to the raw bottom ash. For the mixture giving the best results in terms of mechanical behavior, metal leaching at the natural pH of the material was below the regulatory limits established by the Italian law for utilization; Cr was the only exception, with a release into the leaching solution slightly above the corresponding threshold value.

While the study conducted so far for $CaCl_2$ and, partly, KOH gave encouraging results in terms of mechanical strength development, a deeper insight into the mechanisms acting during the hydration process as a result of chemical activation of bottom ash is still claimed. In this respect, further studies are currently being conducted through TGA, XRD and Raman spectroscopy techniques to derive information on the mineralogical changes occurring during the hardening process in the presence of activators.

As far as the predictive model developed is concerned, a better description of the effects of the hydration phenomena involved may be obtained through proper consideration of higher-order effects and interactions between the factors of interest. Thus, additional levels for the factors “BA dosage” and “activator addition” will be considered in further analysis.

References

Astrup, T., Dijkstra, J., Comans, R.N.J., van der Sloot, H.A. and Christensen, T.H. (2006): Geochemical modelling of leaching from MSWI air-pollution-control residues. Environmental Science & Technology, Vol. 40, pp. 3551-3557.

Blanc, P., Lassin, A., Nowak, C., Burnol, A., Piantone, P. and Chateau, L. (2007): THERMODDEM: a thermodynamic database for waste materials. Available on-line at http://thermoddem.brgm.fr/fichiers/Phreeqc_thermoddem_lvl1_no-org.txt.

Box, G.E., Hunter, S.J. and Hunter, W.G. (2005): Statistics for Experimenters. Design, Innovation and Discovery. Second edition, John Wiley & Sons, Hoboken, New Jersey.

Fan, Y., Yin, S., Wen, Z., and Zhong, J. (1999): Activation of fly ash and its effects on cement properties. Cement and Concrete Research, Vol. 29, pp. 467-472.

Filipponi, P., Polettini, A., Pomi, R., and Sirini, P. (2003): Physical and mechanical properties of incineration bottom ash-based cements. Waste Management, Vol. 23, pp.145-56.

Giampaolo, C., Lo Mastro, S., Polettini, A., Pomi, R., and Sirini P. (2002): Acid neutralisation capacity and hydration behaviour of incineration bottom ash–Portland cement mixtures. Cement and Concrete Research, Vol. 32, pp. 769-775.

Glasser, F.P., Kindness, A. and Stronach, S.A. (1999): Stability and solubility relationships in AFm phases: Part I. Chloride, sulfate and hydroxide. Cement and Concrete Research, Vol. 29, pp. 861-866.

Hyks, J., Astrup, T. and Christensen, T.H. (2009). Long-term leaching from MSWI air pollution control residues: leaching characterization and modelling. Journal of Hazardous Materials, Vol. 162, pp. 80-91.

Lothenbach, B. and Winnefeld, F. (2006): Thermodynamic modeling of the hydration of Portland cement. Cement and Concrete Research, Vol. 36, pp. 209-226.

Montgomery, D.C. (2005): Design and Analysis of the Experiments. Sixth edition, John Wiley & Sons, Hoboken, New Jersey.

Polettini, A., Pomi, R., and Carcani, G. (2005): The effect of Na and Ca salts on MSWI bottom ash activation for reuse as a pozzolanic admixture. Resources Conservation & Recycling, Vol. 43, pp. 404-418.

Polettini, A., Pomi, R., and Fortuna, E. (2009): Chemical activation in view of MSWI bottom ash recycling in cement-based systems. Journal of Hazardous Materials, Vol. 162, pp. 1292-1299.

Pu, X. (1999): Investigation on pozzolanic effect of mineral additives in cement and concrete by specific strength index. Cement and Concrete Research, Vol. 29, pp. 951–955.

Qian, J., Shi, C., and Wang, Z. (2001): Activation of blended cements containing fly ash. Cement and Concrete Research, Vol. 31, pp.1121-1127.

Shi, C. and Day, R.L. (1995): Acceleration of the reactivity of fly ash by chemical activation. Cement and Concrete Research, Vol. 25, pp.1333-1346.

Shi, C. and Day, R.L. (2000_a): Pozzolanic reaction in the presence of chemical activators. Part I. Reaction kinetics. Cement and Concrete Research, Vol. 30, pp.51-58.

Shi, C. and Day, R.L. (2000_b): Pozzolanic reaction in the presence of chemical activators. Part II. Reaction products and mechanism. Cement and Concrete Research, Vol. 30, pp. 607-613.

Shi, C. and Day, R.L. (2001): Comparison of different methods for enhancing reactivity of pozzolans. Cement and Concrete Research, Vol. 31, pp. 813-818.

3rd BOKU Waste Conference April 15 - 17, 2009 Vienna, Austria

An investigation of different activation methods of MSWI bottom ash for blended cement formulation

R. Onori, A. Polettini, R. Pomi
Department of Hydraulics, Transportation and Roads - University of Rome "La Sapienza", Rome, Italy

Abstract

In the present study the feasibility of chemical and mechanical activation to improve the reactivity of incinerator bottom ash in Portland cement mixtures was investigated. Three chemical activators, NaOH, KOH and $CaCl_2$, were selected for the experimental campaign on the basis of the results from previous studies. The experiments were arranged according to a full factorial design of three factors - "bottom ash content", "activator type" and "activator dosage" - set at 2, 3 and 2 levels, respectively. The evolution of mechanical strength and the leaching behavior of activated bottom ash/Portland cement mixtures was a matter of major concern in this study. The results indicated that $CaCl_2$ exhibited by far the best effects on the evolution of the hydration process of the mixtures and metal leaching from the hardened material. As for the other activators used, while an improvement in the mechanical properties was still recognizable when KOH was added to the mixtures, no positive effect could be observed in the presence of NaOH. This study provides some promising indications about the feasibility of incinerator bottom ash utilization for the formulation of blended cements, which however will need to be further assessed through a deeper insight into the mechanisms governing the development of mechanical strength in cementitious systems containing bottom ash.

Background

Bottom ash (BA) represents the major portion of the solid residues generated by waste incineration, accounting for 15-25% by mass of the original waste. The minerals present in BA are formed under high-temperature combustion conditions and are subjected to rapid cooling down to ambient temperatures during quenching at the exit of the combustion unit. This temperature drop explains the metastability of most of such solid phases and accounts for the chemical reactivity of bottom ash under natural conditions, particularly in alkaline and oxidizing environments (Sabbas et al., 2003; Polettini et al., 1998). Incinerator

BA is generally composed of amorphous and vitreous phases, and the most abundant constituents are calcium, silicon and aluminum oxides, which are also major components of typical pozzolanic materials.

Previous studies (Filipponi et al., 2003; Giampaolo et al., 2002) appeared to indicate the capability of bottom ash of exhibiting pozzolanic properties in cement based systems, suggesting potential useful applications for blended cement formulation. Nevertheless, such studies indicated also that the mechanical strength of bottom ash-Portland cement products was always lower than that of pure Portland cement or Portland cement-pozzolanic systems, suggesting the need to enhance the weak pozzolanic properties of bottom ash. More recently, the use of appropriate chemical activators - as suggested by a number of investigators for different materials (Fan at al.,1999; Quian et al., 2001; Shi et al., 1995, 2000, 2001) - combined with thermal and mechanical activation of BA was found to promote the development of mechanical strength for BA-Portland cement mixtures (Polettini et al., 2005, 2009).In the present work, further investigation on the role of chemical activators in the development of physical, mechanical and leaching characteristics of RDF incinerator BA/Portland cement mixtures has been conducted.

Materials and methods

The bottom ash used in the present study comes from an Italian grate-type RDF incinerator. Fresh bottom ash was sampled at the exit of the quenching unit, homogenized by quartering and characterized for elemental composition as well as anion content. The material was sieved to produce five size classes, which were separately characterized for physical and chemical properties. The elemental composition was determined by atomic absorption spectrometry after sample digestion according to an alkaline digestion procedure at 1050 °C using lithium tetraborate as the melting agent. Anions were analyzed by ion chromatography after solubilization according to the Italian UNI 8520 method. On the basis of the anticipated different behavior of the finer fractions when blended with cement, in this study only the 0.425–12.0 mm size classes were selected for the experiments.Different Ca-, Na- and K-based compounds, including $CaCl_2{\cdot}2H_2O$, NaOH, KOH (reagent-grade compounds), were selected as BA activators on the basis of a literature survey and the results from previous studies (Filipponi et al., 2003; Giampaolo et al., 2002; Polettini et al., 2005, 2009; Fan at al.,1999; Quian et al., 2001; Shi et al., 1995, 2000, 2001). The activation procedure applied to BA involved heating at 90 °C for 3 h of slurries (L/S = 2 ml/g) containing the ball-milled (<150 μm) ash and the chemical activator. After the pre-treatment step, BA was oven-dried at 60 °C.Cementitious mixtures were prepared (see *Table 26*) by blending different proportions of ball-milled BA and ordinary Portland cement (OPC) at a water/total solids weight ratio of 0.4. The investigated BA/(BA+ OPC) ratios were 20 and 40 wt.%, while the activator additions adopted (expressed as activator/(BA + OPC) ratios) were 2 and 4 wt.%. Control samples containing 0, 20 and 40 wt.% of BA were also prepared for reference purposes. The experiments were arranged according to a full factorial design of the three factors “BA content”, “activator type” and “activator dosage”, set at 2, 3 and 2 levels, respectively.

Mixture code	BA/(BA+OPC) (%)	Activator/(BA+OPC) (%)		
		KOH	NaOH	$CaCl_2$
OPC	0			
C1	20			
C2	40			
A1	20	2		
A2	20	4		
A3	40	2		
A4	40	4		
A5	20		2	
A6	20		4	
A7	40		2	
A8	40		4	
A9	20			2
A10	20			4
A11	40			2
A12	40			4

Table 29: Composition of the OPC/BA mixtures.

The blends were cast in 30-mm cubic moulds, stored at 40 °C and relative humidity (RH) > 90% for 24 h, then demoulded and allowed to cure at 40 °C and RH> 90% for 7, 28 and 56 days.Measurements of unconfined compressive strength (UCS) were made on triplicate specimens according to the ASTM C109 method. The EN14429 ANC test was applied after mechanical strength testing on ball-milled (< 150 μm) and oven-dried (60 °C) specimens.The analysis of variance (ANOVA) (Box et al., 2005; Montgomery, 2005) was applied to the experimental data to derive an estimation of the statistical significance of the main and linear interaction effects between the factors as well as the error of the experiments. The significant effects were then processed through least-squares linear regression to derive a predictive model, describing the so-called response surface, for the variables of interest. The analytical formulation of the predictive model was as follows:

$$y = a_0 + a_1 x_1 + a_2 x_2 + a_3 x_3 + a_{12} x_1 x_2 + a_{13} x_1 x_3 + a_{23} x_2 x_3 + a_{123} x_1 x_2 x_3 \qquad (1)$$

where y is the response variable (e.g., UCS), x_1, x_2 and x_3 are the levels of the three factors "activator type", "bottom ash content" and "activator dosage" and $a_{i(j)(k)}$ the coefficients of the polynomial function.

Results and discussion

The chemical composition of the three BA size classes investigated (12.0–5.6 mm; 5.6–2.0 mm and 2.0–0.425 mm) is reported in Table 27.

Element	CLASS A (12.0–5.6 mm)		CLASS B (5.6–2.0 mm)		CLASS C (2.0–0.425 mm)	
	TC* (mg/kg)	L** (mg/kg)	TC* (mg/kg)	L** (mg/kg)	TC* (mg/kg)	L** (mg/kg)
Al	64591	57	68087	242	52470	202

As	2	0	3	0	2	0
Ca	228165	663	232945	928	264349	982
Cd	61	0	40	0	7	0
Cr	487	0	467	0	483	0
Cu	6452	0	8499	0	4601	1
Fe	21313	0	18795	0	17632	0
K	4410	221	4852	240	5447	281
Mg	16311	0	16652	1	19403	0
Mn	458	0	475	0	503	0
Mo	128	0	13	0	12	0
Na	14901	242	15175	204	20442	208
Ni	209	0	97	0	100	0
Pb	2441	51	2782	41	3403	83
Sb	102	0	42	0	25	0
Si	118872	5	115175	0	93474	0
Zn	2824	4	2424	1	1892	1
Cl^-	18953		19306		25639	
SO_4^{2-}	13417		10427		8800	

*TC = total content ** L = leachate concentration (EN 12457-2)

Table 30: Chemical composition and leaching of the three size fractions investigated

The trace metals displaying the highest concentrations in BA were Pb (2400-3400 mg/kg), Zn (1900-2800 mg/kg) and Cu (4600-8500 mg/kg). As far as metal leaching was concerned, the Pb and Cr concentrations exceeded the regulatory limits established by the Landfill Directive for disposal in hazardous waste landfills.The results from mechanical characterization of cementitious materials are reported in Figure 1in terms of measured UCS values and calculated specific UCS values (relative to OPC), and in Figure 53 in terms of UCS values as a function of curing time and activator type. SUCS (Pu, 1999) is defined as the mechanical strength of a given mixture divided by its OPC content and is used to identify any additional contribution of cement admixtures to mechanical strength other than that produced by the OPC hydrates.

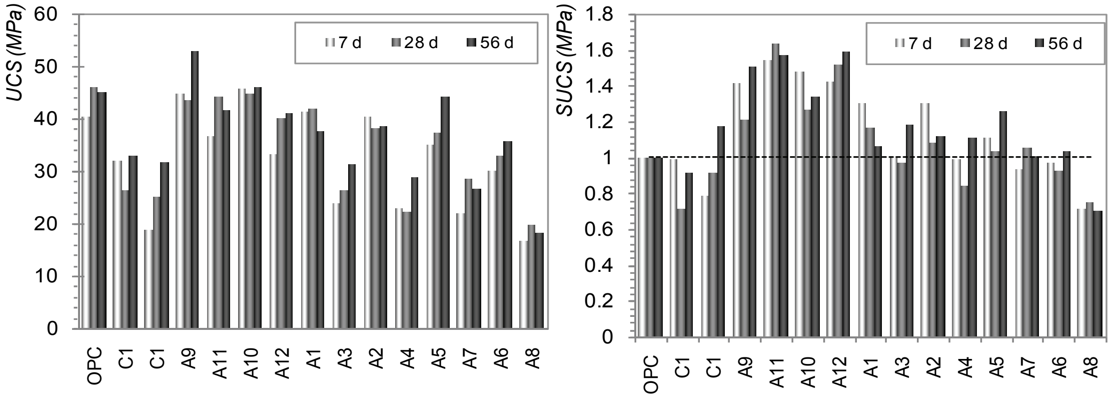

Figure 58: UCS and SUCS values as a function of curing time

The addition of BA to the mixtures with no preliminary activation treatment (samples C1 and C2) was observed to result in decreased mechanical strength values if compared to the control mixture (100% OPC). However, the decrease in UCS depended on BA content in an approximate linear manner at short curing times (7 days), indicating a dilution effect of the cement hydrates system by BA; for longer curing times, the UCS decrease was less than proportional to the BA content, suggesting some possible contribution of the material to the development of mechanical properties.

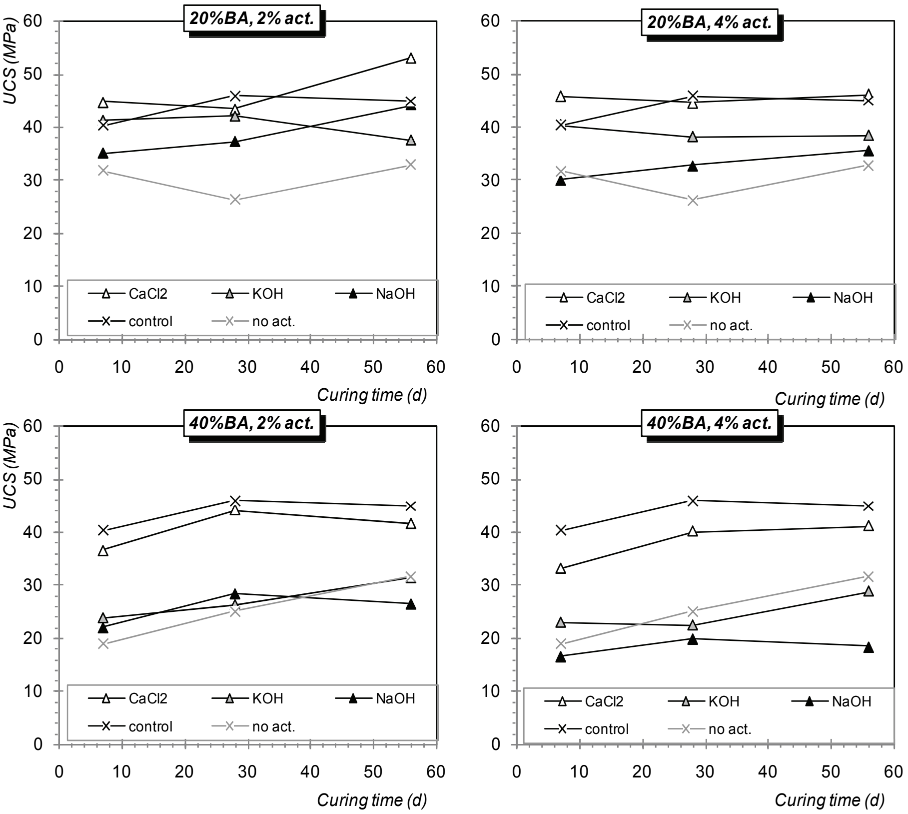

Figure 59: UCS as a function of curing time and activator type

When activated BA was used as a cement admixture, the effects produced on mechanical strength were found to be related to the type of chemical activator used. As a general feature, the three activators tested always resulted in a gain in mechanical strength if compared to the specimens without activator addition. However, the absolute UCS values were found to be largely variable depending on the individual activator used. In particular, as already observed in a previous study on a BA sample from a different source, $CaCl_2$ was found to be capable of improving the mechanical characteristics of cementitious blends in respect to the control mixture. The best results were obtained for a 20% BA content, with UCS values of 44.6, 43.3 and 52.9 MPa after 7, 28 and 56 days, as opposed to 42.0, 45.8 and 44.9 MPa measured for the control sample; increasing the $CaCl_2$ addition from 2% to 4% appeared to have only a minor effect on strength improvement. When the

BA addition was increased to 40%, mechanical strength was reduced only slightly below that of the 100% OPC specimen.As for the two other activators KOH and NaOH, the positive effect on mechanical strength as compared to the non-activated material was by far less evident. Although at 20% BA addition KOH (at both the 2% and 4% dosages) was capable of promoting the hydration process at early curing (7 days) yielding UCS values above that of the control (41.1 and 40.3 MPa, respectively, as opposed to 40.2 MPa), no similar gain was observed at longer curing times. In addition, unlike noted for $CaCl_2$, the decrease in UCS with the BA content when KOH was used as the activator was still considerable at all curing times. This suggested that KOH was only capable to affect hydration to some extent during the early stages of the process and for low BA dosages.The results obtained when BA was activated by NaOH showed that this activator was not suited to significantly contribute to strength development. This occurred irrespectively of the amount of both BA and activator added to the mixtures. Furthermore, an increase in the NaOH dosage was found to adversely effect UCS, likely due to an excess of sodium in the pore solution. The findings commented above become more clear when looking at the specific strength values: while the SUCS of $CaCl_2$-contaning mixtures were all well above the corresponding values for the control specimen, the strength gain was less pronounced for KOH and much less visible (or absent at all) for NaOH. For the reasons explained above, in the following more evidence will be devoted to further examine the mechanical and environmental behavior of the BA/OPC mixtures in the presence of $CaCl_2$.The results of the mechanical strength measurements were processed by means of the ANOVA, which was used to judge the statistical significance of factor effects and interactions, required to build the predictive model described by equation (1). Table 28 reports the ANOVA results for UCS at the three curing times investigated, expressed in terms of sum of squares (SS) for the individual effect/interaction, the corresponding degrees of freedom (DF) and mean squares (MS).

	t = 7 d			**t = 28 d**			**t = 56 d**		
	SS	**DF**	**MS**	**SS**	**DF**	**MS**	**SS**	**DF**	**MS**
SS_1	1194.7	2	**597.3**	1231.2	2	**615.6**	1374.6	2	**687.3**
SS_2	1693.3	1	**1693.3**	814.8	1	**814.8**	1123.4	1	**1123.4**
SS_3	53.1	1	**53.1**	139.9	1	**139.9**	164.4	1	**164.4**
SS_{12}	75.0	2	**37.5**	298.4	2	**149.2**	177.2	2	88.6
SS_{13}	36.3	2	18.1	40.3	2	20.2	87.7	2	43.9
SS_{23}	6.3	1	6.3	22.1	1	22.1	2.6	1	2.6
SS_{123}	9.5	2	4.8	10.9	2	5.4	37.6	2	18.8
SS_E	301.8	24	12.6	1034.0	24	43.1	990.1	24	41.3
SS_T	3369.9	35	96.3	3591.7	35	102.6	3957.6	35	113.1
1 = “activator type”; 2 = “BA dosage”; 3 = “activator addition” E = error; T = total									

Table 31: ANOVA results for UCS

The bold values in Table 28 indicate the significant effects at a 10% significance level. It should be noted that, due to the number of levels used for the two quantitative factors “BA dosage” and “activator addition”, only linear main effects and interactions between factors could be estimated, resulting in a linear predictive model for the response variables. The response surfaces obtained using this approach were plotted in Figure 54 at a constant value for factor 1 (activator type = $CaCl_2$) separately for each curing time.

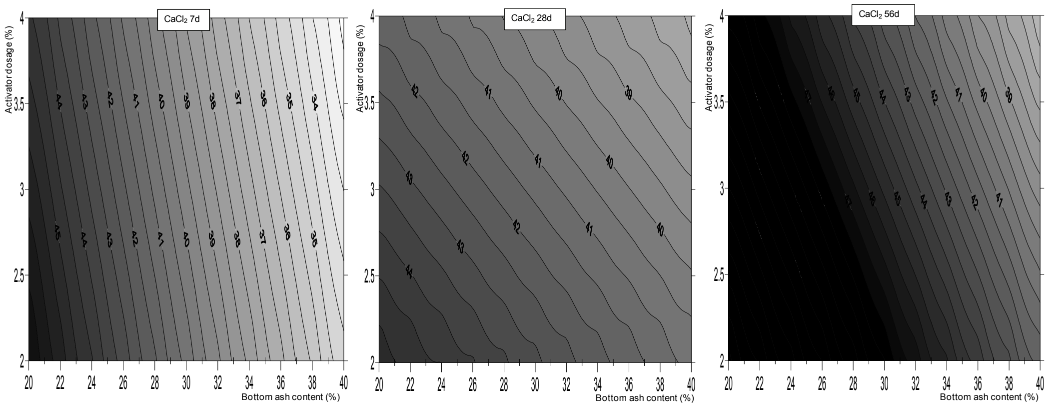

Figure 60: Response surfaces for UCS as derived by equation (1) – values in MPa

The analysis of the contour plots shows the minor effect of an increase of activator dosage at any of the investigated curing times; conversely, UCS was more negatively affected by a corresponding increase in the BA dosage.The mechanical behaviour of mixtures discussed so far was confirmed by the ANC results. The titration curves for the $CaCl_2$-containing blends, depicted in Figure 55 for curing times of 28 and 56 days, appeared to be affected mainly by the BA content while inappreciably by the activator dosage.

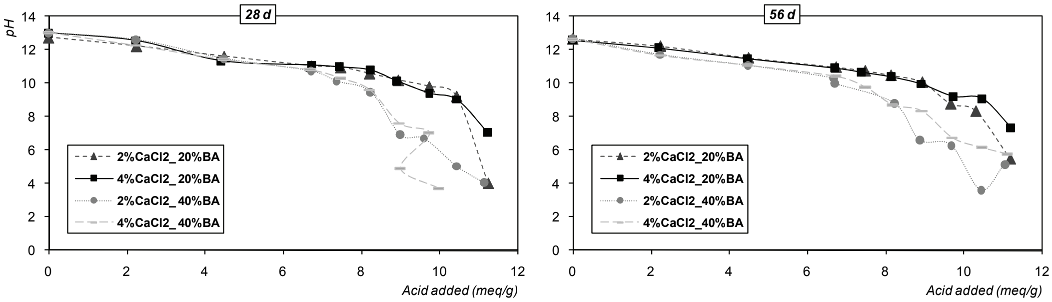

Figure 61: ANC curves for CaCl2-containing blends

It was observed that the ANC to pH 10, which gives a rough estimation of the main hydration phases formed, decreased by about 1-2 meq/g (depending on curing time) as the BA content increased from 20 to 40%. For all the metals under concern, a very dramatic decrease in leaching was observed if compared to the raw BA sample. Metal leaching as a function of pH showed no large differences between the different mixtures investigated. However, as also observed for mechanical strength, the addition of 4% CaCl2 at 20% BA content gave the best results; in particular, in the pH range above 12 metal immobilization efficiency increased by almost an order of magnitude. This is evident in Figure 5, which shows the leaching result obtained for Pb.

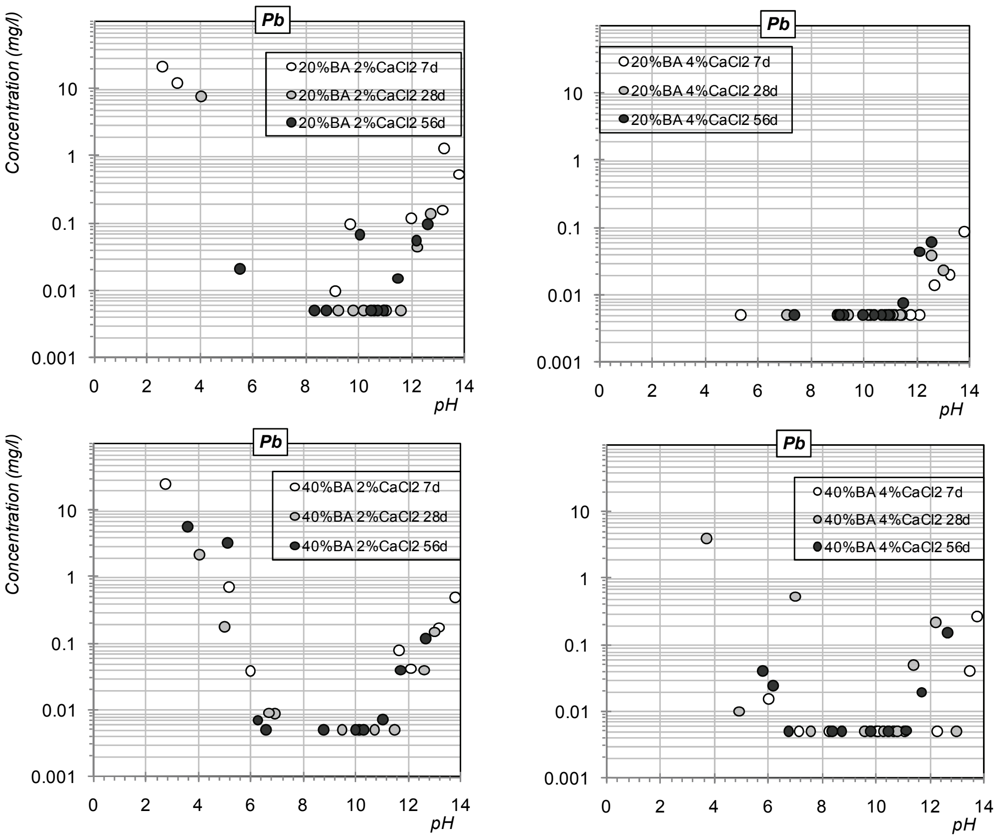

Figure 62: Pb leaching as a function of pH in the ANC test

Conclusions

The preliminary results of a study on the formulation of blended cements using incinerator bottom ash revealed that in order to attain adequate mechanical strength, an activation pre-treatment was required. In all cases, activation contributed to increasing mechanical strength if compared to untreated bottom ash. However, among the activators tested, $CaCl_2$ only was able to increase UCS above that of Portland cement. The environmental performance of the material was also evaluated through leach testing, which showed that metal leaching was drastically reduced if compared to the raw bottom ash. For the mixture giving the best results in terms of mechanical behavior, metal leaching at the natural pH of the material was below the regulatory limits established by the Italian law for utilization; Cr was the only exception, with a release into the leaching solution slightly above the corresponding threshold value.While the study conducted so far for $CaCl_2$ and, partly, KOH gave encouraging results in terms of mechanical strength development, a deeper insight into the mechanisms acting during the hydration process as a result of chemical activation of bottom ash is still claimed. In this respect, further studies are currently being conducted through TGA, XRD and Raman spectroscopy techniques to derive information on the mineralogical changes occurring during the hardening process in the presence of activators.

As far as the predictive model developed is concerned, a better description of the effects of the hydration phenomena involved may be obtained through proper consideration of higher-order effects and interactions between the factors of interest. Thus, additional levels for the factors “BA dosage” and “activator addition” will be considered in further analysis.

References

Box, G.E., Hunter, S.J. and Hunter, W.G. (2005): Statistics for Experimenters. Design, Innovation and Discovery. Second edition, John Wiley & Sons, Hoboken, New Jersey.

Fan, Y., Yin, S., Wen, Z., and Zhong, J. (1999): Activation of fly ash and its effects on cement properties. Cement and Concrete Research, Vol. 29, pp. 467-472.

Filipponi, P., Polettini, A., Pomi, R., and Sirini, P. (2003): Physical and mechanical properties of incineration bottom ash-based cements. Waste Management, Vol. 23, pp.145-56.

Giampaolo, C., Lo Mastro, S., Polettini, A., Pomi, R., and Sirini P. (2002): Acid neutralisation capacity and hydration behaviour of incineration bottom ash–Portland cement mixtures. Cement and Concrete Research, Vol. 32, pp. 769-775.

Montgomery, D.C. (2005): Design and Analysis of the Experiments. Sixth edition, John Wiley & Sons, Hoboken, New Jersey.

Polettini, A., Pomi, R., and Carcani, G. (2005): The effect of Na and Ca salts on MSWI bottom ash activation for reuse as a pozzolanic admixture. Resources Conservation & Recycling, Vol. 43, pp. 404-418.

Polettini, A., Pomi, R., and Fortuna, E. (2009): Chemical activation in view of MSWI bottom ash recycling in cement-based systems. Journal of Hazardous Materials, Vol. 162, pp. 1292-1299.

Pu, X. (1999): Investigation on pozzolanic effect of mineral additives in cement and concrete by specific strength index. Cement and Concrete Research, Vol. 29, pp. 951–955.

Qian, J., Shi, C., and Wang, Z. (2001): Activation of blended cements containing fly ash. Cement and Concrete Research, Vol. 31, pp.1121-1127.

Shi, C. and Day, R.L. (1995): Acceleration of the reactivity of fly ash by chemical activation. Cement and Concrete Research, Vol. 25, pp.1333-1346.

Shi, C. and Day, R.L. (2000_a): Pozzolanic reaction in the presence of chemical activators. Part I. Reaction kinetics. Cement and Concrete Research, Vol. 30, pp.51-58.

Shi, C. and Day, R.L. (2000_b): Pozzolanic reaction in the presence of chemical activators. Part II. Reaction products and mechanism. Cement and Concrete Research, Vol. 30, pp.607-613.

Shi, C. and Day, R.L. (2001): Comparison of different methods for enhancing reactivity of pozzolans. Cement and Concrete Research, Vol. 31, pp. 813-818.

2010 International Solidification/Stabilization Technology Forum 15th-17th June 2010 Cape Breton University (Canada)

International Solidification/ Stabilization Technology Forum
Forum international sur la technologie de la solidification-stabilisation
s/s-tech

Mechanical and leaching properties of blended systems containing OPC and incinerator bottom ash

Roberta Onori
Department of Hydraulics, Transportation and Roads – University of Rome “La Sapienza,” Rome, Italy
Alessandra Polettini, Raffaella Pomi
Department of Hydraulics, Transportation and Roads – University of Rome “La Sapienza,” Rome, Italy

ABSTRACT

In the present study chemical and mechanical activation were applied aiming at improving the reactivity of incinerator bottom ash in Portland cement mixtures. Four chemical activators, NaOH, KOH, $CaCl_2$ and $CaSO_4$, were selected for the experimental campaign on the basis of the results from previous studies. The experiments were arranged according to a full factorial design of three factors: “bottom ash content,”“activator type”and “activator dosage”set at two, four and two levels, respectively. The evolution of mechanical strength and the leaching behaviour of major and trace elements from activated bottom ash/Portland cement mixtures was a matter of major concern in this study. The results indicated that $CaCl_2$ exhibited by far the best effects on the evolution of the hydration process in the mixtures; a positive effect on mechanical strength was also observed when $CaSO_4$ was used as the activator; as for the other activators used, while a slight improvement in the mechanical properties was still recognizable at low curing times when KOH was added to the mixtures, no positive effect could be observed in the presence of NaOH. In all cases investigated, trace metals were found to be efficiently immobilized within the hardened materials. While for major constituents the nature of the main hydration phases formed was investigated through geochemical modelling of leaching solutions, for trace metals no mineral phases could be identified as potential solubility-controlling solids. This is probably an indication of the presence of heavy metals as complex phase assemblages in the hardened materials, or as inclusions in the structure of the hydration products.

RÉSUMÉ

Dans la présente étude, une activation chimique et mécanique ont été appliquées pour améliorer la réactivité des cendres de grilles de l’incinérateur dans les mélanges de ciment portland. Quatre activateurs ont été sélectionnés pour une campagne expérimentale basée sur les résultats d’études antérieures, à savoir NaOH, KOH, $CaCl_2$ et $CaSO_4$. Les expériences se déroulaient selon un plan factoriel complet à trois facteurs – « contenu de cendres de grille», « type d’activateur » et « dosage d’activateur » – établi à 2, 4 et 2 niveaux respectivement. Cette étude s’est particulièrement intéressée à l’évolution de la résistance mécanique et à la lixiviation des éléments traces provenant des mélanges ciment portland /cendres de grille. Selon les résultats, le $CaCl_2$ a obtenu les meilleurs effets sur l’évolution du processus d’hydratation des mélanges; le $CaSO_4$, lorsqu’utilisé comme activateur, a également eu un effet positif sur la résistance mécanique; mais le KOH ajouté aux mélanges n’a donné lieu qu’à une légère amélioration des propriétés mécaniques en ce qui concerne les temps de cure à basse température, et le NaOH n’a eu aucun effet observable. Dans tous les cas, on a noté que les métaux en trace étaient immobilisés de manière efficace dans les matériaux durcis. Si, pour les principaux composants, la nature des principales phases d’hydratation formées a pu être analysée par la modélisation géochimique des solutions de lixiviation, pour les métaux en trace, en revanche, aucune phase de minéralisation n’a été identifiée comme matériaux susceptibles de neutraliser la solubilité. Ceci indique sans doute la présence d’assemblages complexes de métaux lourds dans les matériaux durcis ou leur inclusion dans la structure des produits d’hydratation.

1 INTRODUCTION

Bottom ash (BA) represents the major portion of the solid residues generated by waste incineration, accounting for 15 25% by mass of the original waste. The minerals present in BA are formed under high-temperature combustion conditions and are subjected to rapid cooling down to ambient temperatures during quenching at the exit of the combustion unit. This temperature drop explains the general metastability of such solid phases and accounts for the chemical reactivity of bottom ash under natural conditions, particularly in alkaline and oxidizing environments (Zevenbergen and Comans 1994; Zevenbergen et al. 1996; Meima and Comans 1997, 1998, 1999; Sabbas et al. 2003). Incinerator BA is generally composed of amorphous and vitreous phases, and the most abundant constituents are calcium, silicon and aluminum oxides, which are also major components of typical pozzolanic materials.

In previous studies (Giampaolo et al. 2002; Filipponi et al. 2003) evidence was gained of the capability of bottom ash to exhibit pozzolanic properties in cement-based systems, suggesting potential useful applications for blended cement formulation. Nevertheless, the mechanical strength of bottom ash-Portland cement products was always lower than that of pure Portland cement or Portland cement-pozzolanic systems, suggesting the need to enhance the weak pozzolanic properties of bottom ash.

More recently, the use of appropriate chemical activators ~~–as~~ suggested by a number of investigators for materials of different origin (Poon et al. 2003a, b; Giergiczny 2004; Fan et al. 1999; Quian et al. 2001; Shi et al. 1995, 2000, 2001) ~~–c~~ombined with thermal and mechanical activation of BA was found to promote mechanical strength for BA-Portland cement mixtures (Polettini et al. 2005, 2009; Qiao et al. 2008, 2009).

In the present work, further investigation on the influence of chemical activators on the physical, mechanical and leaching characteristics of refuse derived fuel (RDF) incinerator BA/Portland cement mixtures was conducted to evaluate the possibility for recycling of incinerator BA for the formulation of blended cements.

2 MATERIALS AND METHODS

The bottom ash used in the present study comes from an Italian grate-type RDF incinerator. Fresh bottom ash was sampled at the exit of the quenching unit, homogenized by quartering and analyzed for elemental composition as well as anion content. The material was sieved to produce two size classes (coarse fraction, CF, 0.425 mm < Φ < 12.5 mm and fine fraction, FF, Φ < 0.425 mm), which were separately characterized for physical and chemical properties. The elemental composition was determined by atomic absorption spectrometry after sample digestion according to an alkaline digestion procedure at 1050°C using lithium tetraborate as the melting agent. Anions were analyzed by ion chromatography after dissolution according to the Italian UNI 8520 methods.

Different Ca-, Na- and K-based compounds, including $CaCl_2 \cdot 2H_2O$, $CaSO_4 \cdot 2H_2O$, NaOH, KOH (reagent-grade compounds), were selected as BA activators on the basis of a literature survey and the results from previous studies (Shi et al. 1995, 2000, 2001; Fan et al. 1999; Quian et al. 2001; Giampaolo et al. 2002; Filipponi et al. 2003; Polettini et al. 2005, 2009; Pacewska et al. 2008; Qiao et al. 2008, 2009). The activation procedure involved heating at 90°C for 3 h of slurries (L/S = 2 ml/g) containing the ball-milled (≤50 μm) BA and the chemical activator. The activator additions adopted (expressed as activator/BA ratio) were 2 and 4 wt.%. After the pre-treatment step, BA was oven-dried at 60°C. Cementitious mixtures were prepared (see Table 1) by blending different proportions of un-activated or activated BA and ordinary Portland cement (OPC) at a water/total solids weight ratio of 0.4 and at BA/(BA + OPC) ratios of 0, 20 and 40 wt.%; these were selected on the basis of previous studies, which suggested that above a certain threshold the mechanical properties of the hardened materials are negatively affected (Hanehara et al. 2001; Polettini et al. 2005, 2009). The experiments were arranged according to a full factorial design of the three factors “BA content,” “activator type” and “activator dosage,” set at two, four and two levels, respectively.

The blends were cast in 30-mm cubic moulds, stored at 40°C and relative humidity (RH) >90% for 24 h, then demolded and allowed to cure at 40°C and RH>90% for 7, 28, 56 and 90 days.

Measurements of unconfined compressive strength (UCS) were made on triplicate specimens according to the ASTM C109 method. Simultaneous thermogravimetric (TGA) and differential scanning calorimetry (DSC) analyses were performed on the hardened mixtures; a thermal analyzer operating at a heating rate of 10°C/min in static air over a temperature range of 20–1000°C was used. The EN 14429 ANC test was applied after mechanical strength testing on ball-milled (<150 μm) and oven-dried (60°C) specimens.

Table 1. Composition of the OPC/BA mixtures.

Mix no.	BA/ (BA+OPC) (%)	Activator/ BA (%)	Activator type	BA size fraction
control	0	---	---	
U20	20	---	---	
U40	40	---	---	
K20-2c	20	2	KOH	CF
K20-4c	20	4	KOH	CF
K40-2c	40	2	KOH	CF
K40-4c	40	4	KOH	CF
N20-2c	20	2	NaOH	CF
N20-4c	20	4	NaOH	CF
N40-2c	40	2	NaOH	CF
N40-4c	40	4	NaOH	CF
C20-2c	20	2	$CaCl_2$	CF
C20-4c	20	4	$CaCl_2$	CF
C40-2c	40	2	$CaCl_2$	CF
C40-4c	40	4	$CaCl_2$	CF
S20-2c	20	2	$CaSO_4$	CF
S20-4c	20	4	$CaSO_4$	CF
C20-2f	20	2	$CaCl_2$	FF
C20-4f	20	4	$CaCl_2$	FF
S20-2f	20	2	$CaSO_4$	FF
C20-2cf	20	2	$CaCl_2$	CF+FF
S20-2cf	20	2	$CaSO_4$	CF+FF

The evolution of the hydration process for the investigated mixtures was also studied by means of geochemical modeling of the ANC leaching solutions using Visual Minteq as the mathematical code. To allow for a better description of the speciation of eluates, the standard thermodynamic database was thoroughly updated and extended, including the stability constants of several typical cement hydrates from different literature sources (US Department of Energy 2004; Astrup et al. 2006; Lothenbach and Winnefeld 2006; Blanc et al. 2007; Hills 2009; Hyks et al. 2009). The application of the geochemical speciation code followed a three-step procedure: (1) the program was run using the measured concentrations and pHs as input data and suppressing precipitation for all solid phases; (2) potential solubility-controlling minerals where chosen among those displaying saturation indices (SI) in the range −1.5 ≤ SI ≤ +1.5 and on the basis of the likelihood of formation in cementitious systems; and (3) the predicted concentrations of each element in equilibrium with the selected mineral phases were derived according to the following empirical equation (Astrup et al. 2006):

$$C_{eq} = C_{meas}\left(10^{-SI}\right)^{1/n} \qquad [1]$$

where C_{eq} and C_{meas} are the theoretical and measured element concentrations, respectively, while n is the stoichiometric coefficient of the element in the mineral of concern. In all the modeling calculations, the hypothesis of oxidizing conditions was always assumed.

Table 2. Chemical analysis of the CF and FF of BA.

Element/ Anion	Concentration (mg/kg) CF	Concentration (mg/kg) FF
Al	59700	44000
As	2.1	1.2
Ca	248600	272700
Cd	25.1	3.6
Cr	478	517
Cu	6280	6790
Fe	18470	17700
K	5110	4470
Mg	18030	17830
Mn	488	490
Mo	24.9	14.4
Na	17850	14700
Ni	110	152
Pb	3060	4230
Sb	39.5	34.8
Si	104400	66700
Zn	2190	1960
Cl^-	22520	17860
SO_4^{2-}	11910	10330

3 RESULTS AND DISCUSSION

The chemical composition of the two BA size classes investigated is reported in Table 2. The relative amount of the coarse and fine fractions of the material was 91.2 and 8.8% by weight, respectively. The trace metals displaying the highest concentrations in BA were Cu (6300-6800 mg/kg), Pb (3100-4200 mg/kg) and Zn (2000-2200 mg/kg). As for the leaching of trace metals, Pb was identified as the critical element in BA, exceeding by 50 times the regulatory limit of 0.05 mg/l established by the European Landfill Directive 99/31/EC (1999) for disposal in non-hazardous waste landfills.

The results from mechanical characterization of the cementitious materials are reported in Figure 1 in terms of UCS values for the coarse BA fraction. The addition of un-activated BA (samples U20c and U40c) decreased mechanical strength if compared to the control mixture. When activated BA was used as a cement admixture, the effects produced on mechanical strength were related to the type of chemical activator used. As a general feature, the four activators tested always produced a gain in mechanical strength if compared to the specimens without activator addition; however, the UCS values were largely variable depending on the individual activator used. In particular, as already observed in a previous study on a BA sample from a different source (Polettini et al. 2005, 2009), $CaCl_2$ was found to be capable of improving the mechanical characteristics of cementitious blends in respect to the control mixture; a similar feature was also noted by other authors in the activation of natural pozzolans (Shi and Day 2001). The addition of small amounts of $CaCl_2$ reduces the solubility of $Ca(OH)_2$, at the same time increasing its dissolution rate, in turn improving the rate of pozzolanic reactions (Shi and Day 2000a). Furthermore, $CaCl_2$ is known to decrease the setting time, as well as to promote the formation of monochloroaluminate, $C_3A{\cdot}CaCl_2{\cdot}10H_2O$ (Shi 1998). The best results using $CaCl_2$ were obtained for a 20% BA content at 2% activator addition, with UCS values of 44.6, 43.3, 52.9 and 57.7 MPa after 7, 28, 56 and 90 days, as opposed to 42.0, 45.8, 44.9 and 51.1 MPa measured for the control sample; increasing the $CaCl_2$ addition from 2% to 4% appeared to exert a minor effect on strength improvement. When the BA addition was increased to 40%, mechanical strength was reduced only slightly below that of the control specimen.

As for the other activators, there was still a positive effect on mechanical strength as compared to the un-activated material, although this was less pronounced. The two activators $CaSO_4$ and KOH affected similarly the mechanical properties of the material, although presumably with different mechanisms at the microstructural level. The positive effect of sulphate-based activators is known to be associated to the enhanced formation of AFt phases (Shi and Day 2000b; Poon et al. 2003b). Gypsum also appeared to play a role in the dissolution of the glassy phase of fly ashes (Poon et al. 2003b). In addition to the specific mechanisms described above for $CaCl_2$ and $CaSO_4$, the favourable contribution of Ca-based activators to the hydration process of systems containing alkaline waste materials has been indicated by other authors (Bellmann and Stark 2009) and associated to modified precipitation equilibria resulting from the increased Ca concentration in the pore solution.

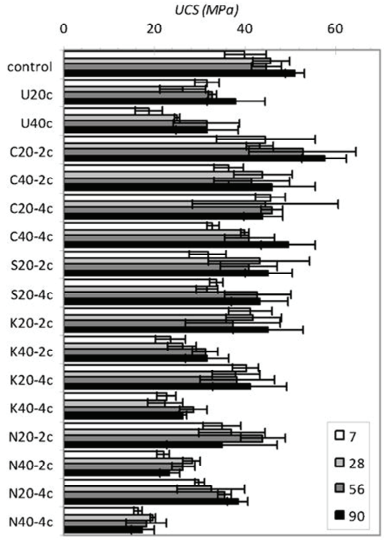

Figure 1. UCS of mixtures containing the CF of BA

The mechanical properties were worsened when NaOH was added to the mixtures, showing that this species was not suited to significantly contribute to strength development, irrespective of the amount of both BA and activator added to the mixtures. Although NaOH is reported in the literature to be a valid activator for a variety of materials, particularly slags rich in C_2AS (Shi and Qian 2000) and low-Ca fly ashes (Arjunan et al. 2001), the effect on strength development has been found to differ depending on the composition of the material to be activated (Shi and Qian 2000). Some investigators have also indicated detrimental effects of NaOH in terms of altered morphology and reduced microstructural uniformity of the hydration products at both early and late ages (Wang et al. 2004). The same authors also highlighted that this negative effect on microstructure is enhanced at elevated curing temperatures, which may explain the results obtained in our experiments.

When comparing the effects of the two alkaline hydroxides used in the present study, the lower contribution of NaOH to mechanical strength development in comparison to KOH is believed to be associated to the higher alkalinity induced in the system at the same weight dosage.

Considering the influence of the BA content of the mixtures, irrespective of the specific activator tested, an increase from 20 to 40% was observed to considerably decrease mechanical strength. From the statistical analysis of UCS values reported in a previous work (Onori et al. 2009), an increase in the activators dosage at any of the investigated curing times was generally found to produce only a minor effect on mechanical strength, indicating the BA content as the main factor affecting the mechanical properties of the hardened materials.

The UCS evolution as a function of curing time for mixtures containing 20% of the coarse BA fraction at 2% activator dosage is reported in Figure 2. It is evident that, in addition to producing higher mechanical strengths, $CaCl_2$ was also shown to exhibit a higher strength gain with time in comparison to all the other mixtures tested, including the control one. Furthermore, $CaSO_4$ and KOH yielded UCS values comparable to that of the control mixture up to 28-day curing, while the residual gain in mechanical strength upon prolonged curing was lower than that of the pure OPC specimen.

A comparison between the mechanical properties of mixtures containing different size fractions of BA is given in Figure 3. Apparently, the fine fraction of the material generally exhibited lower UCS values than the coarse class, likely due to its lower content of alumino-silicate minerals as evidenced by the elemental composition (see Table 2). The mixtures containing the fine fraction also displayed mechanical strength values well below that of the control mixture, even upon chemical activation. When the two size fractions were blended together in the cementitious mixtures, the mechanical behaviour was quite similar to that displayed by the coarse material, obviously due to the prevalence of this in the raw BA. It was also found that, while for the fine material $CaCl_2$ and $CaSO_4$ produced comparable results in terms of UCS, for the coarse fraction $CaCl_2$ was capable of appreciably improving the mechanical properties, with an increase in UCS by 12 26% (depending on curing time) as compared to the corresponding mixture containing the fine fraction.

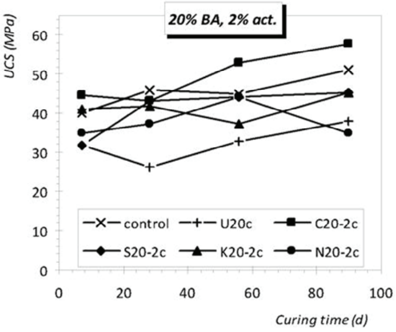

Figure 2. UCS vs. curing time for mixtures containing 20% BA (CF) and 2% activator.

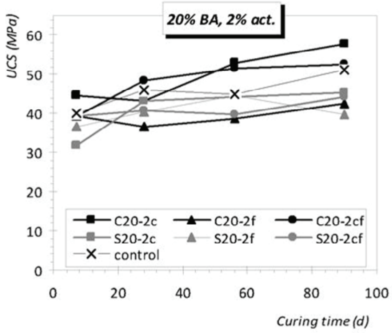

Figure 3. Comparison of UCS of mixtures containing different activated size fractions of BA.

The TGA/DSC patterns for the control, U20c and C20-2c mixtures at 28-day curing are reported in Figure 4. In the TGA patterns, five main regions can be identified on the basis of the characteristic temperature range (see e.g., Alarcon-Ruiz et al. 2005): 1) 20–105℃, corresponding to the loss of the evaporable and part of the bound water; 2) 110–170℃, due to the dehydration of gypsum (displaying a double endothermic peak associated to the subsequent loss of the two water molecules), ettringite and part of the carboaluminate hydrates; 3) 180–300℃, related to the dehydration of C-S-H and carboaluminate phases; 4) 450–550℃, associated to the decomposition of portlandite ($Ca(OH)_2$); and 5) 700–900℃, corresponding to the loss of CO_2 from carbonates.

On the basis of the experimental results depicted in Figure 4, the weight loss associated to the portlandite peak corresponded to a $Ca(OH)_2$ content of 11.5, 10.9 and 6.2 wt.% for the control, U20c and C20-2c mixtures, respectively, which were then corrected to account for the carbonate content of the materials, yielding values of 22.3, 18.5 and 16.0 wt.%. The difference in the portlandite content between the control and the un-activated BA mixture suggests that BA addition to cement produced merely a dilution effect of the hydrate system. When $CaCl_2$ was used as the activator, the portlandite content was found to decrease further; however, given the observed accompanied improvement in mechanical strength (see above), this may be interpreted as a positive influence of chemical activation on the hydration process. In other terms, the lower amount of portlandite measured in the mixture containing $CaCl_2$, along with its improved mechanical properties, may suggest an effect of activation by $CaCl_2$ on the development of pozzolanic reactions within the cementitious system.

The total weight loss (excluding the loss of free water) recorded in the TGA measurements for the control, U20c and C20-2c samples (19.1, 19.4 and 20.4 wt.%, respectively) seems to confirm the increase in the total amount of hydration phases in the presence of $CaCl_2$.

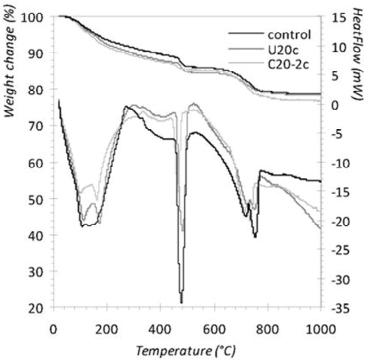

Figure 4. TGA/DSC measurements of selected mixtures.

As for the acid neutralization behaviour of the hydrated mixtures, Figure 5 compares the titration curves obtained for the $CaCl_2$-containing samples at 28 and 56 days. The acid neutralization capacity was observed to decrease with the BA content, as indicated by the increasing slope of the titration curves. Below pH 10 the addition of $CaCl_2$ was also found to reduce the buffering capacity of the material, and this effect became more appreciable at 40% BA dosage.

The results of the ANC test in terms of trace metal leaching as a function of pH are depicted in Figure 6 for the reference mixtures and those containing $CaCl_2$-activated BA (coarse fraction), and compared to the leachate concentrations obtained for the raw BA sample. In general, the trace metal concentrations were found to decrease, in some cases appreciably, with curing, indicating a progressive immobilization with time. Comparing the metal concentrations at the natural pH (leachate without acid addition) with the European Landfill Directive limits for inert waste disposal, it is also clear that the critical elements for the materials under concern include Cr (leachate concentrations in the range 0.05-3.52 mg/L as opposed to a limit of 0.05 mg/L) and Pb (leachate concentrations in the range 0.002-1.90 mg/L as opposed to a limit of 0.05 mg/L). As evident from the ANC curves in Figure 6, the high leaching levels measured for Cr are by no means caused by the contribution of cement, with the control specimen releasing more than 35 mg Cr/kg at 7-day curing; the presence of BA and $CaCl_2$ decreased the leaching level for this metal; however, for the majority of the samples tested the Cr concentration in the leaching solutions exceeded the regulatory threshold limits. This result claims for a very careful control of the chemical composition of the raw materials used for cement production, as this can negatively affect the environmental behaviour of the hardened products obtained, even when they do not include waste materials as admixtures. However, the degree of Cr immobilization in the control mixture was found to increase upon curing, likely due to the incorporation in the hydration phases as indicated by the results from geochemical modeling discussed below. At all ages, an addition of 4% $CaCl_2$ was also observed to exert a more positive effect on Cr leaching in comparison to the 2% dosage.

For both Cu and Pb, the control sample displayed appreciably lower release levels at all pHs since early hydration; however, the differences in leaching between the control and the BA-containing mixtures became fairly less evident as curing progressed, with a similar behaviour being observed for Zn as well. As for Pb, notwithstanding the significant decrease in leaching observed in comparison to the raw BA, the release at the natural pH was often above the regulatory limits due to the typical strongly amphoteric behaviour of this metal. The leaching levels were nevertheless found to benefit from prolonged curing, although with some fluctuations likely due to changes in the pH of the leaching solutions; the best results in terms of Pb release were obtained for the C20-2c specimen after 90 days, with a leachate concentration well below the limits established for disposal in inert waste landfills.

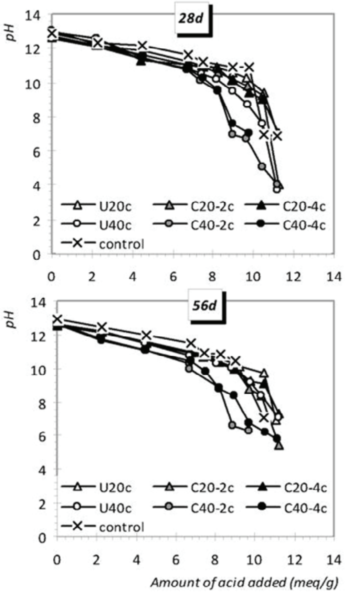

Figure 5. ANC curves for $CaCl_2$-containing mixtures.

The results of geochemical modeling for the investigated trace metals showed that it was not possible to identify common secondary minerals including metal (hydr)oxides, carbonates and sulphates as potential solubility-controlling solids, with leaching solutions being always undersaturated in respect to such phases. Clearly, the difference between the observed and model-predicted leachate concentrations is caused by the role played by additional mechanisms (not accounted for in the model) in the immobilization of trace metals within the investigated materials. This is believed to be related to the role of metal sorption or metal incorporation within the structure of the hydrated matrix, or to the presence of trace metals as complex minerals or phase assemblages which can hardly be described in a univocal manner from the viewpoint of both chemical composition and thermodynamic data. Further investigation on this issue is required to derive information on the immobilization mechanisms of trace metals in BA-OPC blends.

An attempt was made to understand the evolution of the hydration process of OPC in the presence of BA and the activator through geochemical modeling of the leaching solutions obtained from the ANC test. Figures 7 and 8 report the experimental leaching data for Ca, Si and

SO_4^{2-} for the reference mixtures and for the C20-2c sample at curing times of 7 and 56 days, along with the theoretical curves of the solubility-controlling minerals identified on the basis of the modelling calculations. In general, depending on the nature of the mixture tested, different hydration phases were found to control the solubility of major elements/species. For the control sample, at early curing (7 days) ettringite ($Ca_6Al_2(SO_4)_3(OH)_{12}26H_2O$) was observed to control the leaching of Ca and sulphate for pH values in the range 10 12, although at pH 10 11 C-S-H with a Ca/Si ratio of 0.8 also appeared to be a good candidate for solubility control of both Ca and Si. In the alkaline range (pH >12) the leaching of Ca and Si was well described by C-S-H with a Ca/Si ratio of 0.5. The occurrence of C-S-H phases with low Ca/Si ratios as potential solubility-controlling minerals may be explained considering that, due to the large solubility of portlandite in water, even from Ca-rich solutions the equilibrium precipitate has been reported to be always low in Ca/Si ratio (Kersten 1996). It is thus still possible that, although not apparent from the analysis of the ANC eluates, other calcium silicate hydrate phases with higher Ca/Si ratios were actually present in the solid material.

At longer curing times (56 days) Ca leaching from the control mixture was comparably well described by both ettringite and gehlenite hydrate (an AFm phase having the composition $2CaO{\cdot}Al_2O_3{\cdot}SiO_2{\cdot}8H_2O$, also known as strätlingite) at pHs in the range 10 12. Ettringite was also a good candidate for solubility control of sulphate within the same pH range. Ca leaching at pH >12 appeared to be better controlled by the two AFm phases including monosulphate ($Ca_4Al_2(SO_4)(OH)_{12}6H_2O$, which also showed a good fit with sulphate concentration data within the same pH range) and chromium monosulphate ($Ca_4Al_2(CrO_4)(OH)_{12}9H_2O$). The appearance of Cr-monosulphate as a potential solubility-controlling mineral for both Ca and Cr may well explain the incorporation of Cr within the hydration products of Portland cement as the hydration proceeded, with reduced release levels as indicated by the leaching curves in Figure 6. The fit between Si leaching data from the control mixture and the theoretical solubility curves of the above mentioned phases was relatively poor. Only gehlenite hydrate in a limited pH interval (10.5 11.5) appeared to match the experimental data, while Ca/Si=0.5 C-S-H, which gave a good fit with the measured Ca concentrations (see above), was not found to adequately describe the leaching behaviour of Si.

As far as the reference mixture containing un-activated BA (U20c) was concerned, at 7-day curing either anhydrite or gypsum were identified as potential solubility-controlling minerals for both Ca and sulphate in the pH range 8.5 11.5. In the alkaline range (pH >12), while the leaching of Ca was described by Ca oxychloride ($3CaO{\cdot}CaCl_2{\cdot}15H_2O$), no solubility-controlling minerals could be identified for sulphate, with eluates being oversaturated by 1 2 orders of magnitude with respect to both ettringite and monosulphate. It is tempting to hypothesize that the absence of such sulphate-bearing phases in the U20c sample indicates a delay in the hydration process of cement when un-activated BA was added to the mixture.

In the case of Si, again Ca/Si=0.5 C-S-H was identified as the potential leaching-controlling mineral below pH 12.5, while no suitable phases were found to describe Si leaching at higher pH levels. At 56-day curing ettringite appeared to be a good candidate for solubility control for both Ca and sulphate at pH values in the range 9.5 12, although approximately in the same pH interval (10-13) gehlenite hydrate was also found to display a good match with Ca and Si leaching data. At pH values below 9.5, when ettringite becomes unstable as widely reported in the literature (Damidot and Glasser 1992, 1993 a, b; Perkins and Palmer 1999), gypsum appeared to control Ca and sulphate leaching from the material.

When $CaCl_2$-activated BA was added to cement (specimen C20-2c), at 7-day curing gypsum at pH <9 was found to be the most probable candidate for solubility control of both Ca and sulphate. In the case of Ca, monosulphate and Ca oxychloride were also identified as solubility controlling solids in the pH ranges 12 13.8 and 13 13.8, respectively. On the other hand, in the alkaline range (pH >9) sulphate concentrations in the leaching solutions always showed oversaturation with respect to ettringite by a factor of about two, and no mineral appeared to be suitable to explain the release of sulphate from the hardened mixture. As mentioned above for the reference sample containing un-activated BA, the only mineral describing Si leaching (although again with relatively poor fitting of the measured data) was Ca/Si=0.5 C-S-H at pH <10, while at higher pH values none of the phases included in the expanded thermodynamic database was capable of matching the experimental leaching curves.

Upon prolonged curing (56 days), the minerals responsible for solubility control of the major elements/species were found to change. Again, at pH <9 gypsum was selected as the leaching-controlling mineral for both Ca and sulphate; on the other hand, ettringite appeared to be the best candidate for solubility control at pH >10 for both the same species, with a very good fit with the measured concentrations. It should also be mentioned that at the same pH values gehlenite hydrate appeared to adequately describe the release of Ca as well, along with that of Si. In other pH ranges, the dissolution of this element was found to be dictated by quartz (pH <9) and Ca/Si=0.8 C-S-H (pH =12-13).

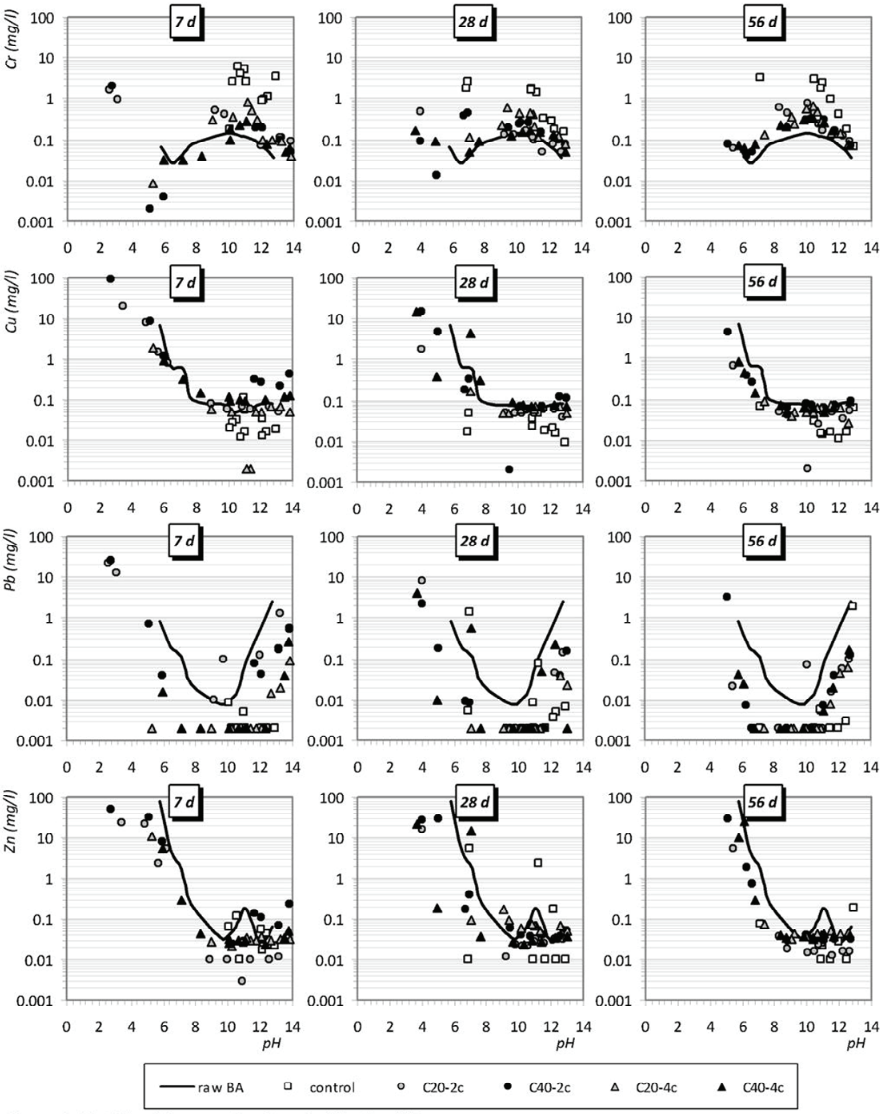

Figure 6. Metal leaching as a function of pH in the ANC test for reference and $CaCl_2$-containing mixtures.

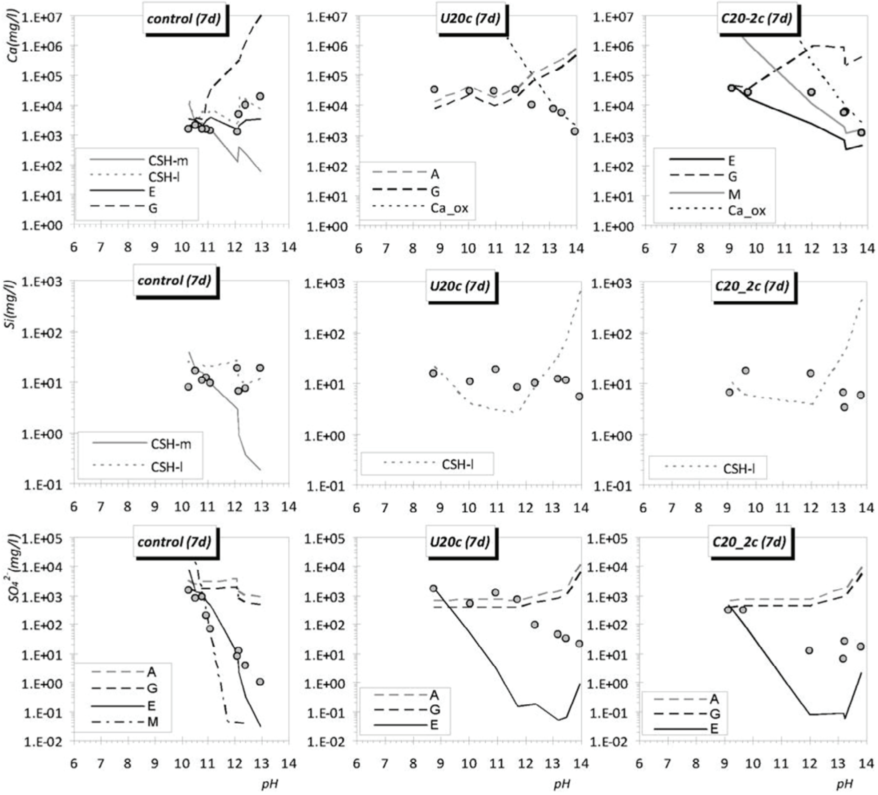

Figure 7. Results of the geochemical modeling for Ca, Si and SO_4^{2-} for the control, U20c and C20-2c mixtures at 7-day curing (A: anhydrite; Caox : Ca oxychloride; CSH-l: C-S-H (Ca/Si = 0.5); CSH-m: C-S-H (Ca/Si = 0.8); E: ettringite; G: gypsum; M: monosulphate).

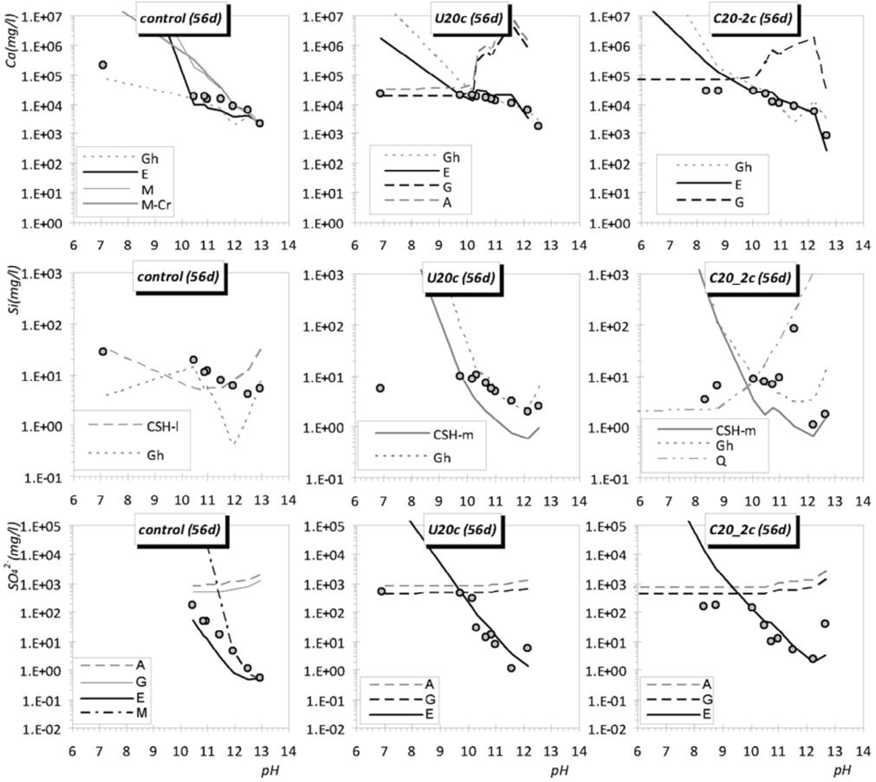

Figure 8. Results of the geochemical modeling for Ca, Si and SO_4^{2-} for the control, U20c and C20-2c mixtures at 56-day curing (A: anhydrite; CSH-l: C-S-H (Ca/Si =0.5); CSH-m: C-S-H (Ca/Si =0.8); E: ettringite; G: gypsum; Gh: gehlenite hydrate; M: monosulphate; MCr: Cr-Monosulphate; Q: quartz).

4 CONCLUSIONS

The preliminary results of a study on the formulation of blended cements using incinerator bottom ash revealed that in order to attain adequate mechanical strength, an activation pre-treatment was required. In all cases, activation contributed to increasing mechanical strength if compared to untreated bottom ash. However, among the activators tested, only $CaCl_2$ was able to increase UCS above that of Portland cement. On the basis of TGA analyses, the effect of $CaCl_2$ appeared to involve to some extent the development of pozzolanic reactions in the cementitious mixtures, with an increase in the total amount of hydration phases present.

The environmental performance of the material was also evaluated through leach testing, which showed that metal relase was reduced if compared to the raw bottom ash as more as curing time was prolonged. For the mixture giving the best results in terms of mechanical behaviour, metal leaching at the natural pH of the material was below the regulatory limits established for disposal in inert waste landfills; Cr was the only exception, with a release into the leaching solution slightly above the corresponding threshold value.

The theoretical description of the composition of the hydrated materials, gained though geochemical modeling of the leaching solutions, indicated the formation of different hydration phases when BA was added to Portland cement. In the case of un-activated BA, the analysis of the modeling results indicated a possible delay in the hydration process in comparison to the normal evolution of pure OPC systems.

REFERENCES

Alarcon-Ruiz, L., Platret, G., Massieu, E. and Ehrlacher, A. 2005. The use of thermal analysis in affecting the effect of temperature on a cement paste, *Cement Concrete and Research*, 35: 609 613.

Arjunan, P., Silsbee, M.R. and Roy, D.M. 2001. Chemical activation of low calcium fly ash. part ii: effect of mineralogical composition on alkali activation, *International Ash Utilization Symposium,* Lexington, Kentucky (USA), October 22–24, 2001, Paper #06.

Astrup, T., Dijkstra, J., Comans, R.N.J., van der Sloot, H.A. and Christensen, T.H. 2006: Geochemical modelling of leaching from MSWI air-pollution-control residues, *Environmental Science & Technology*, 40: 3551 3557.

Bellmann, F. and Stark, J. 2009. Activation of blast furnace slag by a new method, *Cement and Concrete Research*, 39: 644 650.

Blanc, P., Lassin, A., Nowak, C., Burnol, A., Piantone, P. and Chateau, L. 2007. THERMODDEM: a thermodynamic database for waste materials. Available online at http://thermoddem.brgm.fr/fichiers/Phreeqcthermoddemlvl1no-org.txt.

Box, G.E., Hunter, S.J. and Hunter, W.G. 2005. *Statistics for Experimenters. Design, Innovation and Discovery*, 2nd edition, John Wiley &Sons, Hoboken, New Jersey.

Council Directive 99/31/EC 1999. Landfill of waste. Official Journal L 182, 16/07/1999, 0001-0019.

Damidot, D. and Glasser, F.P. 1992. Thermodynamic investigation of the $CaO–Al_2O_3–CaSO_4–H_2O$ system at 50℃ and 85℃, *Cement and Concrete Research*, 22: 1179 1191.

Damidot, D. and Glasser, F.P. 1993a. Thermodynamic investigation of the $CaO-Al_2O_3-CaSO_4-H_2O$ system at 25℃ and the influence of Na_2O, *Cement and Concrete Research*, 23: 221 238.

Damidot, D. and Glasser, F.P. 1993b. Thermodynamic investigation of the $CaO–Al_2O_3–CaSO_4–K_2O–H_2O$ system at 25℃, *Cement and Concrete Research,* 23: 1195 1204.

Fan, Y., Yin, S., Wen, Z. and Zhong, J. 1999. Activation of fly ash and its effects on cement properties, *Cement and Concrete Research*, 29: 467 472.

Filipponi, P., Polettini, A., Pomi, R. and Sirini, P. 2003. Physical and mechanical properties of incineration bottom ash-based cements, *Waste Management*, 23: 145 56.

Giampaolo, C., Lo Mastro, S., Polettini, A., Pomi, R. and Sirini, P. 2002. Acid neutralisation capacity and hydration behaviour of incineration bottom ash–Portland cement mixtures, *Cement and Concrete Research,* 32: 769 775.

Giergiczny, Z. 2004. Effect of some additives on the reactions of the reactions in fly ash-$Ca(OH)_2$ system, *Journal of Thermal Analysis and Calorimetry,* 76: 747 754.

Glasser, F.P., Kindness, A. and Stronach, S.A. 1999. Stability and solubility relationships in AFm phases: Part I. Chloride, sulfate and hydroxide, *Cement and Concrete Research*, 29: 861 866.

Hanehara, S., Tomosawa, F., Kobayakawa, M. and Hwang, K. 2001. Effects of water/powder ratio, mixing ratio of fly ash, and curing temperature on pozzolanic reaction of fly ash in cement paste, *Cement and Concrete Research,* 31: 31 39.

Hills, C.D. 2009. Personal communication. University of Greenwich.

Hyks, J., Astrup, T. and Christensen, T.H. 2009. Long-term leaching from MSWI air pollution control residues: leaching characterization and modelling, *Journal of Hazardous Materials*, 162: 80 91.

Kersten, M. 1996. Aqueous Solubility Diagrams for Cementitious Waste Stabilization Systems. 1. The C-S-H Solid-Solution System, *Environmental Science and Technology*, 30: 2286 2293.

Lothenbach, B. and Winnefeld, F. 2006. Thermodynamic modeling of the hydration of Portland cement, *Cement and Concrete Research*, 36: 209 226.

Meima, J.A. and Comans, R.N.J. 1997. Geochemical modeling of weathering reactions in municipal solid waste incinerator bottom ash, *Environmental Science and Technology*, 31: 1269 1276.

Meima, J.A. and Comans, R.N.J. 1998. Application of surface complexation/precipitation modeling to contaminant leaching from weathered municipal solid waste incinerator bottom ash, *Environmental Science and Technology*, 32, 688 693.

Meima, J.A. and Comans, R.N.J. 1999. The leaching of trace elements from municipal solid waste incinerator bottom ash at different stages of weathering, *Applied Geochemistry*, 14: 159 171.

Montgomery, D.C. 2005. Design and Analysis of the Experiments, 6th edition, John Wiley & Sons, Hoboken, New Jersey.

Onori, R., Polettini, A. and Pomi, R. 2009. An investigation of RDF bottom ash activation for blended cement formulation. Méhu, J., Goumans, J.J.J.M., Heynen, J.J.M., Eds., Proc. *WASCON 2009, International Conference on Sustainable Management of Waste and Recycled Materials in Construction*, Lyon (FR), 3 5 October 2009.

Perkins, R.B., and Palmer, C.D. 1999. Solubility of ettringite $Ca_6[Al(OH)_6]_2(SO_4)_3 26H_2O$ at 5–75°C, *Geochimica et Cosmochima Acta*, 63: 1969 1980.

Polettini, A., Pomi, R. and Carcani, G. 2005. The effect of Na and Ca salts on MSWI bottom ash activation for reuse as a pozzolanic admixture, *Resources Conservation & Recycling*, 43: 404 418.

Polettini, A., Pomi, R. and Fortuna, E. 2009. Chemical activation in view of MSWI bottom ash recycling in cement-based systems, *Journal of Hazardous Materials*, 162: 1292 1299.

Qian, J., Shi, C. and Wang, Z. 2001. Activation of blended cements containing fly ash, *Cement and Concrete Research*, 31: 1121 1127.

Pacewska, B., Wilinska, I. and Blonkowski, G. 2008. Investigations of cement early hydration in the presence of chemically activated fly ash, *Journal of Thermal Analysis and Calorimetry,* 93: 769 776.

Poon, C.S., Qiao, X.C. and Lin, Z.S. 2003a. Pozzolanic properties of reject fly ash in blended cement pastes, *Cement and Concrete Research,* 33: 1857 1865.

Poon, C.S., Qiao, X.C. and Lin, Z.S. 2003b. Effects of flue gas desulphurization sludge on the pozzolanic reaction of reject-fly-ash-blended cement pastes, *Cement and Concrete Research,* 34: 1907 1918.

Qiao, X.C., Tyrer, M., Poon, C.S. and Cheeseman, C.R. 2008. Novel cementitious materials produced from incinerator bottom ash, *Resources, Conservation and Recycling, 52: 496 510.*

Qiao, X.C., Cheeseman, C.R. and Poon, C.S. 2009. Influences of chemical activators on incinerator bottom ash, *Waste Management,* 29: 544 549.

Sabbas, T., Polettini, A., Pomi, R., Astrup, T., Hjelmar, O., Mostbauer, P., Cappai, G., Magel, G., Salhofer, S., Speiser, C., Heuss-Assbichler, S., Klein, R. and Lechner, P. 2003. Management of Municipal Solid Waste Incineration Residues, *Waste Management*, 23: 61 88.

Shi, C. and Day, R.L. 1995. Acceleration of the reactivity of fly ash by chemical activation, *Cement and Concrete Research*, 25: 1333 1346.

Shi, C. 1998. Pozzolanic reaction and microstructure of chemical activated lime-fly ash pastes, *ACI Materials Journal*, 95: 537 545.

Shi, C. and Day, R.L. 2000a. Pozzolanic reaction in the presence of chemical activators. Part I. Reaction kinetics, *Cement and Concrete Research,* 30: 51 58.

Shi, C. and Day, R.L. 2000b. Pozzolanic reaction in the presence of chemical activators. Part II. Reaction products and mechanism, *Cement and Concrete Research,* 30: 607 613.

Shi, C. and Day, R.L. 2001. Comparison of different methods for enhancing reactivity of pozzolans, *Cement and Concrete Research*, 31: 813 818.

Shi, C. and Qian, J. 2000. High performance cementing materials from industrial slags – a review, *Resources, Conservation and Recycling*, 29: 195 207.

US Department of Energy 2004. Qualification of thermodynamic data for geochemical modeling of mineral-water interactions in dilute systems, document no. ANL-WIS-GS-000003.

Wang, K., Shah, S.P. and Mishulovich, A. 2004. Effects of curing temperature and NaOH addition on hydration and strength development of clinker-free CKD-fly ash binders, *Cement and Concrete Research*, 34: 299 309.

Zevenbergen, C. and Comans, R.N.J. 1994. Geochemical factors controlling the mobilization of major elements during weathering of MSWI bottom ash. Goumans, J.J.J.M., van der Sloot, H.A., Aalbers, Th.G., Eds., *Environmental Aspects of Construction with Waste Materials*, Studies in Environmental Sciences 60. Elsevier Sci., Amsterdam, 179 194.

Zevenbergen, C., Van Reeuwijk, L.P., Bradley, J.P. and Comans, R.N.J. 1996. Mechanism and conditions of clay formation during natural weathering of MSWI bottom ash, *Clays and Clay Minerals*, 44: 546 552.

35th International Conference on Advanced Ceramics & Composites (ICACC) 2011

BOTTOM ASH-BASED GEOPOLYMER MATERIALS: MECHANICAL AND ENVIRONMENTAL PROPERTIES

R. Onori, J. Will**, A. Hoppe**, A. Polettini*, R. Pomi*, A.R. Boccaccini***
** Department of Civil and Environmental Engineering, University of Rome "La Sapienza" Rome, Italy*
***Department of Materials Science and Engineering, University of Erlangen-Nuremberg, Erlangen, Germany*

ABSTRACT

The feasibility of geopolymer synthesis using incinerator bottom ash as the source of Si- and Al- containing phases was tested in the present study. Alkaline activation at moderate temperatures was used to force the rearrangement of the alumino-silicate matrix resulting in the production of a geopolymeric material. Different mixtures were investigated for geopolymer production, which differed in the Si/Al ratio (obtained upon addition of sodium silicate and metakaolin at varying proportions) and the NaOH concentration in the alkaline medium. The obtained geopolymeric materials were characterized in terms of physical and mechanical properties, mineralogical and microstructural characteristics as well as chemical durability. Wide variations in the main characteristics of the obtained products were observed, indicating a significant influence of the process variables on the evolution of the geopolymerization reactions. While the physical and mechanical properties correlated well with the Si/Al ratio, no clear trend was found with the NaOH concentration; however, although the strength development upon geopolymerization was clear, the experimental data suggested that the optimal Si/Al ratio was probably beyond the investigated range. SEM, FT-IR, TG and leaching test data showed that, although the onset of the geopolymer-formation reactions was clear, the degree of matrix restructuring was relatively poor, indicating the need for further investigation to promote the development of the geopolymerization reactions.

INTRODUCTION

Bottom ashes (BAs) from waste incineration are generated in relatively large amounts (> 90% of the total solid residues mass) and account for 15-25% by mass of the original waste. BAs are also the residues with technical properties most suited for utilization. The similarities in physical characteristics and major composition of granular construction materials and BA make this residue virtually suited for recycling as a substitute for natural aggregate; construction and building materials are the primary utilization route for BAs in Europe[1]. All the mentioned utilization options rely on the implicit assumption of the predominantly inert characteristics of BA, however, the chemical reactivity of BA under natural conditions has also been widely assessed. Thus, advantage may be taken from the presence of reactive compounds in BA to improve the materials' properties for utilization. Different processing methods have been investigated to improve the mechanical properties of BA in view of engineering applications, which are mostly based on preliminary activation of the material by means of mechanical, chemical or thermal methods (or a combination of the three). In our previous studies[2-6] we applied a number of processes of different nature to transform incinerator BA in a valuable material for various applications. Namely, the studies focused on the production of: 1) sintered ceramics to be used for manufacturing of tiles and linings for pipes and ducts or as an aggregate material; 2) zeolitized materials for the treatment of high-strength industrial wastewaters; 3) pozzolanic materials for the formulation of blended cements. In the present work, we intend to gain insights into the feasibility of production of geopolymeric materials from incinerator BA, considering that the material is known to be composed of amorphous and vitreous phases, the most abundant constituents being Ca-, Si- and Al-containing minerals. While other kinds of inorganic industrial wastes (coal/lignite fly ash[7-15], biomass ash[16], coal bottom ash[9,17], blast furnace slag[18,19], air pollution control ash from waste incineration[20] and wastewater sludge[21]) have been investigated in previous studies for similar applications, to the authors' knowledge no specific study on geopolymer production from incinerator BA has been conducted so far.

MATERIALS AND METHODS

Waste incinerator BA from an Italian grate-type RDF incinerator was used as the starting material for geopolymer synthesis. Fresh BA was sampled at the quenching unit outlet, homogenized by quartering and characterized for elemental composition and anion content. The elemental composition was determined using a Perkin-Elmer 3030B atomic absorption spectrometer after triplicate alkaline digestions at 1050 °C in platinum crucibles using lithium tetraborate as the melting agent. Anions were analyzed using a Metrohm 761 Compact IC ion chromatographer after dissolution according to the Italian UNI 8520 methods. Microstructure was investigated with a Philips XL-30 SEM analyzer, operating at 25 kV with a spot size of 200 nm, a tilt angle of 35º, a take-off angle of 61.34º and equipped with an EDAX DX-4 energy-dispersive spectrometer operated at a count rate of 1200 cps and a live time of 50 s. Samples were first impregnated with an ultra-low viscosity resin, then polished and carbon-coated under vacuum. BA pre-treatment involved ball-milling the dried as-received material to a final mean particle size < 425 μm. The alkaline activator used for geopolymerization included a sodium silicate solution (SiO_2 = 26.91%, Na_2O = 8.68%; SiO_2/Na_2O = 3.1 w/w) and an NaOH solution (10–15.5 M), which were mixed in different proportions to provide the desired reacting medium. Metakaolin (MK) was used to adjust the Si/Al ratio in the desired range of values; metakaolin was obtained from commercial-grade kaolin by calcination at 800°C for 2 hours in air. Milled BA was mixed with the alkaline activator at a solid-to-liquid (S/L) ratio of 4 kg/l except for pastes with the highest metakaolin content, where additional water was required to ensure a suitable workability, resulting in a S/L ratio of 3.3.Different pastes were tested for the geopolymerization process by varying the Si/Al molar ratio (1.28–2.29) and the NaOH concentration (5–9 M) in the alkaline medium, as reported in Table 1 (sample codes include the values of the two parameters in each mixture). The paste preparation procedure involved hand-mixing of the dry BA and metakaolin for 2 minutes, followed by hand-mixing for additional 7 minutes of the resulting dry mixture with previously blended Na silicate and NaOH solutions. The resulting pastes were cast in 20-mm diameter, 45-mm height cylindrical steel moulds, manually compacted with a piston and de-moulded afterwards. The cylindrical specimens were transferred to an oven where they were heated at 75 °C for 24 hours; such operating values were selected on the basis of the results from preliminary tests. After the heat treatment the specimens were wrapped in parafilm foils and cured at room temperature for 7 days.

Table XXXII. Composition of pastes used for the geopolymerization experiments

	Mixture components						Final values	
Sample code	BA	MK	Na silicate sol.	NaOH sol.		S/L ratio	Si/Al	NaOH
	(g)	(g)	(ml)	(M)	(ml)	(g/ml)	(mol/mol)	(M)
S-2.29-5	16	4	2.5	10	2.5	4	2.29	5
S-1.69-5	12	8	2.5	10	2.5	4	1.69	5
S-1.28-5	5.2	14.8	3	10	3	3.3	1.28	5
S-2.29-6	15.8	4.2	3	15	2	4	2.29	6
S-1.69-6	11.7	8.3	3	15	2	4	1.69	6
S-1.28-6	4.6	15.4	3.5	14.5	2.5	3.3	1.28	6
S-2.29-7.5	16	4	2.5	15	2.5	4	2.29	7.5
S-1.69-7.5	12	8	2.5	15	2.5	4	1.69	7.5
S-1.28-7.5	5.2	14.8	3	15	3	3.3	1.28	7.5
S-2.29-9	16.2	3.8	2	15	3	4	2.29	9
S-1.69-9	12.3	7.7	2	15	3	4	1.69	9
S-1.28-9	5.7	14.3	2.5	15.5	3.5	3.3	1.28	9

After 7 days, the products were tested for physical, mechanical, mineralogical, microstructural and leaching properties. Physical and mechanical characterization involved triplicate measurements of bulk density (volume displacement principle), total porosity (pycnometric measurement) and unconfined compressive strength (UCS). Mineralogy and microstructure were investigated through SEM/EDAX, FT-IR and TGA/DTA analyses; while SEM observations were carried out on specimen fragments obtained from mechanical testing, the other analytical techniques were applied on powdered samples. SEM analyses were conducted as already described above. FT-IR absorbance spectra were collected with an Impact 420 Nicolet instrument in the wavenumber range 400–4000 cm−1 with a resolution of 4 cm–1 on pellets with KBr. Simultaneous TGA/DTA analyses were performed at a heating rate of 10 °C/min in static air over a temperature range of 20–1000 °C. The EN 14429 (acid neutralization capacity, ANC) leaching test was applied after mechanical strength testing on ball-milled (<425 µm) specimens to assess the chemical durability of the materials.

RESULTS AND DISCUSSION

Chemical, microstructural and mechanical characterisation the elemental composition of the BA used is reported in Table II. The major constituents of the untreated bottom ash are: Ca (27.5% dry wt.), Si (15.0% dry wt.), soluble chloride (5.4% dry wt.) and Al (4.1%

dry wt.). Appreciable amounts of trace metals were also detected in the material, the highest contents being displayed by Cu (5900 mg/kg), Pb (1400 mg/kg) and Zn (6200 mg/kg).

Table XXXIII. Concentrations (average values ± standard error) of major elements, trace metals and anionic species in the untreated BA

Element/Anion	Concentration (mg/kg)	Element/Anion	Concentration (mg/kg)
Al	41213 ± 2%	Mo	30.4 ± 4%
As	3.4 ± 6%	Na	17496 ± 1%
Ca	274910 ± 7%	Ni	173 ± 22%
Cd	8.3 ± 15%	Pb	1399 ± 12%
Cr	387 ± 4%	Sb	137 ± 15%
Cu	5875 ± 16%	Si	149600 ± 3%
Fe	29377 ± 3%	Zn	6175 ± 6%
K	3869 ± 2%	Cl^-	54423 ± 5%
Mg	18927 ± 4%	SO_4^{2-}	4095 ± 5%
Mn	715 ± 5%		

The SEM micrograph (100× magnification) of the untreated milled BA is shown in Figure 1, which indicates a microstucture with loose particles with large areas characterized by a dark gray level intermixed with lighter gray zones of more limited extension. Both areas were analyzed for elemental composition through EDAX analyses. Dark gray areas mainly contained Ca (16 mol%), Si (13.5 mol%) and Al (5.4 mol%), which could roughly be described by the presence of CaO, SiO_2 and Al_2O_3 at molar ratios of 6:5:1; lower contents of C (4.6 mol%), Na (3.7 mol%), Cl (1.9 mol%) and Mg (1.3 mol%) were also detected. Light gray zones mainly contained Si (24.4 mol%), Na (9.8 mol%) and Ca (7.3 mol%), with smaller concentrations of C (3.9 mol%), Al (2.8 mol%) and Mg (1.4 mol%).The results from mechanical characterization are reported in Figure 2 in terms of UCS values and the relationship between UCS and the Si/Al ratio at given NaOH concentrations in the alkaline medium. Depending on paste composition, large variations in the mechanical properties were observed, with values ranging from a minimum of < 0.1 MPa for sample S-1.28-7.5 to a maximum of 7.4 MPa for sample S-2.29-7.5. While an increase in the Si/Al ratio appeared to improve compressive strength (see Figure 2 b), the influence of NaOH concentration in the reacting medium was less clear, so that at this stage of the investigation it is not possible to derive any conclusive information about the optimal NaOH dosage. For the Si/Al ratio, the results shown in Figure 64Figure 2 b) appear to indicate that the optimum for mechanical strength development should lie beyond the investigated range. While the measured UCS values were relatively weak at the operating conditions tested, the trend reported in Figure 2 b) suggests that improved mechanical characteristics may be obtained when increasing the Si/Al molar ratio above 2.29. Previous studies of geopolymerization of waste materials[7-21] have shown that a very wide range of mechanical strength values can be obtained depending on the initial material composition and processing conditions.

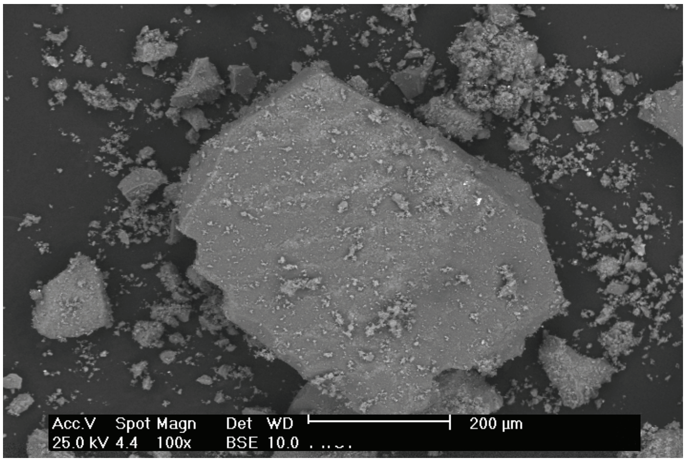

Figure 63. SEM micrographs of polished surfaces for untreated BA.

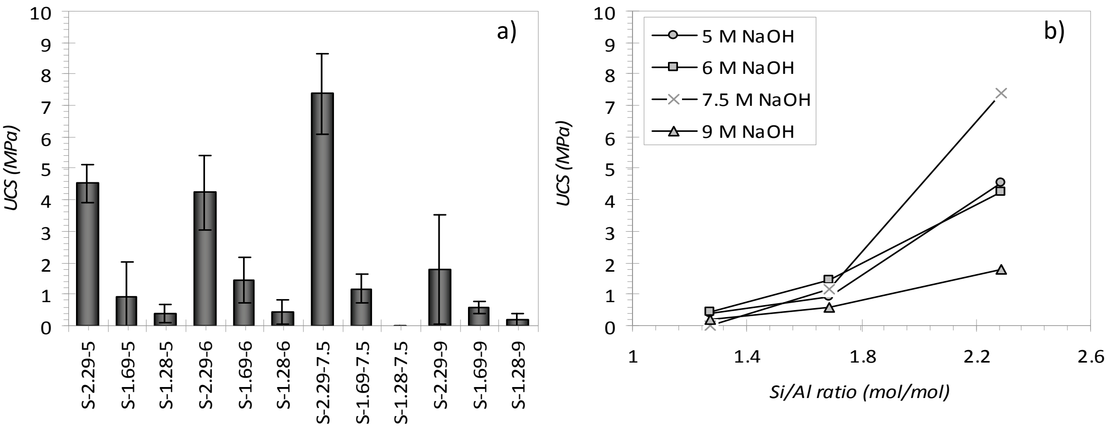

Figure 64. Results of UCS testing on geopolymerized materials (error bars are drawn at one standard deviation of values). The lines in (b) are only for clarify as aid to the eye.

For a more detailed physical and mineralogical/microstructural characterization and to gain knowledge on the microstructure-mechanical strength relationship, four samples were selected among those displaying the best and worst mechanical behaviour; these included S-2.29-7.5 (UCS = 7.38 ± 1.29 MPa), S-2.29-5 (UCS = 4.52 ± 0.59 MPa), S-1.69-7.5 (UCS = 1.18 ± 0.45 MPa) and S-1.28-7.5 (UCS < 0.1 MPa), which differed in the Si/Al ratio and the NaOH concentration. The unit weight and total porosity values for such samples are reported in Table III. Unit weight was found to vary from 10.5 to 15.6 kN/m^3, while total porosity ranged from 40.2 to 66.5%, and both parameters displayed a good correlation with mechanical strength data.

Table XXXIV. Results of physical characterization for selected samples (mean values ± standard deviation)

Sample code	UCS (MPa)	Unit weight (kN/m^3)	Porosity (%)
S-2.29-7.5	7.38 ± 1.29	14.96 ± 0.12	42.8 ± 1.2
S-2.29-5	4.52 ± 0.59	15.57 ± 0.15	40.2 ± 0.5
S-1.69-7.5	1.18 ± 0.45	12.02 ± 0.21	58.9 ± 0.9
S-1.28-7.5	< 0.1	10.54 ± 0.24	66.5 ± 1.2

The SEM micrographs (200× magnification) of polished fragments for samples S-2.29-7.5 and S-2.29-5 (Figure 3) suggest that individual unreacted particles of different size were still present in the material and were surrounded by a layer of small sheets of reacted solids. This effect has been also observed in geopolymers produced using plasma vitrified incinerator air pollution control residues[20]. In the present case, it is apparent that the external layer of reacting material filled the original pores and acted by forming bridges and interconnections between the original grains (Figure 3). The fact that geopolymerization reactions had occurred within the material appears to be indicated by the relatively low pore volume and small void size visible in SEM pictures. Visual observation of the amount and size of pores in the investigated samples also appears to confirm the results from total porosity measurements which indicated that sample S-2.29-7.5 was more porous than sample S-2.29-5. EDAX spot analyses conducted on the 10-μm square areas indicated in Figure 3 showed the main presence of Si (20.9 and 18.0 mol% for samples S-2.29-7.5 and S-2.29-5, resp.) and Al (19.8 and 15.7 mol% for samples S-2.29-7.5 and S-2.29-5, resp.), corresponding to Si/Al molar ratios of 1.05 and 1.15. The Si/Al ratio for these samples thus decreased from 2.29 mol/mol to a final value of ~1.0 mol/mol, which may be explained considering that polysialate-type geopolymers [R_n–(–Si–O–Al–O–)$_n$–], having an Si/Al ratio of 1[22], were formed under the treatment conditions applied.

Sample S-2.29-5 was also found to have a significant Na content (10.8 mol%), which was also appreciably higher than that of sample S-2.29-7.5.

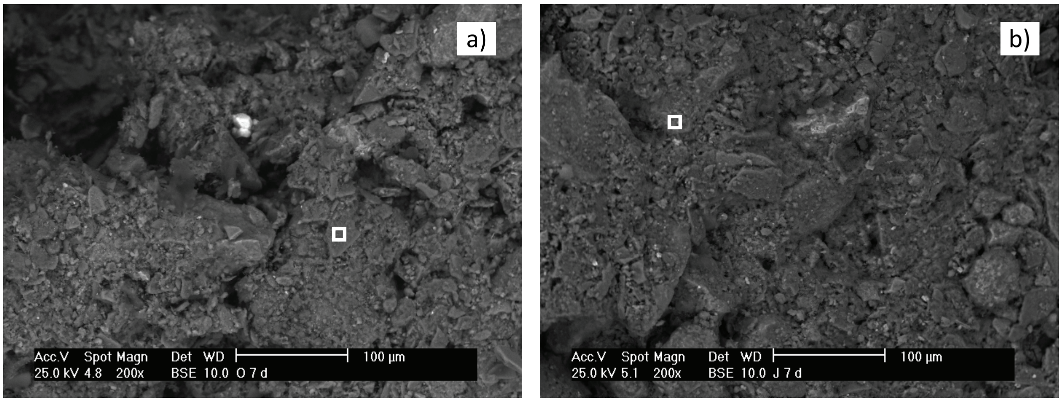

Figure 65. SEM micrographs of fracture surfaces for samples a) S-2.29-7.5 and b) S-2.29-5.

The results of infrared spectroscopy characterization are reported in Figure 4 a) for the untreated BA and the four BA-based geopolymeric materials mentioned above. Five main adsorption bands can be identified in the FT-IR spectra of treated materials, namely: a band at 450–470 cm^{-1} associated to in-plain bending vibration of Si–O–Si[23,26] (referred to as peak 1), a second main band at 980–1040 cm^{-1} associated to asymmetric stretching vibrations of Si–O/Al–O bonds[23-26] (peak 2), a band at ~1450 cm^{-1} due to the presence of O–C–O stretching vibration in carbonate groups[7,23,24,27] (peak 3), two broad bands at 1640–1660 cm^{-1} and 3440–3460 cm^{-1} related to stretching and deformation vibrations of OH and H–O–H groups[9,23,27,28] (peaks 4 and 5). For the untreated BA, a sharp band (although of low intensity) at ~3690 cm^{-1} was also identified (peak 6) and associated to O–H stretching in the $Ca(OH)_2$ structure[29]. According to previous literature studies[23-26], the peaks centered at 980–1040 cm^{-1} and 450–470 cm^{-1} were assumed as the main molecular vibration fingerprints of geopolymeric materials. While the latter was not present in the original BA and was visible in the treated products, the former appeared in the treated materials with a different shape and intensity if compared to the untreated ash. The absorption characteristics in the range of peak 2 suggest that FT-IR spectra display broad and asymmetric curves, which likely result from the overlapping of several characteristic vibrational bands[30]; it is thus possible that not only stretching vibrations of Si–O/Al–O bonds were associated to the observed IR peaks, but that additional vibration modes were also hidden in the spectra. However, a quantitative derivation of such additional characteristic bands has not been performed in the present study. Considering the main peak identified as peak 2, its position tended to shift from wavenumbers of 1020–1040 cm^{-1} (samples S-1.69-7.5 and S-1.28-7.5) towards lower values in the range 985–1007 cm^{-1} (samples S-2.29-5 and S-2.29-7.5), which may be taken as an indication of the increase in the degree of geopolymerization associated to the inclusion of tetrahedrally-coordinated Al in the Si–O–Si skeletal structure[7,12,24,30,31].

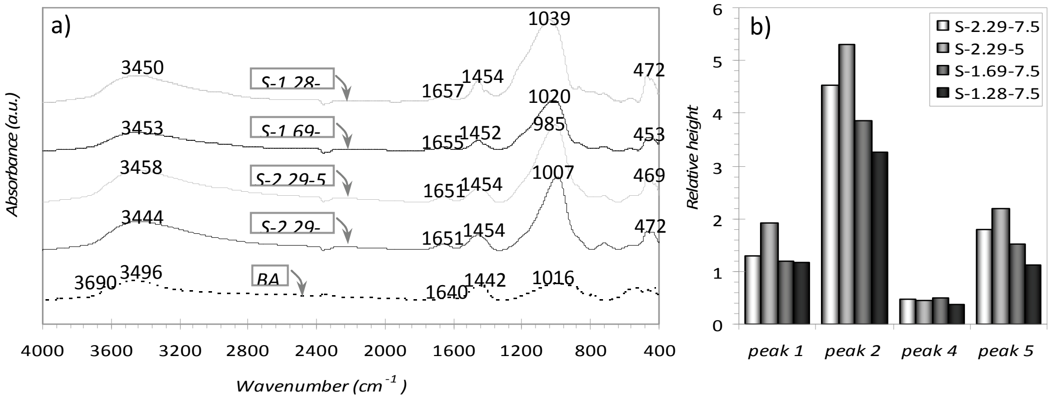

Figure 66. FT-IR spectra (a) and comparison of relative peak intensities (b) for BA-based geopolymers.

A comparison between the intensities of FT-IR peaks for the four BA-based geopolymers is provided in Figure 4 b). Data for each sample were calculated as relative intensities of the peaks of interest normalised to the intensity of peak 3, assuming that the degree of carbonation was the same for all samples tested, so that the carbonate peak should have the same height. The most evident difference in peak height could be observed for peak 2, with samples S-2.29-5 and S-2.29-7.5 displaying higher peak intensities than the other two samples, in agreement with the higher strengths measured; however, the fact that sample S-2.29-7.5 showed a higher UCS than the former could not be related to the information provided by FT-IR data. In general, FT-IR data showed that sample S-2.29-5 displayed higher peak intensities than the other samples. The fact that the height of peak 5, associated to absorbed water, followed the same trend already noted for peak 2 may be considered as an indication of the higher degree of hydration attained for samples S-2.29-5 and S-2.29-7.5, as opposed to the other materials investigated.Another interesting feature noted in the FT-IR spectra was the fact that a small peak appearing at ~800 cm^{-1} for the raw BA, which was attributed to Si–O–Al vibration[23], disappeared in the treated materials and was replaced by several weaker bands at lower wavenumbers, ranging from 700 to 800 cm^{-1}. This may be interpreted assuming that decomposition of Al-containing chemical structures occurred during geopolymerization and that the resulting Al was afterwards incorporated in alumino-silicate structures indicated by peak 2.The thermal analysis results are reported in Figure 5. The thermograms displayed basically four regions characterized by different amounts and rates of mass loss in the following ranges: 20–240 °C, 240–380 °C, 380–700 °C and >700 °C. Within the first region, a major weight loss occurred, accounting for 58–75% of the total weight loss recorded over the temperature range investigated. As outlined by numerous studies[7,12,32-35], a large endothermic peak was observed at temperatures of 120–130 °C, which was related to sample dehydration, with loss of absorbed and loosely bound water. As reported in Table XXXV IV, the weight loss associated to the first temperature region ranged from 4.4 to 5.3% and it was larger for samples S-1.69-7.5 and S-1.28-7.5, for which a poorer geopolymerization degree was also indicated by the other characterization analyses.

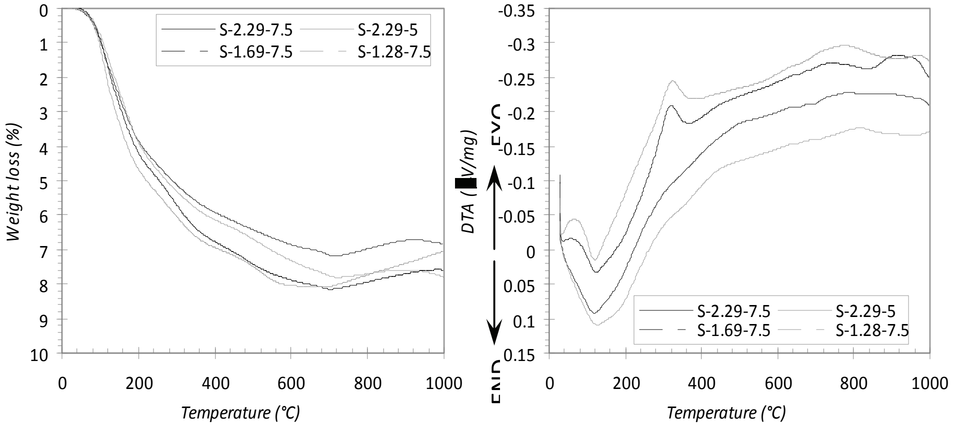

Figure 67. TGA and DTA results for BA-based geopolymers.

Further weight decrease was recorded, although at a lower rate (as also noted by other investigators[33,35]), in the second temperature region and was associated to sample dehydroxylation[7,32]; the mass loss values ranged from 1.4 to 1.8%. However, in the DTA patterns of samples S-1.69-7.5 and S-1.28-7.5, an exothermic peak was identified at about 330 °C, with an associated weight loss of 1.6 and 1.4%, respectively, which indicates the presence of a different phase for such samples if compared to the other materials investigated. Based on the information available, however, no tentative association with any specific phase, the occurrence of which could reasonably be expected only in samples S-1.69-7.5 and S-1.28-7.5, could be made. If the weight loss associated to the decomposition of this unknown phase is subtracted from the overall weight decrease in the temperature region 240–380 °C, net mass loss values are obtained, as shown in Table 1, which suggested a higher degree of hydration for samples S-2.29-7.5 and S-2.29-5, possibly confirming the larger geopolymerization degree attained for such materials.An additional, much slower, mass loss was observed between 380 and 700 °C, which mirrors a more stable thermal behaviour of the materials at temperatures above 380 °C and confirms the results obtained from other studies[33,□]. Finally, a small weight gain (~1%) was observed in the fourth temperature region (> 700 °C).

Table XXXV. Weight loss for different temperature regions as derived from the TGA curves in Figure 5

	Sample code			
Temperature range	S-2.29-7.5	S-2.29-5	S-1.69-7.5	S-1.28-7.5
0-240 °C	4.42	4.57	4.81	5.27
240-380 °C	1.38	1.45	1.83	1.57
240-380 °C (net)	1.38	1.45	0.21	0.19
380-700 °C	1.36	1.74	1.50	1.24
700-1000 °C	-0.33	0.05	-0.56	-1.03

Chemical durability

The ANC curves of the untreated BA and the BA-based geopolymers are shown in Figure 6. Significant changes in the buffering capacity were observed in comparison to the raw ash and between the geopolymerized samples. Due to the high alkali amount added to the mixtures, the natural pH of the original BA (11.84) was found to increase by almost two units in the BA-based geopolymers, reaching values in the range 13.02–13.33. The different mineralogical composition of the untreated and treated materials is mirrored by the different shapes of the titration curves: while the raw BA displayed a sort of plateau in the pH range 10–12, the curves of the treated materials were steeper in this pH range, indicating no significant buffering by mineral phases. The acid buffering capacity of the treated material was generally lower than that of the original BA within the whole range investigated: for the purpose of comparison, while the ANC to pH 8 was 3.2 meq H^+/g for the raw BA, it was reduced to 1.6 meq H^+/g (sample S-1.28-7.5) – 2.9 meq H^+/g (sample S-2.29-7.5). Furthermore, samples S-2.29-5 and S-2.29-7.5 displayed similar ANC curves in the entire pH range investigated and showed stronger buffering capacities with respect to the other two samples; these also appreciably differed from each other, with sample S-

1.28-7.5 displaying the steepest curve. The lower buffering capacity of samples S-1.28-7.5 and S-1.69-7.5 is assumed to confirm the lower degree of geopolymerization reactions occurred for these materials as indicated by the previous analyses.

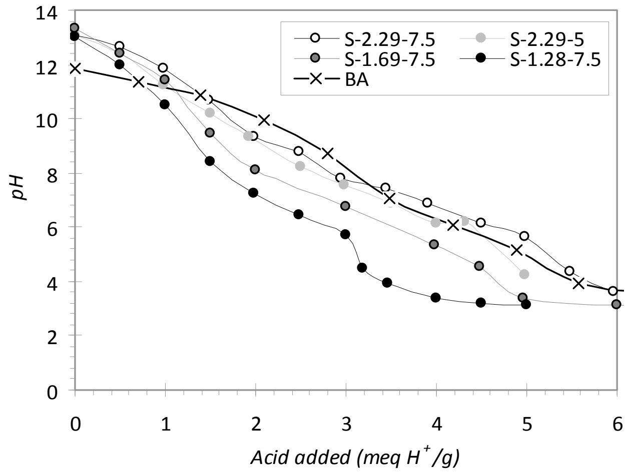

Figure 68. ANC curves for BA-based geopolymers as compared to the untreated BA.

CONCLUSIONS

In the present work, a number of mixtures obtained from BA with the addition of metakaolin, sodium silicate and sodium hydroxide were subjected to a low-temperature thermal treatment in order to induce the formation of geopolymeric materials. Physical, mechanical, microstructural and mineralogical analyses were applied in order to derive information about the influence of the Si/Al ratio and the amount of added NaOH on the main properties of the obtained products. Depending on the process conditions adopted, wide variations in the main characteristics of the materials were observed, indicating a significant influence of the selected process variables on the evolution of the geopolymerization reactions. While the physical and mechanical properties were found to be well correlated with the Si/Al ratio, no clear trend was found with the NaOH concentration in the alkaline medium. Mechanical strength data also suggested that further investigation on the Si and Al content is required to identify the optimal range of values for inducing the highest possible mechanical properties. SEM, FT-IR, TG and chemical durability (ANC) data showed that, although the onset of the geopolymer-formation reactions was clearly confirmed, the degree of matrix restructuring was relatively poor, in agreement with the suggestions provided by the analysis of the mechanical properties.

REFERENCES

[1] T. Astrup, P. Lechner, A. Polettini, R. Pomi, T. Van Gerven, A. van Zomeren, State-of-the-art and outlook on management of waste-to-energy bottom ashes. Part 2: Utilization. Proc. Sardinia 2007, Eleventh International Waste Management and Landfill Symposium, 2007.

[2] C.R. Cheeseman, S. Monteiro da Rocha, C. Sollars, S. Bethanis, and A.R. Boccaccini,

Ceramic processing of incinerator bottom ash, Waste Manage., **23** 907–916 (2003).

[3] A. Polettini, R. Pomi, S. Lo Mastro, and S. Sampieri, Hydrothermal zeolitization of MSWI bottom ash, Proc. WASCON 2006, 6th International Conference on the Environmental and Technical Implications of Construction with Alternative Materials. Science and Engineering of Recycling for Environmental Protection, 439–50.

[4] A. Polettini, R. Pomi, and G. Carcani, The effect of Na and Ca salts on MSWI bottom ash activation for reuse as a pozzolanic admixture, Resour. Conserv. Recy., **43**, 404–18 (2005).

[5] A. Polettini, R. Pomi, and E. Fortuna, Chemical activation in view of MSWI bottom ash recycling in cement-based systems. J. Hazard. Mater., **162**, 1292–9 (2009).

[6] R. Onori, A. Polettini, and R. Pomi, Mechanical properties and leaching modeling of activated incinerator bottom ash in Portland cement blends, Waste Manage., **31**, 298–310 (2011).

[7] S. Andini, R. Cioffi, F. Colangelo, T. Grieco, F. Montagnaro, and L. Santoro, Coal fly ash as raw material for the manufacture of geopolymer-based products, Waste Manage., **28**, 416-23 (2008).

[8] P. Chindaprasirt, T. Chareerat, and V. Sirivivatnanon, Workability and strength of coarse high calcium fly ash geopolymer, Cement Concrete Comp., **29**, 224-9 (2006).

[9] P. Chindaprasirt, C. Jaturapitakkul, W. Chalee, and U. Rattanasak, Comparative study on the characteristics of fly ash and bottom ash geopolymers, Waste Manage., 29, 539-43 (2009).

[10] S. Kumar, and R. Kumar, Mechanical activation of fly ash: effect on reaction, structure and properties of resulting geopolymer, Ceram. Int., **37**, 533-41 (2011).

[11] D. Panias, I.P. Giannopoulou, and T. Perraki, Effect of synthesis parameters on the mechanical properties of fly ash-based geopolymers, Colloid. Surface A, **301**, 246-54 (2007).

[12] F. Škvára, L. Kopecký, V. Šmilauer, and Z. Bittnar, Material and structural characterization of alkali activated low-calcium brown coal fly ash, J. Hazard. Mater., **168**, 711-20 (2009).

[13] J. Temuujin, and A. van Riessen, Effect of fly ash preliminary calcination on the properties of geopolymer, J. Hazard. Mater., **164**, 634-9 (2009).

[14] J. Temuujin, A. van Riessen, and K.J.D. MacKenzie, Preparation and characterisation of fly ash based geopolymer mortars, Constr. Build. Mater., **24**, 1906-10 (2010).

[15] J.G.S. van Jaarsveld, J.S.J. van Deventer, and G.C. Lukey, The effect of composition and temperature on the properties of fly ash- and kaolinite-based geopolymers, Chem. Eng. J., **89**, 63-73 (2002).

[16] S. Songpiriyakij, T. Kubprasit, C. Jaturapitakkul, and P. Chindaprasirt, Compressive strength and degree of reaction of biomass- and fly ash-based geopolymer, Constr. Build. Mater., **24**, 236-40 (2009).

[17] H. Xu, Q. Li, L. Shen, W. Wang, and J. Zhai, Synthesis of thermostable geopolymer from circulating fluidized bed combustion (CBFC) bottom ashes, J. Hazard. Mater., **175**, 198-204 (2010).

[18] T.W. Cheng, and J. P. Chiu, Fire-resistant geopolymer produced by granulated blast furnace slag, Miner. Eng., **16**, 205-210 (2003).

[19] J.E. Oh, P.J.M. Monteiro, S.S. Jun, S. Choi, and S.M. Clark, The evolution of strength and crystalline phases for alkali-activated ground blast furnace slag and fly ash-based geopolymers, Cement Concrete Res., **40**, 189-96 (2010).

[20] I. Kourti, D.A. Rani, D.Deegan, A.R. Boccaccini, and C.R. Cheeseman, Production of geopolymers using glass produced from DC plasma treatment of air pollution control (APC) residues, J. Hazard. Mater., **176**, 704–9 (2010).

[21] C. Lampris, R. Lupo, and C.R. Cheeseman, Geopolymerisation of silt generated from construction and demolition waste washing plants, Waste Manage., **29**, 368–73 (2009).

[22] J. Davidovits, Geopolymer chemistry and applications, Institut Géopolymère, Saint-

Quentin, France, 2nd ed., 2008.

[23] V.F.F. Barbosa, K.J.D MacKenzie, and C. Thaumaturgo, Synthesis and characterisation of materials based on inorganic polymers of alumina and silica: sodium polysialate polymers, J. Inorg. Mater., **2**, 309-17 (2000).

[24] W. Mozgawa, and J. Deja, Spectroscopic studies of alkaline activated slag geopolymers, J. Mol. Struct., **924-926**, 434-41 (2009).

[25] X. Guo, H. Shi, W. Dick, Compressive strength and microstructural characteristics of class C fly ash geopolymer, Cement Concrete Comp., **32**, 142–7 (2010).

[26] J.W. Phair, and J.S.J. Van Deventer, Effect of the silica activator pH on the microstructural characteristics of waste-based geopolymers, Int. J. Miner. Process., **66**, 121-43 (2002).

[27] W.K.W Lee, and J.S.J. Van Deventer, The effects of inorganic salt contamination on the strength and durability of geopolymers, Colloid. Surface A, **211**, 115-26 (2002).

[28] A. Palomo, M.T. Blanco-Varela, M.L. Granizo, F. Puertas, T. Vazquez, M.W. Grutzeck, Chemical stability of cementitious materials based on metakaolin, Cement Concrete Res., **29**, 997–1004 (1999).

[29] M. Yousuf, A. Mollah, P. Palta, T.R. Hess, R.K. Vempati, and D.L. Cocke, Chemical and physical effects of sodium lignosulfonate superplasticizer on the hydration of portland cement and solidification/stabilization consequences, Cement Concrete Res., **25**, 671–82 (1995).

[30] P. Rovnaník, Effect of curing temperature on the development of hard structure of metakaolin-based geopolymer, Constr. Build. Mater., **24**, 1176-83 (2010).

[31] C.A Rees, J.L. Provis, G.C. Luckey, J.S.J. Van Deventer, The mechanism of geopolymer gel formation investigated through seeded nucleation, Colloid. Surface A, **318**, 97–105 (2008).

[32] P. Duxson, G.C. Lukey, J.S.J. van Deventer, Thermal evolution of metakaolin geopolymers: Part 1 – Physical evolution, J. Non-Cryst. Solids, **352,** 5541–55 (2006).

[33] D.L.Y. Kong, and J.G. Sanjayan, Effect of elevated temperatures on geopolymer paste, mortar and concrete, Cement Concrete Res., **40**, 334–9 (2010).

[34] Z. Pan, and J.G. Sanjayan, Stress–strain behaviour and abrupt loss of stiffness of geopolymer at elevated temperatures, Cement Concrete Comp., **32**, 657–64 (2010).

[35] W.D.A. Rickard, and A. van Riessen, Thermal character of geopolymers synthesized from class f fly ash containing high concentrations of iron and α-quartz, Int. J. Appl. Ceram. Technol., **7**, 81–8 (2010).

[36] E. Prud'homme, P. Michaud, E. Joussein, C. Peyratout, A. Smith, S. Arrii-Clacens, J.M. Clacens, and S. Rossignol, Silica fume as porogent agent in geo-materials at low temperature, J. Eur. Ceram. Soc., **7**, 1641–8 (2010).

Waste Management

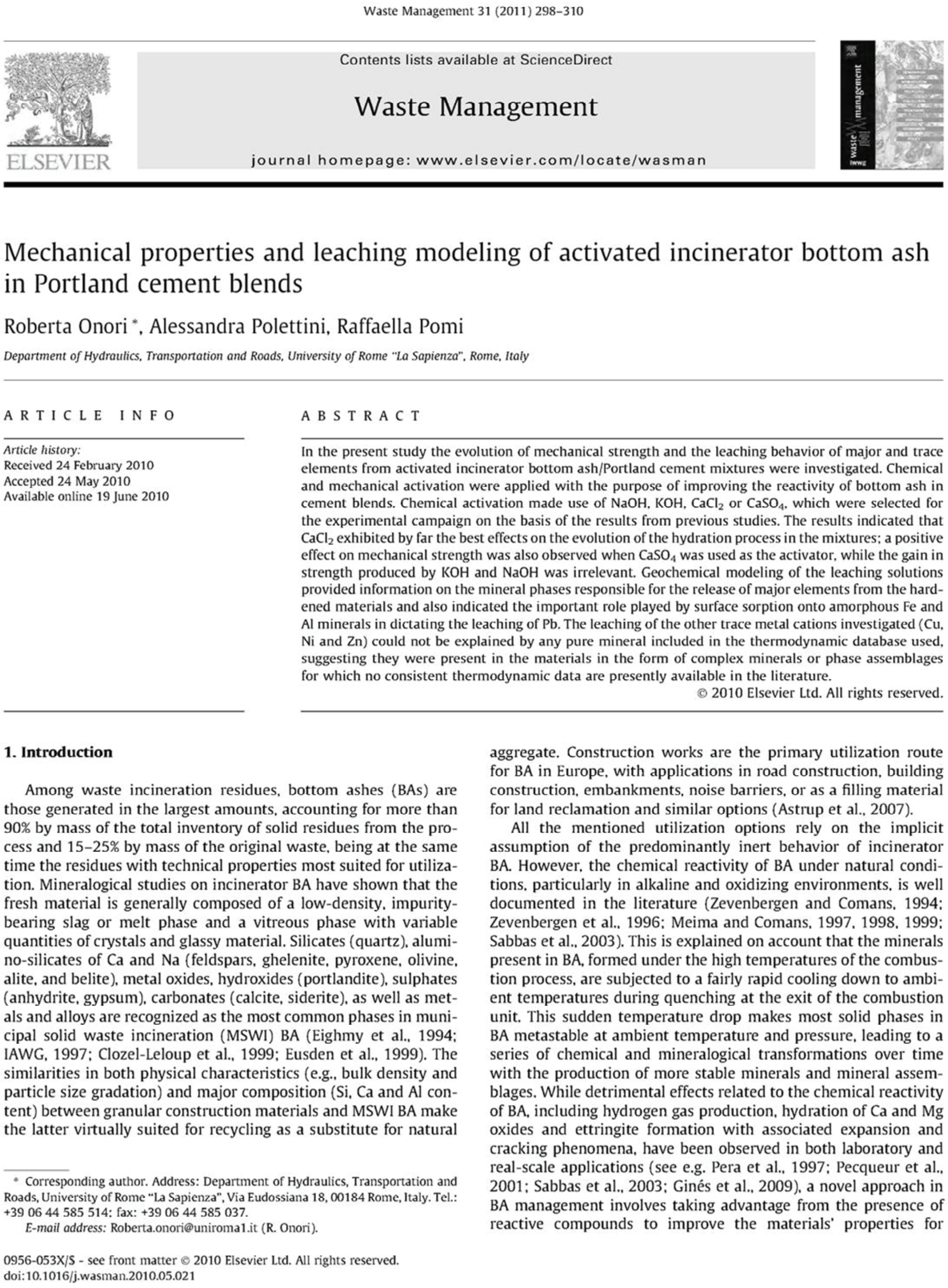

Waste Management 31 (2011) 298–310

Contents lists available at ScienceDirect

Waste Management

journal homepage: www.elsevier.com/locate/wasman

Mechanical properties and leaching modeling of activated incinerator bottom ash in Portland cement blends

Roberta Onori *, Alessandra Polettini, Raffaella Pomi

Department of Hydraulics, Transportation and Roads, University of Rome "La Sapienza", Rome, Italy

ARTICLE INFO

Article history:
Received 24 February 2010
Accepted 24 May 2010
Available online 19 June 2010

ABSTRACT

In the present study the evolution of mechanical strength and the leaching behavior of major and trace elements from activated incinerator bottom ash/Portland cement mixtures were investigated. Chemical and mechanical activation were applied with the purpose of improving the reactivity of bottom ash in cement blends. Chemical activation made use of NaOH, KOH, $CaCl_2$ or $CaSO_4$, which were selected for the experimental campaign on the basis of the results from previous studies. The results indicated that $CaCl_2$ exhibited by far the best effects on the evolution of the hydration process in the mixtures; a positive effect on mechanical strength was also observed when $CaSO_4$ was used as the activator, while the gain in strength produced by KOH and NaOH was irrelevant. Geochemical modeling of the leaching solutions provided information on the mineral phases responsible for the release of major elements from the hardened materials and also indicated the important role played by surface sorption onto amorphous Fe and Al minerals in dictating the leaching of Pb. The leaching of the other trace metal cations investigated (Cu, Ni and Zn) could not be explained by any pure mineral included in the thermodynamic database used, suggesting they were present in the materials in the form of complex minerals or phase assemblages for which no consistent thermodynamic data are presently available in the literature.

1. Introduction

Among waste incineration residues, bottom ashes (BAs) are those generated in the largest amounts, accounting for more than 90% by mass of the total inventory of solid residues from the process and 15–25% by mass of the original waste, being at the same time the residues with technical properties most suited for utilization. Mineralogical studies on incinerator BA have shown that the fresh material is generally composed of a low-density, impurity-bearing slag or melt phase and a vitreous phase with variable quantities of crystals and glassy material. Silicates (quartz), alumino-silicates of Ca and Na (feldspars, ghelenite, pyroxene, olivine, alite, and belite), metal oxides, hydroxides (portlandite), sulphates (anhydrite, gypsum), carbonates (calcite, siderite), as well as metals and alloys are recognized as the most common phases in municipal solid waste incineration (MSWI) BA (Eighmy et al., 1994; IAWG, 1997; Clozel-Leloup et al., 1999; Eusden et al., 1999). The similarities in both physical characteristics (e.g., bulk density and particle size gradation) and major composition (Si, Ca and Al content) between granular construction materials and MSWI BA make the latter virtually suited for recycling as a substitute for natural aggregate. Construction works are the primary utilization route for BA in Europe, with applications in road construction, building construction, embankments, noise barriers, or as a filling material for land reclamation and similar options (Astrup et al., 2007).

All the mentioned utilization options rely on the implicit assumption of the predominantly inert behavior of incinerator BA. However, the chemical reactivity of BA under natural conditions, particularly in alkaline and oxidizing environments, is well documented in the literature (Zevenbergen and Comans, 1994; Zevenbergen et al., 1996; Meima and Comans, 1997, 1998, 1999; Sabbas et al., 2003). This is explained on account that the minerals present in BA, formed under the high temperatures of the combustion process, are subjected to a fairly rapid cooling down to ambient temperatures during quenching at the exit of the combustion unit. This sudden temperature drop makes most solid phases in BA metastable at ambient temperature and pressure, leading to a series of chemical and mineralogical transformations over time with the production of more stable minerals and mineral assemblages. While detrimental effects related to the chemical reactivity of BA, including hydrogen gas production, hydration of Ca and Mg oxides and ettringite formation with associated expansion and cracking phenomena, have been observed in both laboratory and real-scale applications (see e.g. Pera et al., 1997; Pecqueur et al., 2001; Sabbas et al., 2003; Ginés et al., 2009), a novel approach in BA management involves taking advantage from the presence of reactive compounds to improve the materials' properties for

---

* Corresponding author. Address: Department of Hydraulics, Transportation and Roads, University of Rome "La Sapienza", Via Eudossiana 18, 00184 Rome, Italy. Tel.: +39 06 44 585 514; fax: +39 06 44 585 037.
E-mail address: Roberta.onori@uniroma1.it (R. Onori).

0956-053X/$ - see front matter © 2010 Elsevier Ltd. All rights reserved.
doi:10.1016/j.wasman.2010.05.021

utilization. This approach stems from the consideration that incinerator BA is typically composed of amorphous and vitreous phases, the most abundant constituents being Ca, Si and Al minerals, which are also major components of common pozzolanic materials.

Some researchers have investigated different processing methods to improve the mechanical properties of BA for use in engineering applications, which are based on preliminary activation of the material by means of different, often combined, methods: mechanical activation relies on intensive milling of the material to increase the surface area available for reaction; chemical activation is based on the addition of chemical agents capable of breaking down the structure of alumino-silicate minerals, releasing silicate and aluminate ions which can thereafter be transformed into mechanically resistant phases (e.g., in blends with hydraulic binders such as cement and lime, or in geopolymer products); thermal activation involves a moderate-to-high temperature treatment to allow for mineralogical rearrangement of the solid matrix, producing (depending on treatment temperature) either a zeolitized or a predominantly glassy material, the latter being more reactive in alkaline environments, and at the same time immobilizing trace contaminants within the treated material.

In our previous studies (Giampaolo et al., 2002; Filipponi et al., 2003) some evidence was gained of the capability of BA to exhibit pozzolanic properties in cement-based systems, suggesting potential useful applications for blended cement formulation. Nevertheless, such studies also indicated that the mechanical strength of BA-cement products was always lower than that of pure cement or cement–pozzolan systems, suggesting the need to enhance the weak pozzolanic properties of BA. In order to promote the development of mechanical strength for BA–cement mixtures, the use of appropriate chemical activators – as suggested by a number of investigators for materials of different origin (Poon et al., 2003; Giergiczny, 2004; Fan et al., 1999; Qian et al., 2001; Shi and Day, 1995, 2000a,b, 2001) – combined with thermal and mechanical activation of BA was also studied to promote the development of mechanical strength for BA–cement mixtures (Polettini et al., 2005, 2009; Qiao et al., 2008, 2009).

The present work focuses on the technical and environmental behavior of incinerator BA–Portland cement systems with a view to BA recycling in blended cement formulation. In this regard, the role of chemical activators in the development of physical and mechanical properties of hydrated mixtures containing RDF incinerator BA and Portland cement was investigated. The release of major elements and trace metals from the mixtures, which was studied through pH-dependent leaching tests, was one of the main focuses of the work, with the aim to assess the potential environmental impact of the materials and gain an insight into the complex mechanisms governing the release of contaminants from the hardened matrix.

2. Materials and methods

The bottom ash used in the present study comes from an Italian grate-type RDF incinerator. Fresh bottom ash was sampled at the exit of the quenching unit, homogenized by quartering and characterized for elemental composition as well as anion content. The material was sieved to produce two size classes (coarse fraction, CF, 0.425 mm < Φ < 12.5 mm and fine fraction, FF, Φ < 0.425 mm), which were separately characterized for physical and chemical properties. The elemental composition was determined by atomic absorption spectrometry (Perkin–Elmer, model 3030 B) after alkaline digestion of three replicate samples at 1050 °C using lithium tetraborate as the melting agent. Anions were analyzed by ion chromatography (Metrohm, model 761 Compact IC) after dissolution according to the Italian UNI 8520 methods.

Different Ca-, Na- and K-based compounds, including $CaCl_2\cdot 2H_2O$, $CaSO_4\cdot 2H_2O$, NaOH, KOH (reagent-grade compounds), were selected as BA activators on the basis of a literature survey and the results from previous studies (Shi and Day, 1995, 2000a,b, 2001; Fan et al., 1999; Qian et al., 2001; Giampaolo et al., 2002; Filipponi et al., 2003; Polettini et al., 2005, 2009; Pacewska et al., 2008; Qiao et al., 2008, 2009). The activation procedure applied to BA involved heating at 90 °C for 3 h of slurries (L/S = 2 ml/g) containing the ball-milled (<150 μm) ash and the chemical activator. After the pre-treatment step, BA was oven-dried at 60 °C. Cementitious mixtures were prepared (see Table 1) by blending different proportions of dried ball-milled BA and ordinary Portland cement (OPC) at a water/total solids weight ratio of 0.4. The investigated BA/(BA + OPC) ratios were 20 and 40 wt.%, while the activator additions adopted (expressed as activator/BA ratio) were 2 and 4 wt.%. Control samples containing 0, 20 and 40 wt.% of BA were also prepared for reference purposes: in the case of $CaCl_2$, additional reference mixtures were prepared at 0% BA content containing the same amount of activator used for the preparation of mixtures including BA (for example, the sample named Ref. C20–2 in Table 1 is the reference mixture for samples C20–2c, C20–2f and C20–2cf). The blends were cast in 30-mm cubic moulds, stored at 40 °C and relative humidity (RH) > 90% for 24 h, then demoulded and allowed to cure at 40 °C and RH > 90% for 7, 28, 56 and 90 days.

Measurements of unconfined compressive strength (UCS) were made on triplicate specimens according to the ASTM C109 method. Simultaneous thermogravimetric (TGA) and differential scanning calorimetry (DSC) analyses were performed on the hardened materials; a thermal analyzer operating at a heating rate of 10 °C/min in static air over a temperature range of 20–1000 C was used. The EN 14429 (acid neutralization capacity, ANC) leaching test was applied after mechanical strength testing on ball-milled (<150 m) and oven-dried (60 °C) specimens to assess the pH-dependent leaching of both major elements and trace metals from the hardened matrices. After the leaching tests, the pH of the suspensions was measured and the suspensions were centrifuged afterwards, filtered onto 0.45 μm membrane filters and acidified with 1:1 v/v HNO_3 for the subsequent chemical analyses. The analysis of metals in the eluates was carried out using an atomic absorption spectrometer equipped with a graphite furnace for determination of trace concentrations.

To derive information on both the evolution of the hydration process and the mechanisms governing the leaching of contaminants from the hardened materials, geochemical modeling of the ANC eluates was conducted using Visual Minteq as the mathematical code. To allow for a better description of the speciation of eluates from the cement-based materials, the standard thermodynamic database, which presently does not include solid phases typical of hydrated cementitious systems, was thoroughly updated and extended including the stability constants of several cement hydrates from different literature sources (US Department of Energy, 2004; Astrup et al., 2006; Lothenbach and Winnefeld, 2006; Blanc et al., 2007; Hills, 2009; Hyks et al., 2009), which are listed in Table 2 with reference to the corresponding dissolution reaction. In some cases it was required to rearrange the dissolution reaction to fit with the type of components used by Visual Minteq, and recalculate the stability constant accordingly. The application of the geochemical speciation code followed a three-step procedure: (1) the program was run using the measured eluate concentrations and pHs as the input data and suppressing precipitation for all solid phases; (2) potential solubility-controlling minerals where chosen among those displaying saturation indices (SI) in the range $-1.5 \leqslant SI \leqslant +1.5$ and on the basis of the likelihood of formation in cementitious systems; and (3) the predicted concentrations of each element in equilibrium with the selected mineral phases were

Table 1
Composition of the OPC/BA mixtures.

Mix No.	OPC	Mixture composition						BA size fraction
		BA (g/100 g)	Activator (g/100 g)	BA/(BA + OPC) (g/100 g)	Activator/BA (%)	Activator		
						Type	Symbol	
Control	100			0				
U20c	80	20		20				CF
U40c	60	40		40				CF
Ref. C20–2	100		0.4	0		$CaCl_2$	C	
Ref. C20–4	100		0.8	0		$CaCl_2$	C	
Ref. C40–2	100		0.8	0		$CaCl_2$	C	
Ref. C40–4	100		1.6	0		$CaCl_2$	C	
K20–2c	80	20	0.4	20	2	KOH	K	CF
K20–4c	80	20	0.8	20	4	KOH	K	CF
K40–2c	60	40	0.8	40	2	KOH	K	CF
K40–4c	60	40	1.6	40	4	KOH	K	CF
N20–2c	80	20	0.4	20	2	NaOH	N	CF
N20–4c	80	20	0.8	20	4	NaOH	N	CF
N40–2c	60	40	0.8	40	2	NaOH	N	CF
N40–4c	60	40	1.6	40	4	NaOH	N	CF
C20–2c	80	20	0.4	20	2	$CaCl_2$	C	CF
C20–4c	80	20	0.8	20	4	$CaCl_2$	C	CF
C40–2c	60	40	0.8	40	2	$CaCl_2$	C	CF
C40–4c	60	40	1.6	40	4	$CaCl_2$	C	CF
S20–2c	80	20	0.4	20	2	$CaSO_4$	S	CF
S20–4c	80	20	0.8	20	4	$CaSO_4$	S	CF
C20–2f	80	20	0.4	20	2	$CaCl_2$	C	FF
C20–4f	80	20	0.8	20	4	$CaCl_2$	C	FF
S20–2f	80	20	0.4	20	2	$CaSO_4$	S	FF
C20–2cf	80	20	0.4	20	2	$CaCl_2$	C	CF + FF
S20–2cf	80	20	0.4	20	2	$CaSO_4$	S	CF + FF

derived according to the following empirical equation (Astrup et al., 2006):

$$C_{eq} = C_{meas}\left(10^{-SI}\right)^{1/n}, \qquad (1)$$

where, C_{eq} and C_{meas} are the theoretical and measured element concentrations, respectively, while n is the stoichiometric coefficient of the element in the mineral of concern. In the modeling calculations, the hypothesis of oxidizing conditions was always assumed.

To improve the modeling predictions for trace metals, additional runs of the geochemical speciation program were performed, accounting for the binding of trace metals onto the surface of hydrous ferric oxide (HFO). This was described using the diffuse layer model (DLM) proposed by Dzombak and Morel (1990) which is incorporated in the Visual Minteq code. The thermodynamic database for surface complexation was modified by increasing the $\log K$ of the complexation reaction of Pb onto high-capacity/low-affinity sites from 0.3 to 1.7, as suggested by Meima and Comans (1998) and also used by other investigators (see e.g. Martens et al., 2010). Surface sorption onto amorphous aluminum minerals (AAM), which have been demonstrated to have a binding capacity towards metal ions (Stumm and Morgan, 1995; Meima and Comans, 1998), was also taken into account by means of the same surface complexation model as before. Due to the lack of a consistent thermodynamic data set for complexation by AAM, HFO was used as a surrogate sorbent mineral for AAM, considering the similarities in the degree of coordination, charge and reactivity of Fe(III) and Al(III) in such (hydr)oxide forms (Meima and Comans, 1998); the same specific surface area and concentration of binding sites as HFO were used in the calculations, assuming a 1:1 M equivalence between HFO and AAM. The measured leachate concentrations of Fe and Al at $pH < 2$ were taken as a measure of the total amount of HFO and AAM in the samples, as suggested by Engelsen et al. (2009). The amount available for sorption was estimated from low-pH eluates for trace metal cations and from alkaline pH leachates for Cr.

3. Results and discussion

3.1. Bottom ash characterization

The chemical composition of the two BA size classes investigated is reported in Table 3. The relative amount of the coarse and fine fractions of the material was 91.2 and 8.8% by weight, respectively. The trace metals displaying the highest concentrations in BA were Cu (6300–6800 mg/kg), Pb (3100–4200 mg/kg) and Zn (2000–2200 mg/kg). As for the leaching of trace metals (results not shown here), Pb was identified as the critical element in BA, exceeding the regulatory limit established by the European Landfill Directive for disposal in non-hazardous waste landfills.

3.2. Mechanical properties and mineralogy of bottom ash–cement blends

The results from mechanical characterization of the cementitious materials are reported in Figs. 1 and 2 in terms of UCS values for the coarse BA fraction. The addition of un-activated BA (samples U20c and U40c) was observed to result in decreased mechanical strength values in comparison to the control mixture. When activated BA was used as a cement admixture, the effects produced on mechanical strength were dependent on the type of chemical activator used. As a general feature, the four activators tested always produced a gain in mechanical strength in respect to the specimens without activator addition, however the UCS values were largely variable depending on the individual activator used. In particular, as already observed in a previous study on a BA sample from a different source (Polettini et al., 2005, 2009), $CaCl_2$ was capable of improving the mechanical characteristics of cementitious blends in respect to the control mixture, as also observed by other authors in the activation of natural pozzolans (Shi and Day, 2001). The addition of small amounts of $CaCl_2$ is known to decrease the solubility of $Ca(OH)_2$, at the same time increasing its dissolution rate, thus improving the rate of pozzolanic reactions (Shi

Table 2
Stability constants of the new mineral phases added to the standard thermodynamic database in Visual Minteq, based on the dissolution reactions reported.

Mineral	Dissolution reaction	Log K
Sulphate minerals		
K_2SO_4	$K_2SO_4 \rightarrow 2\ K^+ + SO_4$	−1.87[6]
Pentasalt	$(CaSO_4)_5 \cdot K_2SO_4 \cdot H_2O \rightarrow 5\ Ca^{2+} + 2\ K^+ + 6\ SO_4 + 6 \cdot H_2O$	−29.3[6]
$PbSO_4 \cdot PbO$	$PbSO_4 \cdot PbO + 2\ H^+ \rightarrow 2\ Pb^{2+} + SO_4 + H_2O$	−0.19[1]
Syngenite	$K_2Ca(SO_4)_2 \rightarrow Ca^{2+} + 2\ K^+ + 2\ SO_4$	−7.45[6]
C–S–H phases		
Afwillite	$3CaO \cdot 2SiO_2 \cdot 3H_2O + 6\ H^+ \rightarrow 3\ Ca^{2+} + 2\ H_4SiO_4 + 2\ H_2O$	46.90[6]
C–S–H(0.8)	$0.8CaO \cdot SiO_2 \cdot 2.2H_2O + 1.6\ H^+ \rightarrow 0.8\ Ca^{2+} + H_4SiO_4 + H_2O$	11.08[6]
C–S–H(1.1)	$1.1CaO \cdot SiO_2 \cdot 3.9H_2O + 2.2\ H^+ \rightarrow 1.1\ Ca^{2+} + H_4SiO_4 + 3\ H_2O$	16.72[6]
C–S–H(1.7)	$1.7CaO \cdot SiO_2 \cdot 2.617H_2O + 3.4\ H^+ \rightarrow 1.7\ Ca^{2+} + H_4SiO_4 + 2.317\ H_2O$	29.52[2]
C–S–H(1.8)	$1.8CaO \cdot SiO_2 \cdot 5.2H_2O + 3.6\ H^+ \rightarrow 1.8\ Ca^{2+} + H_4SiO_4 + 5\ H_2O$	32.60[6]
Jennite	$1.5CaO \cdot 0.9SiO_2 \cdot (OH)_{4.8} \cdot 0.9H_2O + 3\ H^+ \rightarrow 1.5\ Ca^{2+} + 0.9\ H_4SiO_4 + 2.1\ H_2O$	26.40[4]
Tobermorite	$2CaO \cdot 2.4SiO_2 \cdot 4H_2O + 4\ H^+ \rightarrow 2\ Ca^{2+} + 2.4\ H_4SiO_4 + 1.2\ H_2O$	27.81[4]
AFm phases		
C_4AH_{13}	$2CaO \cdot Al_2O_3 \cdot 13H_2O + 14\ H^+ \rightarrow 4\ Ca^{2+} + 2\ Al^{3+} + 20\ H_2O$	104.42[4]
C_4AH_{19}	$4CaO \cdot Al_2O_3 \cdot 19H_2O + 14\ H^+ \rightarrow 4\ Ca^{2+} + 2\ Al^{3+} + 26\ H_2O$	100.60[2]
C_4FH_{13}	$2CaO \cdot Fe_2O_3 \cdot 13H_2O + 14\ H^+ \rightarrow 4\ Ca^{2+} + 2\ Fe^{3+} + 20\ H_2O$	99.50[4]
C_2AH_8	$2CaO \cdot Al_2O_3 \cdot 8H_2O + 10\ H^+ \rightarrow 2\ Ca^{2+} + 2\ Al^{3+} + 13\ H_2O$	60.43[4]
C_2FH_8	$2CaO \cdot Fe_2O_3 \cdot 8H_2O + 10\ H^+ \rightarrow 2\ Ca^{2+} + 2\ Fe^{3+} + 13\ H_2O$	55.51[4]
C_2ASH_8	$2CaO \cdot Al_2O_3 \cdot SiO_2 \cdot 8H_2O + 10\ H^+ \rightarrow 2\ Ca^{2+} + 2\ Al^{3+} + H_4SiO_4 + 11\ H_2O$	49.35[4]
C_2FSH_8	$2CaO \cdot Fe_2O_3 \cdot SiO_2 \cdot 8H_2O + 10\ H^+ \rightarrow 2\ Ca^{2+} + 2\ Fe^{3+} + H_4SiO_4 + 11 \cdot H_2O$	44.44[4]
$C_4AS'H_{12}$	$3CaO \cdot Al_2O_3 \cdot CaSO_4 \cdot 12H_2O + 12\ H^+ \rightarrow 4\ Ca^{2+} + SO_4^{2-} + 2\ Al^{3+} + 18 \cdot H_2O$	74.29[4]
Cr-monosulphate	$3CaO \cdot Al_2O_3 \cdot CaSO_4 \cdot 15H_2O + 12\ H^+ \rightarrow 4\ Ca^{2+} + CrO_4^{2-} + 2\ Al^{3+} + 21 \cdot H_2O$	71.62[7]
$C_4FS'H_{12}$	$3CaO \cdot Fe_2O_3 \cdot CaSO_4 \cdot 12H_2O + 12\ H^+ \rightarrow 4\ Ca^{2+} + SO_4^{2}- + 2\ Fe^{3+} + 18 \cdot H_2O$	69.37[4]
$C_4AC'H_{11}$	$3CaO \cdot Al_2O_3 \cdot CaCO_3 \cdot 11H_2O + 12\ H^+ \rightarrow 4\ Ca^{2+} + CO_3^{2}- + 2\ Al^{3+} + 17 \cdot H_2O$	70.52[4]
$C_4FC'H_{11}$	$3CaO \cdot Fe_2O_3 \cdot CaCO_3 \cdot 11H_2O + 12\ H^+ \rightarrow 4\ Ca^{2+} + CO_3^{2}- + 2\ Fe^{3+} + 17 \cdot H_2O$	65.60[4]
$C_4AC'_{0.5}H_{12}$	$3CaO \cdot Al_2O_3 \cdot 0.5Ca(OH)_2 \cdot 0.5CaCO_3 \cdot 11.5H_2O + 13\ H^+ \rightarrow 4\ Ca^{2+} + 0.5\ CO_3^{2-} + 2\ Al^{3+} + 18.5 \cdot H_2O$	86.23[4]
$C_4FC'_{0.5}H_{12}$	$3CaO \cdot Fe_2O_3 \cdot 0.5Ca(OH)_2 \cdot 0.5CaCO_{30.5} \cdot 11.5H_2O + 13\ H^+ \rightarrow 4\ Ca^{2+} + 0.5\ CO_3^{2-} + 2\ Fe^{3+} + 18.5 \cdot H_2O$	85.63[4]
Fiedel's salt	$3CaO \cdot Al_2O_3 \cdot CaCl_2 \cdot 10H_2O + 12H^+ \rightarrow 4\ Ca^{2+} + 2\ Al^{3+} + 2Cl^- + 16 \cdot H_2O$	72.04[6]
Kuzel's salt	$3CaO \cdot Al_2O_3 \cdot 0.5CaCl_2 \cdot 0.5CaSO_4 \cdot 12H_2O + 12H^+ \rightarrow 4\ Ca^{2+} + 2\ Al^{3+} + Cl^- + 0.5\ SO_4^{2}- + 18 \cdot H_2O$	71.94[6]
AFt phases		
Cl-ettringite	$3CaO \cdot Al_2O_3 \cdot 3CaCl_2 \cdot 30H_2O + 12H^+ \rightarrow 6\ Ca^{2+} + 2\ Al^{3+} + 6\ Cl- + 36 \cdot H_2O$	56.84[6]
Cr-ettringite	$3CaO \cdot Al_2O_3 \cdot 3CaCrO_4 \cdot 32H_2O + 12\ H^+ \rightarrow 6\ Ca^{2+} + 2\ Al^{3+} + 3\ CrO_4^{2}- + 38 \cdot H_2O$	60.54[7]
Fe-ettringite	$3CaO \cdot Fe_2O_3 \cdot 3CaSO_4 \cdot 32H_2O + 12\ H^+ \rightarrow 6\ Ca^{2+} + 2\ Fe^{3+} + 3\ SO_4^{2}- + 38 \cdot H_2O$	51.98[4]
Tricarboaluminate	$3CaO \cdot Al_2O_3 \cdot 3CaCO_3 \cdot 32H_2O + 12\ H^+ \rightarrow 6\ Ca^{2+} + 2\ Al^{3+} + 3\ CO_3^{2}- + 38 \cdot H_2O$	60.69[4]
(Hydro)garnets		
C_3AS_3	$3CaO \cdot Al_2O_3 \cdot 3SiO_2 + 12\ H^+ \rightarrow 3\ Ca^{2+} + 2\ Al^{3+} + 3\ H_4SiO_4$	52.55[6]
C_3AH_6	$3CaO \cdot Al_2O_3 \cdot 6H_2O + 12\ H^+ \rightarrow 3\ Ca^{2+} + 2\ Al^{3+} + 12 \cdot H_2O$	79.53[4]
$C_3AS_{0.5}$	$3CaO \cdot Al_2O_3 \cdot 0.5SiO_2 \cdot 5H_2O + 12\ H^+ \rightarrow 3\ Ca^{2+} + 2\ Al^{3+} + 0.5\ H_4SiO_4 + 10\ H_2O$	74.12[6]
C_3ASH_4	$3CaO \cdot Al_2O_3 \cdot SiO_2 \cdot 4H_2O + 12\ H^+ \rightarrow 3\ Ca^{2+} + 2\ Al^{3+} + H_4SiO_4 + 8\ H_2O$	69.37[6]
C_3FH_6	$3CaO \cdot Fe_2O_3 \cdot 6H_2O + 12\ H^+ \rightarrow 3\ Ca^{2+} + 2\ Fe^{3+} + 12 \cdot H_2O$	74.61[4]
CAH_{10}		
CAH_{10}	$CaO \cdot Al_2O_3 \cdot 10H_2O + 8\ H^+ \rightarrow Ca^{2+} + Al^{3+} + 14 \cdot H_2O$	38.51[4]
Mg phases		
Hydrotalcite	$Mg_4Al_2(OH)_{14} \cdot 3H_2O + 14\ H^+ \rightarrow 2\ Al^{3+} + 4\ Mg^{2+} + 17 \cdot H_2O$	73.96[4]
CO_3-hydrotalcite	$Mg_4Al_2(OH)_{12} \cdot CO_3 \cdot 2H_2O + 12\ H^+ \rightarrow 4\ Mg^{2+} + CO_3^{2}- + 2\ Al^{3+}$	50.85[4]
Other phases		
Akermanite	$Ca_2MgSi_2O_7 + 6\ H^+ + H_2O \rightarrow 2\ Ca^{2+} + Mg^{2+} + 2 \cdot H_4SiO_4$	46.08[5]
Anorthite	$CaAl_2Si_2O_8 + 8\ H^+ \rightarrow Ca^{2+} + 2\ Al^{3+} + 2\ H_4SiO_4$	25.31[5]
CA	$CaO \cdot Al_2O_3 + 8\ H^+ \rightarrow Ca^{2+} + 2\ Al^{3+} + 4\ H_2O$	45.73[2]
CA_2	$CaO \cdot 2Al_2O_3 + 14\ H^+ \rightarrow Ca^{2+} + 4\ Al^{3+} + 7\ H_2O$	61.77[2]
C_2S	$2CaO \cdot SiO_2 + 4\ H^+ \rightarrow 2\ Ca^{2+} + H_4SiO_4$	38.82[2]
C_3S	$3CaO \cdot SiO_2 + 6\ H^+ \rightarrow 3\ Ca^{2+} + H_4SiO_4 + H_2O$	73.66[2]
C_3A	$3CaO \cdot Al_2O_3 + 12\ H^+ \rightarrow 2\ Al^{3+} + 3\ Ca^{2+} + 6\ H_2O$	113.05[6]
C_4AF	$4CaO \cdot Al_2O_3 \cdot Fe_2O_3 + 20\ H^+ \rightarrow 2\ Al^{3+} + 2\ Fe^{3+} + 4\ Ca^{2+} + 10\ H_2O$	140.51[6]
$C_{12}A_7$	$12CaO \cdot 7Al_2O_3 + 66\ H^+ \rightarrow 12\ Ca^{2+} + 14\ Al^{3+} + 33\ H_2O$	487.20[2]
Ca oxychloride	$3CaO \cdot CaCl_2 \cdot 16H_2O + 6\ H^+ \rightarrow 4\ Ca^{2+} + 2Cl- + 19\ H_2O$	68.75[6]
Ca zincate	$CaZn_2(OH)_6 \cdot 2H_2O + 6\ H^+ \rightarrow Ca^{2+} + 2\ Zn^{2+} + 8\ H_2O$	43.90[3]
Ca-zeolite P	$CaO \cdot Al_2O_3 \cdot 2.6SiO_2 \cdot 3.2H_2O + 8\ H^+ \rightarrow Ca^{2+} + 2\ Al^{3+} + 2.6\ H_4SiO_4 + 2\ H_2O$	20.20[6]
Chabazite	$CaAl_2Si_4O_{12} \cdot 6H_2O + 8\ H^+ \rightarrow Ca^{2+} + 2\ Al^{3+} + 4\ H_4SiO_4 + 2\ H_2O$	13.63[6]
Forsterite	$Mg_2SiO_4 + 4\ H^+ \rightarrow 2\ Mg^{2+} + H_4SiO_4$	28.60[5]
Gehlenite	$Ca_2Al(AlSi)O_7 + 10\ H^+ \rightarrow 2\ Ca^{2+} + 2\ Al^{3+} + H_4SiO_4 + 3\ H_2O$	55.23[5]
Leucite	$KAl(SiO_3)_2 + 2\ H_2O + 4\ H^+ \rightarrow K^+ + Al^{3+} + 2\ H_4SiO_4$	6.42[3]
Merwinite	$Ca_3Mg(SiO_4)_2 + 8\ H^+ \rightarrow 3\ Ca^{2+} + Mg^{2+} + 2\ H_4SiO_4$	69.28[5]
Na-zeolite P	$Na_2O \cdot Al_2O_3 \cdot 2.6SiO_2 \cdot 3.2H_2O + 8\ H^+ \rightarrow Ca^{2+} + 2\ Al^{3+} + 2.6\ H_4SiO_4 + 2\ H_2O$	26.40[6]
$ZnFe_2O_4$	$ZnFe_2O_4 + 8\ H^+ \rightarrow Zn^{2+} + 2\ Fe^{3+} + 4\ H_2O$	9.85[1]
$ZnSiO_3$	$ZnSiO_3 + H_2O + H^+ \rightarrow Zn^{2+} + H_4SiO_4$	2.93[3]
Wairakite	$Ca \cdot Al_2Si_4O_{12} \cdot 2H_2O + 2\ H_2O + 8\ H^+ \rightarrow Ca^{2+} + 2\ Al^{3+} + 4\ H_4SiO_4$	18.87[3]
Wollastonite	$CaSiO_3 + H_2O + H^+ \rightarrow Ca^{2+} + H_4SiO_4$	12.99[3]

1 Dijkstra et al. (2002); 2 US Department of Energy (2004); 3 Astrup et al. (2006); 4 Lothenbach and Winnefeld (2006); 5 Blanc et al. (2007); 6 Hills (2009); 7 Hyks et al. (2009).

Table 3
Chemical composition of the CF and FF of BA.

	Concentration (mg/kg) ± SD error (%)	
Element/anion	CF (%)	FF (%)
Al	59691 ± 8	44051 ± 6
As	2.1 ± 25	1.2 ± 26
Ca	248567 ± 9.0	272715 ± 11
Cd	25.2 ± 25	14.0 ± 25
Cr	478 ± 4	517 ± 4
Cu	6278 ± 21	6790 ± 18
Fe	18467 ± 16	17725 ± 19
K	5110 ± 11	4470 ± 5
Mg	18029 ± 9	17829 ± 6
Mn	488 ± 6	490 ± 4
Mo	12.8 ± 11	14.4 ± 14
Na	17851 ± 20	14695 ± 17
Ni	110 ± 21	152 ± 13
Pb	3064 ± 18	4235 ± 25
Sb	39.5 ± 25	34.8 ± 22
Si	104422 ± 21	66640 ± 25
Zn	2194 ± 17	1964 ± 13
Cl^-	22522 ± 5	17865 ± 7
SO_4^{2-}	11912 ± 8	10331 ± 1

and Day, 2000a). In the present study the best results, as indicated by the insert table in Fig. 2, were obtained for a 20% BA content at 2% $CaCl_2$ addition, with UCS values of 44.6, 43.3, 52.9 and 57.7 MPa after 7, 28, 56 and 90 days, as opposed to 42.0, 45.8, 44.9 and 51.1 MPa measured for the control sample; increasing the $CaCl_2$ addition from 2% to 4% appeared to exert a minor effect on strength improvement. When the BA addition was increased to 40%, mechanical strength was reduced only slightly below that of the control specimen.

Since $CaCl_2$ is known to produce a strength gain in cement and concrete mainly at the early hydration stages, being identified as a set accelerator (see e.g. Rosskopf et al., 1975), control samples containing only cement and $CaCl_2$ were used for comparison with the corresponding activated BA-containing mixtures in order to separate the effect of set acceleration by $CaCl_2$ from that of BA activation by the same species. From Fig. 3a the set acceleration effect exerted by $CaCl_2$ on cement is evident from the UCS values measured at 7- and 28-day curing, while the effect of $CaCl_2$ on BA activation can clearly be found for curing times >28 days. This is demonstrated by the strength gain observed at 56- and 90-day curing for BA-containing mixtures, which attained comparable UCS

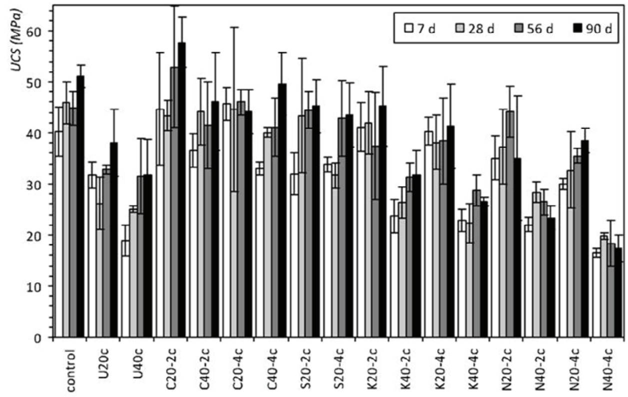

Fig. 1. UCS of mixtures containing the CF of BA.

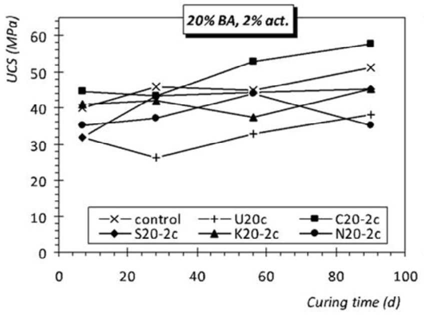

	Curing time (d)			
	7	28	56	90
control	40.2	45.8	44.9	51.2
U20c	31.8	26.2	32.9	38.1
C20-2c	**44.6**	**43.3**	**52.9**	**57.7**
S20-2c	31.9	43.3	44.4	45.2
K20-2c	41.2	41.9	37.4	45.2
N20-2c	35.0	37.2	44.1	35.0

Fig. 2. UCS as a function of curing time for mixtures containing 20% BA (CF) and 2% activator; the table highlights the highest strength values obtained at each curing time.

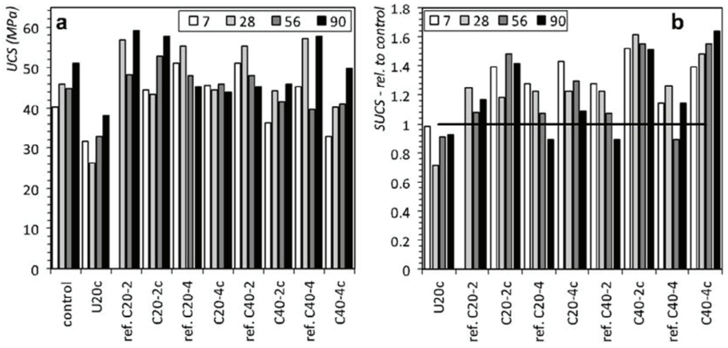

Fig. 3. Comparison of (a) UCS and (b) SUCS of mixtures containing $CaCl_2$ with or without BA addition.

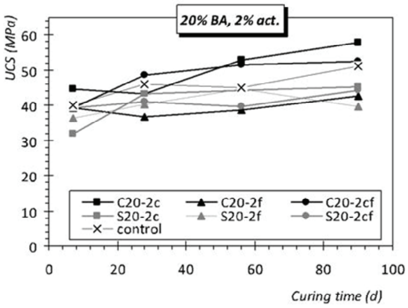

	Curing time (d)			
	7	28	56	90
control	40.2	45.8	44.9	51.2
C20-2c	**44.6**	**43.3**	**52.9**	**57.7**
C20-2f	39.4	36.8	38.8	42.6
C20-2cf	39.5	**48.5**	**51.7**	**52.7**
S20-2c	31.9	**43.3**	**44.4**	45.2
S20-2f	36.6	40.5	44.8	39.7
S20-2cf	39.5	40.9	39.7	44.2

Fig. 4. Comparison of UCS of mixtures containing different activated size fractions of BA.

values to the corresponding reference mixtures, which yet had 20% higher cement content. On account of this issue, the mechanical strength results may be more conveniently interpreted in terms of specific UCS (SUCS) as proposed by Pu (1999), which is calculated as the ratio between the UCS of a given mixture and its cement content. Assuming that in the presence of admixtures mechanical strength is given by two distinct contributions – one from the hydration phases of cement and the other from the additional solid phases formed by the admixtures – the SUCS of the control can be regarded as the contribution of 1% cement to mechanical strength; any SUCS value higher than that of the control thus indicates further contribution of the material to mechanical resistance. From Fig. 3b it is evident that the mixtures containing activated BA displayed higher SUCS values than the corresponding reference mixtures, which in turn displayed higher SUCS values than the control. This indicates that $CaCl_2$ is capable of promoting the mechanical strength development, especially at the early stages of hydration, due to its set acceleration properties; however, a positive contribution of activated BA to the strength of the mixtures is still evident, which proofs the additional effect of $CaCl_2$ on the hydration behavior of BA-containing samples.

As for the other activators, there was still a positive effect on mechanical strength compared to the un-activated material, although this was less pronounced. The two activators $CaSO_4$ and

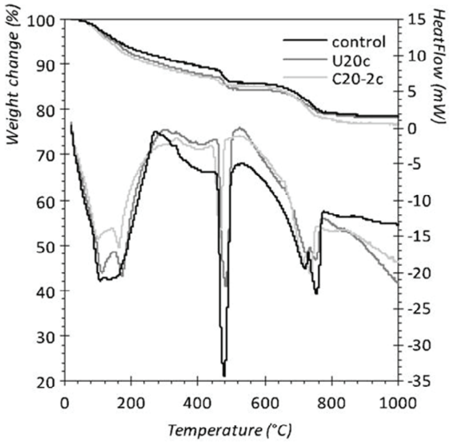

Fig. 5. TGA/DSC measurements of selected mixtures.

KOH affected similarly the mechanical properties of the material. As reported in Fig. 2, $CaSO_4$ and KOH produced strength values in the ranges 31.9–45.2 and 37.4–45.2 MPa, respectively. The positive effect of $CaSO_4$ when this is used as an activator is known to be associated to the enhanced formation of calcium sulfoaluminate-ferrite (tri-substituted) hydrates (or AFt) (Shi and Day, 2000b). The mechanical properties were worsened when NaOH was added to the mixtures, showing that this species was not suited to significantly contribute to strength development, irrespective of the amount of both BA and activator added to the mixtures. The negative effect of NaOH on strength development is believed to be associated to either the higher alkalinity induced in comparison to KOH at the same weight addition, or by an excess of sodium in the pore solution which modified the precipitation equilibria of the main hydration phases.

On the other hand, for all the activators tested, an increase in the BA content of the mixtures from 20 to 40% was observed to considerably decrease mechanical strength. From the statistical analysis of UCS values reported in a previous work (Onori et al., 2009), an increase in the activators dosage at any of the investigated curing times was also generally found to produce only a minor effect on mechanical strength, indicating the BA content as the main factor affecting the mechanical properties of the hardened materials.

The UCS evolution as a function of curing time for mixtures containing 20% of the coarse BA fraction and 2% activator is reported in Fig. 2. It is evident that, in addition to producing higher mechanical strengths, $CaCl_2$ was also shown to exhibit a higher strength gain with time in comparison to all the other mixtures tested, including the control one. Furthermore, $CaSO_4$ and KOH yielded UCS values comparable to that of the control mixture up to 28-day curing, while the residual gain in mechanical strength upon prolonged curing was lower than that of the pure OPC specimen.

A comparison between the mechanical properties of mixtures containing different size fractions of BA is given in Fig. 4, which also reports the numerical UCS data highlighting the best values obtained. For the mixtures activated by $CaCl_2$, the fine fraction of the material exhibited lower UCS values than the coarse class, due to its lower content of alumino-silicate minerals as evidenced by the elemental composition (see Table 3). The strength values of mixtures containing the coarse BA fraction were found to be 12–26% higher (depending on curing time) than the corresponding values obtained using fine fraction. The mixtures containing the fine fraction displayed mechanical strength values well below that of the control mixture, even upon chemical activation. When the two size fractions of $CaCl_2$-activated BA were blended together in the cementitious mixtures, the mechanical behavior was quite similar to that displayed by the coarse material, obviously due to the prevalence of this in the raw BA. When $CaSO_4$ was used as the activator, the strength data for the mixtures containing the coarse or the fine BA fraction were more comparable.

The TGA/DSC patterns for the control, U20c and C20–2c mixtures at 28-day curing are reported in Fig. 5. In the TGA patterns, five main regions can be identified on the basis of the characteristic temperature range (see e.g. Alarcon-Ruiz et al., 2005): (1) 20–105 °C, corresponding to the loss of the evaporable and part of the (physically) bound water (Bazant and Kaplan, 1996); (2) 110–170 °C, due to the dehydration of gypsum (displaying a double endothermic peak associated to the subsequent loss of the two water molecules), ettringite and part of the carboaluminate hydrates; (3) 180–300 °C, related to the dehydration of C–S–H and carboaluminate phases; (4) 450–550 °C, associated to the decomposition of portlandite ($Ca(OH)_2$); and (5) 700–900 °C, corresponding to the loss of CO_2 from carbonates.

On the basis of the experimental results depicted in Fig. 5, the weight loss associated to the portlandite peak corresponded to a $Ca(OH)_2$ content of 11.5, 10.9 and 6.2 wt.% for the control, U20c and C20–2c mixtures, respectively, which were then corrected to account for the carbonate content in the materials, yielding values of 22.3, 18.5 and 16.0 wt.%. The difference in the portlandite content between the control and the un-activated BA mixture suggests that BA addition to cement produced merely a dilution effect of the hydrate system. When $CaCl_2$ was used as the activator, the portlandite content was found to decrease further, however, given the observed accompanied improvement in mechanical strength (see above), this may be interpreted as a positive influence of chemical activation on the hydration reactions. In other terms, the lower amount of portlandite measured in the mixture where $CaCl_2$ was added, along with its improved mechanical properties, may suggest an effect of activation by $CaCl_2$ upon the development of pozzolanic reactions within the cementitious system.

The total weight loss (excluding the loss of free water) recorded in the TGA measurements for the control, U20c and C20–2c samples (19.1, 19.4 and 20.4 wt.%, respectively) seems to confirm a slight increase in the total amount of hydration phases in the presence of $CaCl_2$.

3.3. Acid neutralization behavior and leaching properties of bottom ash–cement blends

Fig. 6 compares the titration curves obtained for the $CaCl_2$-containing samples at 28 and 56 days. The acid neutralization capacity

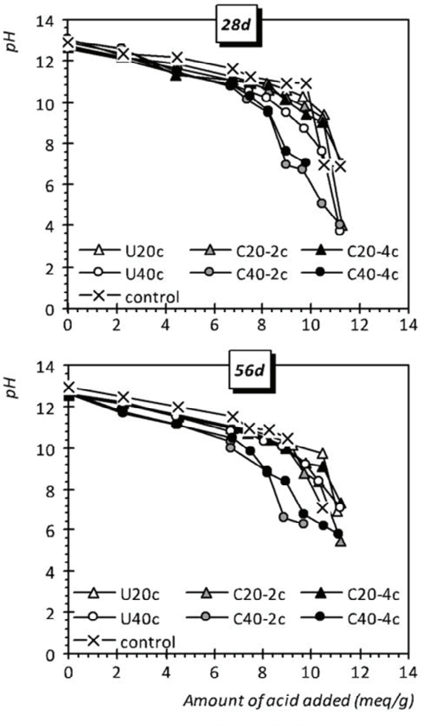

Fig. 6. ANC curves for $CaCl_2$-containing mixtures.

is a key property of cement/waste systems, since the resistance to acid attack may affect the durability and in turn the leaching behavior of such materials, both because the solubility of contaminants is pH-dependent and because the solid matrix integrity depends on the ability to maintain alkaline conditions (Giampaolo et al., 2002). The analysis of the ANC curve of cementitious materials can also provide information on phase composition and contaminant immobilization mechanisms, since, on the basis of the position and width of the observed pH plateaus, it is possible to infer on the presence and amount of solid phases that are stable under specific pH conditions (Glass and Buenfeld, 1999).

The acid neutralization capacity of the tested mixtures was observed to decrease with the BA content, as indicated by the increasing slope of the titration curves. Below pH 10 the addition of $CaCl_2$ was also found to reduce the buffering capacity of the material, and this effect became more appreciable at a 40% BA dosage.

Figs. 7 and 8 report the experimental leaching data for Ca, Si and SO_4^{2-} as obtained from the ANC leaching test on the reference mixtures and the C20–2c sample at curing times of 7 and 56 days; the theoretical curves of the solubility-controlling minerals identified on the basis of geochemical modeling results are also reported. Modeling calculations were conducted to gain a better insight into the evolution of the hydration process of OPC in the presence of BA and the activator and derive information on the mechanisms governing the leaching of major elements and trace metals from the solid matrices. The behavior of the major solid matrix constituents is deemed particularly important to understand the mechanisms of trace contaminant release from the material, since major phases are able to control the leachate pH (which is a key parameter for metal leaching) and to interact with trace elements through several mechanisms including co-precipitation, incorporation, sorption, ion exchange and others.

In general, depending on the nature of the mixture tested, different hydration phases were found to control the solubility of major elements/species. For the control sample, at early curing (7 days) at pH < 11 two AFm phases including gehlenite hydrate ([Gh], also known as strätlingite, having the composition $2CaO{\cdot}Al_2O_3{\cdot}SiO_2{\cdot}8H_2O$, or C_2ASH_8 in the cement chemistry notation) and $3CaO{\cdot}Fe_2O_3{\cdot}(CaSO_4){\cdot}12H_2O$ ($C_4F\overline{S}H_{12}$) were found to describe the leaching of Ca; such two phases also appeared to govern the leaching of, respectively, Si and sulphate in the same pH range. At more alkaline pH values (12–13), the only phase which could explain the release of Ca as well as Si was C–S–H with a Ca/Si ratio of 0.5 [CSH-l]. The occurrence of C–S–H phases with

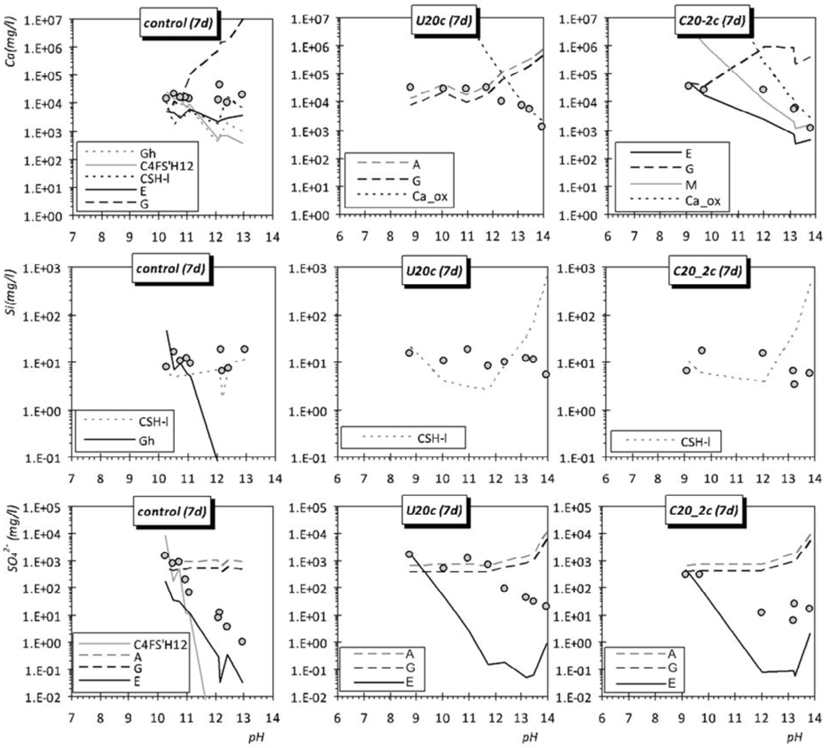

Fig. 7. Results of geochemical modeling for Ca, Si and SO_4^{2-} for the control, U20c and C20–2c mixtures at 7-day curing (A: anhydrite; Ca_ox: Ca oxychloride; $C_4FS'H_{12}$: tetracalcium sulfoferrite hydrate; CSH-l: C–S–H (Ca/Si = 0.5); CSH-m: C–S–H (Ca/Si = 0.8); E: ettringite; G: gypsum; M: monosulphate).

low Ca/Si ratios as potential solubility-controlling minerals may be explained on account that, due to the large solubility of portlandite in water, even from Ca-rich solutions the equilibrium precipitate has been reported to be always low in Ca/Si ratio (Kersten, 1996). It is thus still possible that, although not apparent from the analysis of the ANC eluates, other calcium silicate hydrate phases with higher Ca/Si ratios were actually present in the solid material. In the control sample at early curing the leaching solutions were calculated to be oversaturated by ~1 order of magnitude with respect to ettringite ([E], having the chemical composition $Ca_6Al_2(SO_4)_3(OH)_{12}\cdot 26H_2O$), although the shape of the theoretical solubility curve for this phase was very similar to the experimental leaching curve.

At longer curing times (56 days) Ca leaching from the control mixture was comparably well described by both ettringite and gehlenite hydrate [Gh] at pHs in the range 10–12. Ettringite [E] was also a good candidate for solubility control of sulphate within the same pH range. Ca leaching at pH > 12 appeared to be better controlled by two AFm phases including monosulphate ([M], $Ca_4Al_2(SO_4)(OH)_{12}\cdot 6H_2O$ or $C_4A\overline{S}H_{12}$, which also showed a good fit with sulphate concentration data within the same pH range) and Cr-monosulphate ([MCr], $Ca_4Al_2(CrO_4)(OH)_{12}\cdot 9H_2O$). The appearance of Cr-monosulphate [MCr] as a potential solubility-controlling mineral for both Ca and Cr may well explain the incorporation of Cr within the hydration products of Portland cement as the hydration proceeded, with an associated decrease in the release levels as indicated by the corresponding leaching curves (see Fig. 9 below). The fit between Si leaching data from the control mixture and the theoretical solubility curves of the above mentioned phases was relatively poor. Only gehlenite hydrate [Gh] in a limited pH interval (10.5–11.5) appeared to somehow describe the experimental data, while Ca/Si = 0.5 C–S–H [CSH-I], which gave a good fit with the measured Ca concentrations (see above), was not found to adequately explain the leaching behavior of Si.

As far as the reference mixture containing un-activated BA (U20c) was concerned, at 7-day curing either anhydrite [A] or gypsum [G] were identified as potential solubility-controlling minerals for both Ca and sulphate in the pH range 8.5–11.5. In the alkaline range (pH > 12), while the leaching of Ca was described by Ca oxychloride ([Ca_ox], $3CaO\cdot CaCl_2\cdot 15H_2O$), no solubility-controlling minerals could be identified for sulphate, with eluates being oversaturated by 1–2 orders of magnitude with respect to both ettringite and monosulphate. It is tempting to hypothesize that the absence of such sulphate-bearing phases in the U20c sample indicates a delay in the hydration process of cement when un-activated BA was added to the mixture. In the case of Si, again Ca/

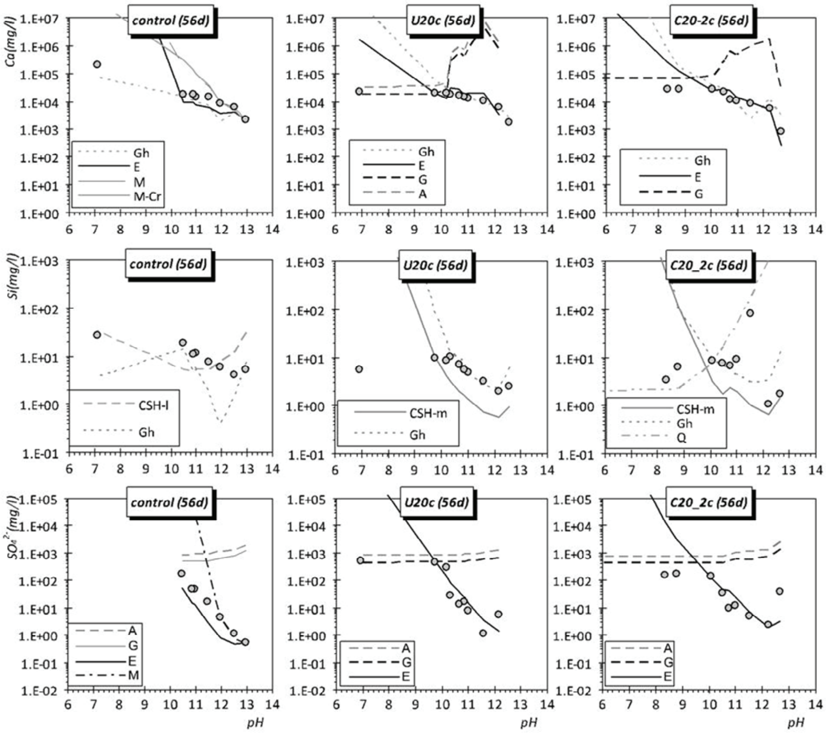

Fig. 8. Results of geochemical modeling for Ca, Si and SO_4^{2-} for the control, U20c and C20-2c mixtures at 56-day curing (A: anhydrite; CSH-l: C–S–H (Ca/Si = 0.5); CSH-m: C–S–H (Ca/Si = 0.8); E: ettringite; G: gypsum; Gh: gehlenite hydrate; M: monosulphate; MCr: Cr-Monosulphate; Q: quartz).

Si = 0.5 C–S–H [CSH-l] was identified as the potential leaching-controlling mineral below pH 12.5, while no suitable phases were found to describe Si leaching at higher pH levels.

At 56-day curing ettringite appeared to be a good candidate for solubility control for both Ca and sulphate at pH values in the range 9.5–12, although approximately in the same pH interval (10–13) ghelenite hydrate [Gh] was also found to display a good match with Ca and Si leaching data. At pH values below ∼9.5, when ettringite [E] becomes unstable as widely reported in the literature (Damidot and Glasser, 1992, 1993; Perkins and Palmer, 1999), gypsum [G] appeared to control Ca and sulphate leaching from the material.

When $CaCl_2$-activated BA was added to cement (specimen C20–2c), at 7-day curing gypsum at pH < 9 was found to be the most probable candidate for solubility control of both Ca and sulphate. In the case of Ca, monosulphate [M] and Ca oxychloride [Ca_ox]

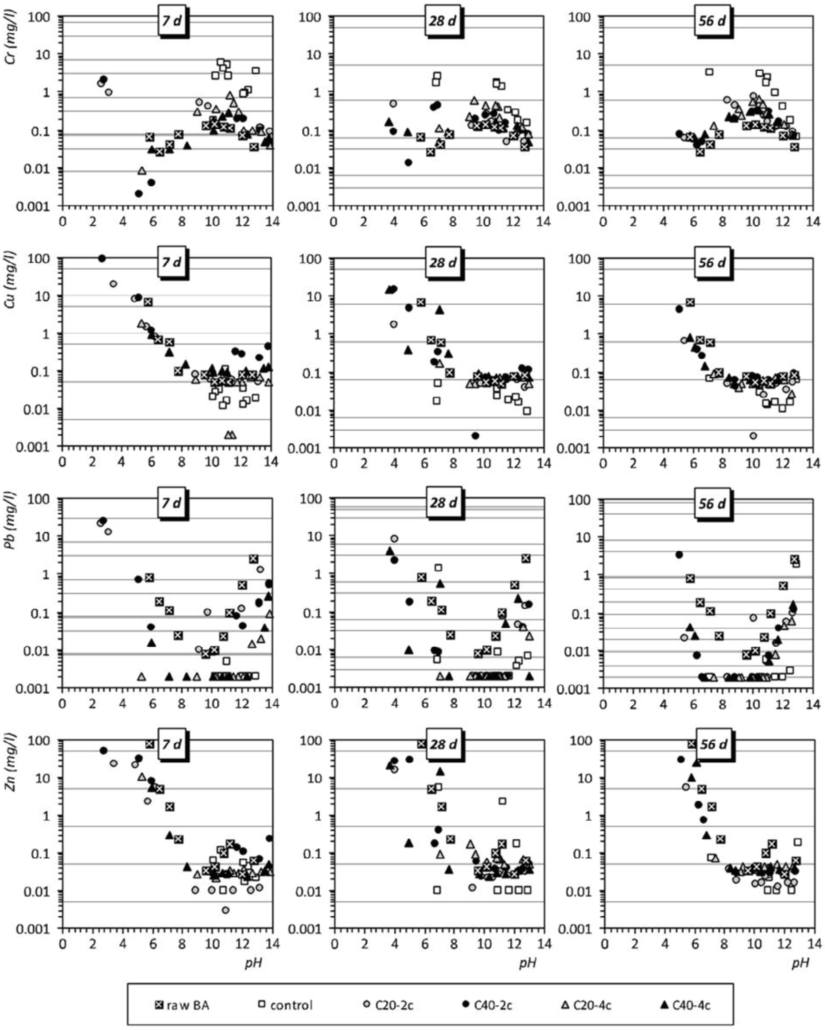

Fig. 9. Metal leaching as a function of pH in the ANC test for reference and $CaCl_2$-containing mixtures.

were also identified as solubility-controlling solids in the pH ranges 12–13.8 and 13–13.8, respectively. On the other hand, in the alkaline range (pH > 9) sulphate concentrations in the leaching solutions always showed oversaturation with respect to ettringite [E] by about 2 orders of magnitude, and no mineral was found suitable to explain the release of sulphate from the hardened material. As mentioned above for the sample containing un-activated BA, the only mineral describing Si leaching (although again with relatively poor fitting of the measured data) was Ca/Si = 0.5 C–S–H [CSH-l] at pH < 10, while at higher pH values none of the phases included in the expanded thermodynamic database was capable of matching the experimental leaching curves.

Upon prolonged curing (56 days), the minerals responsible for solubility control of the major elements/species were found to change. Again, at pH < 9 gypsum [G] was selected as the leaching-controlling mineral for both Ca and sulphate; on the other hand, ettringite [E] appeared to be the best candidate for solubility control at pH > 10 for both species, with a very good fit with the measured concentrations. It should also be mentioned that at the same pH values ghelenite hydrate [Gh] appeared to adequately describe the release of Ca as well, along with that of Si. In other pH ranges, the dissolution of this element was found to be dictated by quartz [Q] (pH < 9) and Ca/Si = 0.8 C–S–H [CSH-m] (pH = 12–13).

The results from the ANC leaching test at natural pH (sub-sample without acid addition) for the trace metals Cd, Cr, Cu, Ni, Pb and Zn are compared in Table 4 with the European regulatory limits for inert waste landfills (EU Council Directive 99/31/EC, 1999) and with the limits established by the Italian law for waste utilization (annex 3 D.M. 05/02/1998, Ministero dell'Ambiente della Repubblica Italiana, 1998). Other trace elements of environmental concern, including the oxyanion-forming elements As, Mo, Sb and V, were not analyzed since for the raw BA either their total content or the leaching levels were below the detection limits. In general, as discussed below in more detail, the leachate concentrations for the investigated heavy metals were found to decrease, in some cases appreciably, with curing, indicating a progressive immobilization with time. According to the values presented in Table 4, it is also clear that the critical elements for the materials under concern include Cr and Pb. As evident from the leaching curves as a function of pH presented below (see Fig. 9), the high leaching levels measured for Cr are clearly caused by the contribution of the cement used, with the control specimen releasing more than 35 mg Cr/kg at 7-day curing; the presence of BA and $CaCl_2$ decreased the leaching level for this metal, however for the majority of the samples tested the Cr concentration in the leaching solutions exceeded the regulatory threshold limits. This result claims for a very careful control of the chemical composition of the raw materials used for cement production, as this can negatively affect the environmental behavior of the hardened products obtained, even when they do not include waste materials as admixtures. As for Pb, notwithstanding the significant decrease in leaching observed in comparison to the raw BA, the release was often above the regulatory limits due to the typical strongly amphoteric behavior of this metal. The leaching levels were also found to benefit from prolonged curing, although with some fluctuations likely due to changes in the pH of the leaching solutions; the best results in terms of Pb release were obtained for the C20–2c specimen after 90 days of curing, with a leachate concentration well below the limits established for both disposal in inert waste landfills and utilization.

The results of the ANC leaching test in terms of trace metal leaching as a function of pH are depicted in Fig. 9 for the control mixture and those containing $CaCl_2$-activated BA (coarse fraction) and compared to the corresponding leaching data obtained for the raw BA sample. Blending BA with cement produced largely different effects on the leaching behavior depending on the trace metal under concern. Apart from the ranges in which the measured concentrations were already below the analytical detection limit, the leaching levels obtained appeared to be positively affected by curing time; when this was increased from 7 to 56 days, the leaching of Cu, Pb and Zn was observed to decrease (although the reduction was not particularly pronounced), indicating a progressive immobilization of metals within the hydrated matrix. Metal leaching as a function of pH showed no large differences between the different mixtures investigated. However, as also observed for mechanical strength, $CaCl_2$ addition at a 20% BA content gave the best results, especially upon prolonged curing.

Among the trace metals of interest, Cr was observed to be released to an appreciably higher degree by the control mixture than by the samples containing BA, due to the contribution of OPC itself. Cr in the control mixture was however found to get progressively more immobilized with curing time, likely due to the incorporation

Table 4

Comparison between leaching test results (natural pH) and regulatory limits for selected heavy metals (bold and underlined values denoting concentrations exceeding the Landfill Directive or Italian regulation limits, respectively).

Concentration (mg/l)							
Element	pH	Cd	Cr	Cu	Ni	Pb	Zn
Untreated	12.71	<0.0005	0.04	0.08	0.0034	**2.52**	0.06
Control (7d)	12.95	<0.0005	**3.520**	0.018	<0.002	<0.002	0.022
Control (28d)	12.92	0.0009	**0.151**	0.009	<0.002	0.007	<0.01
Control (56d)	12.95	0.0008	**0.065**	0.061	0.002	**1.900**	0.179
C20–2c (7d)	13.80	<0.0005	**0.090**	**0.390**	0.060	**0.540**	0.150
C20–2c (28d)	12.74	<0.0005	0.050	0.040	0.060	**0.140**	0.032
C20–2c (56d)	12.66	0.0005	**0.090**	0.054	0.013	**0.100**	0.016
C20–2c (90d)	12.42	<0.0005	**0.060**	0.041	0.033	0.005	0.021
C20–4c (7d)	13.80	<0.0005	0.040	0.050	0.060	**0.090**	0.031
C20–4c (28d)	13.01	<0.0005	**0.080**	0.050	0.004	0.023	0.050
C20–4c (56d)	12.58	**0.0111**	**0.080**	0.027	0.050	**0.061**	0.045
C40–2c (7d)	13.82	<0.0005	0.050	**0.430**	0.004	**0.500**	0.225
C40–2c (28d)	13.01	**0.005**	**0.080**	0.110	0.004	**0.150**	0.051
C40–2c (56d)	12.71	<0.0005	**0.070**	0.090	<0.002	**0.120**	0.031
C40–2c (90d)	12.37	<0.0005	**0.120**	0.140	2.300	**0.270**	0.025
C40–4c (7d)	13.79	<0.0005	**0.060**	0.130	<0.002	**0.270**	0.052
C40–4c (28d)	13.03	<0.0005	0.050	0.070	0.003	<0.002	0.038
C40–4c (56d)	12.65	<0.0005	**0.070**	0.090	0.050	**0.160**	0.041
EU LD (inert waste)		0.004	0.05	0.20	–	0.05	0.40
DM 05/02/1998 (reuse)	5.5–12.0	0.005	0.05	0.05	0.01	0.05	3.00
Detection limit (mg/l)		0.0005	0.0004	0.0002	0.0002	0.0002	0.01

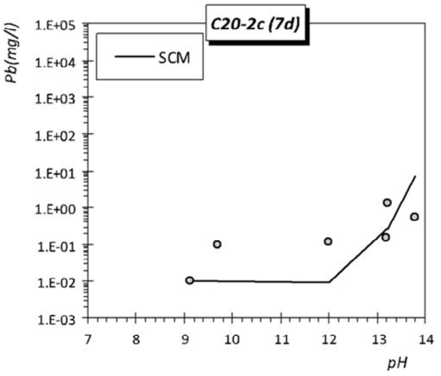

Fig. 10. Results of geochemical modeling of Pb leaching on account of surface complexation by HFO and AAM (SCM = surface complexation model).

in the hydration phases as indicated by the results from geochemical modeling discussed above. At all ages, an addition of 4% $CaCl_2$ was also observed to exert a more positive effect on Cr leaching in comparison to the 2% dosage.

For both Cu and Pb, the control sample displayed appreciably lower release levels at all pHs since early hydration, however the differences in leaching with the BA-containing mixtures became fairly less evident as curing progressed, with a similar behavior being observed for Zn as well.

The results of geochemical modeling for the investigated trace metals showed that it was not possible to identify common secondary minerals including metal (hydr)oxides, carbonates and sulphates as potential solubility-controlling solids, with leaching solutions being always undersaturated in respect to such phases. This is the reason why the modeling predictions were not shown in Fig. 9. When surface complexation was accounted for in the modeling calculations, the results showed reliable predictions only in the case of Pb (see Fig. 10 as an example of the results obtained for specimen C20–2c), which was found to be largely bound to HFO and AAM species in all samples tested (>95% of total leachable Pb, except at pH > 13.5 where the predominantly anionic speciation of Pb in solution likely reduced the amount sorbed). Surface complexation by Fe and Al minerals was thus likely the reason for the strong reduction in Pb leaching within the whole pH range investigated as compared to the raw BA sample. For the other trace metals of concern, the surface complexation model was not able to adequately predict the observed leaching levels, so that the solution concentrations were always strongly overestimated. Clearly, the difference between the observed and model-predicted leachate concentrations is caused by the role played by additional mechanisms (not accounted for in the model) in the immobilization of trace metals within the investigated materials. This is believed to be related to the presence of trace metals as complex minerals or phase assemblages which can hardly be described in a univocal manner from the viewpoint of both chemical composition and thermodynamic data.

4. Conclusions

The results of the present study showed that the positive effect of a number of chemical activators (particularly $CaCl_2$ and to some extent $CaSO_4$) on the development of mechanical properties of blended systems containing incinerator BA and Portland cement. $CaCl_2$ was found to be the most effective activator, being able to increase UCS above that of Portland cement. On the basis of TGA analyses, the effect of $CaCl_2$ appeared to promoting the onset of pozzolanic reactions in the cementitious mixtures, with an increase in the total amount of hydration phases present.

The environmental performance of the material was also evaluated through leach testing, which showed that metal leaching was reduced upon curing if compared to the raw BA, indicating a progressive immobilization of trace metals with time by the hydrate system, although the observed differences in leaching levels were not pronounced. For the mixture giving the best results in terms of mechanical behavior (which contained 20% of BA activated with 2% $CaCl_2$), after 90 days of curing metal leaching at the natural pH of the material was below the regulatory limits established by the Italian law for utilization; Cr was the only exception, with a release into the leaching solution slightly above the corresponding threshold value, which was attributed to a large extent to the contribution of cement.

The theoretical description of the composition of the hydrated materials, gained though geochemical modeling of the leaching solutions, indicated the formation of different hydration phases when BA was added to Portland cement. In the case of un-activated BA, the analysis of the modeling results indicated a possible delay in the hydration process in comparison to the normal evolution of pure OPC systems. The modeling results for trace metal leaching indicated a very strong contribution of surface complexation by Fe and Al minerals in the case of Pb, while poor prediction of the actual leaching behavior for the other trace metals investigated. This was likely related to the complex mineral forms in which trace metals were present in the original material, with association to solid phases for which a chemical and thermodynamic description is not currently available.

References

Alarcon-Ruiz, L., Platret, G., Massieu, E., Ehrlacher, A., 2005. The use of thermal analysis in affecting the effect of temperature on a cement paste. Cement Concrete Res. 35, 609–613.

Astrup, T., Dijkstra, J., Comans, R.N.J., van der Sloot, H.A., Christensen, T.H., 2006. Geochemical modelling of leaching from MSWI air-pollution-control residues. Environ. Sci. Technol. 40, 3551–3557.

Astrup, T., Lechner, P., Polettini, A., Pomi, R., Van Gerven, T., van Zomeren, A., 2007. State-of-the-art and outlook on management of waste-to-energy bottom ashes. Part 2: utilization. In: Margherita di Pula, S. (Ed.), Proc. Sardinia 2007, Eleventh International Waste Management and Landfill Symposium, CA, 1–5 October 2007, Session A13 (on CD ROM).

Bazant, Z.P., Kaplan, M.F., 1996. Concrete at High Temperatures. Longman, London.

Blanc, P., Lassin, A., Nowak, C., Burnol, A., Piantone, P., Chateau, L., 2007. THERMODDEM: A Thermodynamic Database for Waste Materials. <http://thermoddem.brgm.fr/fichiers/Phreeqc_thermoddem_lvl1_no-org.txt>.

Clozel-Leloup, B., Bodénan, F., Piantone, P., 1999. Bottom ash from municipal solid waste incineration: mineralogy and distribution of metals. In: Mehu J., Keck G., Navarro A. (Eds.). Proc. STAB & ENV 99, International Conference on Waste Stabilization and Environment. Lyone Villeurbanne, France, pp. 46–51.

Council Directive 99/31/EC, 1999. Landfill of Waste. Official Journal L 182, 16/07/1999, pp. 0001–0019.

Damidot, D., Glasser, F.P., 1992. Thermodynamic investigation of the $CaO–Al_2O_3–CaSO_4–H_2O$ system at 50 C and 85 °C. Cement Concrete Res. 22, 1179–1191.

Damidot, D., Glasser, F.P., 1993. Thermodynamic investigation of the $CaO–Al_2O_3–CaSO_4–H_2O$ system at 25 °C and the influence of Na_2O. Cement Concrete Res. 23, 221–238.

Dijkstra, J.J., van der Sloot, H.A., Comans, R.N.J., 2002. Process identification and model development of contaminant transport in MSWI bottom ash. Waste Manage. 22, 531–541.

Dzombak, D.A., Morel, F.M.M., 1990. Surface Complexation Modeling: Hydrous Ferric Oxide. John Wiley and Sons, Inc., New York.

Eighmy, T.T., Eusden, J.D., Marsella, K., Hogan, J., Domingo, D., Krzanowski, J.E., Stämpfli, D., 1994. Particle petrogenesis and speciation of elements in MSW incineration bottom ashes. In: Goumans, J.J.J.M., van der Sloot, H.A., Aalbers, Th.G. (Eds.), Waste Materials in Construction. Elsevier Science Publication B.V., Amsterdam, pp. 111–136.

Engelsen, C.J., van der Sloot, H.A., Wibetoe, G., Petkovic, G., 2009. Release of major elements from recycled concrete aggregates and geochemical modeling. Cement Concrete Res. 39, 446–459.

Eusden, J.D., Eighmy, T.T., Hockert, K., Holland, E., Marsella, E., 1999. Petrogenesis of municipal solid waste combustion bottom ash. Appl. Geochem. 14, 1073–1091.

Fan, Y., Yin, S., Wen, Z., Zhong, J., 1999. Activation of fly ash and its effects on cement properties. Cement Concrete Res. 29, 467–472.

Filipponi, P., Polettini, A., Pomi, R., Sirini, P., 2003. Physical and mechanical properties of incineration bottom ash-based cements. Waste Manage. 23, 145–156.

Giampaolo, C., Lo Mastro, S., Polettini, A., Pomi, R., Sirini, P., 2002. Acid neutralisation capacity and hydration behaviour of incineration bottom ash–Portland cement mixtures. Cement Concrete Res. 32, 769–775.

Giergiczny, Z., 2004. Effect of some additives on the reactions of the reactions in fly ash–$Ca(OH)_2$ system. J. Therm. Anal. Calorim. 76, 747–754.

Ginés, O., Chimenos, J.M., Vizcarro, A., Formosa, J., Rosell, J.R., 2009. Combined use of MSWI bottom ash and fly ash as aggregate in concrete formulation: environmental and mechanical considerations. J. Hazard. Mater. 169, 643–650.

Glass, G.K., Buenfeld, N.R., 1999. Differential acid neutralization analysis. Cem. Concr. Res. 10, 1681–1684.

Hills, C.D., 2009. Personal Communication. University of Greenwich.

Hyks, J., Astrup, T., Christensen, T.H., 2009. Long-term leaching from MSWI air pollution control residues: leaching characterization and modeling. J. Hazard. Mater. 162, 80–91.

IAWG (International Ash Working Group), 1997. In: Chandler, A.J., Eighmy, T.T., Hartlén, J., Hjelmar, O., Kosson, D., Sawell, S.E., van der Sloot, H.A., Vehlow, J. (Eds.), Municipal Solid Waste Incinerator Residues, Studies in Environmental Sciences 67. Elsevier Sci., Amsterdam, 1997.

Kersten, M., 1996. Aqueous solubility diagrams for cementitious waste stabilization systems. 1. The C–S–H solid–solution system. Environ. Sci. Technol. 30, 2286–2293.

Lothenbach, B., Winnefeld, F., 2006. Thermodynamic modeling of the hydration of Portland cement. Cement Concrete Res. 36, 209–226.

Martens, E., Jacques, D., Van Gerven, T., Wang, L., Mallants, D., 2010. Geochemical modeling of leaching of Ca, Mg, Al, and Pb from cementitious waste forms. Cement Concrete Res., in press, doi:10.1016/j.cemconres.2010.01.007.

Meima, J.A., Comans, R.N.J., 1997. Geochemical modeling of weathering reactions in municipal solid waste incinerator bottom ash. Environ. Sci. Technol. 31, 1269–1276.

Meima, J.A., Comans, R.N.J., 1998. Application of surface complexation/precipitation modeling to contaminant leaching from weathered municipal solid waste incinerator bottom ash. Environ. Sci. Technol. 32, 688–693.

Meima, J.A., Comans, R.N.J., 1999. The leaching of trace elements from municipal solid waste incinerator bottom ash at different stages of weathering. Appl. Geochem. 14, 159–171.

Ministero dell'Ambiente della Repubblica Italiana, 1998. D.M. 05/02/1998. Individuazione dei rifiuti non pericolosi sottoposti alle procedure semplificate di recupero ai sensi degli articoli 31 e 33 del decreto legislativo 5 febbraio 1997, n. 22. Suppl. Ord. G.U. 16/04/1998 n. 88 (as amended by D.M. 05/04/2006, n. 186).

Onori, R., Polettini, A., Pomi, R., 2009. An investigation of RDF bottom ash activation for blended cement formulation. In: Méhu, J., Goumans, J.J.J.M., Heynen, J.J.M. (Eds.), Proc. WASCON 2009, International Conference on Sustainable Management of Waste and Recycled Materials in Construction. Lyon, FR, 3–5 October 2009.

Pacewska, B., Wilinska, I., Blonkowski, G., 2008. Investigations of cement early hydration in the presence of chemically activated fly ash. J. Therm. Anal. Calorim. 93, 769–776.

Pecqueur, G., Crignon, C., Quénée, B., 2001. Behaviour of cement-treated MSWI bottom ash. Waste Manage. 21, 229–233.

Pera, J., Coutaz, L., Ambroise, J., Chababbet, M., 1997. Use of incinerator bottom ash in concrete. Cement Concrete Res. 27, 1–5.

Perkins, R.B., Palmer, C.D., 1999. Solubility of ettringite $Ca_6[Al(OH)_6]_2(SO_4)_3{\cdot}26H_2O$ at 5–75 °C. Geochim. Cosmochim. Ac. 63, 1969–1980.

Polettini, A., Pomi, R., Carcani, G., 2005. The effect of Na and Ca salts on MSWI bottom ash activation for reuse as a pozzolanic admixture. Resour. Conserv. Recy. 43, 404–418.

Polettini, A., Pomi, R., Fortuna, E., 2009. Chemical activation in view of MSWI bottom ash recycling in cement-based systems. J. Hazard. Mater. 162, 1292–1299.

Poon, C.S., Qiao, X.C., Lin, Z.S., 2003. Pozzolanic properties of reject fly ash in blended cement pastes. Cement Concrete Res. 33, 1857–1865.

Pu, X., 1999. Investigation on pozzolanic effect of mineral additives in cement and concrete by specific strength index. Cement Concrete Res. 29, 951–955.

Qian, J., Shi, C., Wang, Z., 2001. Activation of blended cements containing fly ash. Cement Concrete Res. 31, 1121–1127.

Qiao, X.C., Tyrer, M., Poon, C.S., Cheeseman, C.R., 2008. Novel cementitious materials produced from incinerator bottom ash. Resour. Conserv. Recy. 52, 496–510.

Qiao, X.C., Cheeseman, C.R., Poon, C.S., 2009. Influences of chemical activators on incinerator bottom ash. Waste Manage. 29, 544–549.

Rosskopf, P.A., Linton, F.J., Peppler, R.B., 1975. Effect of various accelerating chemical admixtures on setting and strength development of concrete. J. Test Eval. 3, 322–330.

Sabbas, T., Polettini, A., Pomi, R., Astrup, T., Hjelmar, O., Mostbauer, P., Cappai, G., Magel, G., Salhofer, S., Speiser, C., Heuss-Assbichler, S., Klein, R., Lechner, P., 2003. Management of municipal solid waste incineration residues. Waste Manage. 23, 61–88.

Shi, C., Day, R.L., 1995. Acceleration of the reactivity of fly ash by chemical activation. Cement Concrete Res. 25, 1333–1346.

Shi, C., Day, R.L., 2000a. Pozzolanic reaction in the presence of chemical activators. Part I. Reaction kinetics. Cement Concrete Res. 30, 51–58.

Shi, C., Day, R.L., 2000b. Pozzolanic reaction in the presence of chemical activators. Part II. Reaction products and mechanism. Cement Concrete Res. 30, 607–613.

Shi, C., Day, R.L., 2001. Comparison of different methods for enhancing reactivity of pozzolans. Cement Concrete Res. 31, 813–818.

Stumm, W., Morgan, J.J., 1995. Aquatic Chemistry: Chemical Equilibria and Rates in Natural Waters, third ed. John Wiley and Sons, Inc., New York.

US Department of Energy, 2004. Qualification of Thermodynamic Data for Geochemical Modeling of Mineral–Water Interactions in Dilute Systems, Document No. ANL-WIS-GS-000003.

Zevenbergen, C., Comans, R.N.J., 1994. Geochemical factors controlling the mobilization of major elements during weathering of MSWI bottom ash. In: Goumans, J.J.J.M., van der Sloot, H.A., Aalbers, Th.G. (Eds.), Environmental Aspects of Construction with Waste Materials, Studies in Environmental Sciences 60. Elsevier Science, Amsterdam, pp. 179–194.

Zevenbergen, C., Van Reeuwijk, L.P., Bradley, J.P., Comans, R.N.J., 1996. Mechanism and conditions of clay formation during natural weathering of MSWI bottom ash. Clays Clay Miner. 44, 546–552.

Acknowledgements

I know that it is here where you think that you will find out whether you have meant something in the life of the PhD Candidate… this may be true!

First of all I would like to thank Prof.ssa Polettini and Ing. Pomi without their willingness and suggestions this PhD thesis would not have been written. I would like to mention also Luigi and Gloria for the experimental support in the lab.

Part of the data here presented were collected in the Department of Materials Science and Engineering of University of Erlangen-Nuremberg, taking this into account I would like to thank Prof. Aldo Boccaccini. The last (more or less) three months of my thesis project I spent in Erlangen: to me Erlangen University is also synonymous with "international group of students" with a very good chief that knows as motivate the "young researchers".

A sincere thanks to Prof. Mattia Crespi for the humble and continuous support.

And… leave me some Italian words for my parents and my brother:

"Grazie del continuo supporto anche nei momenti in cui avrei lasciato perdere… grazie per avermi permesso di fare questa esperienza perchè io ci ho messo la volontà e la tenacia ma senza di voi non avrei mai potuto raggiungere questo traguardo!"